DEVELOPING A GENERAL METHODOLOGY FOR EVALUATING COMPOSITE ACTION IN INSULATED WALL PANELS

A report to the Precast/Prestressed Concrete Institute

as part of a Daniel P. Jenny Research Fellowship

By

Jaiden Olsen, Salam Al-Rubaye, Taylor Sorensen, Marc Maguire

UTAH STATE UNIVERSITY
Logan, Utah
2017

ABSTRACT

Developing a General Methodology for Evaluating Composite Action
in Insulated Wall Panels

Precast concrete sandwich wall panels (PCSWPs) have been in use for over 60 years. They provide a very efficient building envelope for many buildings. Characteristic PCSWPs comprise an outer and inner layer (or wythe) of concrete separated by an insulating material. To use all of the material as efficiently as possible, the layers are attached by connectors which penetrate through the insulating layer and are embedded in either concrete wythe. These connectors make it possible for both layers of the wall to work together when resisting loads. The connectors are made out of plastic, or FRP, to prevent heat transfer from one side of the wall to the other.

This research evaluated several different FRP systems by fabricating and testing 41 small scale "push-off" specimens (3 ft. by 4 ft., 0.91 m by 1.22 m) and eight full-scale sandwich panel walls to evaluate the percent composite action of various connectors and compare the results to those provided by the composite connector manufacturers. Testing of push-off specimens was performed by applying loads perpendicular to the connectors and measuring the amount of deformation that occurred. By determining the load-deformation relationship, engineers can make more informed decisions about the full-scale behavior. This project aimed to validate current procedures using these methods, and to develop simpler, more efficient methods for predicting overall strength of this innovative building system. This study concluded that the reported degrees of composite action from each manufacturer are considered conservative in all instances for the connectors tested. Additionally, the intensity and type of connectors are important factors in determining the degree of partial composite action in a panel.

Two methods to predict elastic deformations and cracking were developed (the Beam-Spring model and the Elastic Hand Method) and were compared to the elastic portions of the full-scale testing performed in this study, yielding promising results. A new method (the Partially-Composite Strength Prediction Method) was also created to predict the nominal moment capacity of concrete sandwich wall panels that is easier to implement than current methodologies and shown to be accurate. The results of this method were also compared to the full-scale testing results in this study. Design and analysis examples using these methods are presented in this report. (243 pages)

ACKNOWLEDGEMENTS

The authors are humbly grateful for the support of the Precast/Prestressed Concrete Institute and the Daniel P. Jenny Research Fellowship. The patience of the committee as the team worked through precaster fabrication was infinitely appreciated. Several volunteers and undergraduate researchers helped complete this project, with special thanks due to Gilbert Nichols, Hunter Buxton, Parker Syndergaard, Tyson Glover, and Ethan Pickett for their assistance in the fabrication and testing of the sandwich wall panels. The authors are grateful that Forterra Precast in Salt Lake City, Utah provided the majority of the panels, and Concrete Industries in Lincoln, Nebraska is thanked for their very timely THiN-Wall panel fabrication and delivery. Furthermore, the donation of connectors and insulation materials by Thermomass, Dayton Superior, HK Composites, and Aslan-FRP were greatly appreciate, and an integral part to the completion of this research. Special thanks to Ken Fleck and A. L. Patterson for the donated lifting devices to make the testing of the panels quicker and easier.

CONTENTS

LIST OF TABLES

Table **Page**

LIST OF FIGURES

Figure **Page**

LIST OF SYMBOLS AND NOTATION

The following symbols are used in this paper.

A_{ps}	area of prestressing steel in wythe
A_s	area of mild steel in wythe
b	slab width
C	compression force in wythe
c	depth to neutral axis of wythe from top of wythe
d_1	effective depth of steel in wythe from furthest compression fiber of concrete
E_c	modulus of elasticity of concrete
E_s	modulus of elasticity of steel
F_E	elastic load limit
F_i, $F(i)$	shear force in connector in connector line i
F_{sum}	total shear force, the sum of connector forces in longitudinal location of interest
F_u	ultimate capacity/strength or peak load
f_c'	concrete compressive strength
f_{ps}	stress in prestressing steel in wythe
f_{pu}	ultimate stress of prestressing strands
f_r	modulus of rupture of concrete (psi)
f_s	stress in mild steel in wythe
f_t	concrete tensile strength
f_y	steel yield stress
I_{test}	experimental moment of inertia of sandwich panel
I_{NC}	theoretical moment of inertia of the non-composite sandwich panel
I_{FC}	theoretical moment of inertia of the fully-composite sandwich panel
i	connector line starting at end of panel
K_d	degree of composite action depending on deflection
K_E	elastic stiffness

K_{Ei}	elastic stiffness of connectors in connector line *i*
K_{IE}	inelastic stiffness of plastic stiffness
K_{Mcr}	degree of composite action depending on cracking moment
K_{MN}	degree of composite action depending on maximum moment
L	total length of panel
$M_{cr,test}$	experimental cracking moment of sandwich panel
$M_{cr,NC}$	theoretical cracking moment of non-composite sandwich panel
$M_{cr,FC}$	theoretical cracking moment of fully-composite sandwich panel
M_{FC}	fully-composite moment
$M_{n,test}$	experimental maximum moment of sandwich panel
$M_{n,NC}$	theoretical maximum moment of non-composite sandwich panel
$M_{n,FC}$	theoretical maximum moment of fully-composite sandwich panel
$M_{service}$	moment calculated by service loads
M_{wy2}	cracking moment of wythe 2
N_i	number of connectors in connector line *i*
n	total number of connector rows in half of panel (L/2)
P_{we}	equivalent point load
Span	unsupported span length (support-to-support distance)
T	tension force in wythe
t_{insul}	thickness of insulation
t_{wy1}	thickness of wythe 1
t_{wy2}	thickness of wythe 2
w_c	unit weight of concrete (pcf)
w_{we}	equivalent distributed load
x_i	location of connector line *i* from end of panel
x_P	location of point load from end of panel
Z	distance between centroids of wythe 1 and 2
γ	unit weight of concrete (pcf)

Δ_{axial}	slip of wythes due to axial deformation at end connector
Δ_E	deflection corresponding to elastic load limit
Δ_{Rot}	slip of wythes due to bending at end connector
Δ_U	deflection corresponding to the ultimate capacity
δ_{end}	calculated slip at end connector
$\delta(i)$	slip in connector i
δ_{max}	actual slip in end connector
ε_c	strain in concrete
ε_{ps}	strain in prestressing steel
ε_s	strain in mild steel
ε_y	strain of mild steel at yielding
θ	angle of rotation (radians)
θ_{Pwe2}	angle of rotation for given equivalent point load (radians)
θ_{wwe2}	angle of rotation for given equivalent distributed load (radians)
φ	curvature of wythe

LIST OF ABBREVIATIONS

ACI	American Concrete Institute
BDI-STS	Bridge Diagnostics Inc. - Structural Testing System
CFRP	carbon fiber-reinforced polymer
EPS	expanded polystyrene
FEM	finite element model
FRP	fiber reinforced polymer
GFRP	glass fiber reinforced polymer
HDO	high density overlay
ISO	polyisocyanurate
LEED	Leadership in Energy and Environmental Design
LVTD	linear variable differential transformer
NIST	National Institute of Standards and Technology
PCI	Precast/Prestressed Concrete Institute
PCSWP	precast concrete sandwich wall panels
SMASH Lab	Utah State University's Systems, Materials, and Structural Health Laboratory
SWP	sandwich wall panel
XPS	extruded polystyrene

1 INTRODUCTION

Precast concrete sandwich wall panels (PCSWPs) provide a very efficient building envelope for many buildings. Sandwich wall panels (SWPs) combine structural and thermal efficiencies into a simplistic design where the thermal envelope is integrated into the structural design. This system is advantageous over conventional methods because of its rapid construction and erection methods. Characteristic PCSWPs comprise an outer and inner layer (or wythe) of concrete separated by an insulating material. To achieve maximum structural efficiency, the wythes are connected by shear transfer mechanisms which penetrate through the insulating layer and can provide various levels of composite action. More stringent energy building codes demand greater thermal efficiency and therefore lead to increasing implementation. As these connectors become more widely used, the demand for a reduction in thermal bridging has driven the development of connectors made of many different materials.

With the push for Leadership in Energy and Environmental Design (LEED) Certified buildings, there is a rapidly increasing demand for thermally and cost efficient structural elements. The research performed on PCSWPs in the last two and a half decades has focused on designing with thermally efficient connectors. Thermal bridging is still a significant challenge for PCSWPs, particularly in structurally composite panels. There have been many proposed solutions to enable composite action without thermal bridging and many have been implemented and are currently in use across the United States. Fiber Reinforced Polymer (FRP) connectors make up the largest part of today's cutting edge shear connectors. Unfortunately, PCSWPs with partial or fully-composite action are not well understood from a behavior stand point outside of the often-proprietary data owned by connector companies. Furthermore, composite connector manufacturers have varying degrees of understanding of their own product and often rely on only interpolation of test data to design a panel. Engineers seem to be wary of this approach and have expressed a need a well-founded, simple and quick way to predict PCSWP partial composite action.

The research presented in this report was aimed at developing general tools for PCSWP designers to use in everyday practice specifically through component level testing and simplified modeling. Using this component level testing, the goal of this project was to validate a simple model to predict elastic stresses and deflections in PCSWPs, which are currently a major concern for design engineers, and to evaluate the percent composite action of various connectors and compare the results to those provided by the composite connector manufacturers.

1.1 Background

Precast concrete sandwich wall panels (PCSWPs) have been in use for over 60 years. They provide a very efficient building envelope for many buildings. They combine structural and thermal efficiencies into one simplistic design. They are also advantageous over conventional methods because they eliminate many delays due to field work as well as the need for several sub-contractors. Characteristic PCSWPs comprise an outer and inner layer (or wythe) of concrete separated by an insulating material (Figure 1-1). To achieve maximum structural efficiency, the wythes are connected by shear connectors that penetrate through the insulating layer which can provide various levels of composite action. More stringent energy building codes have demanded greater thermal efficiency. Therefore, these shear connections are often made of various composites to eliminate thermal bridging.

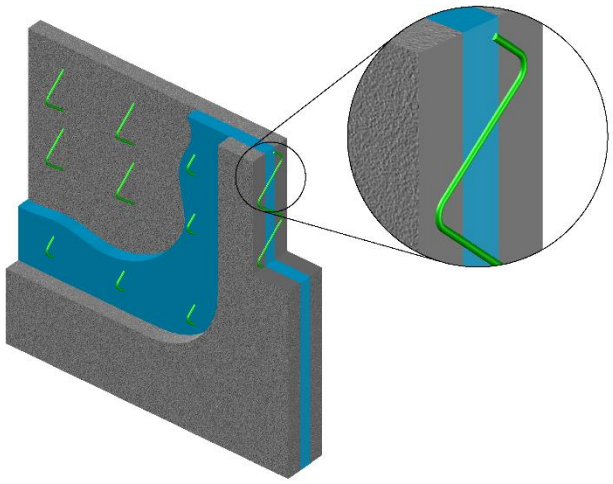

Figure 1-1 Concrete sandwich panel wall

The majority of sandwich panel walls between 1906 and the mid-1990s have had nearly identical components with varying insulation types, dimensions and wythe connection design. Figure 1-2 shows many of the connector configurations used in these early panels. All connectors were made of steel or monolithically cast concrete ribs.

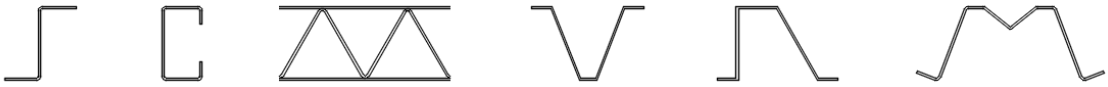

Figure 1-2 Different connector shapes used in sandwich panel walls

Reinforced concrete wythes, insulation, and steel connectors were components of nearly every panel. Thermal bridging is still an expensive problem with precast concrete sandwich panel walls. There have been many proposed solutions and many have been implemented across the United States. The goal of increasing thermal efficiency has led to simple eradication of many steel components within the sandwich panel wall. Though the focus has generally been to prevent any steel from penetrating the thermal barrier, research has proven that elimination of steel components embedded in the concrete can improve thermal efficiency. The most effective solutions are FRP based materials which are currently available to replace steel shear transfer mechanisms like wire trusses.

1.2 Research Objective

This research involves the evaluation of several different proprietary FRP systems by fabricating and testing 41 small scale "push-off" specimens to obtain valuable component testing. Full-scale tests will also be performed using some PCSWP shear connectors from the push-off testing program. The goal of this project is to validate mechanics-based procedures for predicting stresses, deflections and nominal strength using the push-off specimen shear load and deformation data. The results of these newly developed methods will be compared to the results of the full-scale testing.

1.3 Report Outline

Chapter 2 will outline the history of composite action in PCSWP construction and describe the currently available design philosophies. The experimental program, including specimen design and testing protocols, will be described in Chapter 3. Chapter 4 and Chapter 5 will present the results from the push-off testing and full-scale testing, respectively. Chapter 6 will present two general methodologies to predict elastic sandwich panel behavior. Chapter 7 will present a general framework to predict nominal strength of PCSWPs and Chapter 8 will contain the important conclusions from this study.

2 LITERATURE REVIEW

2.1 Concrete Sandwich Panel Wall History

This section contains a history of today's precast concrete sandwich panel walls, starting with its earliest predecessor, tilt-up sandwich panel walls. Records of concrete sandwich panel walls go back as far as 1906. Since their inception, PCSWPs have become a fundamental building envelope alternative in the United States.

2.1.1 1900-1990

Collins (1954) presented a project from the early 1900s. This is the earliest documented project completed using sandwich panel construction. At the time, the new tilt-up sandwich panel system was a novelty to designers and contractors. The panels were constructed by pouring a 2-in. layer of concrete while embedding steel ties into the concrete wythes. Steel tie configuration is unknown. After the concrete cured, a 2-in. layer of sand was poured across the panel on top of which a second 2-in. layer of concrete was poured. After an unspecified amount of time, the panels were tilted on an angle at which the sand was washed out of the panel with a fire hose (See Figure 2-1), leaving an air gap between the inside and outside wythes. This air gap created a simple thermal barrier. After the sand was washed out of the panel, it was tilted upright and fixed into place.

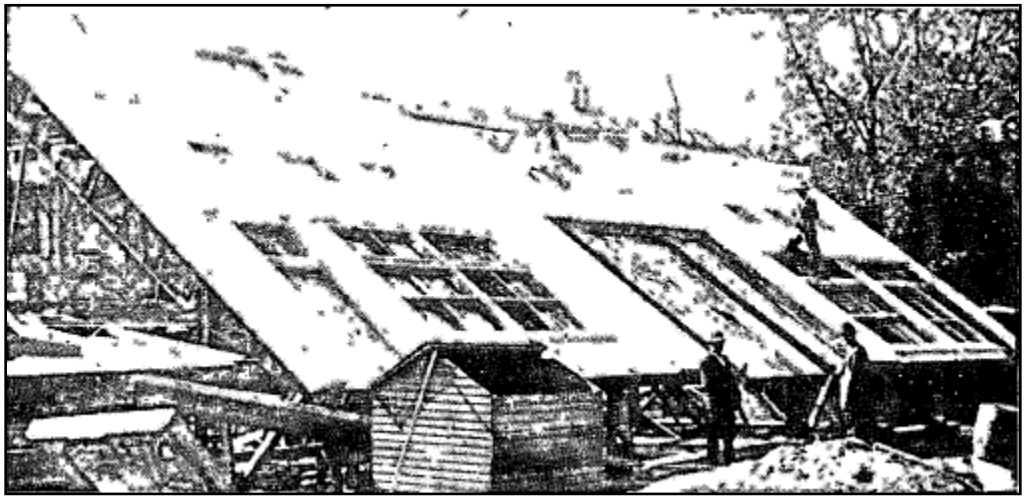

Figure 2-1 SWP tilted while sand is sprayed from center wythe with fire hose (Collins 1954).

Modern machinery enabled the invention of *precast* sandwich wall panels in 1951. Some of the earliest PCSWPs were built in 1951 in New York City, New York. The production lines used to build these precast insulated wall panels were 200 feet long. The panels were six feet high and ten feet wide. The panels were cast and then transported to British Columbia, Canada. "[The panels consisted] of a 2-in. thick layer of cellular glass insulation and two wire-mesh reinforced slabs of 3000-psi concrete, tied together with channel-shaped strips of expanded metal. These ties also serve as shear reinforcing." These panels had an overall thickness of 5.5 inches. Over time, sandwich panel wall designs became much more structurally and thermally efficient.

One project in particular helped Collins develop a design procedure in which he explored different materials to be used as an insulating barrier, different types of shear connectors, and different connector configurations. Figure 2-2 shows one of his twelve-inch (2-8-2) tilt-up sandwich panels. The outer wythes were constructed of reinforced concrete (150 pounds per cubic foot) and the inside wythe was a lightweight foam concrete (28 pounds per cubic foot). The shear connectors used were a thin-gage expanded steel mesh. The available insulating materials (or materials with a high R-value suitable for the constitution of the center wythe) were divided into the following categories:

1. Cellular glass materials and plastic foam
2. Compressed and treated wood fibers in cement
3. Foam concrete
4. Lightweight concrete

Figure 2-2 Lightweight foam concrete tilt-up SWP with 2" outer wythes and 8" center wythe (Collins 1954).

These materials were advantageous for their compressive strength, thermal properties, and unit weight. Insulating concretes are not very common today. The shear connectors that were used were all made of steel: thin-gage expanded mesh, electrically welded wire mesh, bent-wire with welded anchors, and "J" bar (a pin with one hooked end). Collins points out advantages of early sandwich panel walls including thermal efficiency, extended fire rating, and reduced dead weight. These benefits are all similar to contemporary PCSWP.

Collins (1954) suggested that there be a minimum concrete design strength of 3,000 psi for the outside wythes and 2,500 psi for the center insulation (lightweight insulating concrete). He also outlined minimum wythe thicknesses for both the inner and outer wythes. He concluded that the minimum required thicknesses for a panel should be 1.25-2-1.25, or an overall panel thickness of 4.5 inches. The design recommendation took an allowable stress design approach to determine panel dimensions. This iterative design procedure is outlined as follows:

1. Begin with the minimum required wythe thickness to obtain an R-value of 4.5 (°F) ft^2 hr/BTU. This is dependent upon the material used (one of the four categories listed previously) for the center wythe.
2. Calculate biaxial maximum design bending moment by checking wind and seismic forces.
3. Calculate the section modulus and determine the associated required area of steel.

4. Increase the wythe thickness until allowable stresses are met.

Adams et al. (1971) outlined design procedures for precast concrete wall panels that standardized this procedure for designers. The design procedure covered the design of solid, ribbed, hollow core, and sandwich panel walls. The design approach to sandwich panel walls, as indicated by the committee, is to use an "effective section" approach. The recommendation was made that "shearing stress should not be transferred through the nonstructural insulation core. Compressive stress and bending stress should be carried by the concrete sections only (Adams et al. 1971)." The outside wythes of concrete were connected using mechanical steel shear ties or by monolithically cast concrete ribs. It was recommended by the committee that insulation used be either a cellular or mineral based aggregate in lightweight concrete.

The design procedure outlined by Adams et al. (1971) was an allowable stress design approach. By determining the allowable stresses in the panel, an engineer could read a required dimensional ratio of height times width divided by thickness ($h*b/t_e$) from a plot (see Figure 2-3) based on concrete unit weight and compressive strength. In order to determine the correct design stress, two scenarios were considered: vertical compressive stress for concentric loads based on panel buckling stability, and out-of-plane compressive stress for panels between columns, supports, or isolated footings.

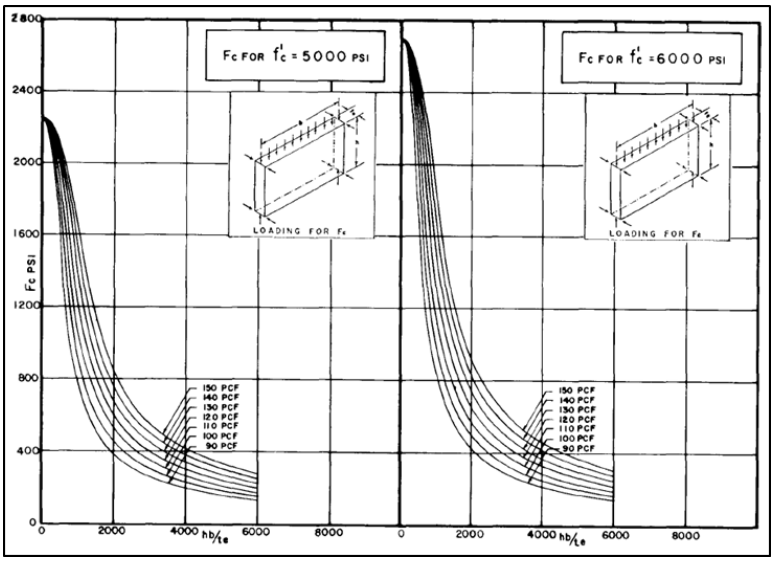

Figure 2-3 Design charts used by designers to extract acceptable dimensional ratios with a calculated stress and predetermined concrete compressive strength (Adams et al. 1971).

Adams et al. (1971) derived equations for determining the allowable stresses in a panel. For vertical compressive stress with $F_a < 0.11f_c'$

$$F_a = 0.225f_c'\left[1 - \frac{\sqrt{f_c'}}{w^{1.5}}\left(\frac{h}{9t_e}\right)^2\right] \quad (2\text{-}1)$$

And for vertical compressive stress with $F_a \geq 0.11f_c'$

$$F_a = 5w^{1.5}\sqrt{f_c'}\left(\frac{t_e}{h}\right)^2 \quad (2\text{-}2)$$

For horizontal compressive stress with $F_c > 0.3f_c'$

$$F_c = 0.45f_c'\left[1 - \frac{f_c'}{w^3}\left(\frac{bh}{75t_e}\right)^2\right] \quad (2\text{-}3)$$

And for horizontal compressive stress with $F_c \leq 0.3f_c'$

$$F_c = 13w^{1.5}\sqrt{f_c'}\left(\frac{t_e}{bh}\right) \quad (2\text{-}4)$$

Where: F_a = allowable direct compressive stress, psi

F_c = allowable horizontal compressive stress, psi

f_c' = specified compressive strength of the concrete at 28 days, psi

w = unit weight of concrete, pcf

h = unsupported height of panel, in

t_e = effective thickness of precast wall, in

The stress which returned the lowest value would govern design. Recommendations were also provided for panel dimension ratio requirements for panels subjected to both vertical and horizontal direct uniaxial or biaxial bending stresses, as follows:

For vertical loads:

$$\frac{f_a}{F_a} + \frac{f_{b1}}{F_b} + \frac{f_{b2}}{F_b} \leq 1 \qquad (2\text{-}5)$$

For horizontal loads:

$$\frac{f_c}{F_c} + \frac{f_b}{F_b} \leq 1 \qquad (2\text{-}6)$$

Adams et al. also provide details on the maximum bearing pressure under a panel (applied on the footprint of the erected panel), to be:

$$F_{br} = 0.4 f_c' \sqrt[3]{\frac{A_c}{A_b}} \leq f_c' \qquad (2\text{-}7)$$

Where: A_c = maximum area of the of supporting member that is geometrically similar to and concentric with the bearing area of the precast panel, in^2

A_b = bearing area of precast panel in contact with supporting frame, in^2

f_a = computed direct compressive stress, psi

$f_b = f_{b1} = f_{b2}$ = computed bending stress, psi, for panels loaded perpendicular to the plane of panel

F_b = allowable maximum bending stress, psi, for panels loaded perpendicular to panel plane

Adams et al. required specific shear connector spacing requirements as well, stating that the connectors should not be placed near the edge of the panel and that the connector composition should be out of a fireproof

ductile material. These requirements were to ensure that connectors would be designed to accommodate all shear, bending, tension, and compression forces even in the case of a fire. The conservative assumption was made that the wythes of sandwich wall panels do not work compositely. Though it was a very conservative approach, it made designing PCSWPs very simple.

2.1.2 1991-2000

Einea et al. (1991) presented detailed information on the design and construction of fully-composite, partially-composite, and non-composite PCSWPs in addition to discussing then common building materials. They discussed the principles of fully-, partially, and non-composite panels (Figure 2-4) and introduced the plausibility of many different types of insulations, outlining details on how to conjoin wall panels. They explored many different configurations of steel shear connectors designed to accommodate some degree of composite action as well as the option of non-composite ties used for attaching architectural cladding and other non-structural elements. Their discussion extensively covered the design and analysis of sandwich panel walls, addressing many failure modes common to PCSWPs.

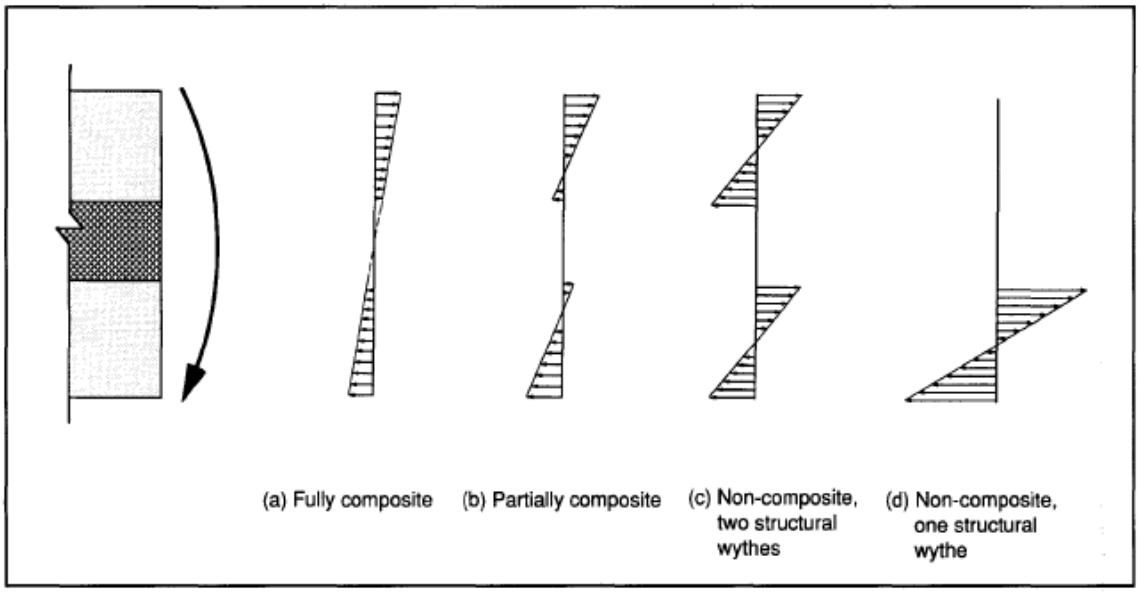

Figure 2-4 Stress distribution diagrams in PCSWPs due to pure bending (Einea et al. 1991)

Einea et al. (1991) introduced the subject of rigid insulation joints. Rigid insulation joints occur when staging the center wythe and preparing to pour the second outside wythe. Rigid insulation comes pre-fabricated in sheets as long as twelve feet. Joints can cause pockets of stagnant air and also concrete ribs that penetrate the thermal barrier, both of which cause a decreased R-value, thus hurting the thermal efficiency of the panel. The easy joint option is called a "butt joint" and is simply two square edges butted up to one another. Recommendations provided by Einea et al. include four much better alternatives, pictured in Figure 2-5; staggered sheets, perpendicular lapping, inclined lapping, and curved lapping.

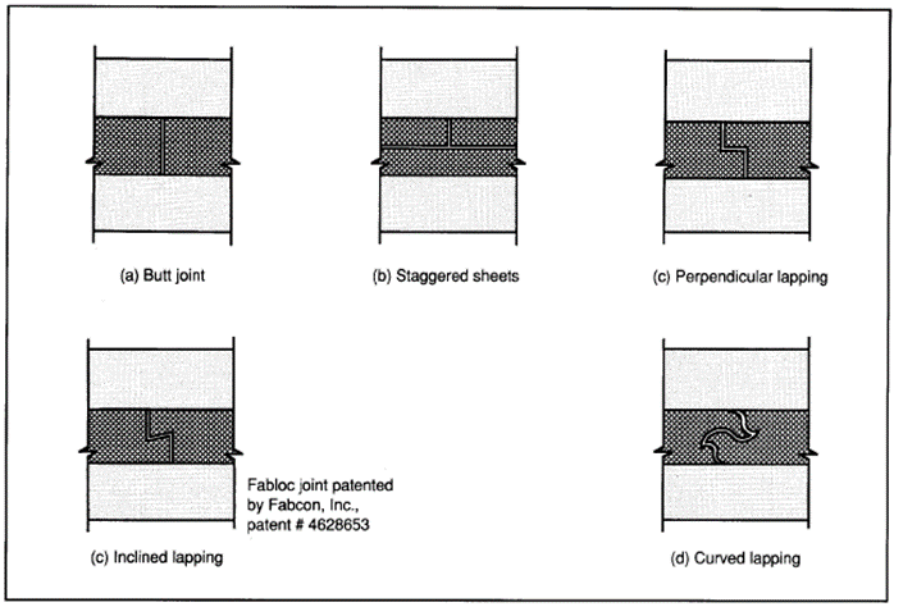

Figure 2-5 Insulation joints in SWPs: a) butt joints, b) staggered sheets, c) perpendicular/inclined lapping, d) curved lapping (Einea et al. 1991)

Studies were performed to plot the reduction in R-value to the percentage of both steel and concrete penetrating through the center wythe. For example, if 0.1% of the area occupied by one wythe is bridged through the panel via stainless steel, there is a 41% reduction in R-value. For concrete penetrations, 1% of the area occupied by one wythe is equivalent to a 37% reduction in R-value. Figure 2-6 and Figure 2-7 plot this relationship of R-value versus percentage of area penetrating the center wythe.

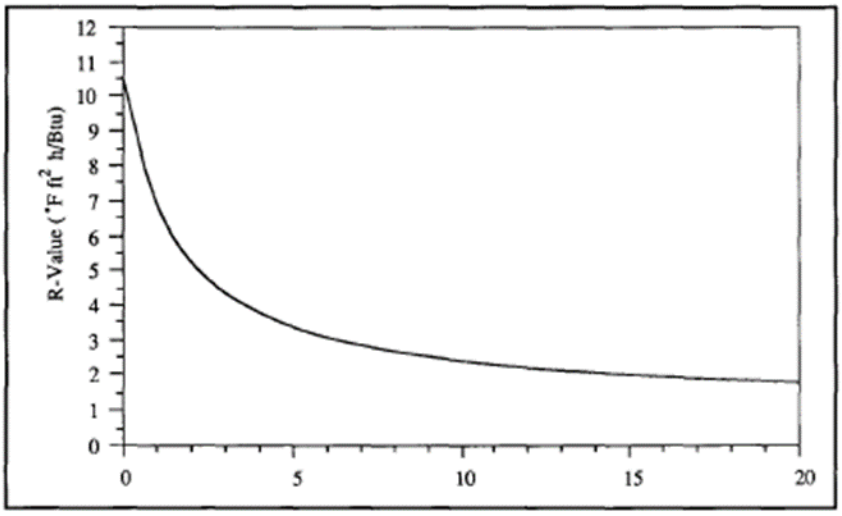

Figure 2-6 R-value vs % area stainless steel connectors in PCSWPs due to thermal bridging (Einea et al. 1991).

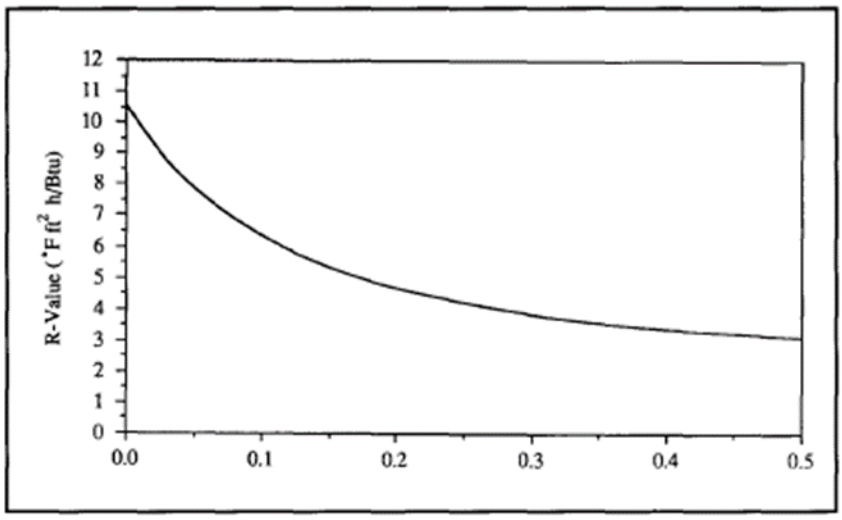

Figure 2-7 R-value vs % area penetration of concrete for PCSWPs due to thermal bridging (Einea et al. 1991).

This study presented the need for further research aimed at maximizing thermal efficiency. Other areas of research they suggested include thermal efficiency, fire protection, volume changes, and transient versus steady-state temperature effects.

Einea et al. (1994), introduced a new sandwich panel system incorporating "fiber-reinforced plastic [polymer]," (FRP) material. Rather than using traditional steel connectors to create a load path between cooperating

wythes, Einea et al. implemented the use of FRP shear connectors. The motivation behind implementing plastic shear connectors as part of a sandwich panel wall was to reduce heat transfer between concrete wythes. Einea et al. identified the thermal insufficiency of using steel connectors, pointing out that it greatly reduces the thermal potential of PCSWPs (Einea et al. 1991). The authors noted that although implementing FRP connectors increases the initial cost, it proves to have positive economic impact through the life of the structure in heating and cooling costs. Another crucial aspect mentioned by Eineia et al. involves the circulation of three components that thermally and structurally efficient precast concrete sandwich panels must incorporate:

1. The connectors must be strong and stiff enough to develop composite behavior of the panels.
2. The connectors must have a high thermal resistance.
3. No concrete penetrations through the insulation layer should exist.

Four different configurations of FRP shear transfer mechanisms were submitted for consideration: wide flange FRP connector, specially fabricated “dog-bone” connector, FRP diagonal strap connectors, and bent bar connector. (See Figure 2-8). The only connector that made it through the first stages of consideration was the bent bar connector. The bent bar connector is a deformed helix that is then threaded with two prestressing strands. Further, the prestressing strands are embedded in either outside wythe to ensure positive connection between the FRP bar and the concrete.

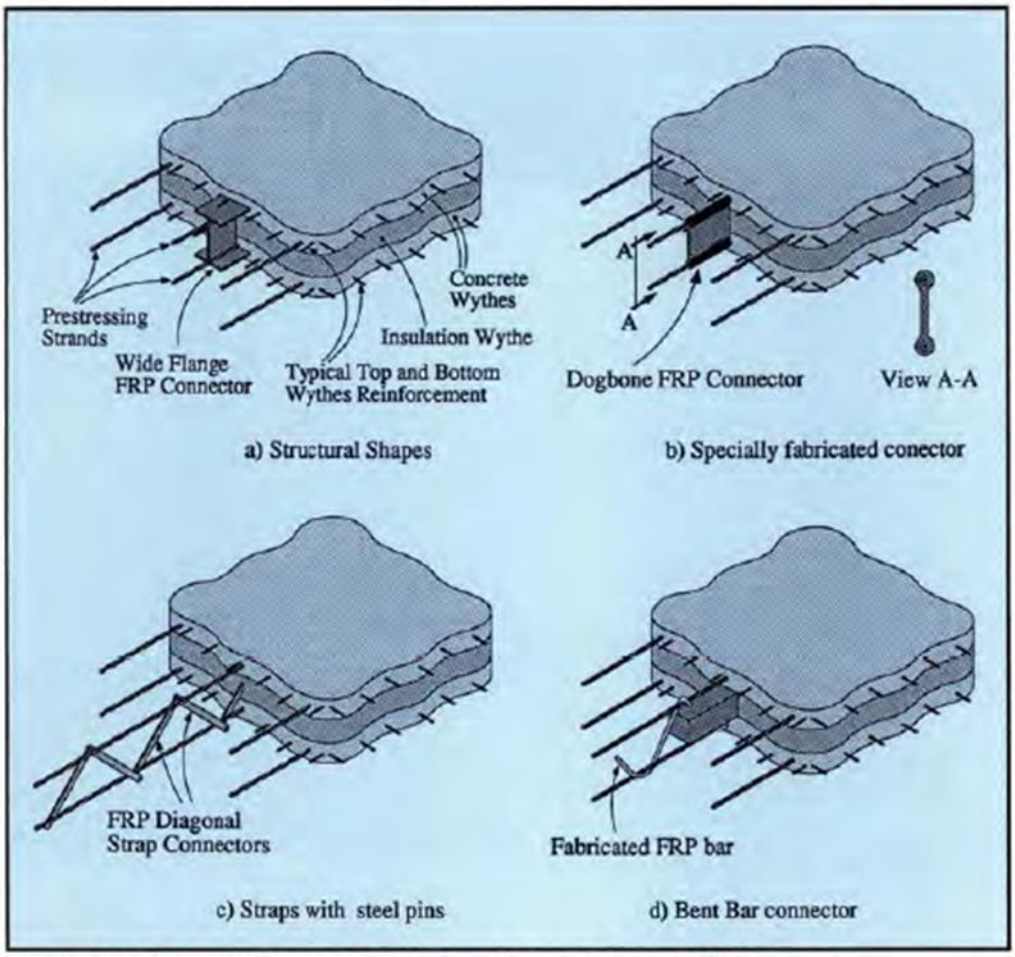

Figure 2-8 Candidate FRP connectors shown in cross-sectional view of PCSWPs (Einea et al. 1994)

Shear testing was performed via push-off specimen to determine the shear capacity and shear stiffness of the connector. It was determined that the shear capacity of the connector is governed by the axial strength of the FRP bar. In other words, the majority of the connectors failed between either of the concrete-foam interfaces. It was also noted that the uninhibited surface of the insulation board bonded with the inner faces of the concrete and contributed up to ten percent of the shear capacity of the specimen.

Flexural testing was also performed to evaluate flexural performance. A single FRP bent bar connector was placed within a three-wythe panel and loaded in two phases. For the first phase, load was applied perpendicular to the panel (Figure 2-9) until the bottom edge of the opposite wythe began to crack. This was done to ensure linearity

during a second loading phase. Once cracking occurred the panel was unloaded. The setup for the second phase of loading mimicked the first, only load was applied until specimen failure. This test was performed on two specimens.

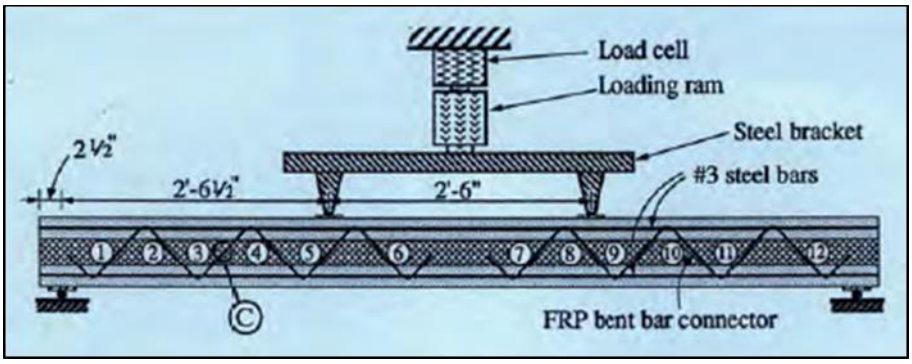

Figure 2-9 Diagram showing the flexural test setup (Einea et al. 1994).

During this initial phase of testing on FRP shear transfer mechanisms, it was determined that in addition to being thermally superior to their predecessors, FRP bars satisfy all structural performance guidelines outlined by the researchers. It was observed that, though FRP is inherently brittle in nature and fractures at ultimate capacity without any warning, ductile behavior was observed. "[This] ductile behavior is likely caused by cracking in the connections between the bent bar connector and the concrete that leads to a gradual loss of composite action and hence, larger deflections (Einea et al. 1994)." Einea et al. suggested that further research be performed in the following categories:

1. "The effect of long term loading on the proposed system.
2. Cyclic load testing to investigate the ductility and energy dissipation characteristics of the panels for use in high seismic risk areas.
3. Development of lifting and connection inserts to maintain the thermal and structural efficiency of panels. Research is required to develop, test, and obtain design parameters for such accessories.
4. Determination of the fire rating of the proposed panel system. FRP material loses a large portion of its strength when exposed to fire or a high temperature environment. Investigation of concrete cover or other means to prolong the fire rating of the system is needed.
5. Determination if lateral support provided by insulation and concrete wythes is sufficient to prevent instability of the connectors when small bars are used.

6. Experiments to determine the nature of load-slip behavior of the connectors inside the wythes to more accurately predict the stiffness of the panels" (Einea et al. 1994).

These suggestions were published more than twenty years ago. Researchers are still searching for many of these solutions today.

Salmon and Einea (1995) sought to determine a method to predict panel deflections. This is one of the first studies to use finite element methods (FEM) in predicting concrete sandwich panel deflections. The first of two determinations made as a result of this research was that predicting deflections caused by thermal bowing using FEM was found to be acceptable. The second was that "long insulated sandwich panels with low connecting-layer stiffness will experience nearly the same amount of thermal bowing as fully-composite panels." In searching for an accurate design procedure, Salmon and Einea looked at an element of a PCSWP being loaded and closely analyzed the deformation (See Figure 2-10). They found that the panel deformation consists of two components. The first is due to the curvature of the panel. The second is as a result of the offset that occurs between wythes as a result of the shear stresses involved. Mathematically, these phenomena can be expressed as:

$$y_{xx} = \frac{M}{EI} + \frac{\alpha^2}{2r} q_x$$

$$\alpha = \frac{(I - 2I_w)}{I} \qquad (2\text{-}8)$$

Where x = distance along the length of the panel

y = upward displacement of the panel

q = relative shearing displacement between the centroids of the top and bottom wythes.

b = width of the panel

M = applied moment

E = wythe modulus of elasticity

I_w = moment of inertia of each wythe

I = moment of inertia of the entire panel cross section

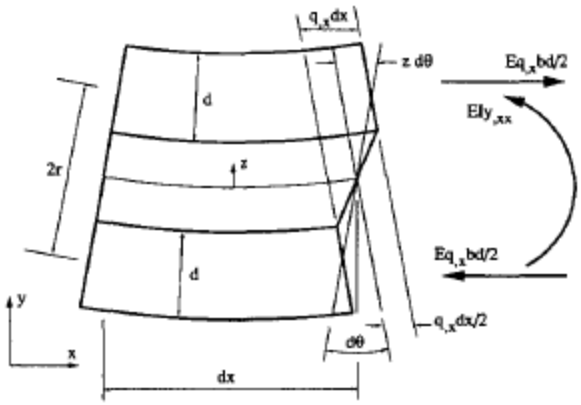

Figure 2-10 Differential Panel Element (Salmon and Einea 1995)

In continuing with the differential equations and performing several derivations similar to the one pictured in Figure 2-10, Salmon and Einea develop an equation to predict displacement they called the continuum model:

$$\delta = \delta_0 \left[1 - \frac{2}{\psi^2}(1 - \operatorname{sech}\psi)\right] \qquad (2\text{-}9)$$

Where

$$\delta_0 = -\frac{M_T L^2}{8EI} \qquad (2\text{-}10)$$

$$\psi = \frac{\chi L}{2\beta} \qquad (2\text{-}11)$$

$$\beta^2 = \frac{1}{1 + 12\left(\frac{r}{d}\right)^2} \qquad (2\text{-}12)$$

$$\chi^2 = \frac{2K}{Ed} = \frac{A_c m}{4\sqrt{2}r^2 b}\frac{E_c}{E}\frac{1}{d} = \frac{1}{4\sqrt{2}}\frac{A_c mn}{rb}\frac{1}{rd} \qquad (2\text{-}13)$$

Where δ = center panel deflection

δ_0 = fully-composite center panel deflection

ψ = $\frac{\chi L}{2\beta}$

M_T = equivalent end moment caused by change in temperature ΔT

L = panel length

E = modulus of elasticity of connectors

I = panel moment of inertia

β = constant: $\beta^2 = 1 - \alpha^2$

χ = constant: $\chi^2 = \frac{2K}{Ed}$

r = distance between structural wythe centroids

d = structural wythe thickness

K = shear stiffness of connecting layer

A_c = cross-sectional area of connectors

m = number of connectors across panel width

E_c = modulus of elasticity of the concrete

n = modular ratio, $\frac{E_c}{E}$

Though no full-scale testing was done at the time of publication, a comparison between the continuum model and finite element model proved quite successful. For the panels analyzed, results were within 1% of each other.

In March of 1997, the Precast Concrete Institute (PCI) published a PCI Committee Report titled, "State-of-the-Art of Precast/Prestressed Sandwich Wall Panels." Kim E. Seeber acted as the chairman for 24-member committee. Unlike the 1991 state-of-the-art paper by Einea et al., wythe and panel dimensions were no longer governed by allowable stress in the panel. A minimum wythe thickness was suggested to be two inches, however, overall panel width could be as low as five inches. Although no maximum wythe thickness was imposed, most designs were to make the panels as thin as possible, with required fire resistivity often designating the thickness of the wall panels. Wythe thickness ratios were dependent upon the type of panel; composite, non-composite, or partially composite. The wythes of composite panels were often symmetrical whereas non-composite panels often had a thicker structural wythe. Panel dimensions were "…limited only by the handling capability of the plant, erection equipment, transportation restrictions, and the ability of the panel to resist the applied stresses" (Seeber et

al. 1997). Panels had been as tall as 75 feet and as wide as 14 feet. Most panels ranged between 6 and 12 inches thick, 8 to 12 feet wide, and 10 to 50 feet tall.

Bowing considerations were addressed by the article as well. There are many variables that make it difficult to predict bowing at any given time. These variables include shrinkage, creep, cracking of the concrete (and, consequently, inconsistent modulus of elasticity), thermal gradients between panels, boundary conditions (including indeterminate fixity), and uncertainty in the degree to which the wythes of the panel are acting compositely. In this report, the researchers noted that bowing most often occurred toward the outside of the building. Panels exposed to the sun in the warmer part of the day experienced more bowing than other panels (i.e. south and west panels see more sunlight throughout the day than the north and east panels). Bowing was also constantly changing throughout the day. Due to differing climate on either side of the wall (post erection), it was also noted that differential shrinkage could occur and cause exaggerated effects. It was also observed that asymmetrical panels (due to differing dimension, concrete strength, or prestressing force) experienced more exaggerated bowing effects as well.

Panel design was also approached differently than the previous state-of-the-art article (Einea et al. 1991). The recommendation for non-composite panels was to simply design them like solid section concrete panels, with the assumption that only one wythe would resist all the vertical loads. In the case of lateral loading, it was considered acceptable to account for the independent flexural stiffness of each wythe. An example is provided for calculating the stresses associated in a 2-1-3 panel in Figure 2-11.

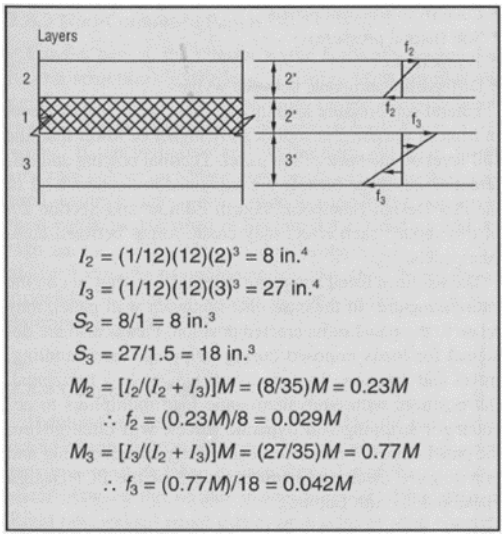

Figure 2-11 Stress distribution in a non-composite sandwich panel (Seeber et al. 1997)

The approach recommended for composite panels was to design the panel similar to that of a solid panel with the same cross-sectional thickness. It was assumed that the panel would remain fully-composite for the entire life of the structure. The authors noted that consideration must be taken for the horizontal shear load that needs to be transferred between the wythes. They also mention that when determining the section properties for design, an account must be made for the lack of stiffness in the center wythe as pictured in Figure 2-12. Recommendations were provided for calculating the force required to be transferred through the shear transfer mechanisms as found in the PCI Design Handbook (Section 4.3.5) (Seeber et al. 2004).

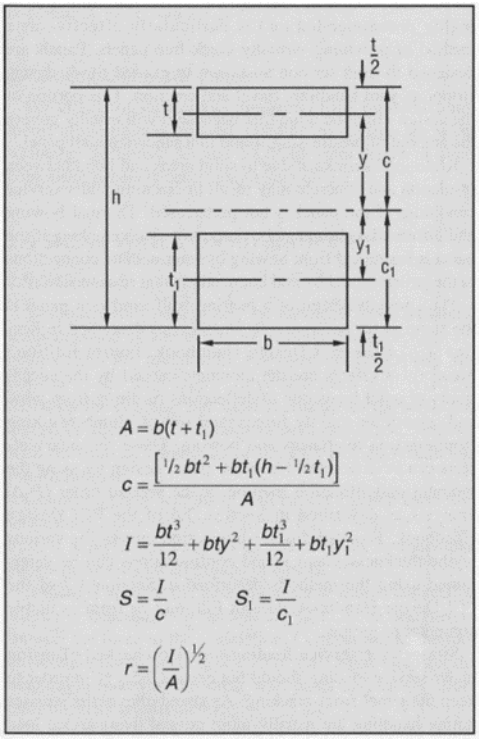

Figure 2-12 Sample calculations for determining section properties of fully-composite SWP (Seeber et al. 1997)

Semi-composite panels were designed for two different stages. The assumption was made that the panel works compositely through stripping, release, handling, transportation, and erection processes. The panel was then assumed to be non-composite following erection. This assumption was made because of the concrete-foam interface bond that was initially present in PCSWPs. This bond was known to deteriorate with time. It was unsafe to rely on this bond for the life of the structure. In reality, composite action can be assumed for the panel at the time of release

because of the shear capacity of the concrete-foam interface bond in conjunction with shear connectors. After the concrete-foam interface bond is broken, there is still a degree of composite action that takes place as a result of the shear connectors. This was not understood at the time. Another suggested design procedure for partially composite panel was to perform lateral load tests on an experimental panel that is an exact replication of the design panel. By loading the experimental panel and comparing measured deflections to the calculated fully-composite and non-composite dimensional equivalent, a degree of composite action could be derived by linear interpolation.

For bearing wall design of non-composite panels, the structural wythe was designed to accommodate all bearing loads, including the dead weight of the non-structural wythe if the non-structural wythe did not bear on the structure below. The design was required to comply with the design prescriptions outlined in the PCI Handbook for bearing walls (Seeber et al. 2004).

For composite panels, the bearing loads were required to be positively transferred to both structural wythes. Measures were to be taken to ensure transfer between wythes via positive shear transfer mechanisms. Again, the design was required to comply with the design prescriptions outlined in the PCI hand book for bearing walls.

Semi-composite panels had to be considered as non-composite for bearing loads. In checking for buckling, the independent moments of inertia were to be used. Note this is not the composite section, but the independent wythe section properties.

For shear wall design, lateral load resistance was to be attributed to the structural wythe for non-composite panels. For composite panels, the composite section was allowed to be used to accommodate lateral loads. Semi-composite panels were designed just like non-composite panels.

Included in the article, Seeber et al. outlined design procedures for external connections, panel roof connections, corner connections, floor connections, and panel to panel connections. Also discussed were detailing considerations, reinforcement requirements, fire resistance, insulation types, energy performance, and sandwich panel wall fabrication, transportation, erection, and inspection. This article was ascribed as the most comprehensive design provision published at the time.

Salmon et al. (1997) tested four full-scale specimens to compare results from a control group (two panels with a standard steel truss shear connector) to the results of panels containing the FRP truss introduced by the same group of researchers in 1994 (Einea et al. 1994). This research was geared towards the observation of partially-

composite action and ultimate strength comparison. It was determined by the researchers that results between each type of shear connector were very similar.

The beam elements in the FEM model, shown in Figure 2-13, were assigned a moment of inertia corresponding to each wythe. The truss elements represented the FRP truss or steel truss, depending on the model. Load was applied to the model to generate elastic performance. The results were compared to determine accuracy. Salmon et al. derived an equation from the linear analysis to predict the effective moment of inertia for partially composite panels.

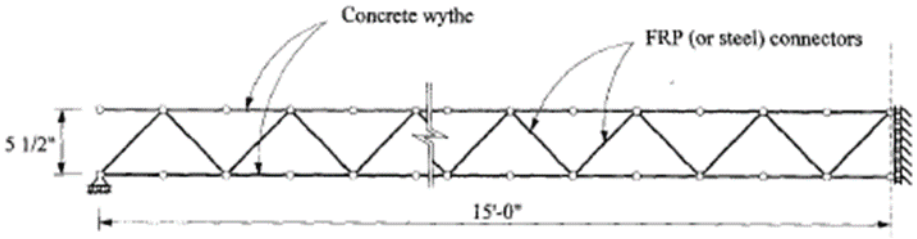

Figure 2-13 A depiction of the FEM/linear analysis model (Einea et al. 1997)

$$I_e = \frac{Mh}{f_b - f_t} \qquad (2\text{-}14)$$

Where I_e = the effective moment of inertia

f_b = the stress at the bottom face of the panel

f_t = the stress at the top face of the panel

M = applied moment

h = unsupported length of the panel

Note, Eq. (2-14) does predict the effective moment of inertia. However, the FEM model is optimized to mimic the data determined from experimental methods. After the researchers calculated the effective moment of inertia, the cracking moment was calculated as follows:

$$M_{cr} = \left(6\sqrt{f_c'} + \frac{f_{ps}A_{ps}}{A_w}\right)\frac{I_e}{c} \qquad (2\text{-}15)$$

Where: M_{cr} = bending moment that causes cracking

f_c' = concrete compressive strength

f_{ps} = effective prestress in the strand

A_{ps} = prestressed steel area in tension wythe

A_w = cross sectional area of the concrete wythe

c = distance from panel centroid to compression face

The design recommendations given included specifications on adequate FRP to achieve composite action, and not over-reinforcing the concrete wythes.

2.1.3 2001-2010

Pessiki and Mlynarczyk (2003) performed a series of research projects on PCSWPs containing steel truss shear connectors. This project involved the evaluated composite behavior of PCSWP. By designing four full-scale 3-wythe panels of identical dimensions, Pessiki and Mlynarczyk derived an equation to determine the experimental moment of inertia shown in Eq. (2-16). Because this value is an experimental value, it was the actual moment of inertia of the partially composite panel. Pessiki and Mlynarczyk were able to evaluate the degree of composite action using Eq. (2-17), which calculated the percent composite action using the assumption that the relationship between non-composite and fully-composite panels is linear.

$$I_{exp} = \frac{5wL^4}{384\Delta E_c} \qquad (2\text{-}16)$$

$$\kappa = \frac{(I_{exp} - I_{nc})}{(I_c - I_{nc})} \qquad (2\text{-}17)$$

Where: I_{exp} = experimentally determined moment of inertia

w = uniformly distributed load per length

L = span length of test panel

Δ = midspan lateral deflection

E_c = modulus of elasticity of concrete

κ = factor to describe percent composite action of panel

I_c = moment of inertia of the fully-composite section

I_{nc} = moment of inertia of the non-composite section

The first full-scale specimen was a typical PCSWP. Shear forces were transferred between wythes via regions of solid concrete, steel shear connectors, and concrete-insulation interface bond. The other three specimens were constructed such that only one shear transfer mechanism was incorporated into each panel. By testing all four panels with a uniform lateral pressure and determining relative stiffnesses, it was found that the solid concrete regions provided the majority of the composite action in the wall panel. The recommendation of the researchers was that "solid concrete regions be proportioned to provide all of the required composite action in a precast sandwich wall panel." Though significant, this research fueled a need to create a more efficient shear connector and spurred research on full-scale panels that did not contain any solid concrete regions in the panel.

Lee and Pessiki (2008) performed testing involving the lateral load testing of three-wythe (three concrete wythes, two foam wythes) panels with steel truss shear connectors. They tested two panels, each with a different cross-section (See Figure 2-14). This research was performed to enhance the knowledge acquired as a result of Lee and Pessiki (2007), proving that five-wythe panels were more thermally efficient than their three-wythe counter parts. This motivated research to determine structural performance of different five-wythe configurations. The PCSWPs were tested by placing each specimen horizontally on top of an air bladder and placing reaction beam structures on each end to mimic pin-and-roller end conditions. Upon inflation of the bladder, the panel would experience a uniformly distributed loading condition. This uniformly distributed load was incrementally increased until failure. Load and deflection were measured for both panels and then compared. It was determined that Panel 2 was stiffer than Panel 1. Because of the abrupt failure noted, Lee and Pessiki made the recommendation that the design tensile strength should be reduced for five-wythe panels. They also noted that current codified design methods were acceptable for five-wythe sandwich panel design. The recommendation made to reduce the tensile strength is a result of Eq. 2-18.

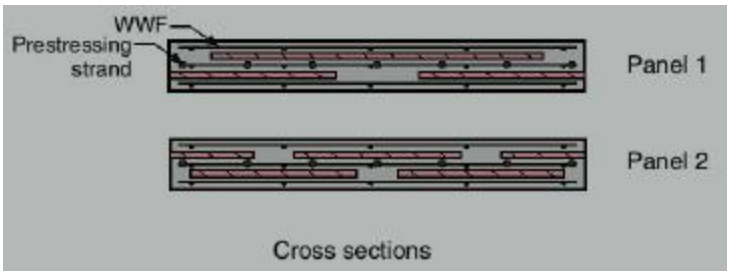

Figure 2-14 Cross sectional view of the two panels tested by Lee and Pessiki (2008)

$$\alpha\sqrt{f_c'} = \frac{Mc}{I} + f_{pe} \qquad (2\text{-}18)$$

Where: α = is a multiplier (typically = 7.5)

f_c' = compressive strength of concrete

M = the moment when cracking occurs

c = distance from the centroid to extreme tension fiber

f_{pe} = effective prestress of the panel

Lee and Pessiki observed a considerably reduced cracking moment. As a result of Eq. (2-18), they recommended that the value of α be equal to 3.7 rather than 7.5 for PCSWP design. Another aspect of this research incorporated the generation of design graphs to help designers determine the maximum transverse stresses for various end conditions. These graphs are shown in Figure 2-15, where each line is representative of a different type of panel. The graphs were interpreted by the number of strands or the initial prestress in the panel (psi). The upper graph is for center wythe stresses, while the lower schematic shows the outer wythe stresses.

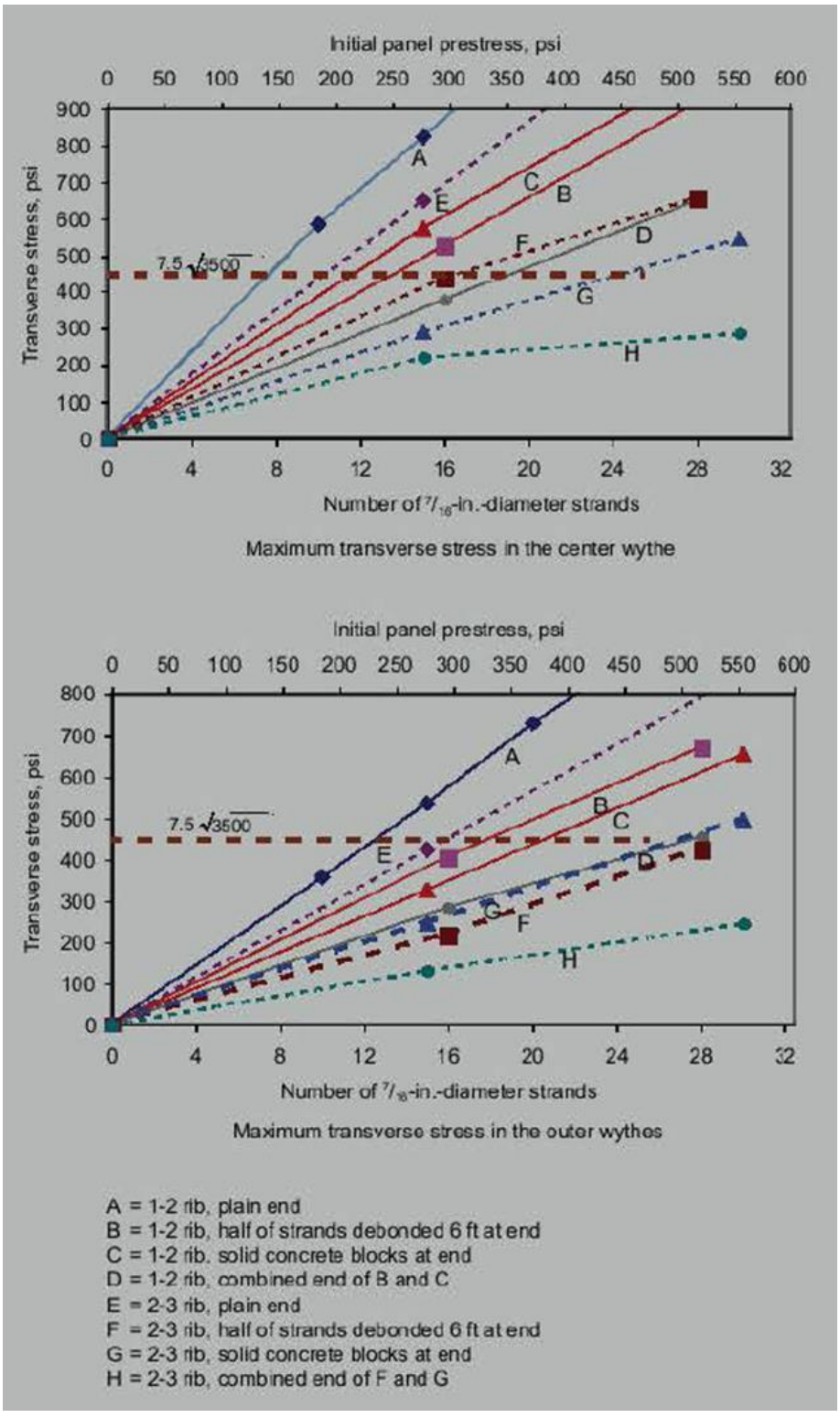

Figure 2-15 Maximum transverse stresses for various end conditions (Lee and Pessiki 2008)

The most relevant observations and recommendations of Lee and Pessiki's project included that

- early flexural cracking was observed for both panels (leading to the recommendation that design tensile strength be $3.7\sqrt{f_c'}$),
- the design for transverse bending stresses could be addressed by incorporating additional stiffness at either terminal of the panel (i.e. shear connector, debonded strands, or discontinuous concrete ribs),
- a correlation existed between the experimental results and FEM analysis, indicating that the FEM analysis could be used to predict cracking,
- design codes of the day proved sufficient for three-wythe panel design,
- a T-beam approach was recommended to predict flexural capacity, and
- transverse stresses could be checked using Figure 2-15.

Pantelides et al. (2008) sought to determine the adequacy of a new hybrid glass fiber-reinforced polymer (GFRP) composite shell steel connector in PCSWPs. This connector mimicked the design of a steel truss in geometry, but utilized FRP in the web in place of steel. This greatly reduced thermal bridging through the panel. Other FRP connectors were also used in the research. Specimens were created using the FRP shear connectors and were laterally loaded to determine the stiffness of the panels. It was determined that for the panels tested, composite action was achieved with the FRP shear connectors. Pantelides et al. developed a bilinear approximation to predict the deflection at yield:

$$\Delta_{my} = \frac{(0.5P_y)a}{24E_c I_{cr}}(3L^2 - 4a^2) \qquad (2\text{-}19)$$

Where: Δ_{my} = midspan deflection at yield

P_y = total applied load at yield

A = shear span

E_c = modulus of elasticity of the concrete

I_{cr} = moment of inertia of the fully-cracked section

L = clear span length

The elastic and plastic regions can be visually estimated from the results of their testing (Figure 2-16).

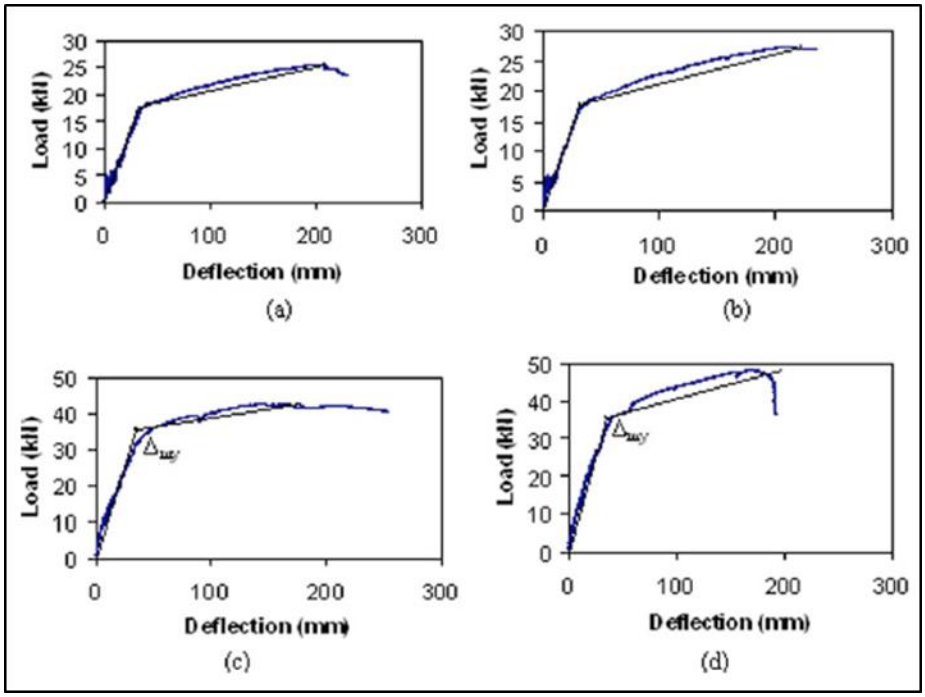

Figure 2-16 Lateral load vs mid-span deflection with analogy model: a) epoxy-cured GFRP single cage; b) urethane-cured GFRP single cage; c) epoxy-cured double cage; and d) urethane-cured double cage (Pantelides et al. 2008)

2.1.4 2011-Present

Naito et al. (2011) performed research on non-load bearing sandwich panel walls that is considered one of the most comprehensive studies done on PCSWPs. Naito et al. tested fifty-six full-scale specimens to failure using a variety of connectors including metallic, carbon fiber-reinforced polymer (CFRP), and GFRP shear connectors. The research covered both prestressed and regular reinforced concrete wythes, and both structural and non-structural scenarios were also considered. Wythe configurations had various symmetries and also asymmetries. Fully-composite, partially composite, and non-composite shear ties were tested. Three different insulation types were tested as well. For every configuration, the test was duplicated either two or three times depending on material availability, with 21 different configurations in total. The specimens were constructed off sight and transported to the testing facility. For this reason, concrete types varied significantly. Various pre-casting companies helped to

fabricate the specimens. Every specimen configuration was accompanied by an idiosyncratic schematic. Every specimen was tested by applying an iterative loading sequence across the unsupported length of the panel (see Figure 2-17). End conditions were considered pin-and-roller during the experimental procedure. In reality, the specimen was not fixed in the longitudinal direction, but was fixed laterally. This was the case to ensure any panel deformation inconsistencies, or slip, could be measured (See Figure 2-18). Equation (2-20) shows the calculation for rotation at the support.

$$\theta = tan^{-1}\left[\frac{2\Delta_{mid}}{L}\right] \qquad (2\text{-}20)$$

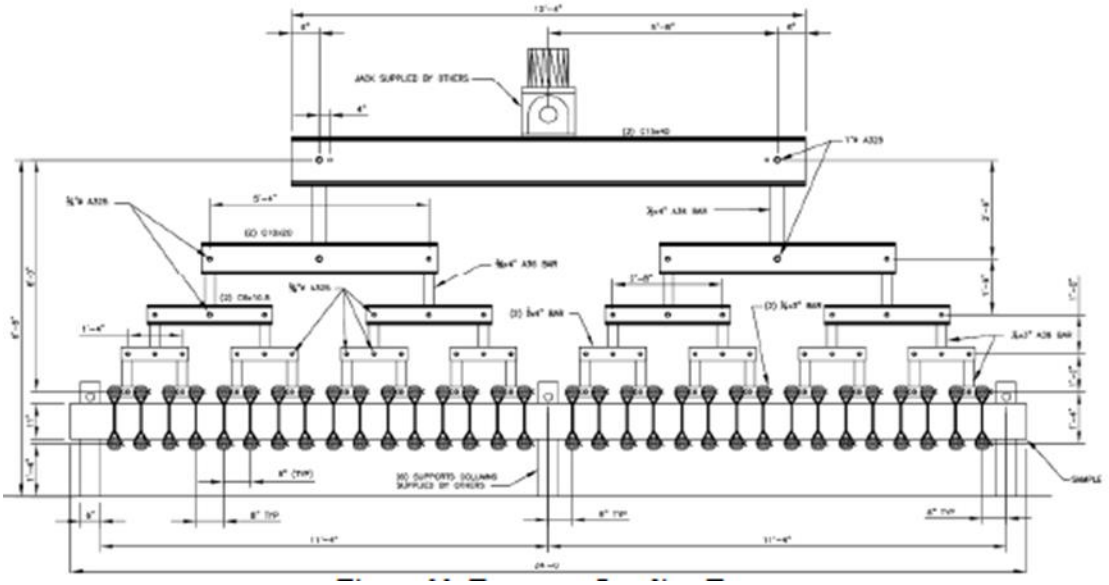

Figure 2-17 Loading pattern applying point loads across unsupported span of panel (Naito et al. 2011)

Figure 2-18 Photograph depicting the loading tree and end-slip measurement (Naito et al. 2011)

The load pattern was applied in order to simulate a uniformly distributed load. After loading each specimen to failure, plots were created displaying pressure vs. midspan displacement. Tabulated values of specimen name, age of concrete, max load, max pressure, corresponding displacement, east and west slip, boundary rotation, and measured moment capacity were also created for each specimen configuration. An example of specimen "PCS5" is included. Data from Figure 2-19 was also referenced by Bai and Davidson (Bai and Davidson 2015).

Specimen	Age at Test [days]	Max Load [lbs]	Max Pressure [psi]	Corresponding Displacement [in]	East Slip [in]	West Slip [in]	Rot. [deg]	Measured Moment Capacity [k-in]
PCS5-A	101	17770	4.628	4.765	0.527	0.604	4.541	266.55
PCS5-B	112	19910	5.185	5.118	0.500	0.562	4.875	298.65
PCS5-C	113	18252	4.753	5.536	0.633	0.637	5.272	273.78
	Average	18644	4.86	5.14	0.55	0.60	4.90	279.7

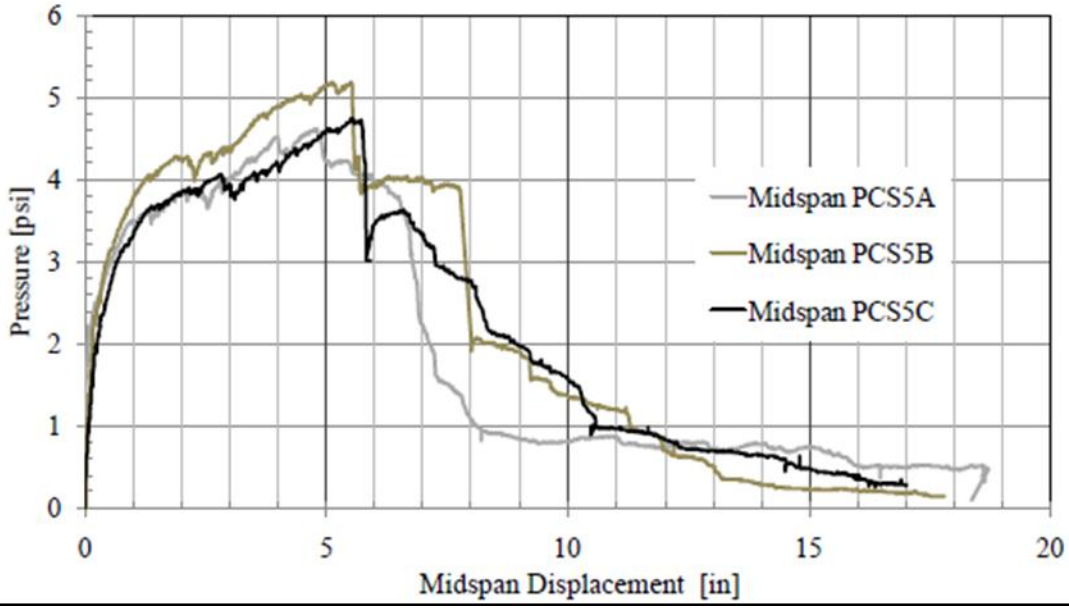

Figure 2-19 Data collected for Naito et al.'s testing of Connector B (Naito et al. 2011)

Frankl et al. (2011) researched behavior of PCSWP reinforced with CFRP shear grid connectors. This research was modeled after research performed by Naito et al. in the previous section, except that loading was performed vertically. Full-scale panels were tested by applying two equidistant point loads to generate a constant moment region across the midspan of the panel (See Figure 2-20). Similar plots were derived and strain profiles were generated. Frankl et al. included in their report several of the observed failure modes of the CFRP shear grid. The researchers implemented the following equation, Eq. (2-21), from Bischoff and Scanlon to determine the effective moment of inertia.

$$I_{eff} = \frac{I_{cr}}{1 - \left(\frac{M_{cr}}{M_a}\right)^2 \left[1 - \frac{I_{cr}}{I_g}\right]} \leq I_g \qquad (2\text{-}21)$$

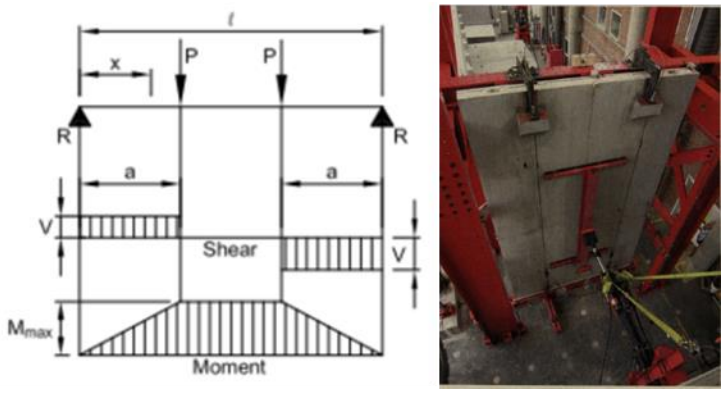

Figure 2-20 Shear and Moment Diagram from PCI Handbook (left) and testing of vertical panel (right) (Seeber et al. 2004; Frankl et al. 2011)

Another state-of-the-art paper was published by Losch et al. in the March 2011 PCI Journal regarding PCSWPs. Like many of the previous "State-of-the-Art" papers published by the PCI, this article highlighted many of the iconic PCSWP buildings constructed in the past decade. This article served the purpose of updating much of the current design procedures to include recommendations for FRP shear connectors and other pertinent information and findings of recent research. It goes into extensive detail about wythe thickness and prestressing strand sizing, wythe connectors, panel width thickness and span, bowing, flexural design, load bearing design, shear wall considerations, external connections, detailing considerations, thermal performance, manufacturing processes, product tolerances, transportation, erection and inspection of PCSWPs. This is the most recent document published by PCI regarding PCSWP design for engineers, though it is nearly identical to the standards presented in the PCI Handbook published in 2004 (Seeber et al. 2004). A few changes included consideration of fully-composite as well as non-composite shear connectors and there is also a lot more detail on panel connections.

Bunn (2011) published data on push-off specimens rather than full-scale specimens. The data collected considered vertical and transverse alignment of the connectors; foam to concrete interface bond variations; panels without shear connectors; panels with missing shear connectors; variations in panel dimensions, grid spacing, wythe

thickness, and foam type. For every specimen tested, plots were generated displaying shear flow versus deflection. This was done to compare specimen and connectors stiffness. The design approach taken by Bunn, is to predict a Nominal shear flow capacity based on four variables and one constant. The equation is shown in Eq. 2-22.

$$q_n = \gamma_{type} * \gamma_{thickness} * \gamma_{spacing} * \gamma_{orientation} * q_{baseline} \qquad (2\text{-}22)$$

Where: q_n = Nominal shear flow capacity of grid, lb/in

γ_{type} = factor for insulation type (either EPS or XPS)

$\gamma_{thickness}$ = factor for insulation thickness

$\gamma_{spacing}$ = factor for grid spacing

$\gamma_{orientation}$ = factor for grid orientation (either vertical or transverse)

$q_{baseline}$ = constant of 100 lb/in (based on the shear flow capacity of the grid)

Table 2-1 Table to determine factors for Equation (2-22) (Bunn 2011)

	γ_{Type}	Insulation Thickness (in.)	$\gamma_{thickness}$	Spacing (in.)	$\gamma_{spacing}$	Orientation	$\gamma_{orientaion}$	$q_{baseline}$
EPS	1.77	2	1.53	12	0.95	Vertical	1	100
		4	1.34	18	1.12			
		6	1.11	24	1.18	Transverse	0.8	
		8	1.11	36	1.56			
	γ_{Type}	Insulation Thickness (in.)	$\gamma_{thickness}$	Spacing (in.)	$\gamma_{spacing}$	Orientation	$\gamma_{orientaion}$	$q_{baseline}$
XPS	1.28	2	1.27	12	1.34	Vertical	1	100
				18	1.19			
		4	1.18	24	1.05	Transverse	0.8	
				36	0.99			

Equation (2-22) takes a relatively straight forward approach but was proven accurate when predicting the experimentally tested specimens. The equation was optimized using a spreadsheet and derived from the test results collected from the experimental program.

Woltman, Tomlinson, and Fam (2013) investigated the performance of non-composite GFRP shear connectors. The connector tested was simply a GFRP dowel, which is deformed on either end to achieve sufficient embedment in the outer concrete wythes in a push-off specimen (Figure 2-21). The setup allowed the concrete to be poured monolithically.

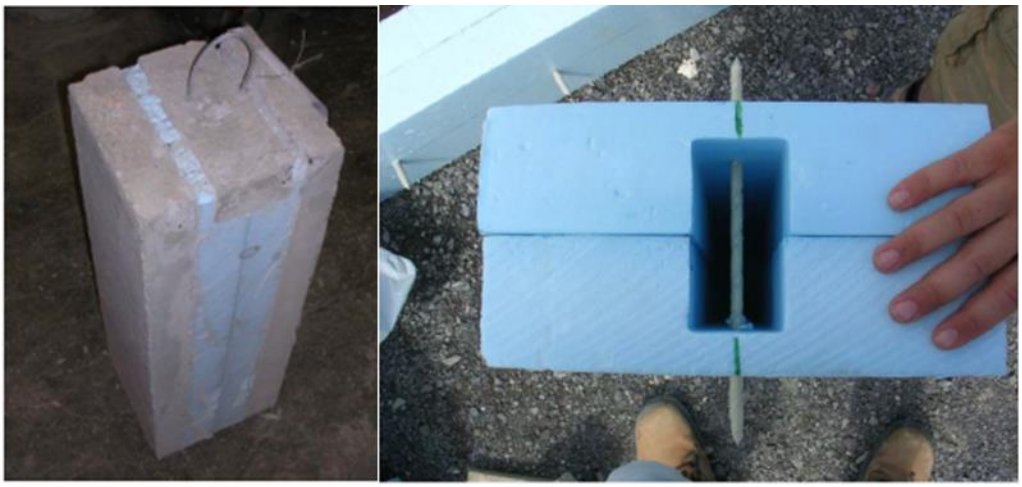

Figure 2-21 Push-off Specimen cured (left) and before concrete poured (right) (Woltman et al. 2013)

Push-off specimens were tested to failure, load and deflection were measured and plotted to compare stiffness. Woltman et al. makes significant observations regarding the modes of failure. The specimens experienced both strong and weak axis failures of the connector, cracking of the concrete embedment, as well as dowel action of the GFRP dowel (See Figure 2-22).

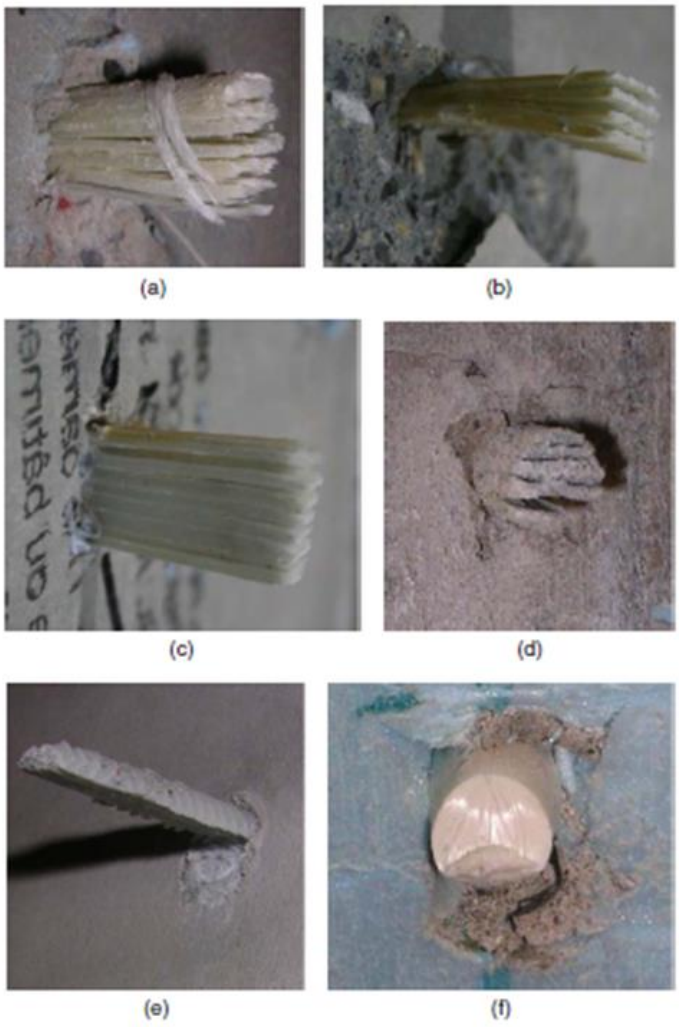

Figure 2-22 Observed failure modes in SWP: a) weak axis and b) strong axis fracture, c) dowel action, d) concrete cracking, e) polymer brittle fracture (Woltman et al. 2013)

Woltman et al. (2013) were able to create an analytical model that explained the behavior of the FRP shear connectors and also correlated the dowel shear strength based on the thickness of the insulation, observing that shear strength is reduced as thickness increases. It was determined that if flexural failure governs, then Eq. (2-23) ought to be used. If shear failure governs, however, then Eq. (2-24) would be appropriate.

$$M = \frac{2If_u}{D} \quad (2\text{-}23)$$

$$\tau_{mas} = k\frac{V}{A} \quad (2\text{-}24)$$

Where: M = governing moment of the connector

I = cross-sectional

f_u = flexural capacity of the GFRP connector

D = the diameter of the GFRP connector

τ_{max} = governing shear stress of the connector

k = shape factor (1.33 for round connectors)

A = cross-sectional area of the connector

V = $2M/X$

- M = governing moment of the connector
- X = thickness of the foam wythe

It was determined that for the non-composite shear connectors the load displacement curves have an initial elastic peak response due to the added shear strength of the foam-concrete interface bond. After this bond deteriorates, the connectors begin to plasticize and form longitudinal cracks. A rapid and significant deformation takes place at this instant. Because of this plasticization, the response continues, but at a reduced stiffness. Once ultimate capacity is reached, the load gradually decreases as connectors fail one by one. As previously stated, the connectors fail mostly by delamination or dowel action.

Bai and Davidson (2015) analyzed partially composite, foam-insulated, concrete sandwich structures to derive mathematically the correlation between the degree of composite action (for partially composite panels) and the combined stiffness of the shear connectors within the panel. They did this to predict bearing and flexural behavior of PCSWPs. Bai and Davidson derived the non-trivial mathematical solution to predict deflection, bending moment, axial force, slip between wythes, and middle layer shear stress. These equations are as follows:

Panel Deflection:

$$y_1 = \frac{5}{384}\frac{qbl^4}{E_w I_{total}}\left[1 - \frac{24}{5}\left(\frac{x}{l}\right)^2 + \frac{16}{5}\left(\frac{x}{l}\right)^4\right]\ldots$$
$$+\frac{1}{16}\frac{qbl^4}{E_w I_{total}}\left(\frac{\alpha}{\beta}\right)^2\left(\frac{2\beta}{\chi l}\right)^2\left[\left(\frac{2\beta}{\chi l}\right)^2\left(\frac{\cos h\left(\frac{\chi}{\beta}\right)\chi}{\cos h\left(\frac{\chi l}{2\beta}\right)} - 1\right) + \frac{1}{2}\left(1 - \left(\frac{2\chi}{l}\right)^2\right)\right] \quad (2\text{-}25)$$

$$y_2 = \pm\frac{q}{4k} \quad (2\text{-}26)$$

$$y_3 = \pm\frac{\sqrt{2}}{2}\frac{qbl}{E_w I_{toatl}}\frac{l_0}{\beta^2}\frac{1}{\Psi}\left(\phi_1^0\phi_1 + \phi_3^0\phi_3\right) \quad (2\text{-}27)$$

$$\begin{cases} y^{ex} = |y_1| + |y_2| + |y_3| \\ y^{in} = |y_1| - |y_2| - |y_3| \end{cases} \quad (2\text{-}28)$$

Bending Moment:

$$M1{=}18qbl2\alpha 22\beta\chi l21{-}cosh\chi\beta\chi cosh\chi l2\beta{+}12\beta 21{-}2\chi l2 \quad (2\text{-}29)$$

$$M2{=}0 \quad (2\text{-}30)$$

$$M3{=}\,{-}24abl2l0l1\psi\ \phi 30\phi 1{+}\phi 10\phi 3 \quad (2\text{-}31)$$

$$Mex{=}M1{-}M3Mex{=}M1{+}M3 \quad (2\text{-}32)$$

Axial Force:

$$N_1 = \frac{1}{8}\frac{qbl^2}{r}\ \alpha^2\left[-\left(\frac{2\beta}{\chi l}\right)^2\left(1 - \frac{\cosh\left(\frac{\chi}{\beta}\right)\chi}{\cosh\left(\frac{\chi l}{2\beta}\right)}\right) + \frac{1}{2}\left(1 - \left(\frac{2\chi}{l}\right)^2\right)\right] \quad (2\text{-}33)$$

$$N_2 = 0 \quad (2\text{-}34)$$

$$N_3 = 0 \quad (2\text{-}35)$$

$$\begin{cases} N^{ex} = -|N_1| \\ N^{ex} = |N_1| \end{cases} \quad (2\text{-}36)$$

Slip Between Wythes:

$$\phi = \frac{1}{4}\frac{qrbl^3}{E_w I_{total}}\left(\frac{2\beta}{\chi l}\right)^2 \frac{1}{\beta^2}\left[\frac{2\beta}{\chi l}\left(\frac{\sinh\left(\frac{\chi}{\beta}\right)\chi}{\cosh\left(\frac{\chi l}{2\beta}\right)}\right) - \frac{2\chi}{l}\right] \quad (2\text{-}37)$$

Middle Layer Shear Stress:

$$\tau = \frac{1}{4}\frac{ql}{r}\alpha^2\left[\frac{2\beta}{\chi l}\left(\frac{\sinh\left(\frac{\chi}{\beta}\right)\chi}{\cosh\left(\frac{\chi l}{2\beta}\right)}\right) - \frac{2\chi}{l}\right] \quad (2\text{-}38)$$

Where: y_1, y_2, *and* y_3 = deflection cases used for super-position

M_1, M_2, *and* M_3 = moment cases used for super-position

N_1, N_2, *and* N_3 = axial force cases used for super-position

y^{ex} = external deflection

y^{in} = internal deflection

M^{ex} = external bending moment

M^{in} = internal bending moment

N^{ex} = external axial force

N^{in} = internal axial force

Φ = slip between wythes

τ = shear stress in the middle layer

q = lateral pressure applied to the face of the wythe

k = vertical compressive stiffness of middle wythe

b = wythe width

d = thickness of wythe

l = span length

$l_0 = \sqrt[4]{E_w \cdot \frac{i}{2k} \cdot b}$

$i = 2 \cdot I_{sgl}$

$I_{sgl} = \frac{bd^3}{12}$ = moment of inertia of each wythe

E_w = moduli of elasticity of wythes

I_{Total} = $2I_{sgl} + 2r^2A$ = moment of inertia of the whole cross-section

A = cross-sectional area of wythe

χ = $\sqrt{\frac{2Kb}{E_w A}}$

K = shear stiffness of the middle layer

α = $\sqrt{\frac{2r^2A}{I_{total}}}$

β = $\sqrt{1-\alpha^2}$

k = vertical compressive stiffness of middle layer

Ψ = $\phi_1^0(\phi_2^0 + \phi_4^0) - \phi_3^0(\phi_2^0 + \phi_4^0)$

$\phi_1{}^0$ = $\cos\lambda \cdot \cosh\lambda$

$\phi_2{}^0$ = $\cos\lambda \cdot \sinh\lambda$

$\phi_3{}^0$ = $\sin\lambda \cdot \sinh\lambda$

$\phi_4{}^0$ = $\sin\lambda \cdot \cosh\lambda$

$\lambda = \frac{\sqrt{2}}{4}\left(\frac{l}{l_0}\right)$

ϕ_1 = $\cos\varepsilon \cdot \cosh\varepsilon$

ϕ_3 = $\sin\varepsilon \cdot \sinh\varepsilon$

r = distance from neutral axis of wythe to the overall neutral axis

Predicted panel behavior was then compared to observed behavior from Naito's 2011 research (Naito et al. 2011), where most predictions were relatively close, though some were significantly inaccurate. Unfortunately, these equations are too cumbersome for most engineers.

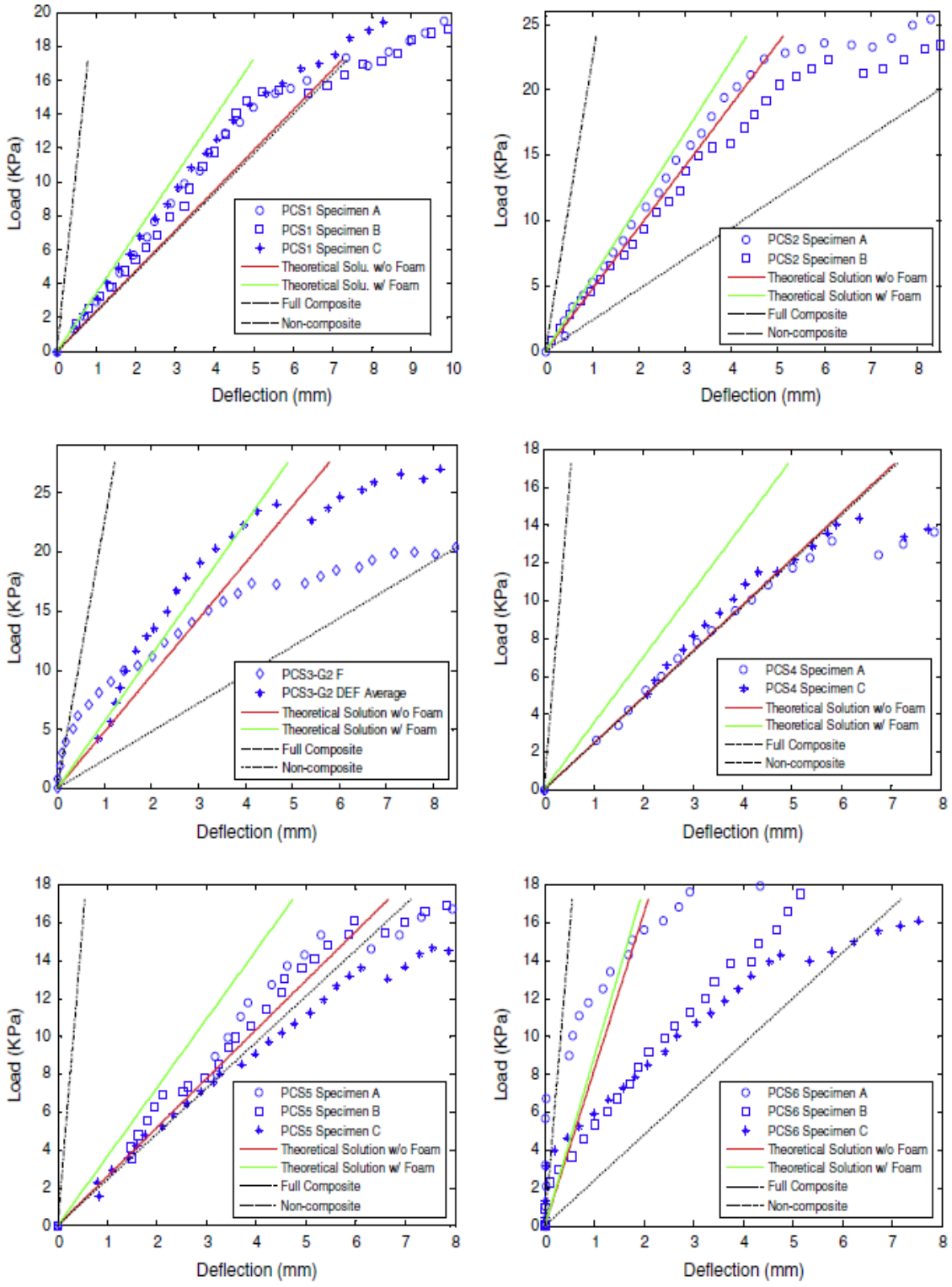

Figure 2-23 Naito et al.'s data (2011) vs Bai and Davidson's predictions (Bai and Davidson 2015)

2.2 Composite Action

Composite action is a principle that describes the degree to which two or more independent bodies cooperate to accommodate a specified loading scenario. The principle of composite action is used to design composite beams (beams which are made up of multiple materials) and reinforced concrete, but more applicable to this research, it is also used to design sandwich panel walls. Sandwich panel walls can be designed as fully-composite, partially composite, or non-composite. Composite action occurs when there is a shear transfer mechanism which transfers load from one element to another. Essentially a shear transfer mechanism creates a point of fixity or partial fixity between two interfaces.

From the history of PCSWPs, it is apparent that the creation of the concrete sandwich panel wall was intended entirely for thermal purposes. The structural capacity of these elements was not fully realized for many more years. Designing PCSWPs to be 100% composite is still a major challenge today. It is currently unknown how to design for partial composite action.

2.3 Thermal Efficiency

Thermal efficiency has been the main goal of PCSWPs since their inception. However, previous research has shown that there is room for improvement. The goal is to achieve as much thermal resistance as possible to prevent heat transfer from one side of the panel to the other. It is clear that the most efficient system currently achievable would be to have no steel penetrate the insulating layer, and eliminate as much steel as possible throughout the panel. There has been much research on different materials to use as shear connectors, the most successful of which are FRP based materials.

The most attractive characteristic for constructing PCSWPs are that they are an environmentally friendly, thermally efficient, and cost effective solution as a building envelope. Primarily, they serve as a thermally resistant building envelope. By improving their thermal performance, the desire to integrate these elements into all buildings increases. Though there are already significant economic incentives for taking advantage of the structural capacity of PCSWPs, they need to be thermally exceptional to optimize their benefits and make PCSWPs more marketable.

2.4 FRP Shear Transfer Mechanism

Shear transfer mechanisms, also known as shear connectors, are elements that tie the concrete wythes together. This fixity prevents independent association of structural elements. If the elements are fully-composite, this forced interaction requires equivalent load distribution and strain compatibility. As discussed in the history portion of this report, these connectors have varied greatly from simple steel pins to FRP trusses. Compared to steel, GFRP has a higher tensile strength while being 75% lighter. It is both electrically and thermally non-conductive. There are many different ways to form, or mold, GFRP. It can be extruded, injected, or woven. The different manufacturing processes create different structural properties.

2.4.1 Mold Injected GFRP

Mold injected GFRP becomes very brittle due to the random alignment of fibers within the component. There are many advantages to mold injecting GFRP. It is extremely cost effective when compared to other processes. Molding is a very fast process when compared to extruding or weaving. The constraints on shape are almost nonexistent.

2.4.2 Extruded GFRP

When GFRP is extruded, all the fibers are aligned in the same direction and essentially "cast" in the polymer. This polymer can be many different things but is usually epoxy based. When the fibers are all aligned, the component becomes ductile because all of the fibers are being loaded in the same direction. Fiber alignment can be optimized to accommodate many different loading scenarios as long as the loading scenario is known previous to design. When GFRP is extruded, the component develops a strong and weak axis. If the component is loaded parallel to the alignment of the strands, it is extremely strong. If the component is loaded perpendicular to the alignment of the strands, it is less-strong. The extrusion process is difficult and time consuming causing individual component costs to rise dramatically. The shape of the component with extruded GFRP simply requires a homogenous cross-section perpendicular to the fiber alignment. After the component is cast in polymer, additional machining may take place to create the desired final product. For the purpose of creating a shear connector, machining is performed to create the necessary deformations to embed the connector into the concrete.

2.4.3 Weaved GFRP

The last common manufacturing process is weaving. To weave GFRP, you must align the fibers in the desired pattern. This is done with either a machine, or often by hand. The fibers are frequently situated loosely, if the fibers were stretched tightly, the desired shape may become unattainable. After the fibers are placed in the desired configuration, the polymer is poured around the fibers and allowed to cure. This process is advantageous, especially when the desired outcome is dependent on fiber alignment, and that alignment is not continually parallel throughout the component. For the application of this project to PCSWPs, the most common application of weaving GFRP results in a truss like configuration. This is because elements within the component are designed to experience different forces (compression and tension) at different times. This requires the fibers to be aligned, but in various directions. Weaving is time consuming, and therefore expensive. Another downside to this procedure is that components are not going to be identical every time. The standard deviation of the product is very large.

2.5 Design Methods

As noted in Section 2.1, the design methods for PCSWPs have varied greatly over time. As with any building element, the longer it has been in use, the greater the understanding of the system becomes. A history of the design of PCSWPs was covered in Section 2.1. In most studies presented in that section, the number of shear connectors was never addressed. There are three methods that address this issue. These are the principles of mechanics, the ACI simplified method, and the PCI method.

2.5.1 Principles of Mechanics

Using the principles of mechanics, the analogous shear stress, τ, can be obtained for any given load. By applying the appropriate load factor, the design shear force can be determined. This force is calculated at the concrete-foam interface, where the force is at an associated maximum (Figure 2-24).

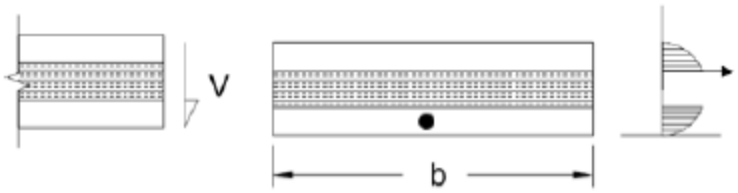

Figure 2-24 Evaluation of shear by principles of mechanics (Bunn 2011)

$$\tau = \frac{V_{max} Q_t}{I_{total} b} \quad (2\text{-}39)$$

$$q_{req} = \frac{V_{max} Q_t}{I_{total}} \quad (2\text{-}40)$$

Where: τ = maximum shear stress to be transferred

V_{max} = maximum shear force due to the applied loading

Q_t = first moment of area above the concrete-foam interface

I_{total} = cross-sectional moment of inertia of the entire panel

b = width of the panel cross-section

q_{req} = maximum applied shear flow

After the required shear flow, q_{req}, is obtained, calculating the number of required shear connectors equals:

$$N_{req} \geq \frac{q_{req}}{q_{connector}} \quad (2\text{-}41)$$

Where: N_{req} = number of connectors required at a certain cross-section

q_{req} = from Eq. (2-40)

$q_{connector}$ = shear flow capacity of the connector

2.5.2 ACI Simplified Method

By ACI 318 (2014), shear stress, τ, is the maximum shear force acting on the panel. The shear stress acting at the concrete-foam interface is based on b*d, or the full effective cross-section. Because of this, shear flow is calculated as:

$$q_{req} = \frac{V_{max}}{d} \qquad (2\text{-}42)$$

Where: d = distance between resultant tension and compression forces (Figure 2-25)

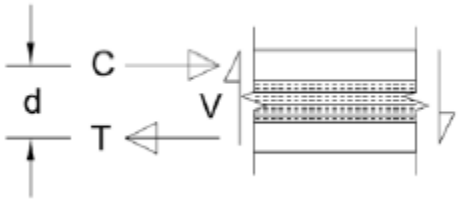

Figure 2-25 Definition of distance, d, from Eq. (2-42) (Bunn 2011)

By substituting the required shear flow associated with Eq. (2-42) into Eq. (2-41), one can determine the required number of shear connectors at any given panel cross-section.

2.5.3 PCI Method

The third method, requires that the full capacity of the panel be used when calculating the associated composite action. The shear stress, τ, is calculated at the maximum moment region (Seeber et al. 2004). It is allowed to use the lesser of the tension, T_{max}, or compression, C_{max}, forces when calculating the shear stress at the maximum moment region. Another assumption made, is that due to composite action, the entire depth of the exterior wythe is acting in compression. The required shear flow capacity, q_{req}, can be computed as follows:

$$V_{req} = \min \begin{cases} T_{max} \\ C_{max} \end{cases} \quad (2\text{-}43)$$

$$T_{max} = A_{ps} f_{ps} + A_s f_y \quad (2\text{-}44)$$

$$C_{max} = 0.85 f_c' b t_c \quad (2\text{-}45)$$

$$q_{req} = \frac{V_{req}}{d_L} \quad (2\text{-}46)$$

Where: A_{ps} = area of prestressing steel in tension wythe

f_{ps} = stress in prestressing strand

A_s = area of steel in tension wythe (excluding prestressing)

f = yield stress of steel in tension wythe (excluding prestressing)

f_c' = concrete compressive strength

b = width of cross-section

t_c = thickness of compression wythe

d_L = length of panel from M_{max} to the nearest support

Just as in the ACI method, one can determine the required number of connectors by substituting Eq. (2-46) into Eq. (2-41).

3 EXPERIMENTAL PROGRAM

3.1 Introduction

The experimental portion of this research was to test several different proprietary and non-proprietary FRP shear connector systems by fabricating and testing 41 small scale "push-off" specimens to apply direct shear to the connectors, as well as test eight full-scale sandwich panel walls. The purpose of this testing was to for an experimental basis to develop a general methodology for calculating partial composite action elastic behavior and capacity. This chapter of this report contains an outline of the experimental program including specimen configuration and testing setup.

3.2 Push-off Tests

3.2.1 Specimen Configurations and Test Matrix

A test matrix was created to provide information on each of the specimens that needed to be constructed (Table 3-1). This was based on three variables: 1) connector type, 2) foam type, and 3) concrete/foam interface bond. This study included 5 different connectors. For convenience of data presentation, each connector was assigned a letter descriptor and are as follows: Nu-Tie connector (Connector A), Thermomass CC Connector (Connector B), Thermomass X Connector (Connector C), HK Composite Connector (Connector D), and Delta Tie (Connector E). The blank spaces in the table below exist only because Thermomass (Connector B and C) does not supply expanded polystyrene foam with their connectors.

Table 3-1 Test Matrix for Five-Wythe Push-Off Specimens

TEST MATRIX FOR FIVE-WYTHE PUSH-OFF SPECIMENS							
			A	**B**	**C**	**D**	**E**
Foam Type	**Wythe**	**Bond**					
Expanded Polystyrene (EPS)	3"	B	AEPS3B	-*	-*	DEPS3B	EEPS3B
		UB	AEPS3UB	-*	-*	DEPS3UB	EEPS3UB
	4"	B	AEPS4B	-*	-*	DEPS4B	EEPS4B
		UB	AEPS4UB	-*	-*	DEPS4UB	EEPS4UB
Extruded Polystyrene (XPS)	3"	B	AXPS3B	BXPS3B	CXPS3B	DXPS3B	EEPS3B
		UB	AXPS3UB	BXPS3UB	CXPS3UB	DXPS3UB	EEPS3UB
	4"	B	AXPS4B	BXPS4B	CXPS4B	DXPS4B	EEPS4B
		UB	AXPS4UB	BXPS4UB	CXPS4UB	DXPS4UB	EEPS4UB
Polyisocyanurate (ISO)	3"	B	AISO3B	BISO3B	CISO3B	DISO3B	EEPS3B
		UB	AISO3UB	BISO3UB	CISO3UB	DISO3UB	EEPS3UB
	4"	B	AISO4B	BISO4B	CISO4B	DISO4B	EEPS4B
		UB	AISO4UB	BISO4UB	CISO4UB	DISO4UB	EEPS4UB
*Fabricator does not use EPS with their system							

All push-off test specimens were created with three concrete wythes that were each separated by a wythe of foam insulation, and were either 3-3-6-3-3 panels (meaning that wythe thicknesses were 3 inches for all wythes except for a 6 inch center wythe) or 4-4-8-4-4 panels (where wythe thicknesses were all 4 inches except for an 8 inch center wythe), with only connector spacing number changing per manufacturer recommendations. Each specimen was 3 feet wide by 4 feet tall and contained a variety of connectors and configurations from the connector companies (Figure 3-1). Foam types that were used include: Extruded Polystyrene (XPS), Polyisocyanurate (ISO), and Expanded Polystyrene (EPS). The concrete was reinforced concentrically with No. 3 grade 60 rebar spaced every 6 inches (exact spacing of rebar was contingent upon the accommodation of connectors).

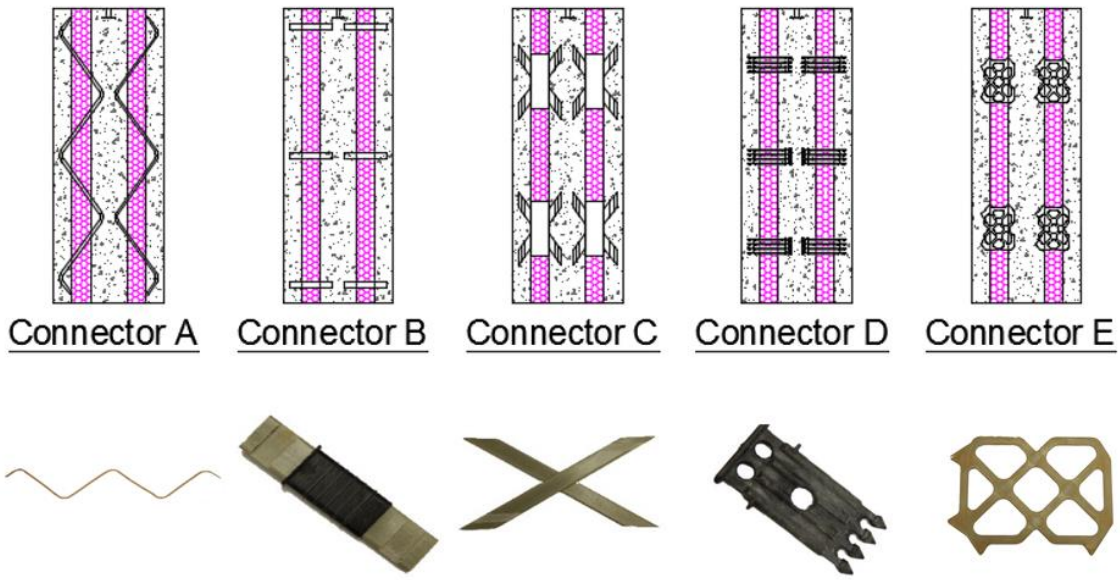

Figure 3-1 Push-off Specimen diagram and photographs of each connector

Each connector group tested was manufactured using Glass Fiber Reinforced Polymer (GFRP). However, not all companies used the same manufacturing process. Each Connector is discussed in detail in the following section.

3.2.1.1 Connector A (Nu-Tie)

Connector A (Figure 3-2) is a pultruded GFRP truss (Section 2.4.3). For the push-off specimens in this study, connectors were designed to occupy a 48" section and varied in width depending on the thickness of the insulating wythe. Four connectors were evenly spaced throughout each specimen, two in each wythe. Spacing of six inches off of center was recommended by the manufacturer and was used as the spacing in this report. A detailed diagram of the push-off specimen is shown in Figure 3-3.

Figure 3-2 Connector A close-up

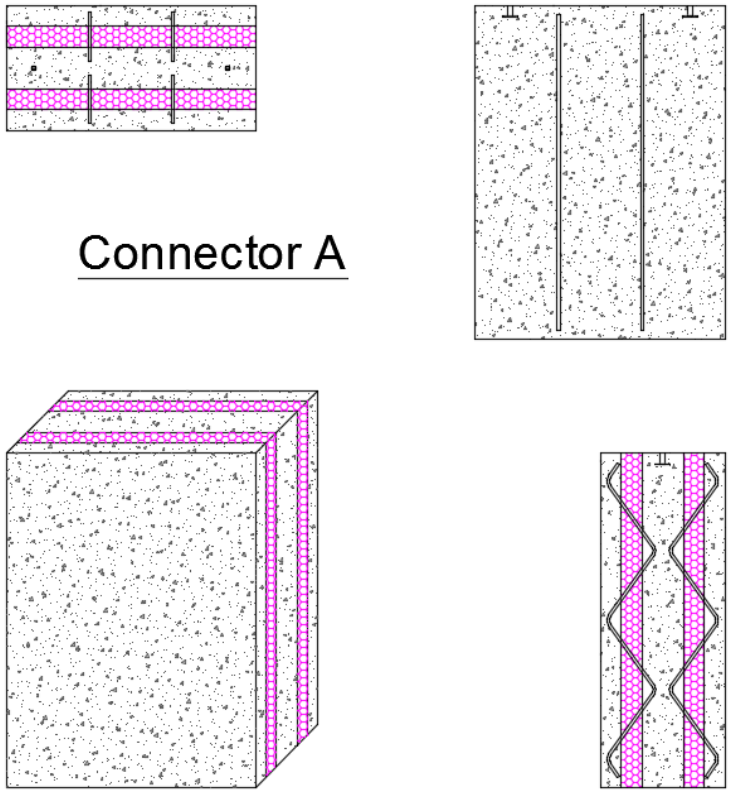

Figure 3-3 Detailed diagram of the push-off specimen design for connector A

3.2.1.2 Connector B (Thermomass CC-connector)

Connector B (Figure 3-4) is an extruded GFRP connector and is considered a structurally-composite connector (Section 2.4.2). The main structural component is an extruded GFRP flat bar, which has machined ends such that the specimen is able to enable interlock with the concrete for enhanced bond. The connector is designed

for a 2 in. embedment length in the concrete wythes. Twelve connectors were used in each specimen, six in each wythe. Two rows of three were spaced nine inches from center leaving nine inches of cover to the outside edge of the panel (Figure 3-5).

Figure 3-4 Connector B close-up

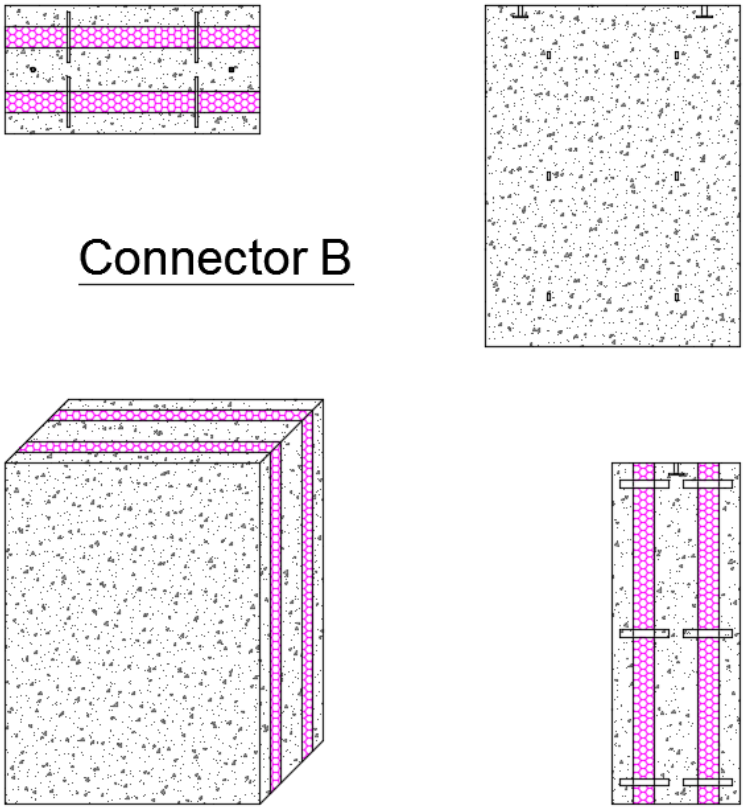

Figure 3-5 Detailed diagram for push-off specimen for connector B

3.2.1.3 Connector C (Thermomass X-connector)

Also an extruded GFRP product, Connector C (Figure 3-6) uses extruded GFRP bars, oriented in an X shape. Connector C is actually the combination of two GFRP flat bars, similar to Connector B, embedded into the concrete. The combination of the two independent connectors that form an "X," will be considered one connector. As with Connector B, this GFRP connector required post extrusion machining to enhance mechanical interlock with the concrete. Eight connectors were placed in each specimen, with four specimens inserted in each wythe. There were two rows of two connectors, each spaced nine inches from center (See Figure 3-7).

Figure 3-6 Connector C close-up

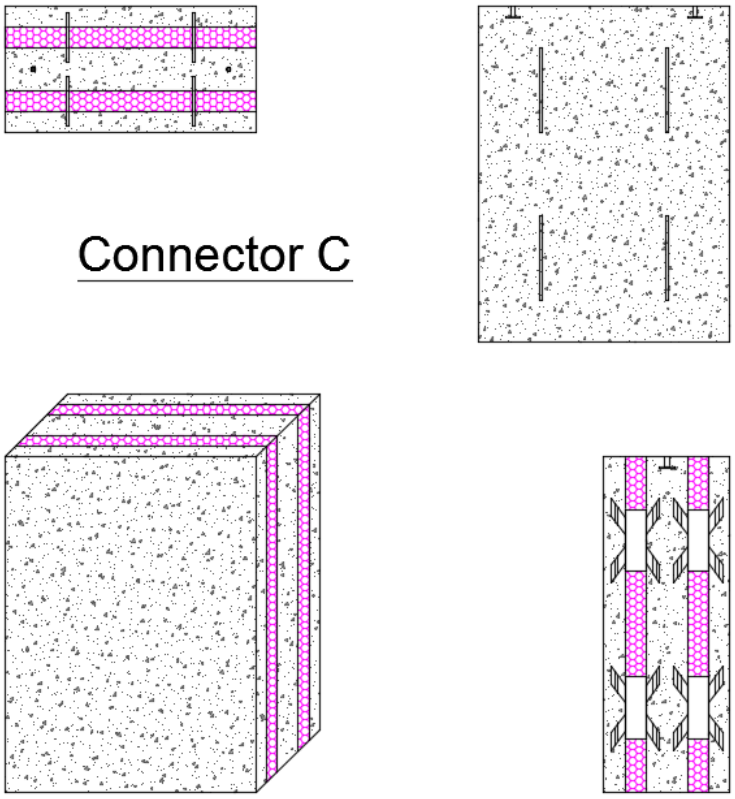

Figure 3-7 Detailed diagram for push-off specimen for connector C

3.2.1.4 Connector D (HK Composite Connector)

Connector D (Figure 3-8) is a mold injected GFRP product (Section 2.4.1) that has randomly aligned and distributed glass fibers in a thermoplastic matrix. Connector D is designed for 1.5 in. embedment into a concrete wythe and is 3 inches wide and ½ inch thick. Connector D has an asymmetrical design developed for construction efficiency. Connector D is a mold injected product with randomly distributed glass fibers, greatly reducing the cost of each connector and increasing production rate. For this report, twelve connectors were used in each specimen. Connectors were spaced at two rows of three, each spaced nine inches from center, per the manufacturer's recommendation (Figure 3-9).

Figure 3-8 Connector D close-up

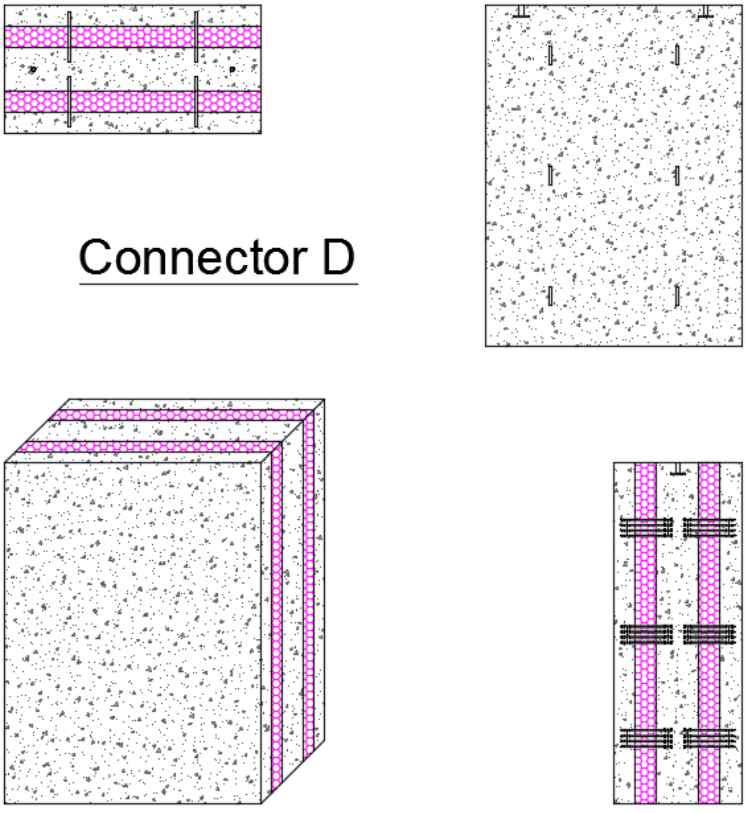

Figure 3-9 Detailed diagram for push-off specimen for connector D

3.2.1.5 Connector E (Delta Tie Connector)

Connector E (Figure 3-10) is a GFRP shear connector. This connector is designed like a small truss. It is 5 in. wide, 7 in. long, and 1/8 in. thick. Four connectors were used in each wythe, eight connectors per specimen. Each row of two connectors was spaced nine inches off center (Figure 3-11).

Figure 3-10 Connector E close-up

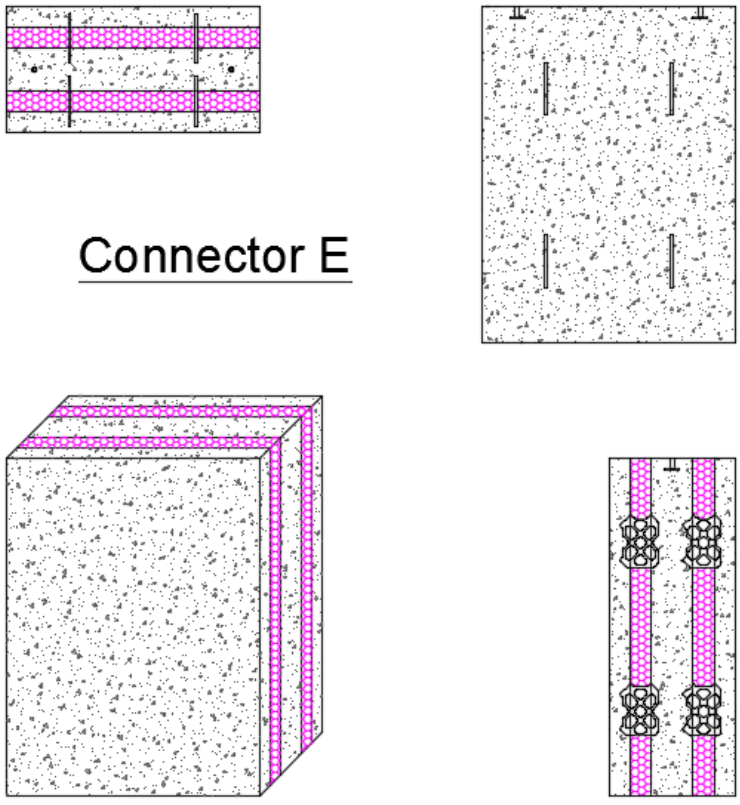

Figure 3-11 Detailed diagram for push-off specimen for connector E

3.2.2 Construction of Push-off Specimen

Specimens were cast horizontally, one layer at a time. Forms were built out of HDO (high-density overlay) plywood manufactured by Plum Creek Company. The first wythe would be cast immediately followed by the insertion and vibration of the connectors and foam. The forms would be stripped and taller forms constructed in their place. Once taller forms were in place, the center wythe would be poured and immediately followed by the insertion and vibration of the connectors and foam. Forms would be stripped and the tallest forms would be constructed, after which the final concrete wythe would be poured. The unbonded specimens used a plastic sheet between the foam and concrete surfaces to eliminate the bond, duct tape was used to ensure no concrete leaked where connectors penetrated the plastic (Figure 3-12). Once concrete strength was achieved (greater than 4000 psi), the specimens were prepared for testing.

Figure 3-12 Seaming of the bond inhibitor using duct tape

For Connectors B, C, and D, preparation involved placement of the bond inhibitor for unbonded specimens and insertion of connectors for all specimens. The foam used for Connectors B, C, and D was provided by the manufacturer. The foam came pre-cut to proper dimensions and included apertures for connector insertion. Connectors are shown inserted into foam in Figure 3-13.

Figure 3-13 Left: Connector B, Middle: Connector C, Right: Connector D

For Connector E, foam was ordered independently of the connectors. Therefore, preparation of the foam required sizing the foam to correct dimension, creating apertures for connectors, and providing the bond inhibitor where applicable. The cutting was done with a hot knife, which was adequate, but was much less precise than the water jetted and machined specimens sent from other fabricators. Connector E is shown placed in the foam (after concrete was poured) in Figure 3-14.

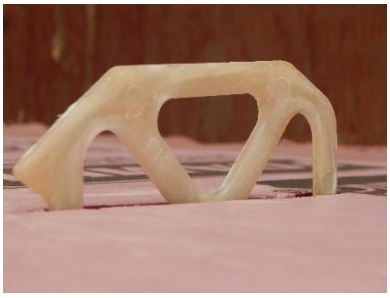

Figure 3-14 Connector E placed in foam

3.2.2.1 Casting Concrete

Concrete was cast one wythe at a time. After forms were set, foam was prepared, and connectors staged, concrete was delivered and pouring into the formwork. Special care was taken to ensure that the separators remained perpendicular to the base and stayed in place. Uneven lateral pressures were eliminated by manually equalizing the amount of concrete on either side of the separator. Concrete was vibrated into the forms using a pencil vibrator. A screed was drawn across the top of the formwork walls to ensure maximum volume occupancy. After the proper

amount of concrete was in the formwork, a trowel was used to smooth the surface of the fresh concrete in preparation of placing the foam and connectors into the concrete.

Part way through the concrete pour, a sample was taken from near the middle of the truck batch to create nine 4-inch diameter cylinders, and determine the unit-weight of the concrete. All of this was done according to the appropriate document published by the American Society for Testing and Materials; ASTM C143, ASTM C31, and ASTM C138 respectively.

Upon troweling the surface of the concrete, foam was placed on top of the wet concrete and connectors were inserted into the wythe. After the connectors and foam were in place, a pencil vibrator was put in contact with every connector to ensure the concrete would adhere to the connector.

Once the concrete, foam, and connectors were all in place, special care was taken to clean off all equipment and surfaces. An example of the completed first layer can be seen in Figure 3-15. After the concrete had set up, the walls of the formwork were removed (Figure 3-16). After the formwork was clean, the second set of forms were fixed into place. This included the insertion of the rebar, propping the rebar on the chairs, and gluing the rubber recess for the pick point into place (Figure 3-17). Attention was given to location of each connector specimen prior to concrete placement. This was done to ensure that an unbonded EPS foam wythe containing Connector A, received an unbonded EPS foam wythe containing Connector A on top of the second wythe.

Once the necessary preparations were made to pour the second wythe, concrete was ordered and the same process used to construct the first wythe was repeated for the second wythe, with one exception; because the second wythe contained the lifting anchors, a manual check was preformed to ensure that none of the pick-points were removed during the pouring process. After the concrete was allowed to cure, the formwork was removed (Figure 3-18) and the last set of forms were put into place (Figure 3-19).

After the formwork was in place and the necessary preparations were made, the process outlined for the first wythe was repeated, except no additional foam or connectors were placed on the top of the top wythe. Because the exposed surface of the concrete was a final product, special care was taken to finish the concrete surface (Figure 3-20). The finished product was allowed to harden before the forms were removed (Figure 3-21).

Figure 3-15 Completed first wythes with foam and connectors in place

Figure 3-16 Clean-up following formwork removal of first wythe

Figure 3-17 Second wythe preparation with rebar, pick-points, and form work in place

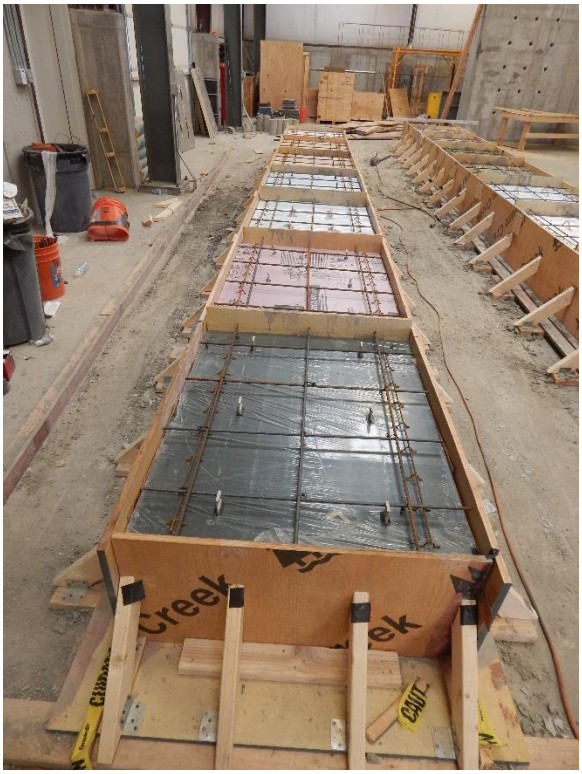

Figure 3-18 Formwork removed after concrete for the second wythe is allowed to cure

Figure 3-19 The highest set of forms is in place ready to pour the last concrete wythe

Figure 3-20 Taking special care to put a finished surface on the final wythe of the concrete

Figure 3-21 Finished Product Waiting to Cure

3.2.3 Push-off Test Setup

The push-off specimen test setup is illustrated in Figure 3-22. Push-off specimens were loaded by placing a ram and load cell on the wide center wythe and supported at the bottom of the outer wythes. The load was transferred to the specimen through a spreader beam which in turn passed the load into the specimen directly in line with the connectors. The specimen was supported only on the outer wythes at the bottom. Extra care was taken to ensure the specimen was flush on the supports. Relative displacement of the inner wythe to the outer wythes was measured in four places and averaged to determine the reported displacements. The Linear Variable Differential Transformers (LVDTs) were attached to the outer wythes using a custom-built bracket (Figure 3-23 and Figure 3-24). Displacements were measured by fixing a small piece of mild steel to the center wythe, providing a reference point for LVDTs to measure from (See Section 3.2.4). A load cell was placed at the ram-to-spreader beam interface to measure the overall applied load. As a safety precaution, a loose chain was firmly attached to the center wythe to prevent catastrophic failure or related injury. Careful observation was given to the tautness of the chain. Never was the chain taut during loading.

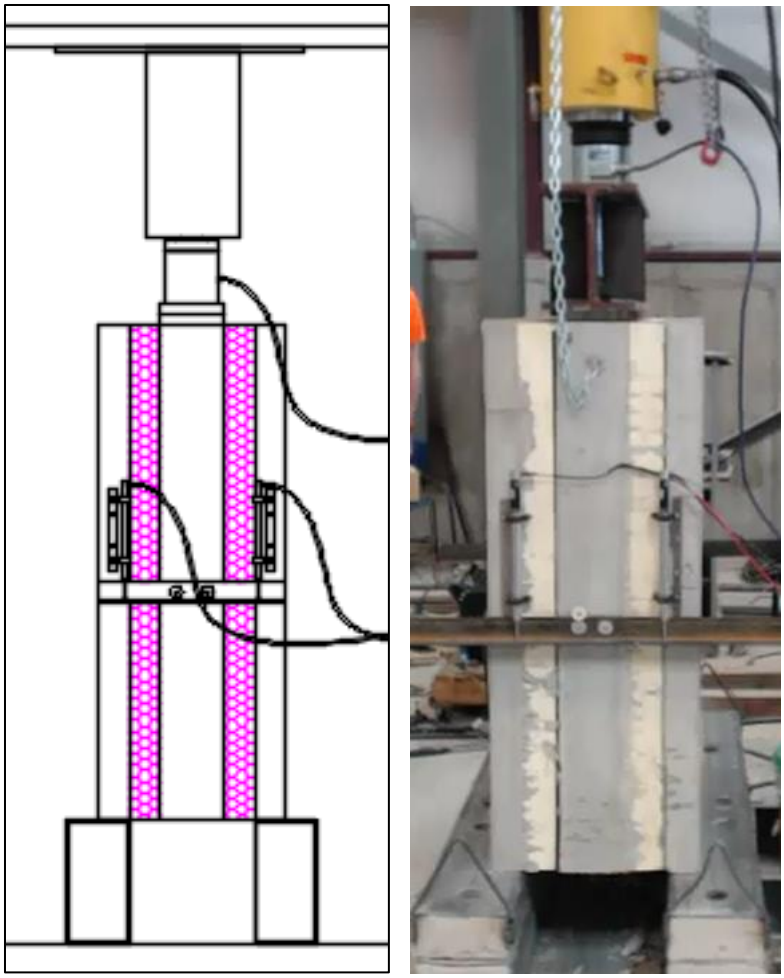

Figure 3-22 Diagram (left) and photograph (right) of test set up

3.2.4 Instrumentation

The LVDTs used for this testing were newly purchased with NIST traceable calibration in February 2015 and are verified periodically on a NIST traceable universal testing machine, according to the SMASH lab Management System Manual. The transducers were attached to the specimen using the specially fabricated bracket shown in Figure 3-23. The two holes closest to the left and right edges in the diagram, where threaded to accommodate a #10-32 machine screw. The inner holes were used to nail the bracket to the specimen. Nails were pounded using a powder actuated 0.22 caliber fastening tool. The bracket can be seen in use in Figure 3-24.

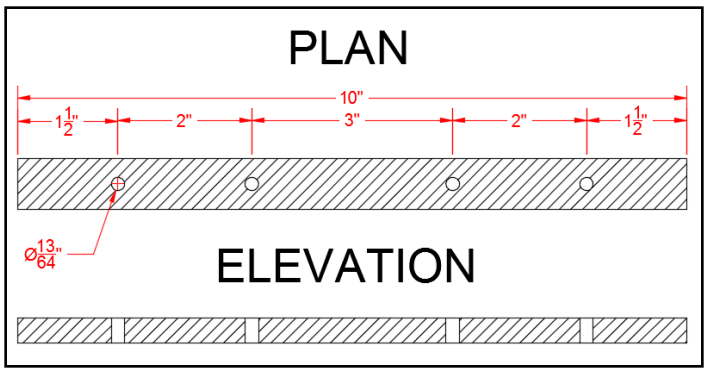

Figure 3-23 Specially designed mounting bracket used to attached LVDTs to specimen

Figure 3-24 Special bracket fixed to specimen with LVDT

The Geokon load cell calibration was verified in February 2015 using a Tinius Olsen testing machine with NIST traceable calibration, last calibrated March 2014. The equipment used to collect data was the Bridge Diagnostics Inc.-Structural Testing System (BDI-STS).

The Linear Variable Differential Transformers (LVDT) were mounted such that the contact point between the mild steel angle and the plunger of the LVDT was at the vertical midpoint of the associated wythe. There was an LVDT attached to the edge of each exterior wythe, to make a total of four shear displacement measurements. These measurements were averaged to determine the actual shear displacement of the center wythe relative to the exterior wythes.

3.3 Full-scale tests

3.3.1 Full-scale Specimen Configurations and Test Matrix

Two 16-ft long and six 15-ft long concrete sandwich wall panels were tested to evaluate their flexural strength and the composite action of different shear connectors. This part of the study included 4 different connectors (presented in Figure 3-25). For convenience of data presentation, each connector was assigned a letter descriptor like the Push-Off Testing in Section 3.2.1 as follows: Nu-Tie connector (Connector A), Thermomass CC Connector (Connector B), Thermomass X Connector (Connector C), and HK Composite Connector (Connector D). Two panels were tested with Connector A (NU-Tie 3/8 in. diameter connectors), two with only Connector B (Thermomass CC connectors), two with a combination of Connectors C and D (Thermomass CC and X connectors), and two with only Connector D (HK Composite connectors). All connectors were a type of glass fiber reinforced polymer (GFRP). Connector A was a GFRP rebar fabricated into a "zig-zag" pattern, 3/8-in. diameter rebar with longitudinally aligned fibers. Connectors B and C were also an aligned fiber flat bar of GFRP (like Connector A) that were either oriented in an X shape or orthogonal to the concrete wythes. Connector D was a mold-injected product with randomly aligned fibers. The manufacturing process and alignment of the fiber significantly changes the failure mode and ductility of the connectors (Olsen and Maguire 2016).

Figure 3-25 Shear Connectors Tested, Left to Right: Connector A, B, C, and D

All panels were fabricated with XPS insulation, and utilized shear connectors to attain some degree of composite action by transferring shear between the both wythes through the insulation.

Connector A panels had a 3-4-3 in. configuration with prestressed reinforcement in the longitudinal direction and shear connectors as shown in Figure 3-26 and Figure 3-27. The prestressing consisted of three low-relaxation 270 ksi strands with a 3/8-inch diameter tensioned to $0.70f_{pu}$. The panels were designated A-2 (Figure

3-26) and A-4 (Figure 3-27) with the 2 and 4 designating the number of shear connectors in each row. Shear connectors were distributed uniformly with a total of eight in the A-2 panel and sixteen in the A-4 panel. The difference in the number of connectors was intended to demonstrate the dependence of the panel performance upon the number of connectors within the panel. At the authors' request, the A-2 panel used connectors at a lower level than typically used by the manufacturer for this panel configuration.

The B, BC, and D panels had mild reinforcement and a 4-3-4 in. configuration. The reinforcement of these panels included four Grade 60 #3 bars in the longitudinal direction for each wythe and three shear connectors in each row. In the B panels, only Connector B shear connectors were distributed uniformly at sixteen-inch spacing for a total of 33 in each panel (see Figure 3-28). In the BC panels, 33 Connector B shear connectors were uniformly distributed with an additional six Connector C shear connectors spread throughout the panel (see Figure 3-29). Like the B panels, D panels had Connector D shear connectors distributed uniformly at sixteen-inch spacing for a total of 33 in each panel (see Figure 3-30).

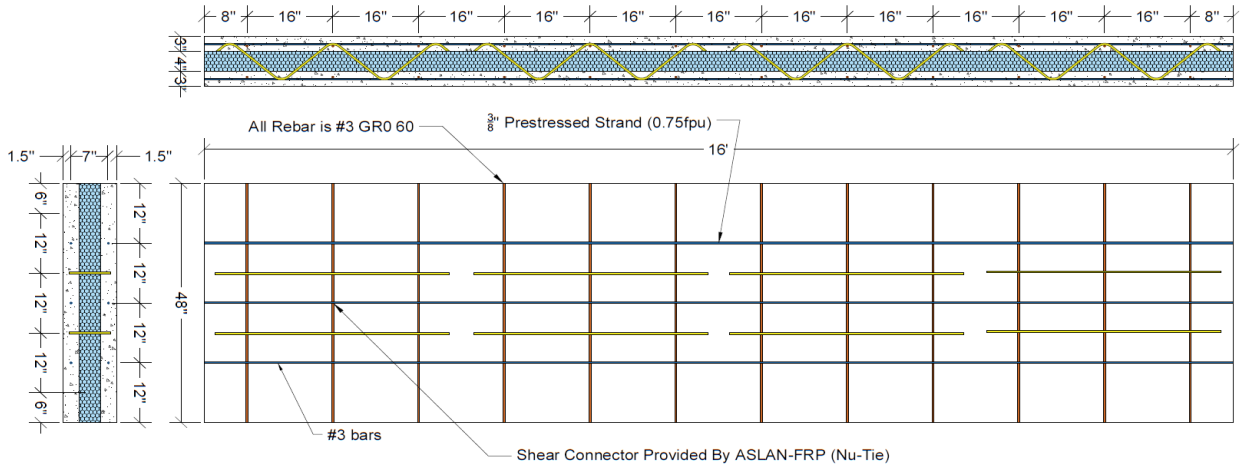

Figure 3-26 A-2 panel details

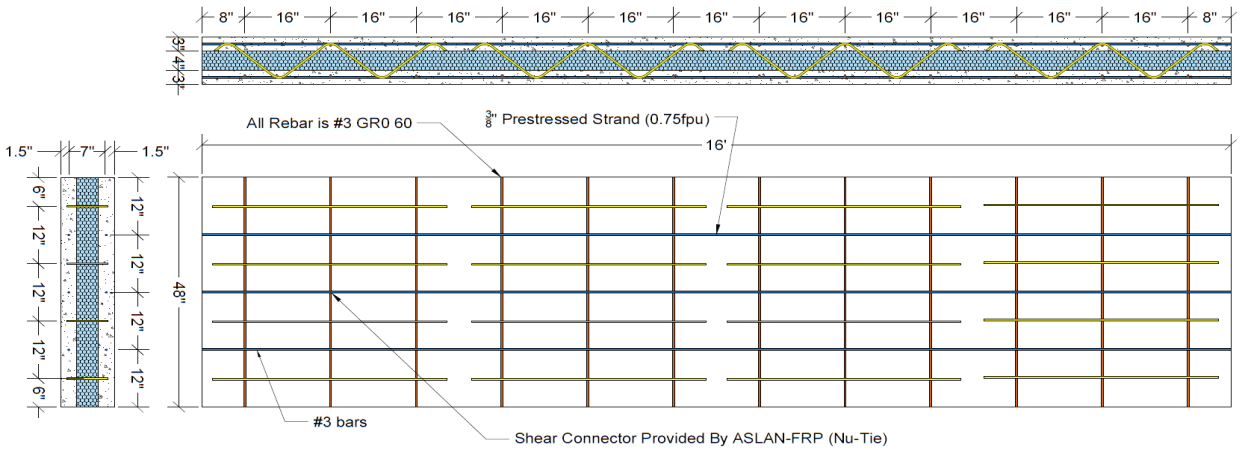

Figure 3-27 A-4 panel details

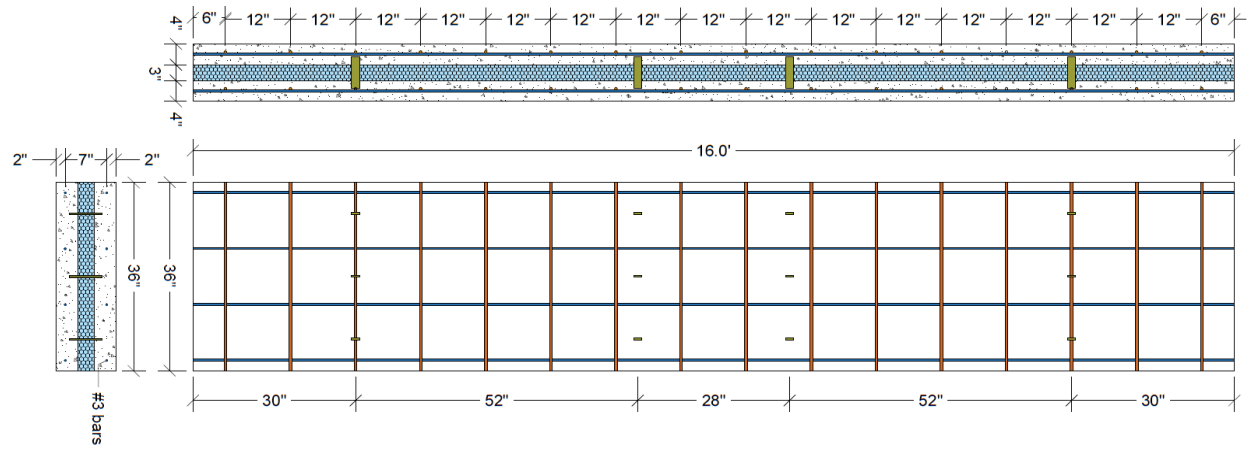

Figure 3-28 B panel details

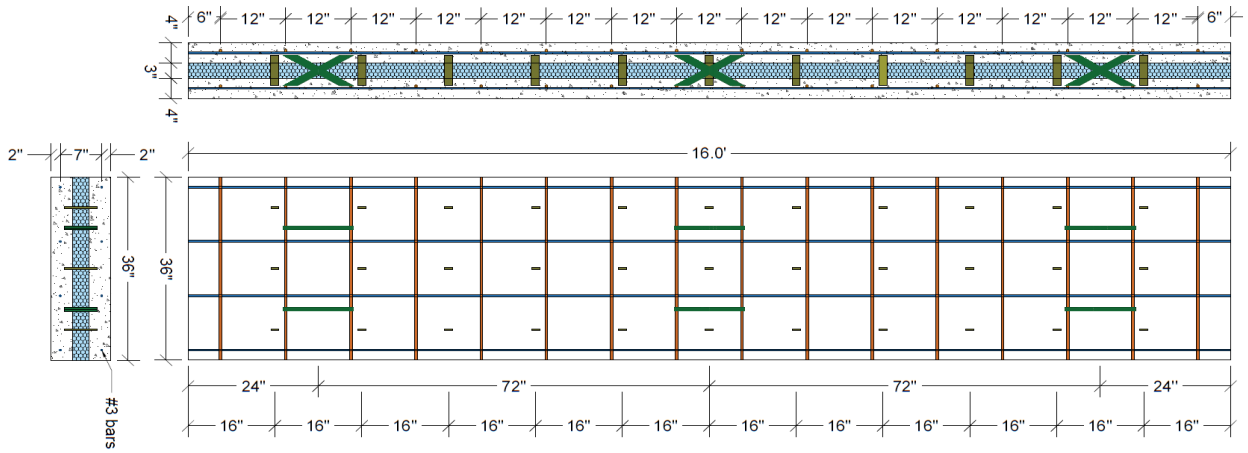

Figure 3-29 BC panel details

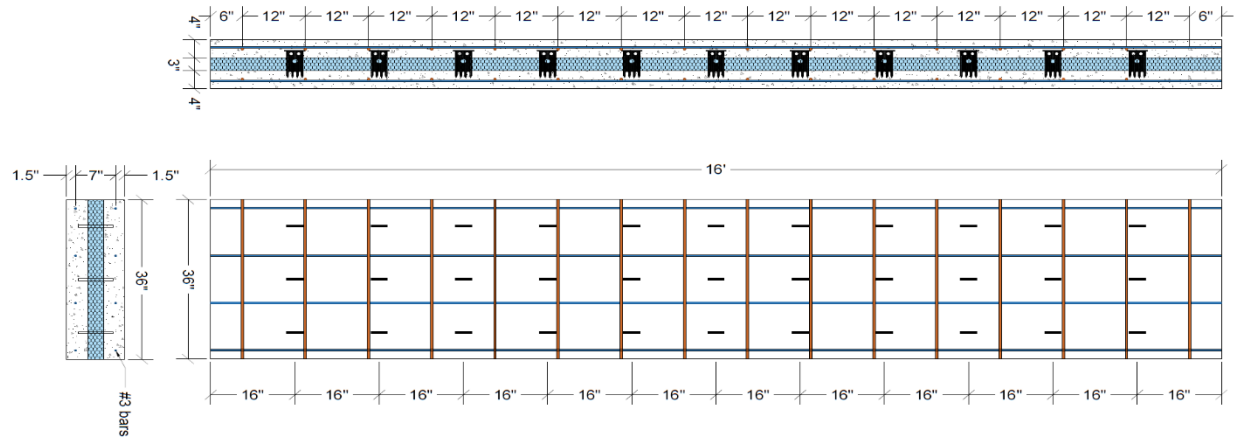

Figure 3-30 D panel details

3.3.2 Construction of Wall Panels

All panels were fabricated with XPS insulation, and utilized shear connectors to attain a certain degree of composite action by transferring the shear flow between the both wythes through the insulation. The design of the panels was performed in conjunction with representatives from Forterra Structural Precast (Salt Lake City, Utah) and Concrete Industries (Lincoln, Nebraska).

3.3.3 Full-scale Test Setup

Each 16-ft long panel was placed on simple supports with a 15-ft span for A-2 and A-4 panels, and a 14-ft span for the B, BC, and D panels. A single hydraulic actuator applied four point loads with a spreader beam assembly to simulate a distributed load, as shown in Figure 3-31.

Deflection was measured at midspan on both edges (north and south) of the panel. Relative slip between concrete wythes was measured using LVDTs at each panel corner (northeast, southeast, northwest and southwest). Prior to testing, dead load deflection was measured at midspan with a total station and high accuracy steel ruler by finding the elevations of the supports and at midspan. This procedure provided a dead load midspan deflection with an accuracy of 1/32 in.

Concrete compression strengths were measured using ASTM C39 procedures from 4 in. x 8 in. concrete cylinders sampled and provided by the precasters. Rebar and prestressing steel samples were obtained from each panel after testing by breaking out the concrete from the ends, where there was no plasticity.

Rebar were tested according to ASTM A370 and the full stress strain curved developed using a 2-in. extensometer. Because of gripping limitations of the tensile testing machine available, standard reusable chucks were used to test the 3/8 in. prestressing strand. Using chucks during tensile testing is known to limit both elongation and provide slightly lower ultimate stresses (Morcous et al. 2012; Maguire 2009). Only ultimate tensile stress was recorded for the prestressing strand because a proper (24 in. gauge length, rotation capable) extensometer was not available.

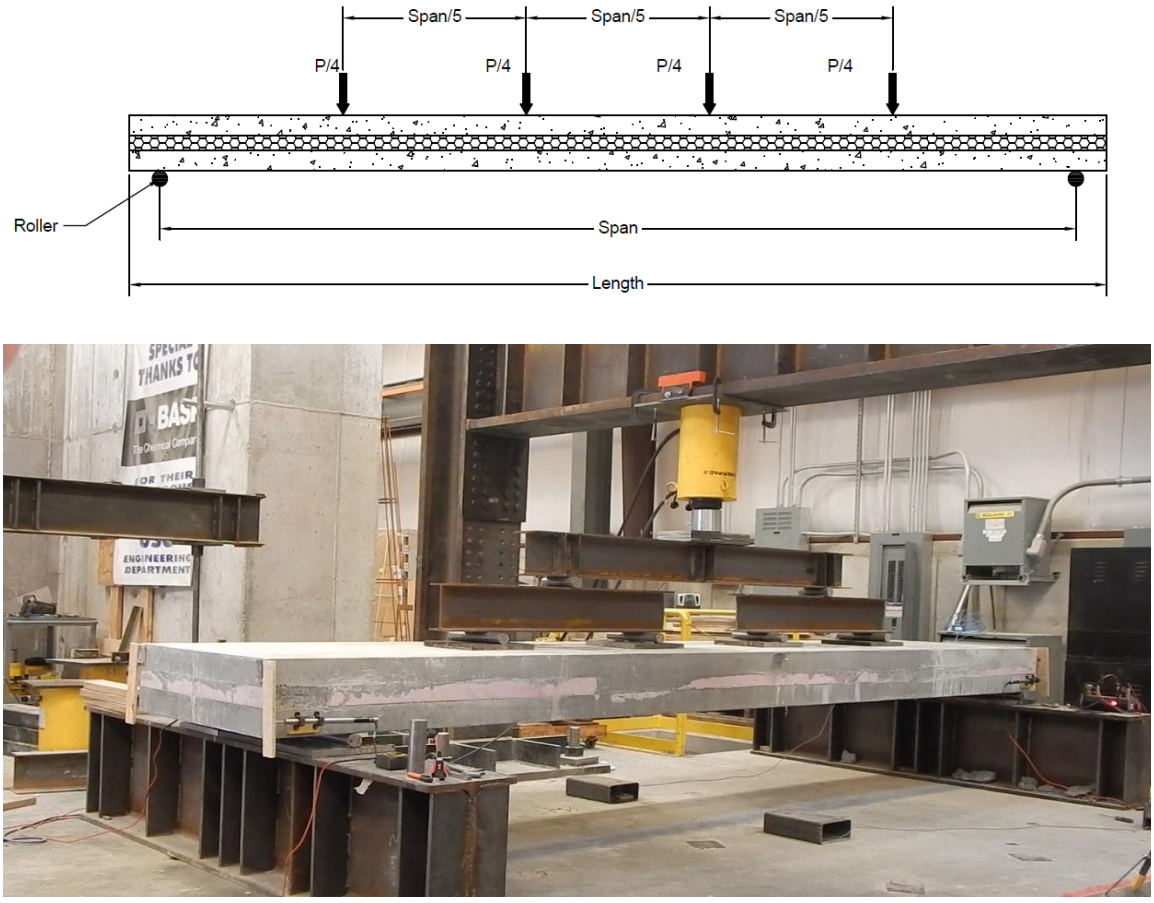

Figure 3-31 Full-scale specimen test setup

3.3.4 Full-Scale Test Sensors

The data acquisition, LVDTs for slip measurement and load cell for ram load measurement are the same as described in the previous section for the push-off specimen. The deflection measurements were made with LX-PA-20 (UniMeasure) string potentiometers with calibration verified on a NIST traceable Tinius Olsen Universal Testing Machine to an accuracy of 0.001 in.

3.4 Material Testing

Concrete cylinder compressive tests were performed for all specimens tested. For full-scale tests, concrete cylinders were provided by the respective precaster to be tested on the day of specimen testing. Due to limited material, space, and budget, all of the push-off specimens could not be poured at once. Each specimen required three

separate concrete pours (one per wythe), and specimens were created in three different sets due to space restrictions for a total of nine pours (three sets with three pours each). Cylinders were created from the concrete midway through each pour. All cylinders were 4-inch diameter, with compressive tests performed according to ASTM C39.

3.5 Summary

The preceding chapter described the test setup for the experimental program. Push-off specimens were fabricated and tested at the Utah State University SMASH lab. The full-scale specimens were fabricated by Concrete Industries and Forterra Precast and tested at the Utah State University SMASH lab. The following chapters present the results and analysis of the push-off and full-scale tests.

4 TEST RESULTS FOR PUSH-OFF TESTS

4.1 Introduction

In this study, 41 pure shear push-off specimens were created to evaluate the shear stiffness of the various commercially available sandwich panel wall shear connectors. This chapter presents the results of this testing. The variables studied were connector type, foam thickness, foam type and foam bond. This study included 5 different connectors. For convenience of data presentation, each connector was assigned a letter descriptor and are as follows: Nu-Tie connector (Connector A), Thermomass CC Connector (Connector B), Thermomass X Connector (Connector C), HK Composite Connector (Connector D), and Delta Tie (Connector E). Due to project constraints, only a single specimen of each type could be constructed so there is no statistical information available regarding the connector strength and stiffness values, making some comparisons difficult. Design, fabrication, and test setup for the push-off specimens is presented in the preceding chapter.

4.2 Material Testing

Concrete cylinder compressive tests were performed for all specimens tested. Due to limited material, space, and budget, all the push-off specimens could not be poured at once. Each specimen required three separate concrete pours (one per wythe), and specimens were created in three different sets due to space restrictions for a total of nine pours (three sets with three pours each). Cylinders were created from the concrete midway through each pour. All concrete cylinders were 4-inch diameter, with compressive tests performed according to ASTM C39.

Tabulated values of the push-off specimen material properties are shown in Table 4-1 below with other pertinent information regarding the concrete shown in Table 4-2. These values are calculated from ACI 318-14 (American Concrete Institute 2014). A visual comparison of the concrete compressive strength is shown in graphical form in Figure 4-1.

Table 4-1 Material properties of concrete for push-off specimens

Set	Pour	Slump	Unit Weight of Concrete	Compressive strength (psi) (Days of Curing)			
	(#)	(in)	(lb/ft^3)	28	14	7	3
1	1	9	138.79	5124.39	3736.49	1823.03	911.52
	2	7.5	139.80	5550.13	4152.13	2690.58	1345.29
	3	5	133.95	6264.74	4925.24	4134.74	2067.37
	Average	**-**	**137.51**	**5646.42**	**4271.29**	**2882.78**	**1441.39**
2	1	6.5	141.54	5861.28	4445.88	3402.88	1701.44
	2	7.5	134.70	5531.03	4184.03	2497.87	1248.93
	3	9.25	136.60	4979.96	3613.96	1593.76	796.88
	Average	**-**	**137.61**	**5457.42**	**4081.29**	**2498.17**	**1249.08**
3	1	8.5	139.65	5211.53	3815.03	2084.91	1042.46
	2	5	139.20	6195.50	4803.50	2766.32	1383.16
	3	6	138.65	5916.19	4529.69	3562.60	1781.30
	Average	**-**	**139.17**	**5774.41**	**4382.74**	**2804.61**	**1402.31**

Table 4-2 Material Properties of Concrete for push-off specimens

	w_c	f'_c	f_t	E_c
Set	pcf	psi	psi	psi
1	137.51	5646.42	563.56996	3998690
2	137.61	5457.42	554.0578	3935487
3	139.17	5774.41	569.92137	4116901

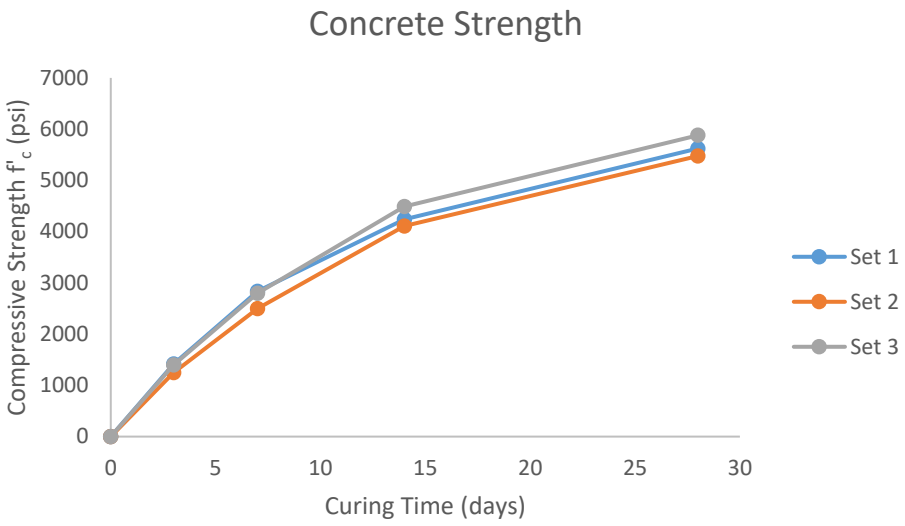

Figure 4-1 Graphical representation of average concrete compressive strengths in Table 4-2

4.3 Push-off Test Results

Each push-off specimen was loaded through failure. Figure 4-2 presents an example Shear Load versus Shear Deformation plot. All load displacement curves had an initial elastic peak response. After this initial peak, the connectors began to exhibit reduced stiffness until peak load. Many of the connectors maintained significant load past this peak load while continuing to deform, whereas, others failed soon after they reached peak load. This section will provide a brief overview and summary of all connector types and each connector will be reviewed specifically in the following subsections.

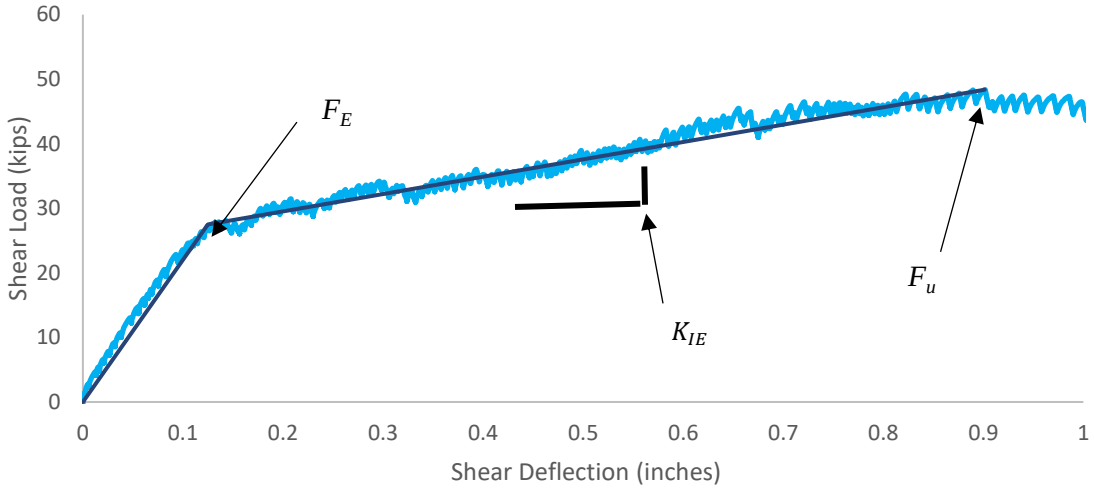

Figure 4-2 Load-Deformation Curve & Visually Identifying the Yield Point

On a load-deflection diagram, the elastic stiffness of the specimen the initial slope of the load deformation curve. For design purposes, this curve is idealized into two categories: the elastic portion, K_e, and the plastic portion, K_{ie} (Figure 4-2). The stiffness can be calculated as the derivative of the curve, which for our idealized case of two sections is equal to:

$$K_E = \frac{F_E}{\Delta_E} \qquad (4\text{-}1)$$

$$K_{IE} = \frac{F_u - F_E}{\Delta_U - \Delta_E} \qquad (4\text{-}2)$$

Where: K_E = elastic stiffness

K_{IE} = inelastic stiffness of plastic stiffness

F_E = elastic load limit

F_u = ultimate capacity or peak load

Δ_E = deflection corresponding to the elastic load limit

Δ_U = deflection corresponding to the ultimate capacity

Utilizing Equations (4-1) and (4-2), elastic and plastic stiffnesses were calculated for each connector and calculated per connector.

Figure 4-3 presents an ultimate strength (F_u) comparison for all specimens. Connector A with 3-in. bonded XPS insulation produced the strongest individual shear connection (16.8 kips each), while connector D with 4-in. unbonded EPS insulation produced the smallest shear connection (1.39 kips each), though in this instance there may have been a fabrication issue. There was a consistent reduction in strength between 3-in. and 4-in. wythe specimens, but connector C with ISO and connector D with XPS experienced little to no reduction in strength.

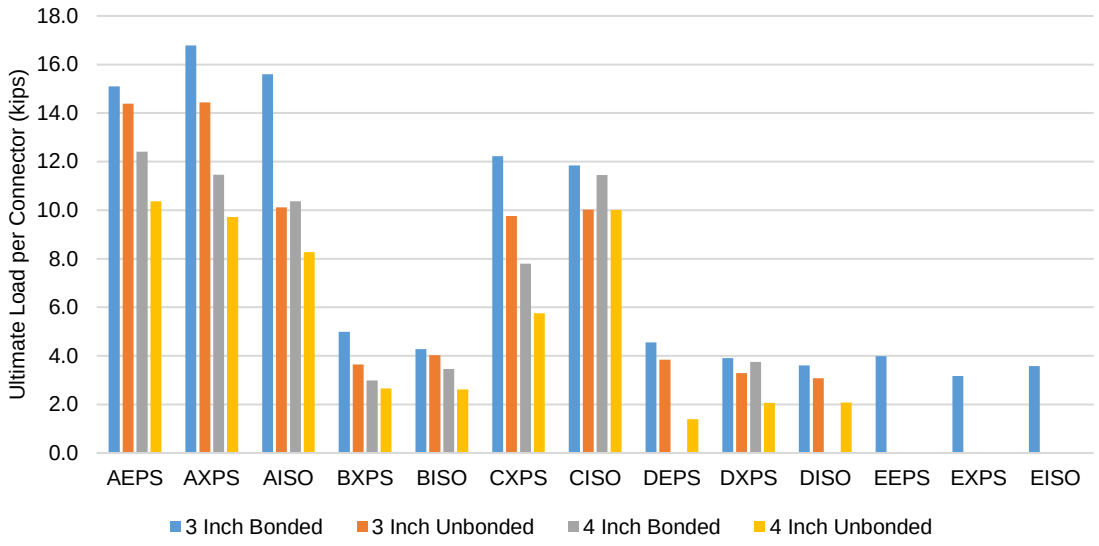

Figure 4-3 Ultimate Load Comparison for All Connectors Individually

Each unbonded specimen produced a reduction in ultimate strength for its respective connector. The amount of reduction in ultimate strength varied greatly, however. For example, connector A with EPS produced a reduction of approximately 10% when unbonded, while connector D with EPS produced an approximately 70% difference when unbonded.

Foam type did contribute to the ultimate strength as well, but the results were also inconsistent (especially with the ISO). This variation is expected to be because the ISO surfaces were not consistent between manufacturers. The ISO foam selected for each was part of the manufacturer's system/recommendation, and therefore what a precast producer would receive upon purchase. Some ISO surfaces were smooth plastic or metallic foil while others

had a paper surface (Figure 4-4). The vastly differing properties of each of these materials causes them to bond differently with the concrete, possibly leading to inconsistencies in bonded and unbonded behavior for the ISO. Ultimate strengths were typically higher with XPS, but connector D experienced higher loads with EPS.

Figure 4-4 Different types of polyisocyanurate foam and their associated face finishing

An "elastic limit" load (F_E) and "elastic" stiffness (K_E) were identified from the load deformation curve of each push-off specimen. This was done by visually identifying the yield point as shown in Figure 4-2. Figure 4-5 shows the maximum elastic force (F_E) observed during testing for each connector configuration. Although fatigue testing was not performed, it was assumed that F_E should be the maximum force allowed in the connector during service loading scenarios as damage may accumulate at higher loads. Figure 4-5 allows a visual comparison of elastic load limits for all push-off specimens in this paper. The connectors that exhibited a high ultimate strength, F_u, in Figure 4-3 also presented with a similar F_E, relative to the other connectors. Connector A with XPS had the highest F_E value (9.5 kips), but Connector A with ISO was significantly lower than the EPS and XPS combinations. This is likely due to the difference in ISO surface treatment used with the fabricators system as previously discussed, which might cause inconsistent bond. There was relatively little difference between the Connector A ISO bonded and unbonded. Similar relationships between insulation, wythe thickness and bond performance are observed with respect to F_E.

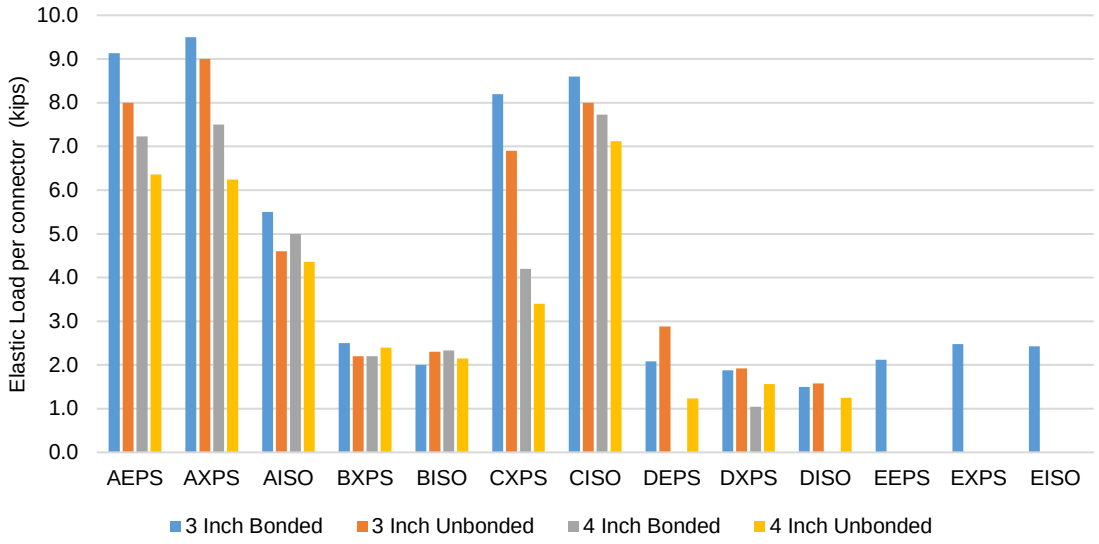

Figure 4-5 Elastic Load Limit (F_E) Comparison for All Specimen Configurations

Figure 4-6 presents the elastic stiffness values for the push-off specimens tested in this program. Connector B resulted in the lowest K_E values with as low as 6 kips/in in combination with the 4-in. unbonded specimens, whereas several Connector A specimens exceeded 150 kips/in. Surprisingly, although Connector D specimens had displayed lower relative strengths with respect to the other connectors, they had a similar stiffness to the other connector specimens in many instances. Connectors A and C showed significantly higher stiffness and strength. This is likely due to their truss-like fiber orientation which allows more efficient horizontal load transfer as opposed to the load transfer mechanism of Connectors B and D, which is more like dowel action or pure shear.

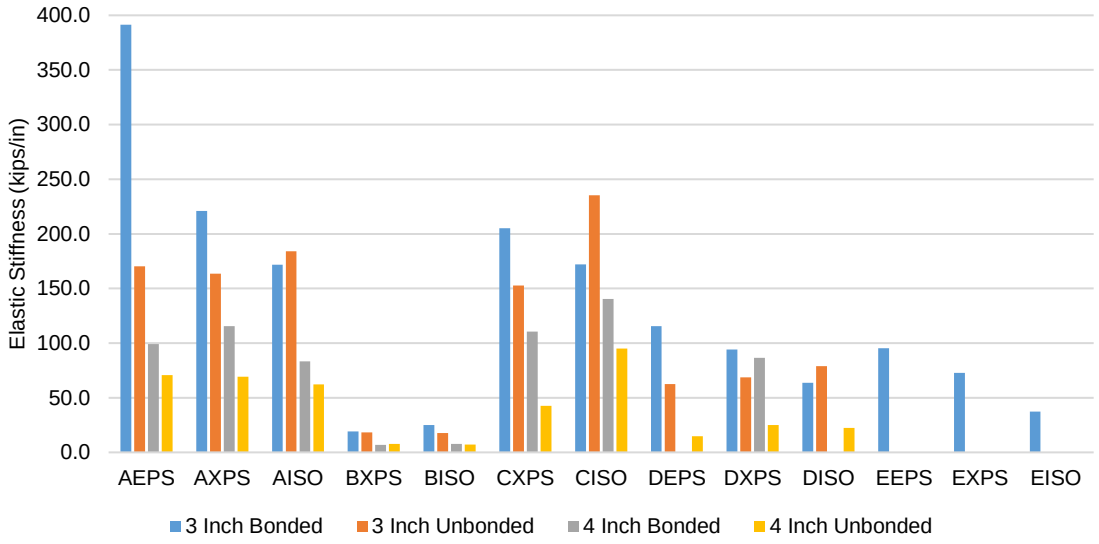

Figure 4-6 Elastic Stiffness Comparison for All Connector

Both unbonded ISO scenarios for connectors A and C displayed higher elastic stiffness values than their bonded counterparts. This was unexpected and may be evidence of highly variable bond behavior and/or insulation behavior. Generally, 4-in. wythes, bonded and unbonded, exhibit significantly lower stiffness than the observed reductions in strengths in Figure 4-2 and Figure 4-5. Similar observations can be made from the inelastic stiffnesses presented in Figure 4-7.

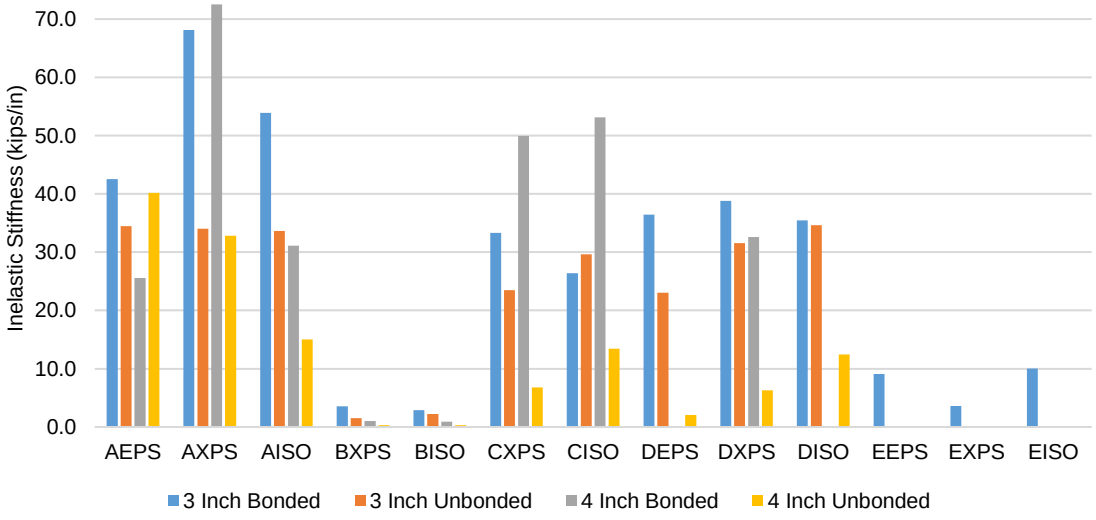

Figure 4-7 Inelastic Stiffness Comparison for All Connector

It should be expressly noted that the differences in strength and stiffness should not be the sole factor in selecting a shear component. Cost, durability, ease of fabrication and customer support should also be considered when selecting a system. Also, connector configuration is important to performance (Olsen and Maguire 2016).

4.3.1 Experimental Results for Connector A

Figure 4-8 and Figure 4-9 display plots of shear load versus shear deflection for all Connector A 3-in. and 4-in. specimens, respectively. There is a reduction in all mechanical values when comparing the 4 in. specimens to the 3 in. specimens, as expected. Connector A seems to be affected by the bond of the foam to the concrete since, in all cases, the bonded specimens have larger strengths and stiffnesses than the unbonded specimens. This did not hold true for all the other connectors as presented in the following sections. Table 4-3 and Table 4-4 present the tabulated capacities of the specimen and the stiffnesses, respectively.

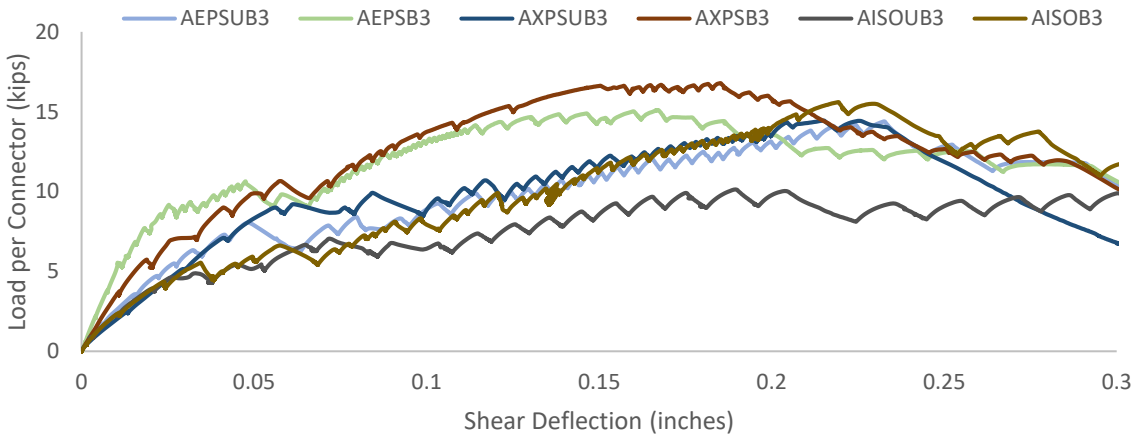

Figure 4-8 Chart of all 3-in. specimens for Connector A

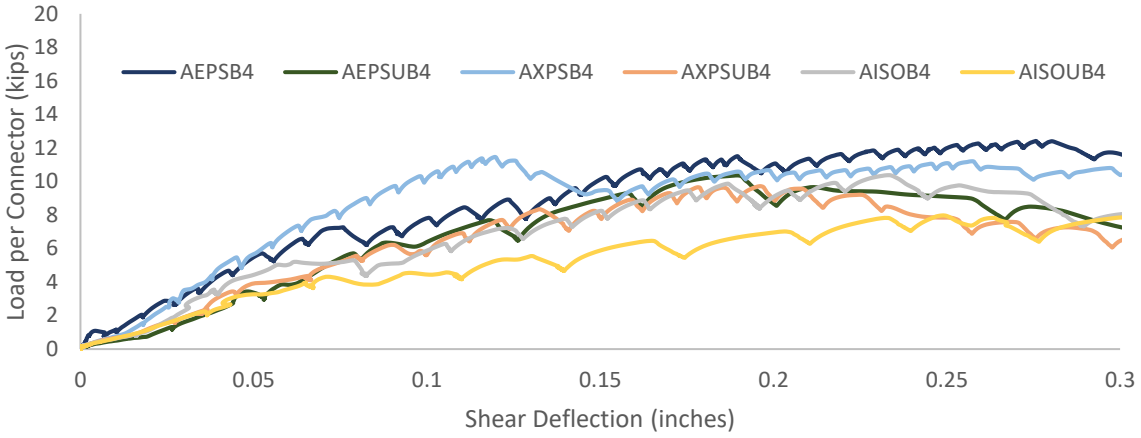

Figure 4-9 Chart of all 4-in. specimens for Connector A

Table 4-3 Observed Experimental Capacity of Connector A

	Ultimate Capacity of Specimen				Ultimate Capacity of Connector			
	3 Inch		4 Inch		3 Inch		4 Inch	
	(kips)	*(kips)*	*(kips)*	*(kips)*	*(kips)*	*(kips)*	*(kips)*	*(kips)*
	B	UB	B	UB	B	UB	B	UB
AEPS	60.4	57.6	49.7	41.5	15.1	14.4	12.4	10.4
AXPS	67.2	57.8	45.9	38.9	16.8	14.4	11.5	9.7
AISO	626	40.5	41.5	33.1	15.6	10.1	10.4	8.3

Table 4-4 Elastic and plastic stiffness for all Connector A push-off specimens

Specimen			AEPS3B	AEPS3UB	AEPS4B	AEPS4UB	AXPS3B	AXPS3UB	AXPS4B	AXPS4UB	AISO3B	AISO3UB	AISO4B	AISO4UB
Elastic Stiffness	K_E	(kips/in)	391	170	100.0	69.4	221	163.6	115.4	69.3	172	184	83.3	62.5
Inelastic Stiffness	K_{EL}	(kips/in)	42.2	34.3	24.5	41.3	68	34.0	72.5	31.3	54.7	32.7	31.1	15.0

4.3.2 *Experimental Results for Connector B*

Figure 4-10 and Figure 4-11 display plots of shear load versus shear deflection for all Connector B 3-in. and 4-in. specimens, respectively. There is a reduction in all mechanical values when comparing the 4 in. specimens to the 3 in. specimens, as expected. Connector B seems to behave similarly whether the foam is bonded or not. Table 4-5 and Table 4-6 present the tabulated capacities of the specimen and the stiffnesses, respectively.

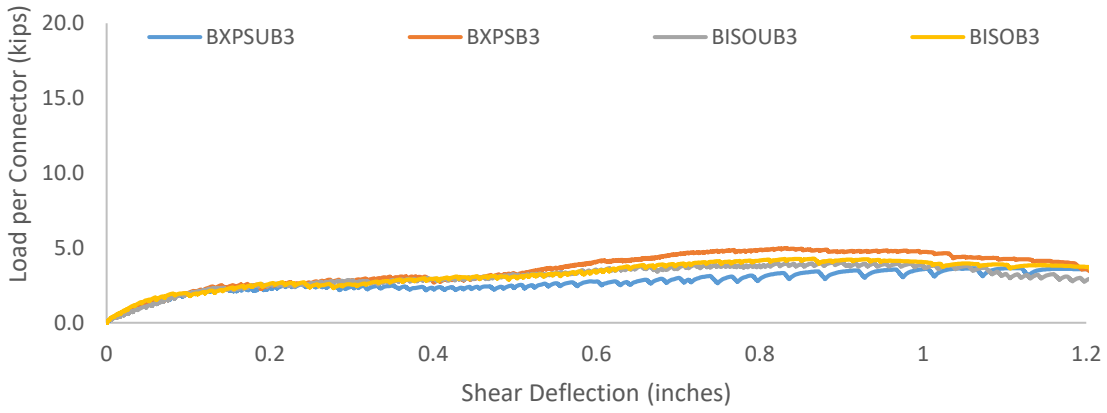

Figure 4-10 Chart of all three-inch specimens for connector B

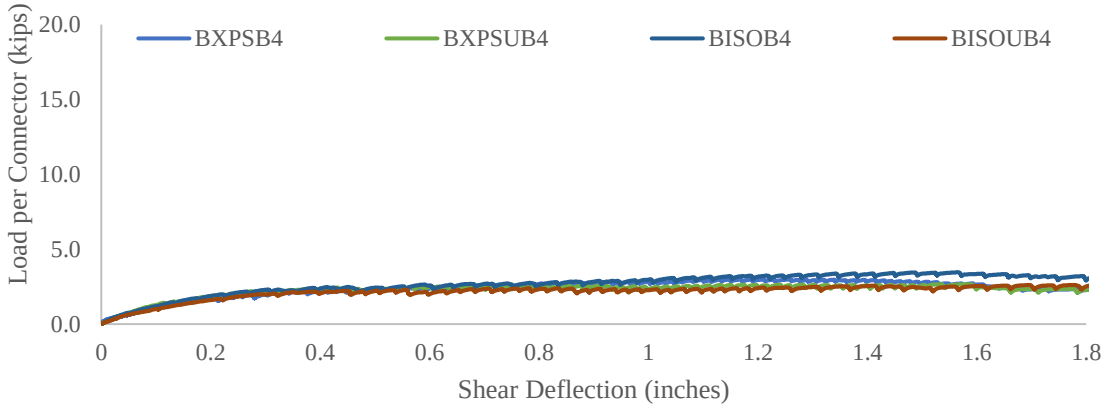

Figure 4-11 Chart of all 4-in. specimens for Connector B push-off specimens

Table 4-5 Observed experimental capacity of Connector B

	Ultimate Capacity of Specimen				Ultimate Capacity of Connector			
	3 Inch		4 Inch		3 Inch		4 Inch	
	B	UB	B	UB	B	UB	B	UB
BXPS	59.91	43.71	35.77	31.95	4.99	3.64	2.98	2.66
BISO	51.32	48.38	41.49	31.42	4.28	4.03	3.46	2.62

Table 4-6 Elastic and plastic stiffness for all Connector B push-off specimens

Specimen			BXPS3B	BXPS3UB	BXPS4B	BXPS4UB	BISO3B	BISO3UB	BISO4B	BISO4UB
Elastic Stiffness	K_{EL}	(kips/in)	19.2	18.3	7.0	7.7	25	17.7	7.8	7.2
Inelastic Stiffness	K_{EL}	(kips/in)	3.5	1.5	1.0	0.3	2.9	2.2	0.9	0.3

4.3.3 Experimental Results for Connector C

Figure 4-12 and Figure 4-13 display plots of shear load versus shear deflection for all Connector C 3-in. and 4-in. specimens, respectively. There is a reduction in all mechanical values when comparing the 4 in. specimens to the 3 in. specimens, except for the Connector C ISO bonded 4 in. specimen, which had very similar values compared to the 3 in. specimens in the same series. Connector C was affected by the foam to concrete bond, although is it less pronounced in the 3 in. specimens and in nearly every case the strength and stiffness is significantly reduced when unbonded. Note that the manufacturer does not recommend Connector C for 3 in. specimens and some connectors in the 3 in. wythes experienced compression blow out as discussed later in this chapter. Table 4-7 and Table 4-8 present the tabulated capacities of the specimen and the stiffnesses, respectively.

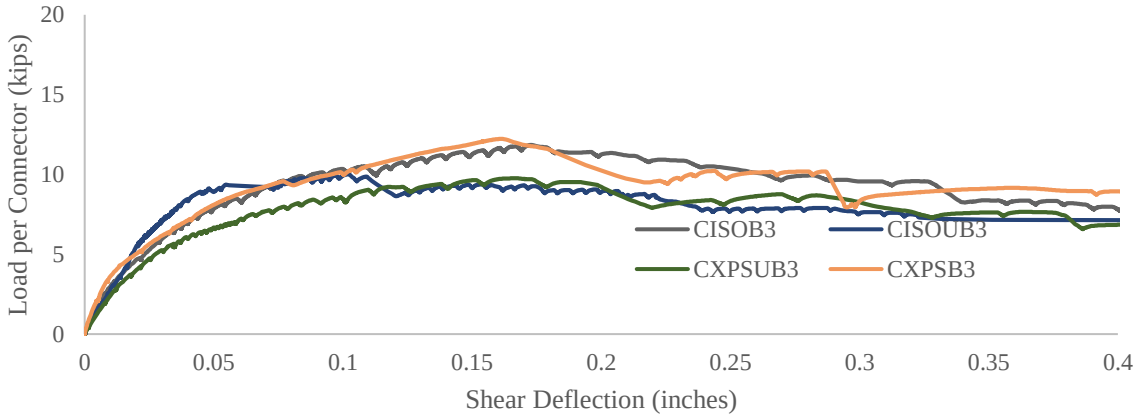

Figure 4-12 Chart of all 3-in. specimens for Connector C

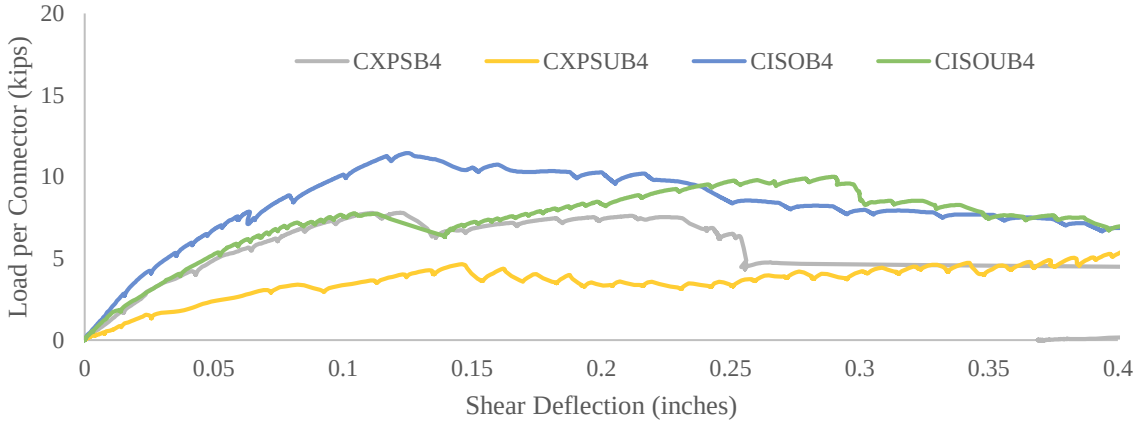

Figure 4-13 Chart of all 4-in. specimens for Connector C

Table 4-7 Observed Experimental Capacity of Connector C

	Ultimate Capacity of Specimen				Ultimate Capacity of Connector			
	3 Inch		4 Inch		3 Inch		4 Inch	
	B	UB	B	UB	B	UB	B	UB
CXPS	97.85	78	62.37	46	12.23	9.76	7.8	5.75
CISO	94.74	80.21	91.61	80.04	11.84	10.03	11.45	10.01

Table 4-8 Elastic and plastic stiffness for all Connector C push-off specimens

Specimen			CXPS3B	CXPS3UB	CXPS4B	CXPS4UB	CISO3B	CISO3UB	CISO4B	CISO4UB
Elastic Stiffness	K_{EL}	(kips/in)	205	153	110	42.5	172	235	140	94
Inelastic Stiffness	K_{EL}	(kips/in)	34.7	23.5	50	6.8	26.5	29.4	53.1	13.6

4.3.4 Experimental Results for Connector D

Figure 4-14 and Figure 4-15 display plots of shear load versus shear deflection for all Connector B 3-in. and 4-in. specimens, respectively. There is a reduction in all mechanical values when comparing the 4 in. specimens to the 3 in. specimens. Connector D had significantly reduced ductility when compared to the other connectors, especially for the 3 in. specimens. This is due to its randomly aligned fibers and dowel action failure mode. Based on these results, it appears that foam type and has little effect on the strength and stiffness of Connector D. Bond does influence strength and stiffness, however it negligible. Table 4-9 and Table 4-10 present the tabulated capacities of the specimen and the stiffnesses, respectively. Interestingly, considering its overall strength, Connector D has a very high elastic stiffness, which would be a very favorable property for controlling elastic deflections and cracking.

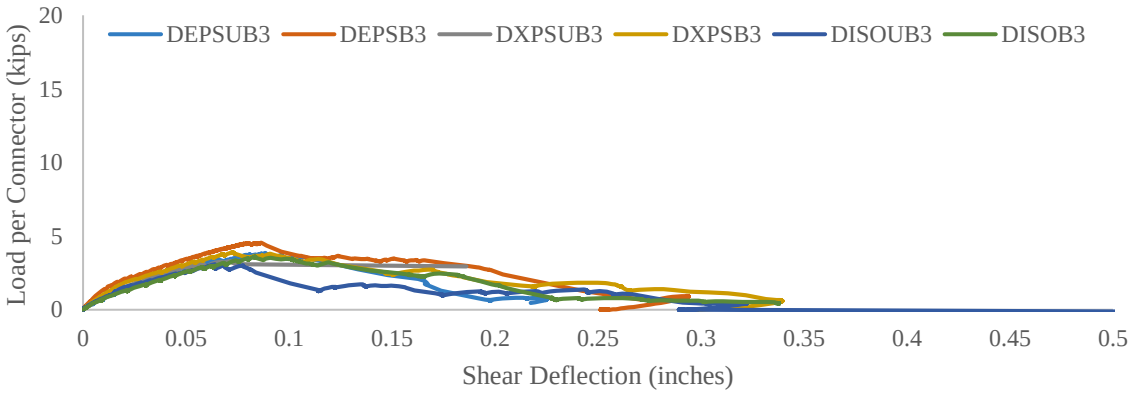

Figure 4-14 Chart of all 3-in. specimens for Connector D

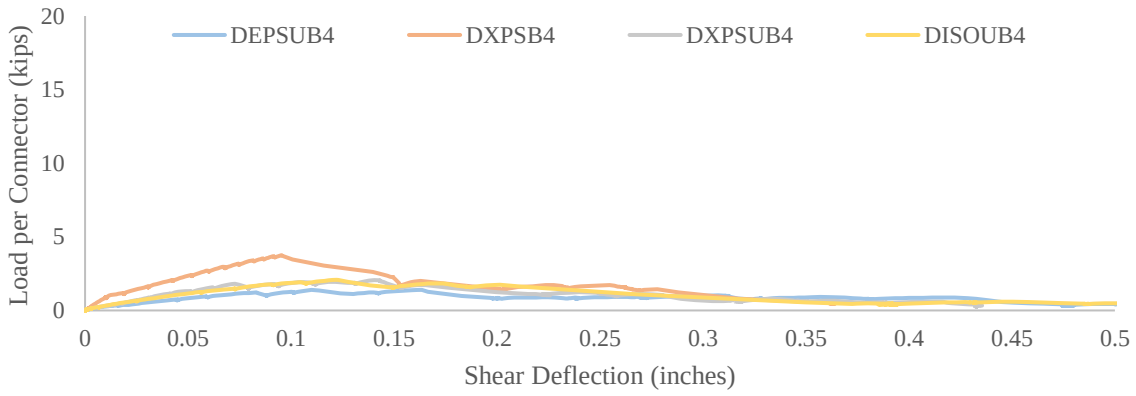

Figure 4-15 Chart of all 4-in. specimens for Connector D

Table 4-9 Observed experimental capacity of Connector D

	Ultimate Capacity of Specimen				Ultimate Capacity of Connector			
	3 Inch		4 Inch		3 Inch		4 Inch	
	B	UB	B	UB	B	UB	B	UB
HKEPS	54.00	46.18	-	16.73	4.50	3.85	-	1.39
HKXPS	46.92	39.52	45.08	24.74	3.91	3.29	3.76	2.06
HKISO	43.26	37.03	-	24.98	3.60	3.09	-	2.08

Table 4-10 Elastic and plastic stiffness for all Connector D push-off specimens

Specimen			DEPS3B	DEPS3UB	DEPS4B	DEPS4UB	DXPS3B	DXPS3UB	DXPS4B	DXPS4UB	DISO3B	DISO3UB	DISO4B	DISO4UB
Elastic Stiffness	K_{EL}	(kips/in)	115	62.9	-	14.8	94.8	68.6	86.7	25.2	63.6	79.0	-	22.2
Inelastic Stiffness	K_{EL}	(kips/in)	37.6	23	-	2.0	38.8	31.6	32.6	6.3	35.4	34.6	-	12.4

4.3.5 Experimental Results for Connector E

Figure 4-16 displays a plot of shear load versus shear deflection for all Connector E specimens. For Connector E, only 3-in. specimens were tested because the 4-in. specimens were unacceptable for testing. Based on the little information gathered, there does not seem to be a significant influence of foam type on the strength, but the ISO specimen had reduced elastic stiffness. Connector E had lower ductility than the rest, except for connector D.

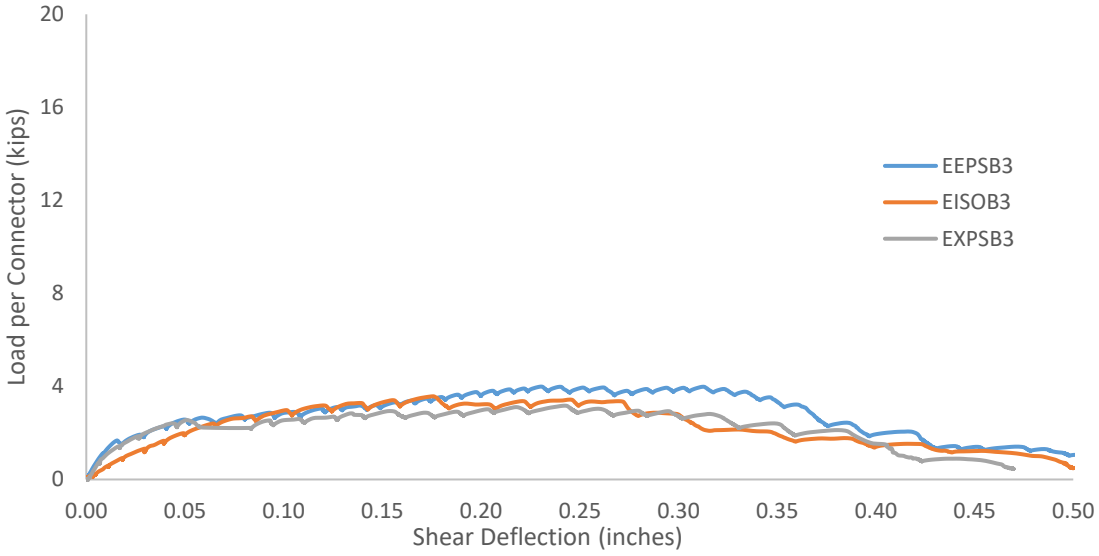

Figure 4-16 Chart of all 3-in. specimens for Connector E

Table 4-11 Elastic and plastic stiffness for all Connector E push-off specimens

Specimen			EEPS3B	EEPS3UB	EEPS4B	EEPS4UB	EXPS3B	EXPS3UB	EXPS4B	EXPS4UB	EISO3B	EISO3UB	EISO4B	EISO4UB
Elastic Stiffness	K_{EL}	(kips/in)	95.5	-	-	-	72.7	-	-	-	37.4	-	-	-
Inelastic Stiffness	K_{EL}	(kips/in)	9.1	-	-	-	3.6	-	-	-	10.0	-	-	-

4.3.6 Failure Modes of Shear Connectors

In general, glass fiber-reinforced polymer (GFRP) and nearly all other polymers and FRP products are considered brittle when compared to material like steel. However, the GFRP shear connectors tested, have exhibited many different modes of failure including: delamination, rupture, pull-out, push through and dowel action (pure shear).

4.3.6.1 Connector A (Nu-Tie Connector)

Connector A was a pultruded GFRP bar. It was 48 inches long and there were four of them in each specimen. Load was applied parallel to the connector and engaged the connector by putting the legs of the truss into either tension or compression. All specimens were loaded to failure. Figure 4-17 shows specimen AISOUB3. This failure was very typical for all connector A specimens. It shows a tensile rupture caused by rupture of the tension leg of the truss. Figure 4-18 shows specimen AISOUB4, which failed in pullout. Pullout was not common for this connector type and is likely to have been fabrication related. Figure 4-19 is failure due to shear fracture an unbonded EPS specimen.

Figure 4-17 Tensile rupture in unbonded specimen with ISO foam

Figure 4-18 Pullout failure in unbonded specimen with ISO foam

Figure 4-19 Shear fracture failure in unbonded specimen with EPS foam

4.3.6.2 Connector B (Thermomass CC Connector)

Connector B was an extruded connector symmetric in cross-section except for the machined deformations constructed to aid in the creation of bond development. Twelve connectors were equally and symmetrically spaced in each specimen. Load was applied perpendicular to the long axis of the connector and loaded to failure. Because these connectors were loaded perpendicular to the grain of the connector, relatively large deformations were observed, leading to greater variety of failures as well. Dowel action and the delamination of fibers, was the most common failure. Figure 4-20, Figure 4-21 and Figure 4-22 depict different connector delamination patterns. Another

commonly observed failure was that of shear rupture, also caused by pure shear. (see Figure 4-23). Pull-out was also observed with Connector B. When a connector failed due to pull-out, other failure mechanisms were also present. Figure 4-24 shows connector B failing in pullout, but bending fracture is also observable. Figure 4-25 shows a clean and clear shear fracture of connector B.

Figure 4-20 Dowel action causing delamination occurring along the width of Connector B

Figure 4-21 Dowel action failure of Connector B

Figure 4-22 Dowel action occurring along the length of Connector B

Figure 4-23 Shear fracture observed in Connector B

Figure 4-24 Pullout occurring with Connector B in combination with bending fracture

Figure 4-25 Shear fracture of Connector B

4.3.6.3 Connector C (Thermomass X Connector)

Much like Connector B, Connector C is a pultruded connector with machined ends to enable mechanical bond. Unlike Connector B, Connector C is loaded axially due to the compression and tension struts which develop because of its shape. Eight Connectors were equally and symmetrically spaced in each specimen. Load was applied in line with the connectors. Delamination and rupture were the most common cases of failure. In the case of the 3-in. specimens, the connector punched through the concrete on the outside of the specimen. This was somewhat expected as these connectors are not recommended for 3 in. concrete wythes, but were tested that way for the comparison study. Figure 4-26, Figure 4-27, and Figure 4-28 show various types of rupture and delamination. Figure 4-29 is a great example of a shear fracture. This fracture takes place in the compression leg of the "X.". Figure 4-30 and Figure 4-31 show the failure of 3-in. specimens caused by punch through of the connector.

Figure 4-26 Delamination observed in a 4-in. unbonded XPS specimen

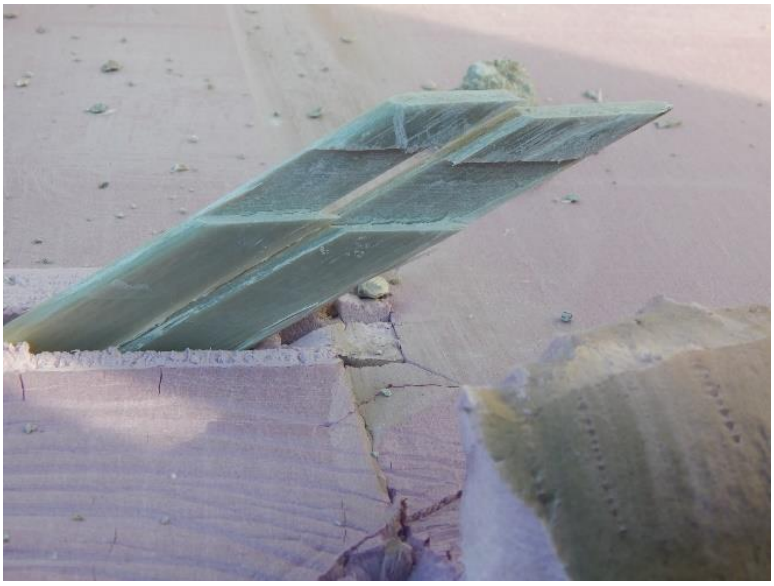

Figure 4-27 Dowel action in a 4-in. bonded XPS specimen

Figure 4-28 Delamination / shear rupture in a 4-in. bonded XPS specimen

Figure 4-29 Shear fracture and dowel action of Connector C

Figure 4-30 Punch through observed in all 3-in. specimens with Connector C

Figure 4-31 Punch through close-up

4.3.6.4 Connector D (HK Composite Connector)

Connector D was a mold injected connector with randomly aligned fibers. Twelve connectors were equally and symmetrically spaced in each specimen. Load was applied in line with the connectors. Shear rupture / dowel action was the only observable failure mode in Connector D. Fracture always occurred on both ends of the connector. There were no instances where fracture occurred on one end and not the other. Pull out was not observed. Connector D does, however, have the most uniquely shaped embedment regions of all the connectors. Figure 4-32 through Figure 4-34 show the shear fractures of connector D from multiple angles.

Figure 4-32 Shear fracture of Connector D (full specimen)

Figure 4-33 Shear fracture of Connector D, both ends fractured

Figure 4-34 Close-up of shear fracture of connector D

4.3.6.5 Connector E (Delta Tie Connector)

For Connector E, eight connectors were equally and symmetrically spaced in each specimen. Load was applied in line with the connectors. Connector E exhibited only one type of failure: tensile rupture. This woven connector displayed a consistent failure mode. The truss formation of Connector E always failed in its tension members. Figure 4-35 shows the completely ruptured specimen. Figure 4-36 and Figure 4-37 depict the tension legs of the truss failed while the compression leg is mostly intact. Due to internal truss shape of Connector E, it fails with rupture of the tension leg of the connector, but the overall shape of the connector is similar to that of Connector B and D and also its behavior. For Connector E, the foam was not engaged as much as it was for A and C, which had more angled connectors.

Figure 4-35 Three inch bonded EPS connector E tensile rupture of all connectors

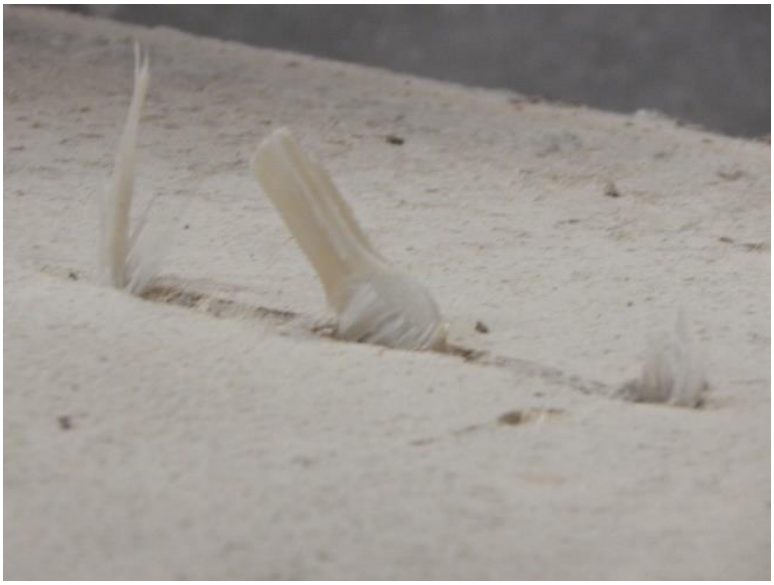

Figure 4-36 Tensile rupture of connector E, note compression leg still intact

Figure 4-37 Tensile rupture of tension strut in truss.

4.3.7 Recommended Design Curves

The shear load versus deformation information from the above connectors is a valuable design value for partially composite sandwich panel walls. Using the concept illustrated in Figure 4-2 one can use the values summarized in Table 4-12. Future effort should investigate statistical information regarding the shear strength and stiffness in order to properly and safely set limits on elastic stresses and failure stresses in the connectors during different loading scenarios. As of now it seems prudent to limit connector forced to the elastic range (F_E, Δ_E) for elastic behavior like cracking and deflections. Furthermore, for the ultimate limit state it may be prudent to limit connector forces and deformations to F_U and Δ_U to force failure of the wythes rather than a probably more brittle failure of the connectors.

Table 4-12 Summary of recommended design curves for all connectors

Connector	Foam	Bond Interface	F_E (Kips)	K_E (Kips/in.)	F_U (Kips)	K_{IE} (Kips/in.)	Δ_E (in.)	Δ_U (in.)
A	3EPS	Bonded	9.13	391.30	15.10	42.54	0.023	0.166
	3EPS	Unbonded	8.00	170.21	14.39	34.45	0.047	0.233
	4EPS	Bonded	7.23	99.04	12.41	25.58	0.073	0.276
	4EPS	Unbonded	6.36	70.67	10.36	40.20	0.090	0.190
	3XPS	Bonded	9.50	220.93	16.79	68.11	0.043	0.150
	3XPS	Unbonded	9.00	163.64	14.44	34.04	0.055	0.215
	4XPS	Bonded	7.50	115.38	11.46	72.53	0.065	0.120
	4XPS	Unbonded	6.24	69.33	9.72	32.82	0.090	0.196
	3ISO	Bonded	5.50	171.88	15.60	53.91	0.032	0.219
	3ISO	Unbonded	4.60	184.00	10.12	33.66	0.025	0.189
	4ISO	Bonded	5.00	83.33	10.37	31.12	0.060	0.233
	4ISO	Unbonded	4.36	62.29	8.27	15.01	0.070	0.331
B	3XPS	Bonded	2.50	19.23	4.99	3.55	0.130	0.833
	3XPS	Unbonded	2.20	18.33	3.64	1.53	0.120	1.064
	4XPS	Bonded	2.20	7.00	2.98	1.02	0.314	1.168
	4XPS	Unbonded	2.40	7.67	2.66	0.29	0.313	1.535
	3ISO	Bonded	2.00	25.00	4.28	2.89	0.080	0.867
	3ISO	Unbonded	2.30	17.69	4.03	2.24	0.130	0.901
	4ISO	Bonded	2.33	7.77	3.46	0.89	0.300	1.565
	4ISO	Unbonded	2.15	7.17	2.62	0.32	0.300	1.778
C	3XPS	Bonded	8.20	205.00	12.23	33.29	0.040	0.161
	3XPS	Unbonded	6.90	152.78	9.76	23.51	0.045	0.168
	4XPS	Bonded	4.20	110.53	7.80	49.95	0.038	0.110
	4XPS	Unbonded	3.40	42.50	5.75	6.79	0.080	0.426
	3ISO	Bonded	8.60	172.00	11.84	26.40	0.050	0.173
	3ISO	Unbonded	8.00	235.29	10.03	29.65	0.034	0.102
	4ISO	Bonded	7.73	140.55	11.45	53.13	0.055	0.125
	4ISO	Unbonded	7.12	94.93	10.01	13.41	0.075	0.290
D	3EPS	Bonded	2.08	115.56	4.56	36.47	0.018	0.086
	3EPS	Unbonded	2.88	62.61	3.85	23.05	0.046	0.088
	4EPS	Unbonded	1.23	14.84	1.39	2.05	0.083	0.163
	3XPS	Bonded	1.88	94.80	3.91	38.78	0.020	0.073
	3XPS	Unbonded	1.92	68.57	3.29	31.57	0.028	0.072
	4XPS	Bonded	1.04	86.67	3.76	32.61	0.012	0.095
	4XPS	Unbonded	1.56	25.16	2.06	6.27	0.062	0.142
	3ISO	Bonded	1.50	63.56	3.60	35.43	0.024	0.083
	3ISO	Unbonded	1.58	79.00	3.09	34.62	0.020	0.064
	4ISO	Unbonded	1.25	22.24	2.08	12.45	0.056	0.123
E	3EPS	Bonded	2.12	95.45	3.99	9.09	0.022	0.230
	3XPS	Bonded	2.48	72.73	3.17	3.63	0.034	0.245
	3ISO	Bonded	2.43	37.38	3.58	10.04	0.065	0.177

4.4 Summary and Conclusions

The preceding chapter describes the testing of 41 pure shear push-off specimens, created to evaluate the shear stiffness of the various commercially available sandwich panel wall shear connectors. The variables studied were connector type, foam thickness, foam type and foam bond. Due to project constraints, only a single specimen of each type could be constructed so there is no statistical information available regarding the connector strength and stiffness values. The following conclusions can be made from the push-off testing:

- For pin type connectors that fail mainly in dowel action (Connectors B and D) or behave like a pin connector (Connector E) foam type and bond play a negligible role in strength and stiffness.
- For truss type connectors (Connectors A and C) that are loaded mainly in tension or compression when shear is applied to the specimen, foam type and bond plays a more significant role in strength and stiffness.
- Connector types vary widely in stiffness, strength, and ductility
- Due to inherent variability associated with concrete bond, it is not recommended that designers use the fully bonded values for strength and stiffness for long term strength without long term testing.
- Future effort should investigate statistical information regarding the shear strength and stiffness in order to properly and safely set limits on elastic stresses and failure stresses in the connectors during different loading scenarios.

5 TEST RESULTS FOR FULL-SCALE PANELS

5.1 Material Testing

Concrete cylinder compressive tests were performed for all specimens tested. For full-scale tests, concrete cylinders were provided by the respective precaster to be tested on the day of specimen testing. The results of the ASTM C39 compression testing is presented in Table 5-1. Each value presented in Table 5-1 is the average of three cylinders from the compression wythe taken on the day of testing. For convenience of data presentation, each connector was assigned a letter descriptor as explained in Section 3.2 as follows: Nu-Tie connector (Connector A), Thermomass CC Connector (Connector B), Thermomass X Connector (Connector C), and HK Composite Connector (Connector D). Two panels were tested with Connector A (NU-Tie 3/8 in. diameter connectors), two with only Connector B (Thermomass CC), two with a combination of Connectors B and C (Thermomass CC and X connectors), and two with only Connector D (HK Composite connectors).

Table 5-1 Concrete Compression Strength for Full-scale Specimens

Specimen	**Average f_c'** *(psi)*	**Split tension** *(psi)*	**Modulus of Elasticity** *(psi)*
A-2	10,400	766	6,191,000
A-4	10,400	766	6,191,000
B-1	9,230	691	5,824,000
B-2	8,000	699	5,986,000
BC-1	9,230	691	5,824,000
BC-2	8,000	699	5,986,000
D-1	9,230	691	5,824,000
D-2	8,000	699	5,986,000

Figure 5-1 presents the stress vs strain curves for the rebar in the B, BC, and D sandwich panels. The average yield stress was 72.2 ksi and the ultimate stress was 110 ksi. The average ultimate capacity for the prestressing strands was 259 ksi. It is likely the testing method described in Section 3.2 above affected the ultimate capacity of the strands.

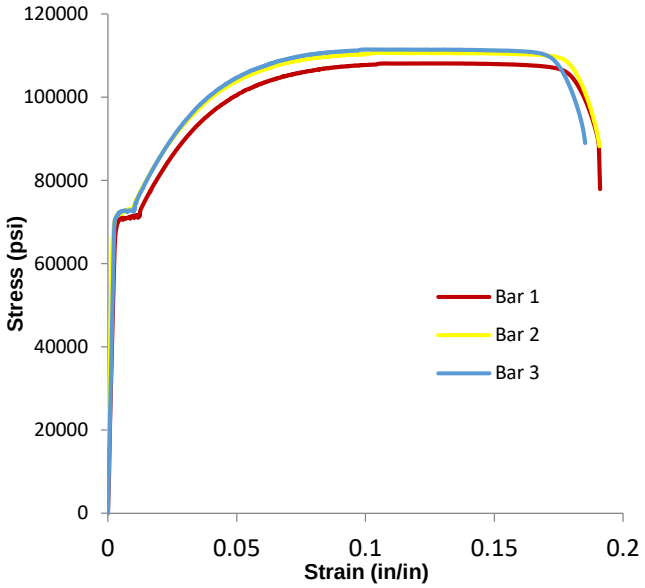

Figure 5-1 Stress vs. Strain for rebar in B, BC, and D panels

5.2 Full-scale Test Results

5.2.1 Load vs. Deflection for Entire Data Set

All loads shown herein include self-weight, and all deflections include deflection due to self-weight as measured by a total station. Figure 5-2 presents the load versus deflection plot for A-2 and A-4 panels. The maximum loads attained by the two panels were considerably different. The maximum loads attained were 30% different (compare 463 psf to 333 psf in Figure 5-2). Observed slip at the maximum load in the A-4 panel was 0.167 inches, whereas the slip at maximum load observed in the A-2 panel was 0.24 inches at failure. Clearly the shear tie intensity, at the level tested in these two panels, had a large effect on maximum load and slip.

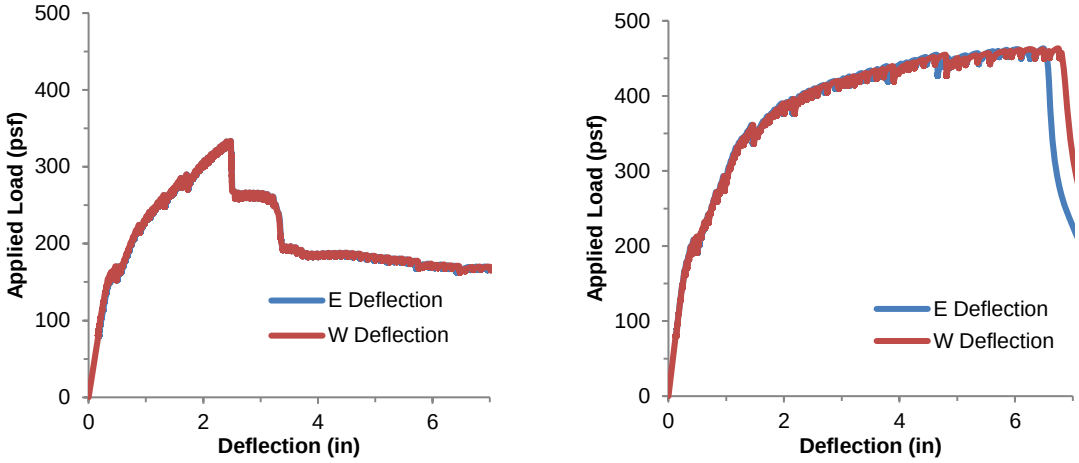

Figure 5-2 Load vs Deflection for A-2 (left) and A-4 (right)

The load vs. deflection results of B-1 and B-2 panels are presented in Figure 5-3. The maximum loads for these panels were also very similar with a difference of only 13% (comparing 355 psf for B-1 and 307 psf for B-2 in Figure 5-4). The amount of slip measured in the panels at maximum capacity was 0.74 in.

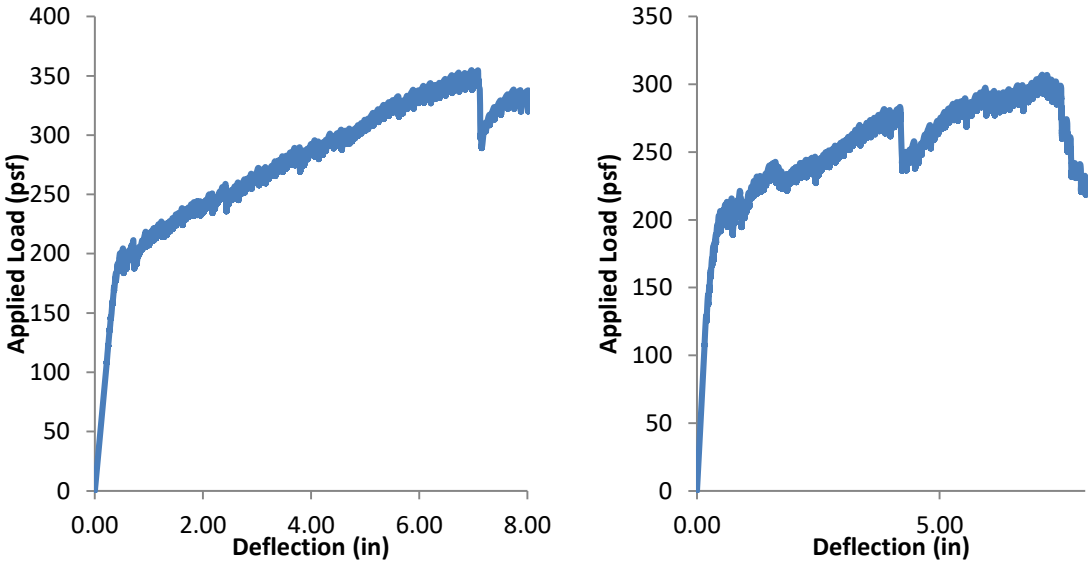

Figure 5-3 Load vs. Deflection for elastic only for B-1 (left) and B-2 (right) panels

The load vs. deflection results of BC-1 and BC-2 panels are presented in Figure 5-4. The maximum loads for these panels were also very similar with a difference of only 8% (comparing 528 psf for BC-1 and 485 psf for BC-2 in Figure 5-4). The amount of slip measured in the panels at maximum capacity was 0.05 in.

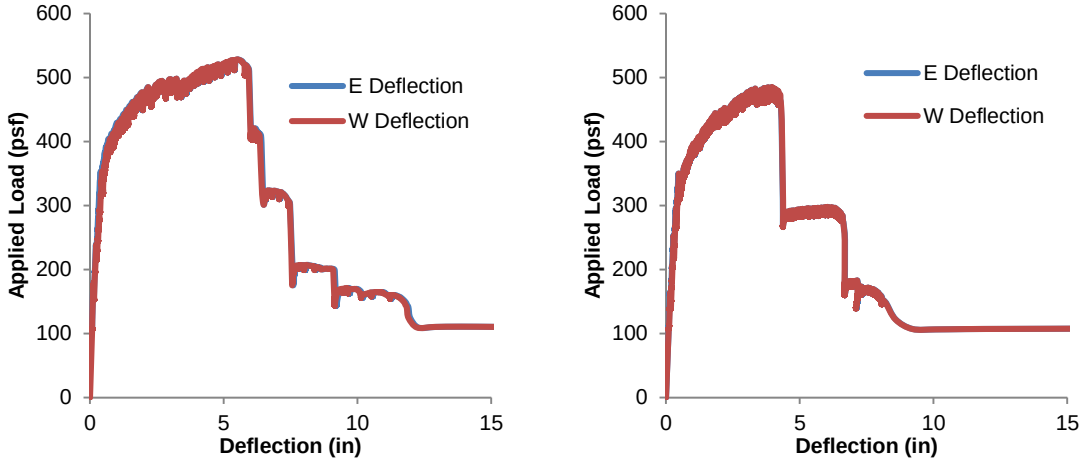

Figure 5-4 Load vs. Deflection for BC-1 (left) and BC-2 (right) panels

Figure 5-5 presents the Load versus Deflection plots for the D-1 and D-2 panels. The maximum loads attained by the two panels were similar. The maximum loads attained had only a 6% difference (comparing 529.5 psf to 498.8 psf in Figure 5-5). The amount of slip measured in the panels at maximum capacity was 0.08 in. in both panels.

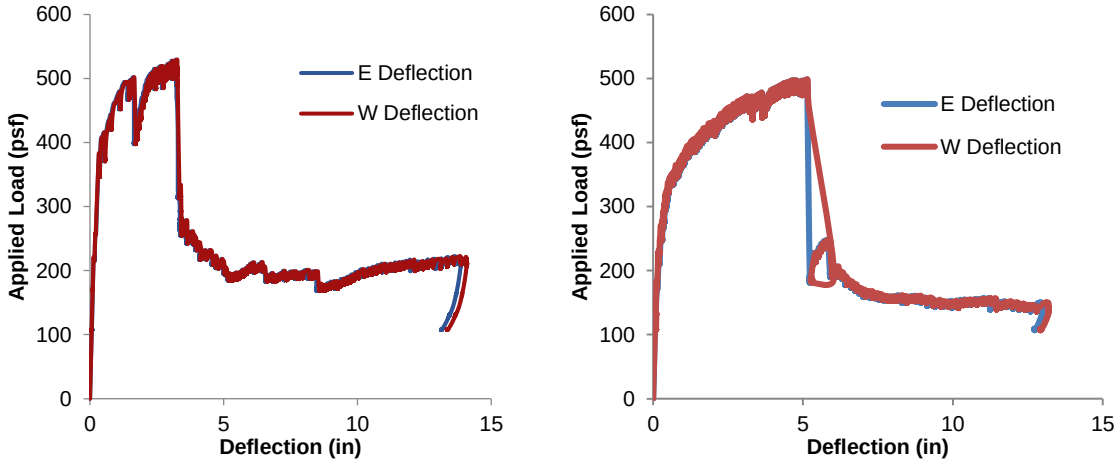

Figure 5-5 Load vs Deflection for D-1 (left) and D-2 (right) panels

The maximum loads and slip values are also summarized numerically later in Table 5-2 of Section 5.2.3.

5.2.2 *Load vs. Deflection for Elastic Only*

Figure 5-6 through Figure 5-9 show the load vs deflection for the elastic only.

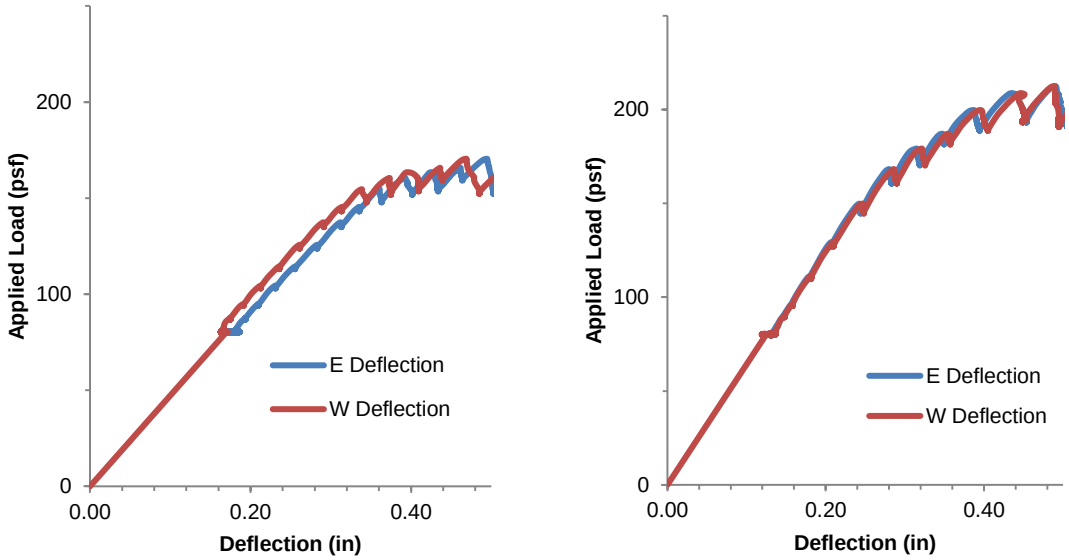

Figure 5-6 Load vs Deflection for elastic only for A-2 (left) and A-4 (right)

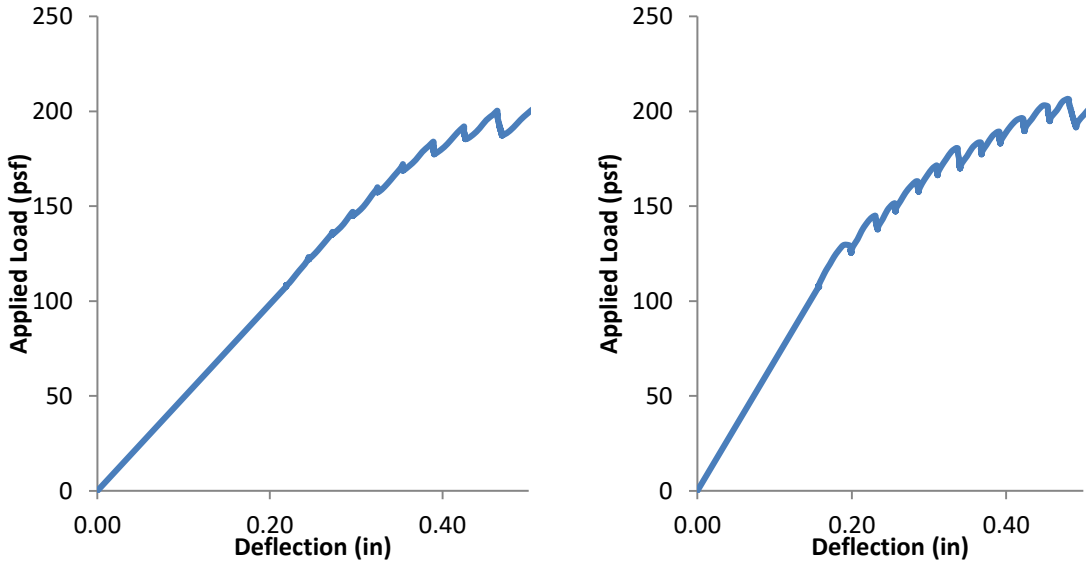

Figure 5-7 Load vs. Deflection for elastic only for B-1 (left) and B-2 (right) panels

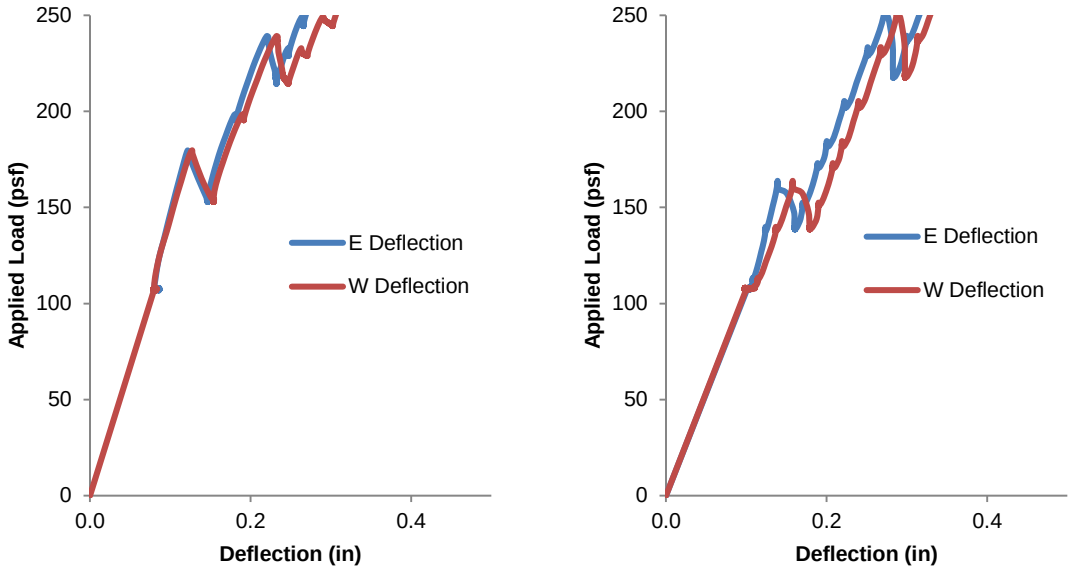

Figure 5-8 Load vs. Deflection for elastic only for BC-1 (left) and BC-2 (right) panels

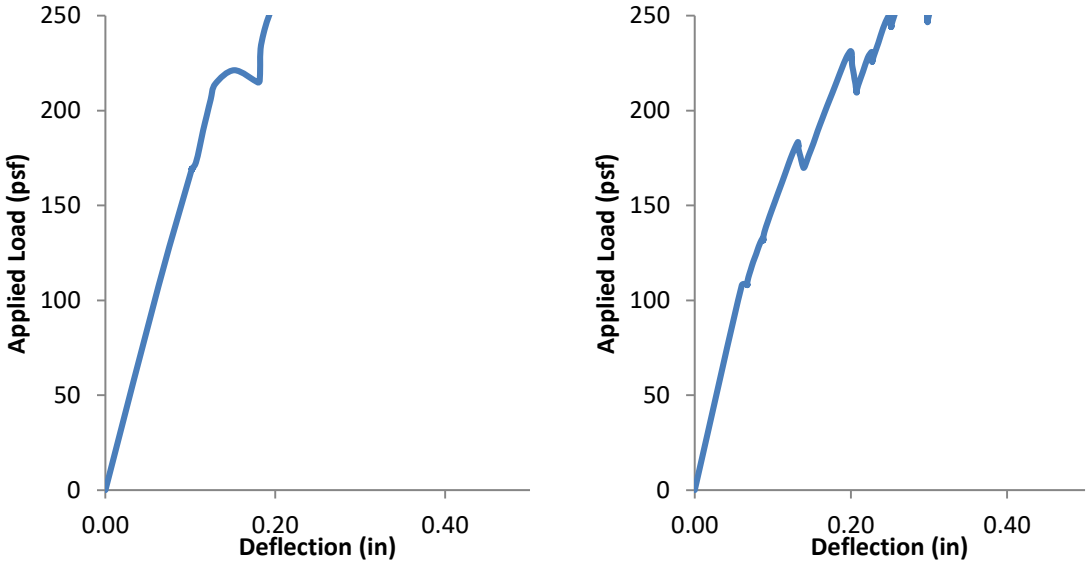

Figure 5-9 Load vs Deflection for elastic only for D-1 (left) and D-2 (right) panels

5.2.3 *Load vs. Slip for Entire Data Set*

Slip of the wythes was measured during testing to calculate the composite action within each panel. Table 5-2 summarizes the maximum loads and slips measured for all tested panels.

Table 5-2 Full-Scale Specimen Panel Test Results

Specimen	**Wythe configuration** *(in)*	**Span length** *(ft)*	**Maximum Load** *(psf)*	**Slip at Maximum Load** *(in)*
A-2	3-4-3	15.0	334	0.26
A-4	3-4-3	15.0	463	0.18
B-1	4-3-4	14.0	355	0.74
B-2	4-3-4	14.0	307	0.74
BC-1	4-3-4	14.0	528	0.11
BC-2	4-3-4	14.0	485	0.05
D-1	4-3-4	14.0	530	0.08
D-2	4-3-4	14.0	499	0.08

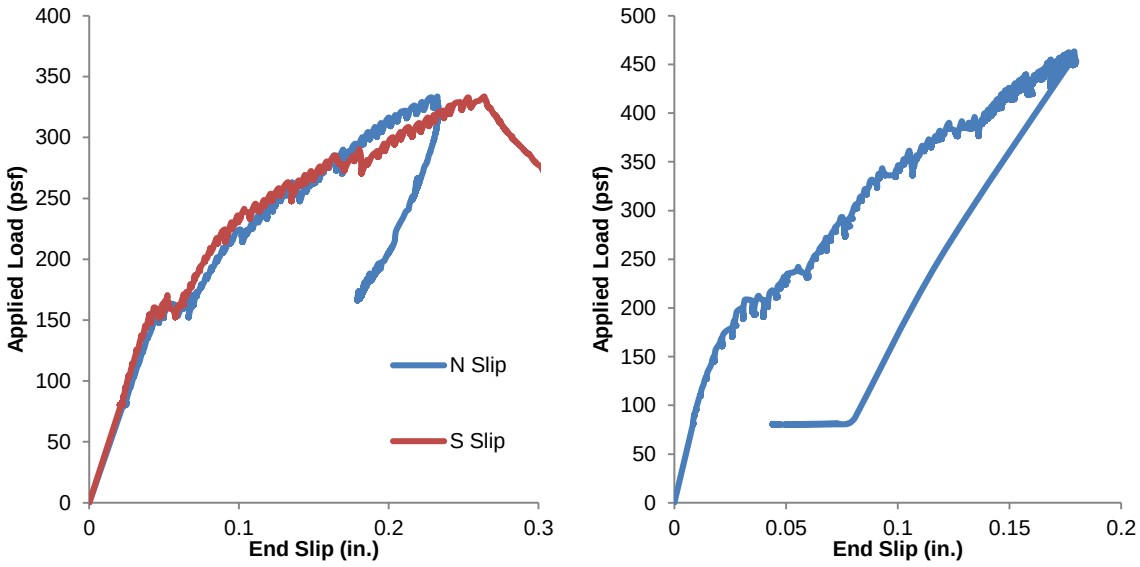

Figure 5-10 Load vs. slip for A-2 (left) and A-4 (right) panels

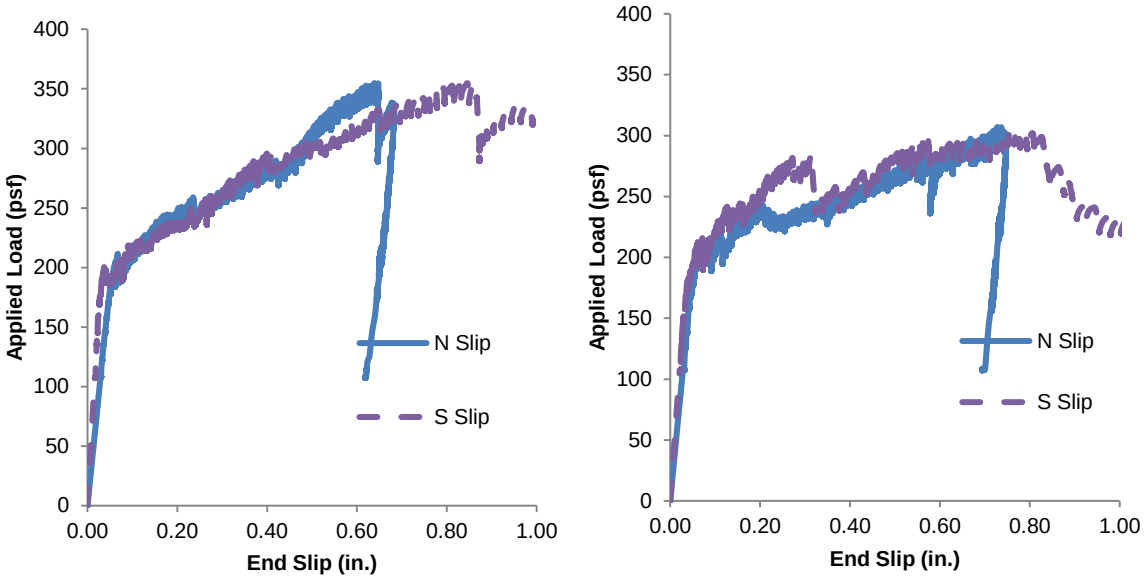

Figure 5-11 Load vs. slip for B-1 (left) and B-2 (right) panels

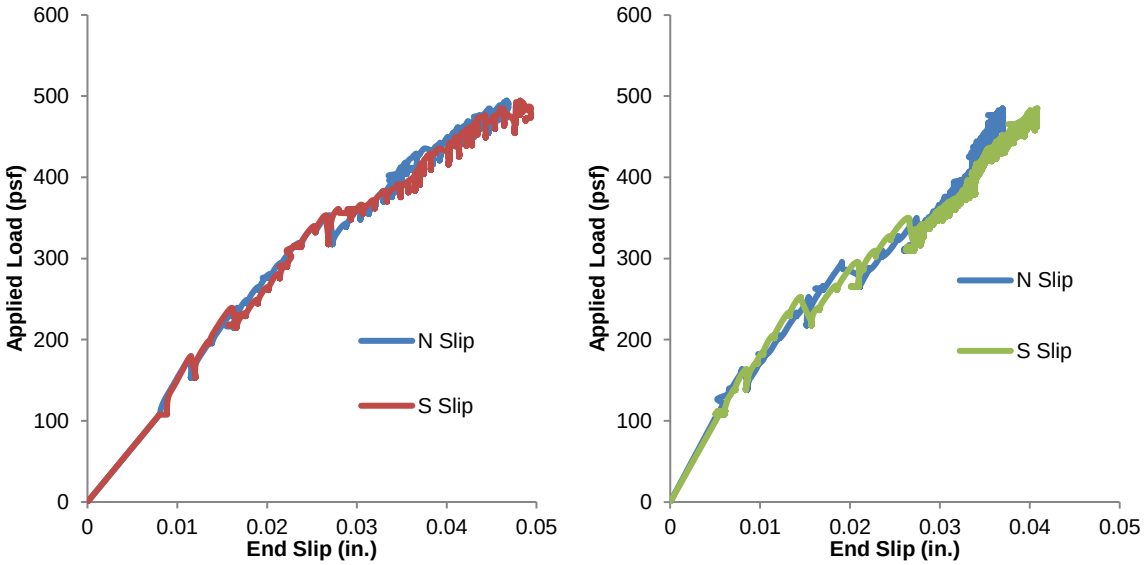

Figure 5-12 Load vs. slip for BC-1 (left) and BC-2 (right) panels

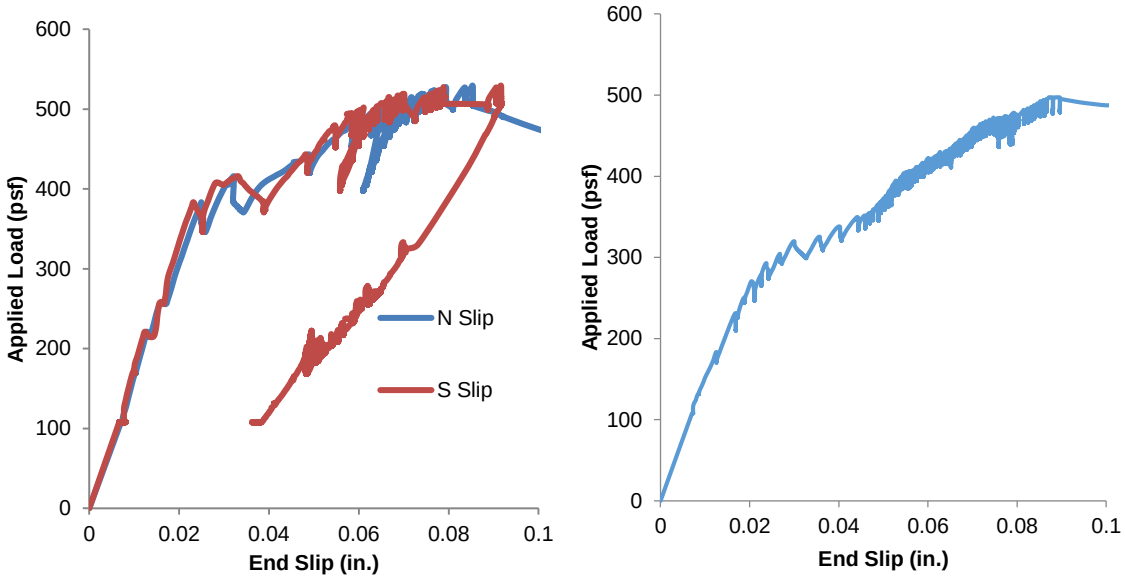

Figure 5-13 Load vs. slip for D-1 (left) and D-2 (right) panels

5.2.4 Composite Action Results

Utilizing the theoretical fully-composite moment, theoretical non-composite moment, and the actual measured moment from the test results, the degree of composite action, K_{Mn}, can be determined as shown in for different panels using Eq. (5-1).

$$K_{Mn} = \frac{M_{n,test} - M_{n,NC}}{M_{n,FC} - M_{n,NC}} \qquad (5\text{-}1)$$

Where Mn_{test} = experimental maximum moment of the sandwich panel

Mn_{NC} = theoretical maximum moment of the non-composite sandwich panel

Mn_{FC} = theoretical maximum moment of the fully-composite sandwich panel

For the degree of composite action depending on cracking moment using Eq. (5-2).

$$K_{Mcr} = \frac{M_{cr,test} - M_{cr,NC}}{M_{cr,FC} - M_{cr,NC}} \qquad (5\text{-}2)$$

Where Mcr_{test} = experimental cracking moment of the sandwich panel

Mcr_{NC} = theoretical cracking moment of the non-composite sandwich panel

Mcr_{FC} = theoretical cracking moment of the fully-composite sandwich panel

For the degree of composite action depending on deflection using Eq. (5-3).

$$K_d = \frac{I_{test} - I_{NC}}{I_{FC} - I_{NC}} \qquad (5\text{-}3)$$

Where I_{test} = experimental moment of inertia the sandwich panel

I_{NC} = theoretical moment of inertia of the non-composite sandwich panel

I_{FC} = theoretical moment of inertia of the fully-composite sandwich panel

Figure 5-14 graphically demonstrates the degree of composite action shown in Eq. (5-1), (5-2), and (5-3).

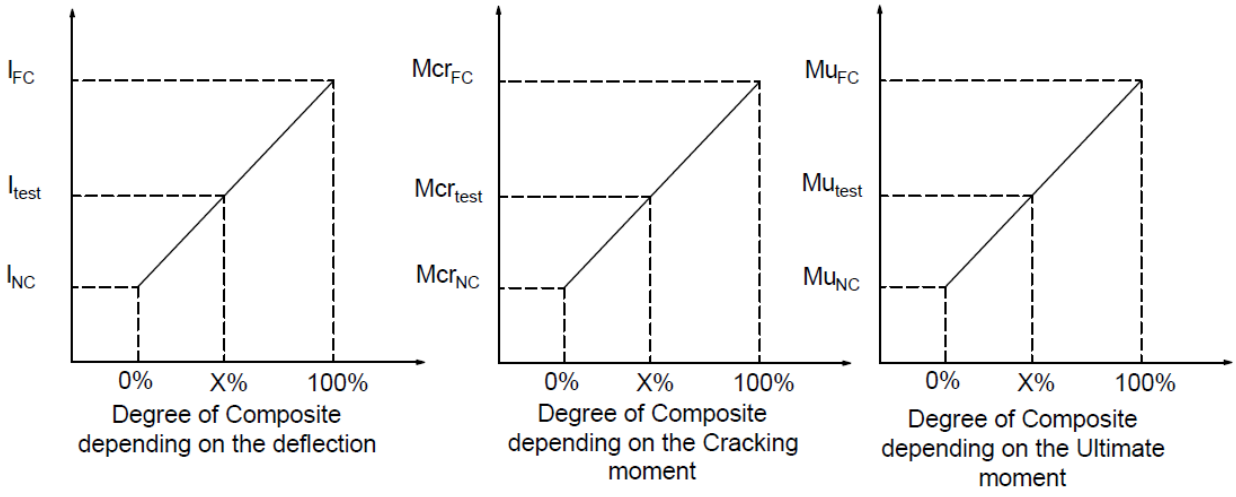

Figure 5-14 Visual demonstration of degree of composite action

Table 5-3 presents the midspan moment comparisons for the full-scale panels. The measured maximum moments of the sandwich panels were used to evaluate the composite action achieved. The measured maximum moment was calculated at midspan, using the self-weight of the panel (a distributed load) and the four point loads. The fully-composite nominal moment was calculated using strain compatibility and actual material properties for the concrete and steel as presented above, assuming the entire cross section was active. The non-composite moment strength was calculated in the same manner using only the properties of a single wythe and multiplying by two.

Table 5-3 Measured vs. Manufacturer-reported composite action for maximum moment

Specimen	**M_{nFC} (lb*ft)** *(lb*ft)*	**M_{nNC} (lb*ft)** *(lb*ft)*	**Measured Composite Action** *(%)*	**Manufacturers Reported Composite Action** *(%)*
A-2	55,000	15,800	70%	-*
A-4	55,000	15,800	115%	100%
D-1	44,100	12,800	104%	80%
D-2	43,400	12,200	97%	80%
BC-1	44,100	12,800	103%	70%
BC-2	43,400	12,200	93%	70%
B-1	44,100	12,800	41 %	-*
B-2	43,400	12,200	57 %	-*
* Purposely reinforced lower than usual – not a typical panel				

The A-4 panel resulted in 115% composite action. Other programs have noticed over 100% in the past, which is likely due to material variability as it would be impossible for a panel to be stronger than theoretically composite. Had the manufacturer designed this panel, it would have been designed at 100% composite. The A-2 panel would not have been a design coming from the manufacturer, but was prepared to demonstrate what would come from under-detailing such a panel. Doubling the number of connectors resulted in a 30% increase in composite action at ultimate.

The Connector B panels had a lower connector number due to manufacture error. This resulted in an average of 50% composite action, and is not realistic of actual design used in the field.

The Connector BC panels resulted in a composite action of 103% and 93% (Table 5-3). However, the manufacturer would recommend only 70% composite action at nominal strength for these connectors

The D-1 and D-2 panels at the as-built 16 in. spacing would have resulted in a panel designed at 80% composite action per manufacturer recommended guidelines. Both panels achieved far more that 80% composite (see 104% and 97% in Table 5-3).

From the panels tested with the recommended connectors, it is clear that the manufacturer recommended empirically based composite actions are accurate and conservative.

5.3 Conclusions

Eight concrete sandwich panels were tested to failure at the Utah State University Structures Lab. The purpose of the testing was to evaluate the percent composite action for the connector configurations and compare the results to those reported by composite connector manufacturers. The following conclusions can be made from the experimental program:

- The type and intensity of shear connectors significantly affect the degree of composite action achieved in a concrete sandwich panel wall. Doubling the number of shear connectors in the Connector A panels (Nu-Tie connector) resulted in a large gain in percent composite action. (Note that the A-2 panel is reinforced much lighter than would be detailed for an actual building)
- The manufacturer-reported degree of composite action can be considered conservative for the panel configurations and connectors and connector patterns tested in this paper.

6 PREDICTING ELASTIC BEHAVIOR

Predicting concrete sandwich panel elastic stresses and deformations is paramount for design to prevent cracking and limit second order effects. Several researchers have developed techniques to predict sandwich panel deformations (e.g. Bunn 2011; Frankl et al. 2011; Bai and Davidson 2015; Woltman et al. 2013). Prediction methods vary significantly in complexity and accuracy. This section presents two proposed methods that were developed and used during this testing that may give engineers a quick and accurate prediction of the elastic behavior of PCSWPs in the future: the Beam-Spring Model, and the proposed Elastic Hand Method.

6.1 Beam-Spring Model

The first model investigated was an analytical model created using a commercial matrix analysis software package and is a more general variation of what many connector manufacturers do currently using usually specialized techniques for their connector shape/configuration. This model could easily be replicated using any commercial or personally written matrix analysis software, and could also be easily built into commercial wall panel analysis and design software and should work for any connector type. This approach modeled the PCSWP using only beam and spring elements (Figure 6-1) combined with the appropriate material values, boundary conditions, and shear connector stiffnesses (attained from the tested push-off specimens discussed earlier in Chapter 4). Other research programs (e.g., modified truss [Pantelides et al. 2008] and beams and springs [Teixeira et al. 2016]) have described similar methods using matrix software. This concept has been around for decades when discussing multi-wythe masonry (Drysdale, Hamid, and Baker 1994). Many connector manufacturers use a truss analysis with matrix software, usually a Vierendeel truss, but some angled connectors, like Connector A (Nu-Tie connector), use angled truss elements. The purpose of developing a simple model that relies only on springs and beam elements is that it can be used to model a panel with any connector type, repetitively, with little to no change between analyses, and relies only on shear testing data, which most connector companies already have from ICC-ES acceptance criteria, specifically ICC-ES AC320 and ASTM E488-96.

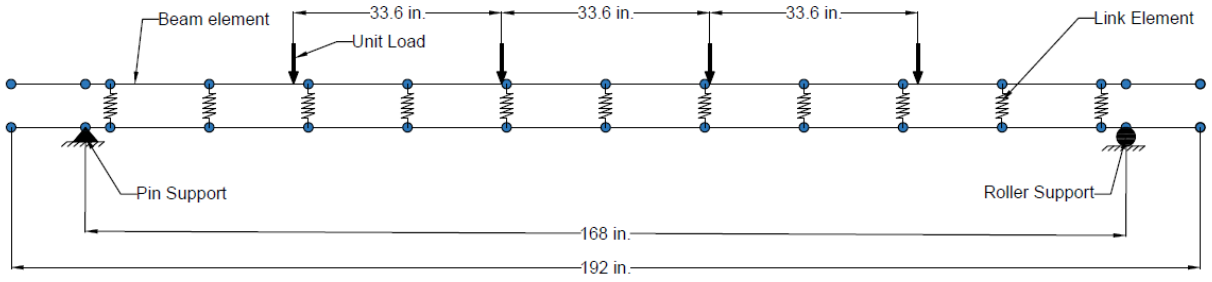

Figure 6-1 Example of Full-scale specimen modeled using the Beam-Spring Model

The proposed two-dimensional model consists of two frames with cross-sectional areas equal to the area of the wythes of the panel they represent. These beam elements can be assigned the individual gross properties of each wythe and separated by a distance equal to the distance between the centroids of the wythes. Shear and axial spring elements are then used to model the transfer of shear force between wythes, and are assigned shear stiffnesses corresponding to the actual stiffnesses of the connectors as measured in the previous sections. Support conditions are modeled as pin (translation fixed, rotation free) and roller (longitudinal translation free, transverse translation fixed, rotation free) and should be placed at the appropriate location on the panel.

To verify this method, each test specimen was modeled from the previous chapter, and elastic deflections and stresses were compared to the test results. Because each test specimen had a different connector configuration and spacing, links connecting the beam elements were placed at locations corresponding to each of the shear connectors. The values of shear stiffness, K_E, used in each model are shown in Table 6-1. These shear connector stiffnesses from the push-off tests included both the stiffness of the connector and the lumped insulation stiffness. For design, it may be prudent to use the unbonded values, but to verify the accuracy of the panels in this study the bonded values for K_E were used.

Table 6-1 Panel Properties

Panel	**Width** *in.*	**Configuration** *in.*	**Span** *in.*	**Modulus of Elasticity of Concrete** *psi*	**Split Tension of Concrete** *psi*	**Connector Stiffness (K_E)** *kips/in*	**Modulus of Elasticity of Insulation** *psi*
A-2	48	3-4-3	180	6,191,000	766	118	670
A-4	48	3-4-3	180	6,191,000	766	118	670
B-1	36	4-3-4	168	5,824,000	691	17.9	670
B-2	36	4-3-4	168	5,986,000	699	17.9	670
BC-1	36	4-3-4	168	5,824,000	691	17.9 205	670
BC-2	36	4-3-4	168	5,986,000	699	17.9 205	670
D-1	36	4-3-4	168	5,824,000	691	94.8	670
D-2	36	4-3-4	168	5,986,000	699	94.8	670

The model included four point loads applied to the top face of the model, imitating the full-scale testing performed in this study. In addition, self-weight was added to the total load. Links were also assigned longitudinal stiffnesses based on the tributary geometry and on an assumed Young's modulus of XPS insulation (since XPS was the only insulation used for the full-scale specimens). Tension/compression values for the connectors were not measured in this study, but most connector companies have tension testing performed according to ICC-ES AC320. With this model, the deformations and deflections were easily predicted along with axial forces and bending moments in the concrete wythes, which can be resolved into stresses. The results will be discussed in Section 6.3.

6.2 Elastic Hand Method Analysis Procedure

6.2.1 Elastic Hand Method Description

The proposed Elastic Hand Method for predicting deflections and cracking requires a sectional analysis as well as a full member analysis in order to incorporate panel geometry and connector forces. This method was based on the following assumptions:

1. Standard Euler-Bernoulli beam theory applies to the individual wythes (i.e. plane sections remain plane and normal to the deflected axis)
2. Linear elastic material behavior (including the shear connectors).

3. The Principle of Superposition is valid

4. The slip varies linearly along the length of the panel as shown in Figure 6-2. This implies that the shear forces will vary linearly too if the connectors are identically distributed. This is not always true, but is a reasonable simplification as will be demonstrated below.

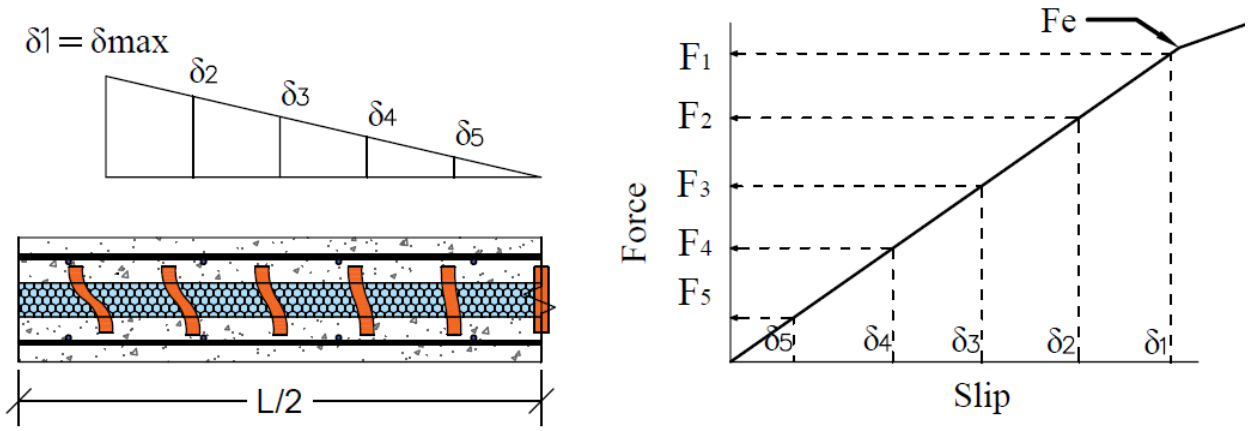

Figure 6-2 Slip Diagram along the length of the panel

Using the above assumptions, the engineer must perform an iterative procedure due to the nature of determining slip for various connector patterns. Once the connector force is determined based on the end slip, a sectional analysis is performed for the controlling wythe (the cracking wythe) and deflections can be easily determined using elastic beam equations. The guessed slip will need to be checked using slip kinematic relationships, but this is accomplished using familiar mechanics equations and equivalent loads.

6.2.2 Elastic Hand Method Procedure

The cracking moment and deflection predictions of the Elastic Hand Method depend mainly on the section geometry, modulus of rupture of the concrete, the elastic modulus, and the connector forces. For the purposes of discussion, wythe 1 is considered the wythe that would be in compression during positive bending of a fully-composite sandwich panel and wythe 2 is considered the wythe that would be in tension during positive bending of a fully-composite sandwich panel. The following steps comprise the procedure for the Elastic Hand Method.

1. Calculate the material and section properties assuming the sandwich panel acts non-compositely. The following equations are an example. These may vary depending on the type of reinforcement.

$$E_c = 33.0 * \gamma^{1.5} * \sqrt{f'c} \quad (6\text{-}1)$$

$$f_r = 7.5 * \sqrt{f'c} \quad (6\text{-}2)$$

$$I_{NC1} = \frac{bt_{wy_1}^3}{12}$$

$$I_{NC2} = \frac{bt_{wy_2}^3}{12} \quad (6\text{-}3)$$

$$Z = \frac{t_{wy_1} + t_{wy_2}}{2} + t_{insul} \quad (6\text{-}4)$$

Where E_c = modulus of elasticity of the concrete (psi)

γ = unit weight of the concrete (pcf)

f_c' = concrete compressive strength (psi)

f_r = modulus of rupture of concrete (psi)

I_{NC1} = moment of inertia of non-composite wythe 1 (in^4)

I_{NC2} = moment of inertia of non-composite wythe 2 (in^4)

b = slab width (in)

t_{wy1} = thickness of wythe 1 (in)

t_{wy2} = thickness of wythe 2 (in)

Z = distance between compression and tension wythe centroids (in.)

t_{insul} = insulation thickness (in)

2. Assume an end slip, which is the slip at the end connector line (see Figure 6-2). Calculate the slips in the other connectors using similar triangles or Eq. (6-5).

$$\delta(i) = \delta_{max} * \frac{\left(\frac{L}{2} - x_i\right)}{\left(\frac{L}{2} - x_1\right)} \qquad (6\text{-}5)$$

Where $\delta(i)$ = slip in connector i (in)

δ_{max} = Slip in the end connector (in), also assumed to be the max. slip in the panel

L = total length of the sandwich wall panel (in)

x_i = location of the connector from the end of the panel (in)

3. Calculate the forces in each connector and connector line using Equations (6-6) and (6-7).

$$F_i = \delta(i)\, N_i * K_E \qquad (6\text{-}6)$$

$$F_{sum} = \sum F_i \qquad (6\text{-}7)$$

Where $F(i)$ = is the force in connector line i (in)

N_i = is the number of connectors in connector line i

K_{Ei} = is the elastic stiffness from shear testing for the connectors in connector line i

F_{sum} = is the sum of the connector forces at the longitudinal location of interest

4. Calculate the cracking moment for a mild reinforced non-composite wythe (assuming wythe 2 will crack before or simultaneously with wythe 1) as shown below, with appropriate addition of prestressing forces if necessary (not shown), and including the axial force generated by the connector forces from Equation (6-7) and as demonstrated by Figure 6-3:

$$\frac{M_{wy_2} * \frac{t_{wy_2}}{2}}{I_{NC2}} + \frac{F_{sum}}{b * t_{wy_2}} = f_r$$

$$M_{wy_2} = 2 * I_{NC2} * \left(\frac{f_r}{t_{wy_2}} - \frac{F_{sum}}{b * {t_{wy_2}}^2}\right) \qquad (6\text{-}8)$$

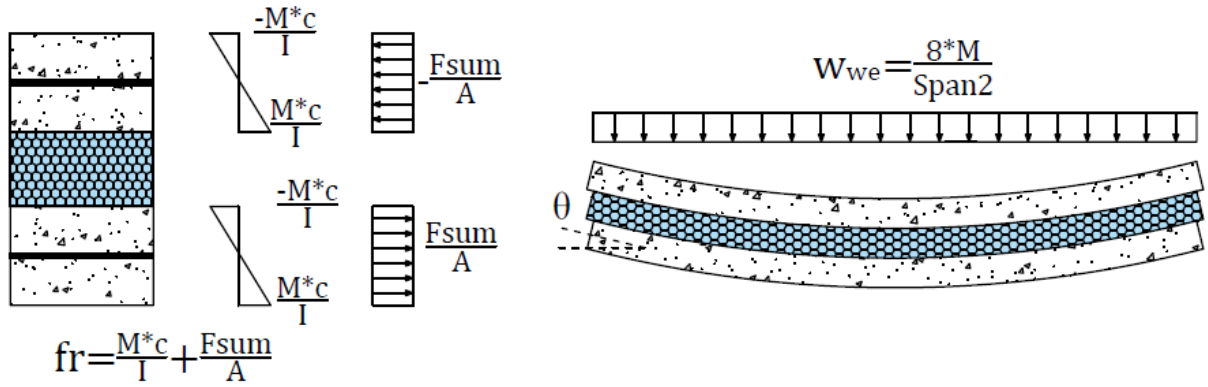

Figure 6-3 Load and stress profile of sandwich panel (left) equivalent load (right)

5. Now, the applied load that causes this cracking moment can be back calculated which will aid in determining deflections and rotations. Calculate the equivalent load that wythe 2 can carry using equations (6-8) and (6-9). Figure 6-3 shows the stress profile and the equivalent distributed load to produce the cracking moment in a reinforced concrete section. An equivalent load can be a distributed load, a point load, four point loads etc. depending on load condition. Equation (6-9) demonstrates the equivalent distributed load for the moment carried by only the bottom wythe at cracking assuming the wythes share load equally ($t_{wy1} = t_{wy2}$).

$$M_{wy_2} = \frac{w_{we2} Span^2}{8}$$

$$w_{we2} = \frac{8 * M_{wy_2}}{Span^2} \qquad (6\text{-}9)$$

To determine if the above assumption of slip is correct, the slip needs to be recalculated for verification. This iteration is deemed necessary only because solving for the slip (in a closed form) directly is very cumbersome (but possible). Slip calculation is accomplished by finding the different components of slip (axial and rotational, see Figure 6-4) at the end connector line and comparing it to the assumptions using the equivalent load above. For additional accuracy, the same process could be used at each connector line (with additional iteration), but will be shown to be unnecessary with respect to accuracy.

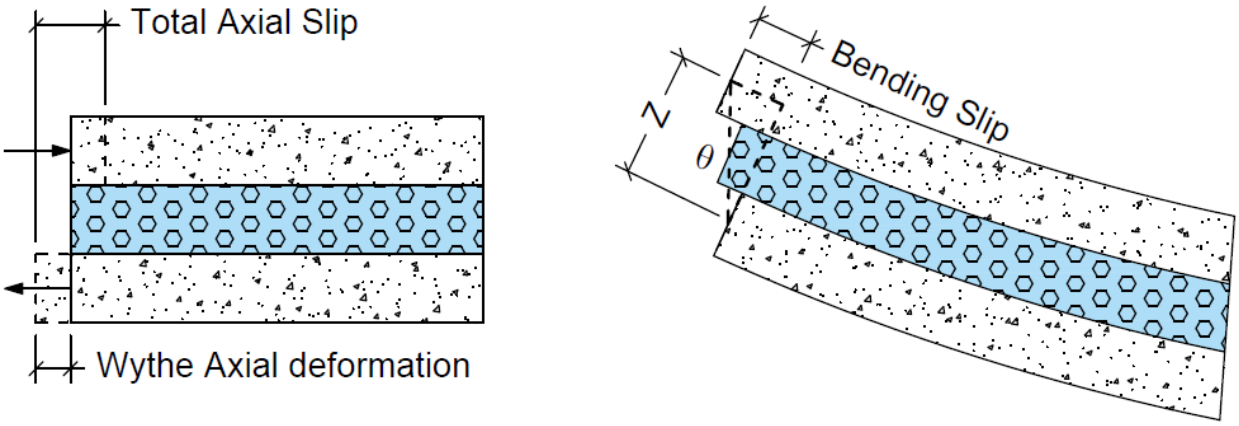

Figure 6-4 Axial and Bending Slip

6. Using the equivalent load from the previous step, calculate axial and rotational displacement at the end connector. Rotation (θ) of the wythe at the end connector location can be calculated using published equations (available in the PCI Design Handbook) or an elastic structural analysis method (e.g. Castiglione's Theorem, Virtual Work) for the applied load (e.g., distributed, point loads). For this explanation, it is assumed a distributed load is most common and is presented in Equation (6-10). Equation (6-10) uses the moment of inertia of only wythe 2 and the equivalent load calculated in the previous step for wythe 2.

$$\theta = \frac{w_{we2} * Span^3}{24 * E * I_{NC2}} \qquad (6\text{-}10)$$

$$\Delta_{Rot} = \theta * Z \qquad (6\text{-}11)$$

Where w_{we} = equivalent distributed load of the wythe (lb/in)

θ = angle of rotation (radians)

Span = support to support distance (in)

Δ_{Rot} = slip of the wythes due to bending (in) at the end connector

n = total number of connector rows on *L*/2

To calculate the axial slip, one must account for each of the connector forces along the beam based on the assumed slip distribution. Then the axial forces from the connectors combined with their locations on the panel are used with the well-known elastic axial deformation equation (*PL*/*AE*) for both wythes. This process is demonstrated in Figure 6-5 for a single wythe. Equation (6-12) below could be simplified for direct solution of standard connector patters (e.g., uniform, triangular) if desired.

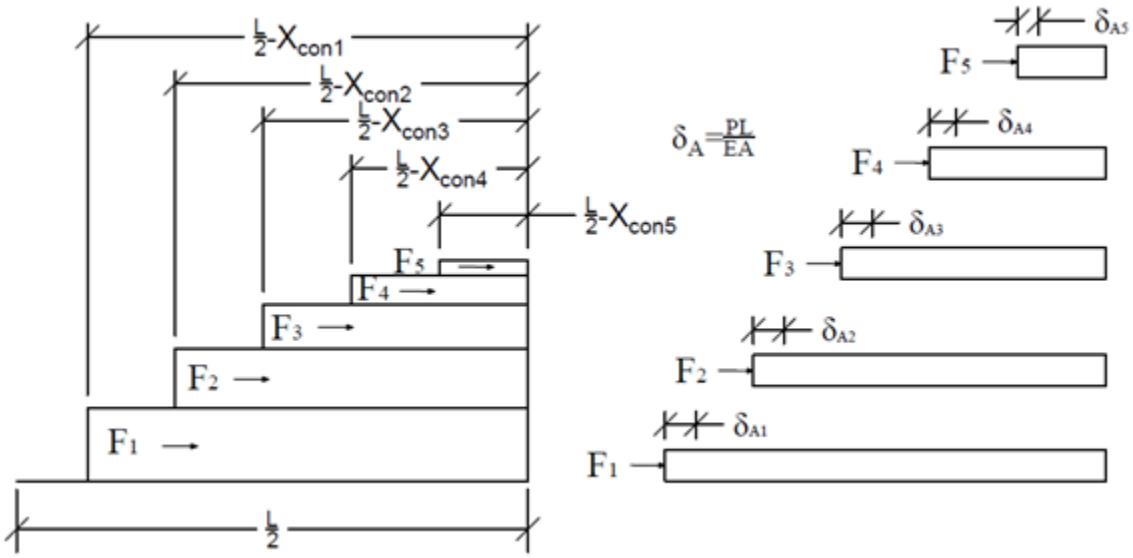

Figure 6-5 Axial slip

$$\Delta_{Axial} = \left[\left(\frac{1}{b * E * t_{wy_1}}\right) + \left(\frac{1}{b * E * t_{wy_2}}\right)\right] * \sum_{i=1}^{n} F_i * \left(\frac{L}{2} - x_i\right) \qquad (6\text{-}12)$$

Where Δ_{Axial} = slip of the wythes due to axial deformation at the end connector (in)

n = total number of connector rows on $L/2$

i = connector line starting at the end of the panel

F_i = force in connector i (lb)

x_i = location of connector line i

7. Finally, using Equation (6-11) and (6-12), the slip at the end connector can be calculated as

$$\delta_{end} = \Delta_{Rot} - \Delta_{Axial} \qquad (6\text{-}13)$$

Total slip at every connector is the result of two components: the axial deformation and the bending slip, as shown in Figure 6-4. I may also be noted that the axial slip and the rotation slip act in different directions. Because they are calculated as absolute deformations in Equation (6-11) and (6-12), they lose their sign and Equation (6-13) requires the negative sign.

Compare this slip value to that assumed in Step 2, and repeat Steps 2 through 6 until δ_{end} assumed (Step 2) is equal to δ_{end} calculated (Step 6). This is most easily accomplished using a spreadsheet or computer program.

8. Calculate the cracking moment using equation (6-14).

$$M_{cr} = M_{wy_2} * 2 + F_{sum} * Z \qquad (6\text{-}14)$$

Where M_{cr} = applied moment (lb-in)

Calculate deflection using Equation (6-15) for a uniform distributed load. For different loading pattern, a different formula should be used.

$$\Delta = \frac{5 * w_{we2} * Span^4}{384 * E_c * I_{NC2}} \qquad (6\text{-}15)$$

Where Δ = predicted overall deflection of the midspan of the sandwich wall panel (in)

The above steps and explanation outline the approach using only first principles and equations most engineers are familiar with. Some examples of using this method for analysis are included in Appendix A. Below, this methodology will be checked against the experimental results in previous chapters which include panels with prestressing only, mild reinforcing only, different depths, different concrete strengths, different connectors, and different connector patterns. In theory, this method could also be used to predict behavior of panels with holes and at any location along the length of the panel, with some modifications.

6.3 Validation of the Beam-Spring Model and Elastic Hand Method

Predictions of cracking moment, deflection, and slip of the eight full-scale test panels were made using the Beam-Spring Model and Elastic Hand Method above, and then compared to the actual measured values to validate these predictions. Both methods returned very favorable results. Figure 6-6 presents the actual results and predictions of both models for the full-scale A-2 sandwich panel. In this figure and those similar in the following, the Beam-Spring and Elastic Hand Method (labeled as HM), are plotted up through cracking, which is the last point at which they are valid. In the plots, a slightly bi-linear relationship for the HM and the Beam-Spring model can be observed (which is counterintuitive for an elastic method) this is because the method was applied for a uniform load to simulate dead load and then four point loads (as it was tested).

Both models show excellent agreement with the observed behavior. The cracking moment differs only by 0.5% and 0.8% for the Beam-Spring Model and Elastic Hand method, respectively. Deflection at the cracking moment differs by 14% and 4% for the Beam-Spring model and Elastic Hand method, respectively. The actual slip of the A-2 panel was measured to be 0.05 inches, with the Beam-Spring Model predicting 0.045 inches and the Elastic Hand Method predicting 0.0423 inches. Furthermore, in the below figures, it is easy to see the experimental load deformation plots and the slip plots become non-linear just as the HM and Beam-Spring model predict cracking.

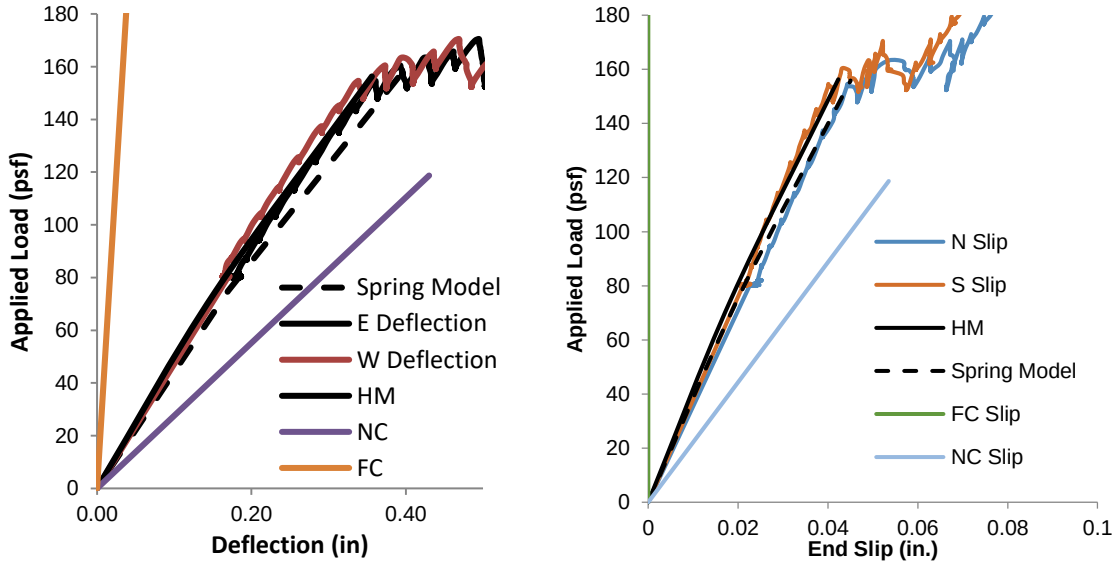

Figure 6-6 Load versus Deflection (left) and Load versus End Slip (right) for A-2 Panel

The Beam-Spring Model and the Elastic Hand Method underpredicted the cracking moment of the A-4 panel by 5% and 4% percent respectively. Figure 6-7 shows that the applied load at cracking was around 200 psf, which differed slightly from the predictions of both methods. Both methods overpredicted the slip in this specimen, the Beam-Spring Model doing so by 11% and the Elastic Hand Method by 14%.

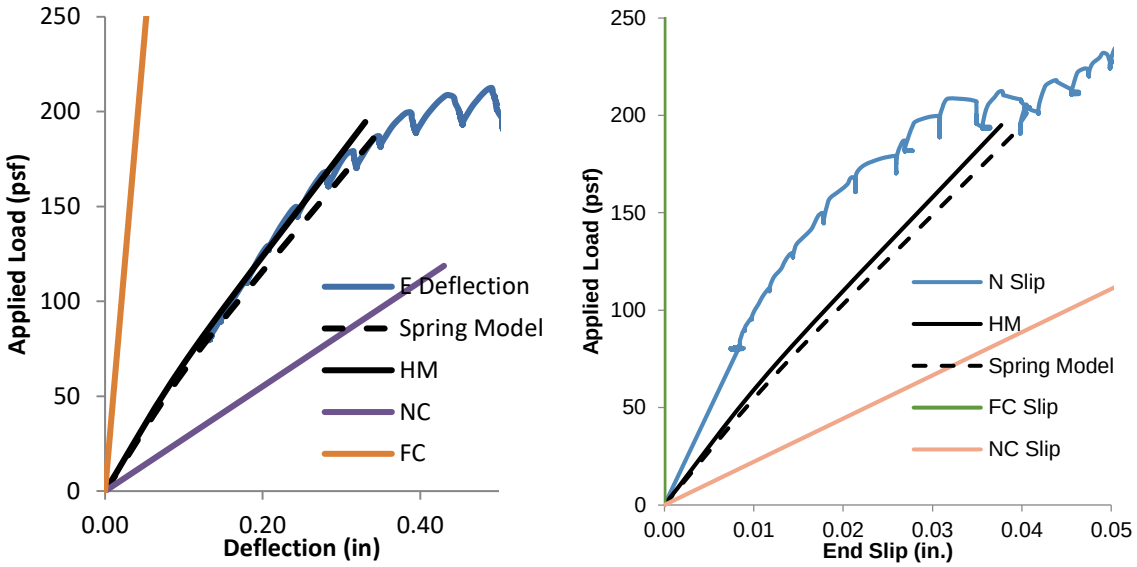

Figure 6-7 Load versus Deflection (left) and Load versus End Slip (right) for A-4 Panel

The Connector B specimens are included in this section only for completeness. The full-scale Connector B specimens were fabricated incorrectly and transported improperly, arriving to the USU facility cracked. As such, deflection and cracking predictions are not valid by the methods presented here and are not indicative of a real-life panel reinforced per manufacturer recommendations. The load vs. deflection and load vs. slip for the Connector B specimens are shown in Figure 6-8 and Figure 6-9. The Beam-Spring Model and Elastic Hand Method for this case predicted the same cracking load and slip values. A comparison of the actual values to the predicted values was not possible for these specimens since the panels had cracked during transportation.

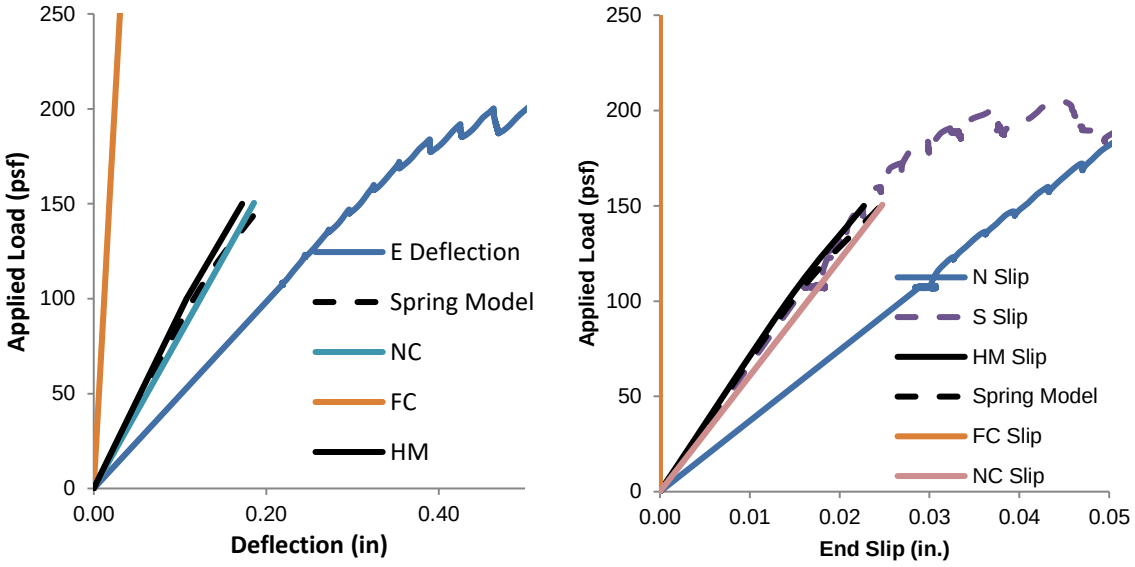

Figure 6-8 Load versus Deflection (left) and Load versus End Slip (right) for B-1 Panel

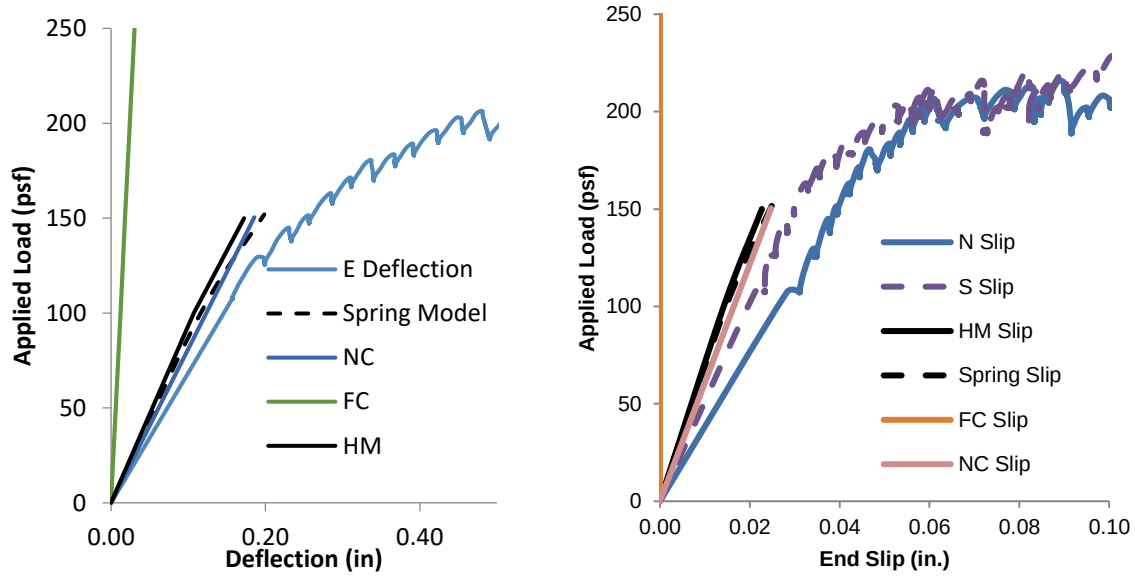

Figure 6-9 Load versus Deflection (left) and Load versus End Slip (right) for B-2 Panel

Both methods overpredicted the cracking load, the Beam-Spring Model by 10% and the Elastic Hand Method by 10% as shown in Figure 6-10 and Figure 6-11 for the BC-1 and BC-2 panels. The slip for the BC specimens was overpredicted by 80% for both methods.

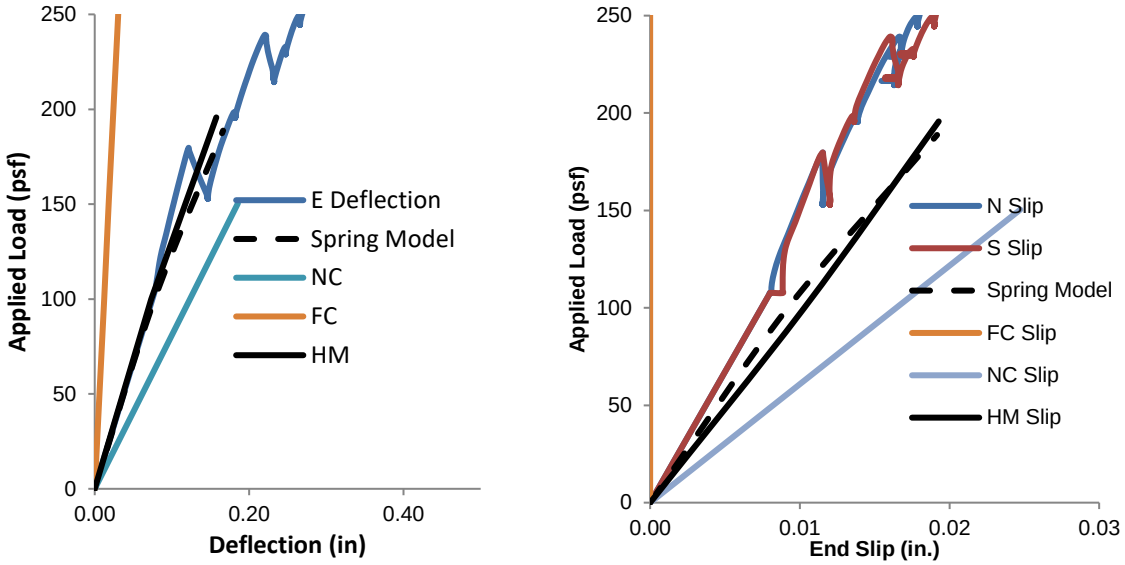

Figure 6-10 Load versus Deflection (left) and Load versus End Slip (right) for BC-1 Panel

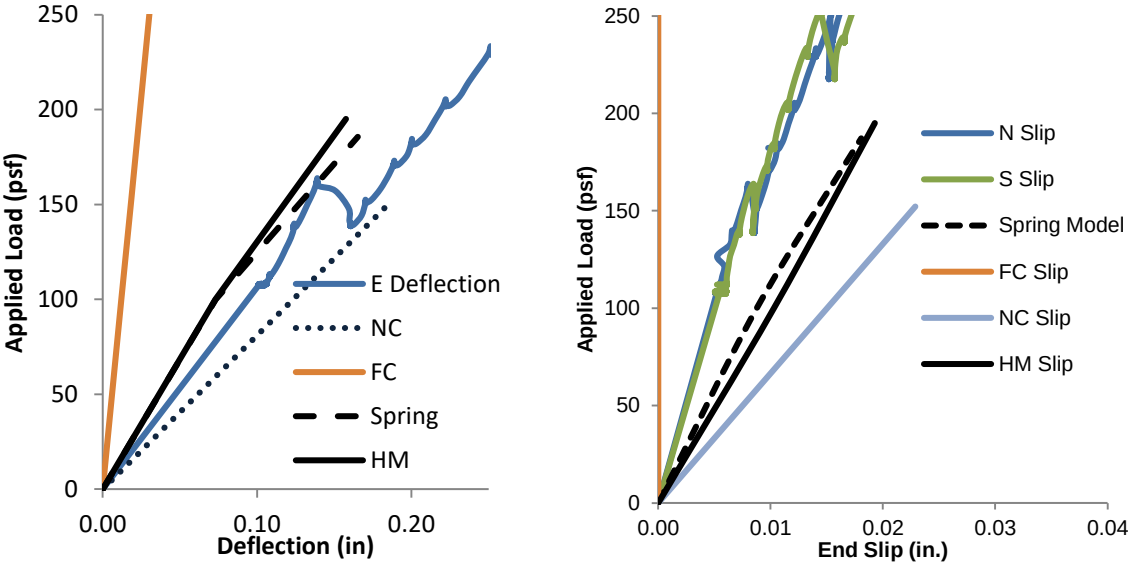

Figure 6-11 Load versus Deflection (left) and Load versus End Slip (right) for BC-2 Panel

Figure 6-12 and Figure 6-13 display the predicted values vs. the actual values for the D-1 and D-2 specimens. The cracking load predicted by the Beam-Spring Model matched the average result of the full-scale D panel specimens. However, the Elastic Hand Method overpredicted the cracking load by 9%. The Beam-Spring Model overpredicted the slip by 18%, and the Elastic Hand Method overpredicted the slip by 40%.

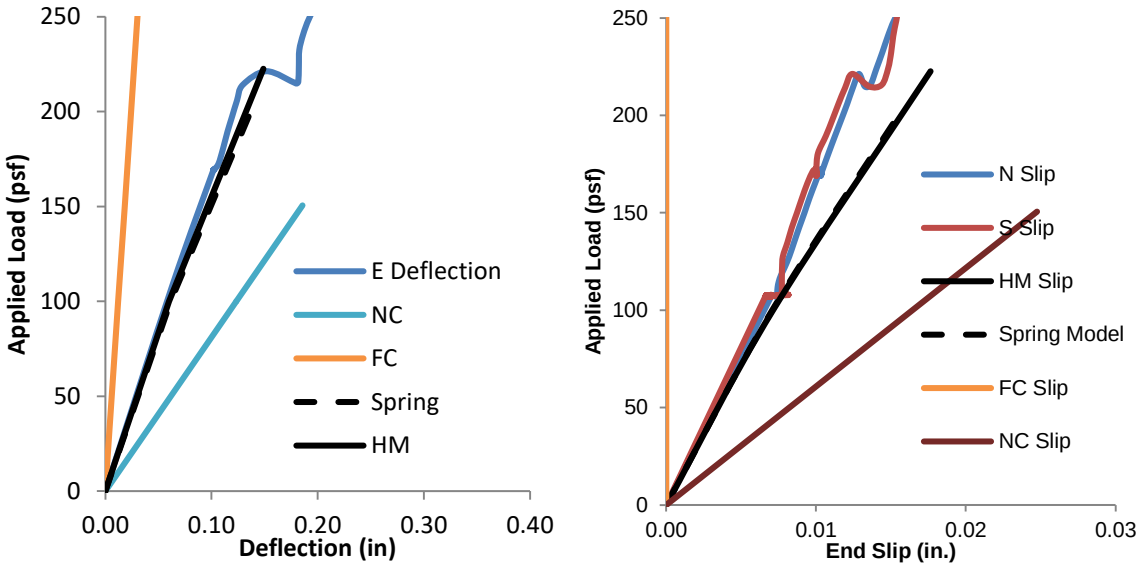

Figure 6-12 Load versus Deflection (left) and Load versus End Slip (right) for D-1 Panel

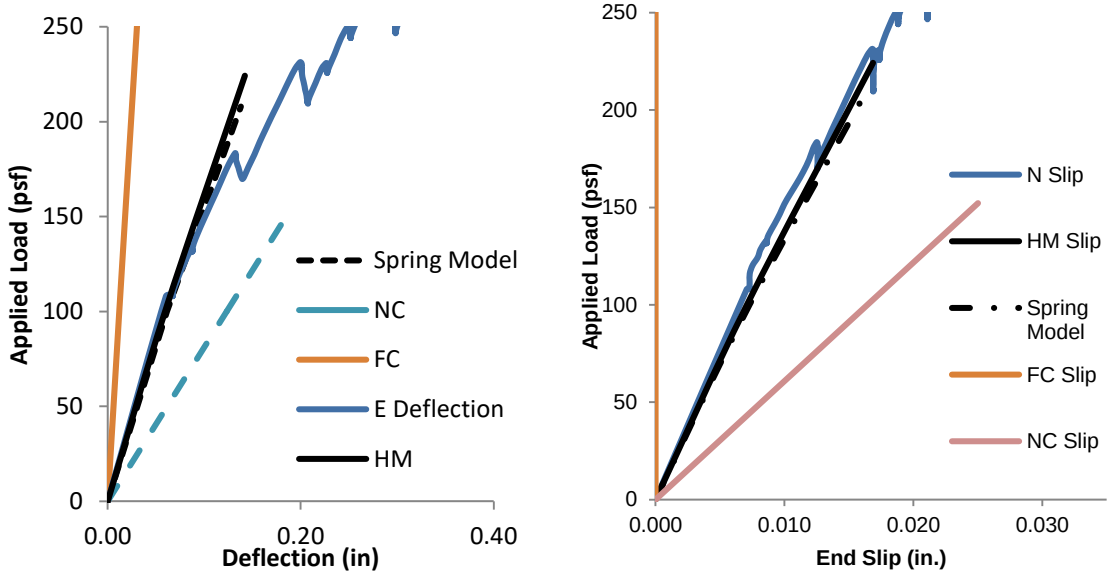

Figure 6-13 Load versus Deflection (left) and Load versus End Slip (right) for D-2 Panel

Table 6-2 presents a comparison of the measured cracking load and deflection at cracking for each full-scale test in this study to the Beam-Spring Model and Elastic Hand Method, respectively. Both methods are very accurate except for the D-2 and BC-2 specimens. The reason for this is unclear and may be due to measurement error. Table 6-3 and Table 6-4 contain the measured-to-predicted ratios for the Beam-Spring Model and the Elastic Hand Method, respectively. As is shown in these tables, on average, the predictions are very good at 0.95 and 0.97 for the Beam-Spring and 0.94 and 0.98 for the Elastic Hand Method for cracking and deflection at cracking, respectively. These accuracies are similar to those of other analysis methods for structures like reinforced and prestressed concrete beams as well as steel members (Nowak and Collins 2000). If the BC-2 and D-2 panels are not included, the measured-to-predicted ratios are nearly 1.0.

Table 6-2 Summary of measured and predicted cracking and deflections

Panel	Measured		Elastic Hand Method		Beam-Spring Model	
	Cracking Load	**Deflection**	**Cracking Load**	**Deflection**	**Cracking Load**	**Deflection**
	(psf)	*(in)*	*(psf)*	*(in)*	*(psf)*	*(in)*
A-2	155	0.34	156	0.36	156	0.39
A-4	202	0.44	194	0.33	192	0.352
B-1	-	-	150	0.17	152	0.198
B-2	-	-	150	0.17	152	0.198
BC-1	180	0.12	195	0.16	198	0.155
BC-2	164	0.15	195	0.16	197	0.157
D-1	221	0.14	222	0.15	209	0.144
D-2	184	0.13	222	0.15	208	0.138

Table 6-3 Beam-Spring Model Measured-to-Predicted Ratios

Panel	Cracking Load	Deflection
A-2	0.99	0.87
A-4	1.05	1.25
B-1	-	-
B-2	-	-
BC-1	0.91	0.79
BC-2	0.83	0.96
D-1	1.06	1.00
D-2	0.88	0.96
Average	**0.95**	**0.97**

Table 6-4 Elastic Hand Method Measured-to-Predicted Ratios

Panel	Cracking Load	Deflection
A-2	0.99	0.96
A-4	1.04	1.33
B-1	-	-
B-2	-	-
BC-1	0.92	0.77
BC-2	0.84	0.95
D-1	1.00	0.97
D-2	0.83	0.89
Average	**0.94**	**0.98**

6.4 Elastic Hand Method and Beam-Spring Model Comparison

One of the critical assumption of the Elastic Hand Method is the slip distribution along the length of the member. As noticed by previous research, the slip is not truly a triangular distribution, like the distribution of vertical shear in a simply supported beam with a distributed load (Olsen and Maguire 2016). The distribution seems to look more like a parabola or "hourglass" shape. Figure 6-14 compares the connector force distribution for two different panels using the Elastic Hand Method and Beam-Spring Model, where the distributions do not match, although they are very close. Table 6-5 shows that predictions made with the Elastic Hand Method were similar to those of the Beam-Spring Model (all ratios between 0.93 and 1.15) indicating there is very little difference in the predictions and indicates the linear slip assumption is good enough for design, especially for cracking.

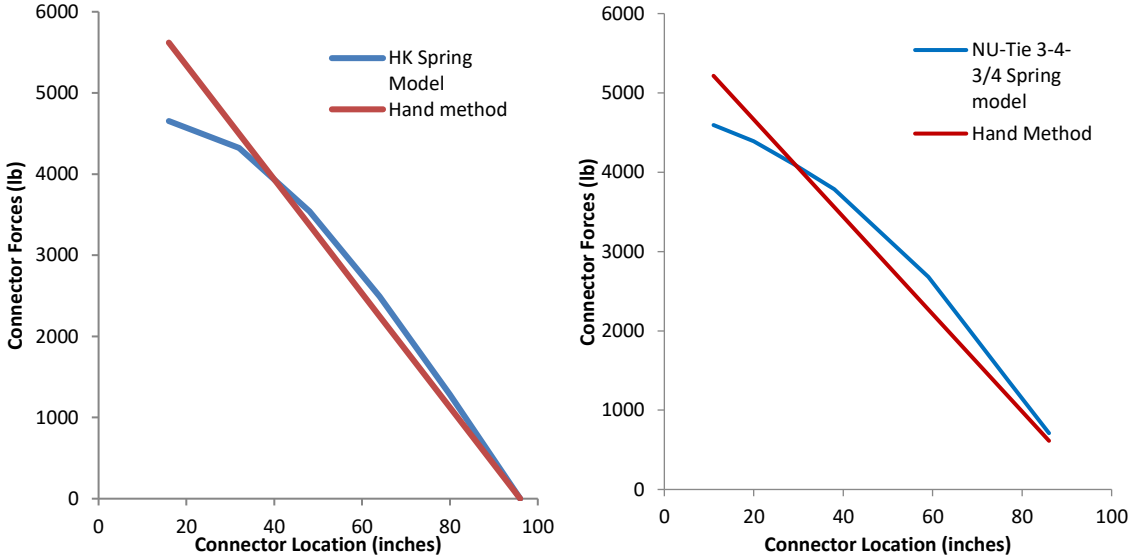

Figure 6-14 Connector forces diagram using the Elastic Hand Method and the Beam-Spring Model

Table 6-5 Ratio of the Beam-Spring Prediction to the Elastic Hand Method Prediction

Panel	**Cracking Load** *(psf)*	**Deflection** *(in.)*
343-2	1.00	1.10
343-4	0.99	1.07
HK 1	0.94	0.97
HK 2	0.94	0.93
T A1	1.02	0.98
T A2	1.01	1.00
T B1	1.01	1.15
T B2	1.01	1.15

Because engineers are currently used to the concept of percent composite action, Table 6-6 and Table 6-7 show the composite action prediction for cracking moment and deflection, respectively, for the Elastic Hand Method and Beam-Spring model. There is very good agreement again except for the BC-2 and D-2 panels.

Table 6-6 Measured Composite Action for cracking moment

Specimen	**M_{crFC}** *(lb*ft)*	**M_{crNC}** *(lb*ft)*	**Measured Composite Action** *(%)*	**Elastic Hand Method Composite Action** *(%)*	**Beam-Spring model Composite Action** *(%)*
A-2	66,583	12,804	12	12.3	12.2
A-4	66,583	12,804	24	21.8	21.2
B-1	41,481	11,067	-	2.3	2.9
B-2	41,866	11,184	-	1.9	2.5
BC-1	41,481	11,067	11	15.3	13.5
BC-2	41,866	11,184	6	14.8	12.5
D-1	41,481	11,067	23	23.2	18.0
D-2	41,866	11,184	11	22.6	17.0

Table 6-7 Measured Composite Action for deflection

Specimen	I_{FC}	I_{NC}	Measured Composite Action	Elastic Hand Method Composite Action	Beam-Spring Model Composite Action
	(in^4)	*(in^4)*	*(%)*	*(%)*	*(%)*
A-2	3744	216	5.1	4.0	3.7
A-4	3744	216	5.4	7.7	7.5
B-1	3912	384	-	-	-
B-2	3912	384	-	-	-
BC-1	3912	384	11.1	6.2	5.4
BC-2	3912	384	1.0	7.4	6.9
D-1	3912	384	12.7	10.0	10.2
D-2	3912	384	7.5	12.4	10.9

6.5 Elastic Hand Method Design Procedure

The following procedure outlines the design approach for service loads using the Elastic Hand Method (see Appendix B for a Design Example). This procedure is for sandwich panels with equal wythe thicknesses; however, it can also be used for sandwich panels with unequal wythe thicknesses if appropriate modifications are made.

1. Calculate the material and section properties assuming the sandwich wall panel acts non-compositely.
2. Assume the number and spacing of connectors, and the slip at the end connector line. Calculate the forces in each connector and connector line using Equations (6-6) and (6-7), repeated here for convenience.

$$F_i = \delta(i)\, N_i * K_E \qquad (6\text{-}16)$$

$$F_{sum} = \sum F_i \qquad (6\text{-}17)$$

3. Calculate the cracking moment for a mild reinforced non-composite wythe using Equation (6-18).

$$M_{wy_2} = \frac{M_{service} - F_{sum} * Z}{2} \qquad (6\text{-}18)$$

4. Calculate the equivalent load using Equation (6-9), repeated here for convenience.

$$w_{we2} = \frac{8 * M_{wy_2}}{Span^2} \qquad (6\text{-}9)$$

5. Using the equivalent load, calculate the axial and rotational displacement assuming the equivalent load distribution using equations (6-10) through (6-12), again repeated here for convenience.

$$\theta = \frac{w_{we2} * Span^3}{24 * E * I_{NC2}} \qquad (6\text{-}10)$$

$$\Delta_{Rot} = \theta * Z \qquad (6\text{-}11)$$

$$\Delta_{Axial} = \left[\left(\frac{1}{b * E * t_{wy_1}}\right) + \left(\frac{1}{b * E * t_{wy_2}}\right)\right] * \sum_{i=1}^{n} F_i * \left(\frac{L}{2} - x_i\right) \qquad (6\text{-}12)$$

6. Calculate a new value of δ_{end} using Equation (6-13). Check if δ_{end} is less than the Elastic Slip limit. If it is not, iterate steps 2-6 until this limit state is satisfied.

$$\delta_{end} = \Delta_{Rot} - \Delta_{Axial} \qquad (6\text{-}13)$$

7. Check tension stress to verify it is less than modulus of rupture of the concrete with Equation (6-19).

$$f = \frac{M_{wy_2} * t_{wy_2}}{2 * I_{NC2}} + \frac{F_{sum}}{b * t_{wy_2}} \leq f_r \qquad (6\text{-}19)$$

8. Calculate the midspan deflection. For a uniform distributed load, use Equation (6-15).

$$\Delta = \frac{5 * w_{we2} * Span^4}{384 * E_c * I_{NC2}} \qquad (6\text{-}15)$$

6.6 Conclusions

In this section, two methods to predict elastic deformations and cracking were developed. First, the Beam-Spring model is a simple, general, matrix analysis framework that allows for accurate prediction of sandwich panel behavior. The proposed Elastic Hand Method was also developed which uses some simplifications and enforces equilibrium and slip kinematics. This method is general enough to predict cracking and deflections in most panels, but requires some iteration. Both models are limited to elastic behavior, although if inelasticity were introduced to the Beam-Spring model (non-linear springs and beam elements), ultimate deflections and ultimate strength could likely be determined, though this may not be necessary (see next chapter).

The Beam-Spring Model presented here is a promising option for elastic analysis of precast concrete sandwich panel walls using composite shear connector systems, including those with unsymmetrical wythes, axial forces and irregular connector patterns, including P-δ and P-Δ effects.

The Elastic Hand Method presented here relies on iteration, which is inconvenient, but easily programmed into excel or anther design aiding program. The iteration could be eliminated, but is difficult due to the summations of force required, and this would limit the method's versatility and may require additional simplifying assumptions. The Elastic Hand Method is only evaluated on equal wythe panels from this program, but could be extended to unsymmetrical wythes, axial forces, panels with openings and alternate connector patterns.

Both methods were compared to the elastic portions of the full-scale tests from previous sections. Table 6-8 below simply consolidates Table 6-3 and Table 6-4 from the chapter as a summary of the accuracy of the cracking and deflection predictions for the panels tested in this study by displaying the Measured-to-Predicted ratios for each method. Additional validation on more varied panels should be performed, but the results are very promising.

Table 6-8 Measured-to-Predicted ratio

Panel	Elastic Hand Method		Beam-Spring Model	
	Cracking Load	**Deflection**	**Cracking Load**	**Deflection**
A-2	0.99	0.96	0.99	0.87
A-4	1.04	1.33	1.05	1.25
B-1	-	-	-	-
B-2	-	-	-	-
BC-1	0.92	0.77	0.95	0.71
BC-2	0.84	0.95	0.88	0.97
D-1	1.00	0.97	1.06	1.00
D-2	0.83	0.89	0.88	0.96
Average	**0.94**	**0.98**	**0.97**	**0.96**

The following conclusions can be made from the result in this chapter:

- A versatile, general matrix-based procedure, termed the Beam-Spring Model, can be used to predict elastic deflections and cracking very accurately, with a 0.97 and 0.96 test-to-prediction ratio for cracking load and deflections, respectively.
- Using first principles and a series of assumptions, a hand based method can be used to predict elastic deflections and cracking very accurately, with a 0.94 and 0.98 test-to-prediction ratio for cracking load and deflections, respectively.

7 PREDICTING STRENGTH BEHAVIOR

7.1 Introduction

There are a handful of recently introduced methods proposed to predict the ultimate moment capacity of a concrete sandwich panel wall (Tomlinson 2015; Hassan and Rizkalla 2010; Naito et al. 2012). In addition to being few in number, they are difficult to use for engineers in practice, requiring complicated moment curvature analyses. Furthermore, they rely on empirical data and interpolation rather than a general approach, or a combination of these things. There is a significant need to develop an easy-to-use method based on first principles and good design assumptions that is easily fit into an engineer's design routine. To simplify the design process of concrete sandwich panel walls so that a greater number of engineers can safely design them, this chapter presents a new method, the Partially-Composite Strength Prediction Method, to predict the nominal moment capacity of concrete sandwich wall panels that is easy to implement and shown to be accurate. The results of the method are compared to those in the full-scale testing chapter and use the results generated in the shear-testing chapter.

7.2 Calculating Percent Composite Action

Design engineers are familiar with the calculations of non-composite and fully-composite sandwich wall panels. The following sections reiterate this for completeness of the below discussion, as well as introduce a formal definition of percent composite action for ultimate moment. The latter is necessary because there is no standard definition within the industry, although the most popular one is adopted for this discussion.

7.2.1 Non-Composite Ultimate Moment

The ultimate moment for an ideally non-composite panel is the sum of the ultimate moments of the individual wythes, as shown in Figure 7-1. When reinforced with mild steel, the following calculations (based on strain compatibility) can be used to calculate the ultimate moment, with minor variation for a prestressed panel:

$$a_1 = \frac{A_{s1} f_{s1}}{0.85 f_c' b} \qquad (7\text{-}1)$$

$$a_2 = \frac{A_{s2} f_{s2}}{0.85 f_c' b} \qquad (7\text{-}2)$$

$$M_{NC} = A_{s1} f_{s1} \left(d_1 - \frac{a_1}{2}\right) + A_{s2} f_{s2} (d_2 - \frac{a_2}{2}) \qquad (7\text{-}3)$$

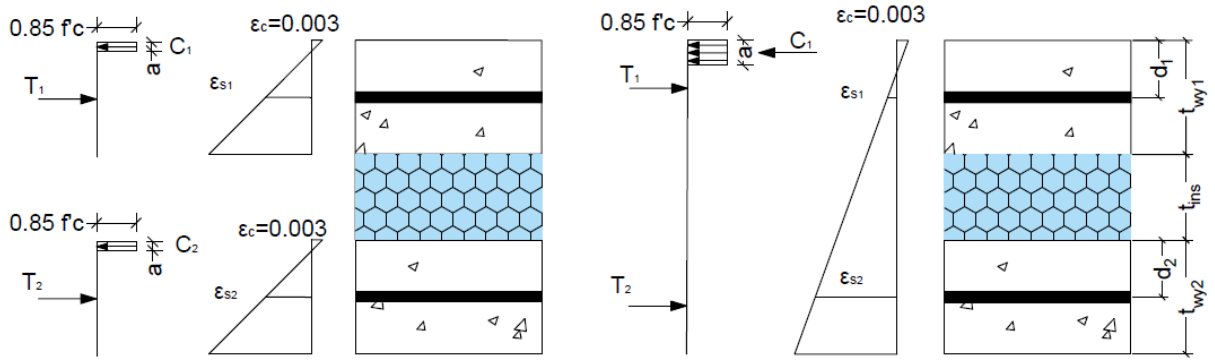

Figure 7-1 Strain and load profile for the non-composite SWP (left) and fully-composite SWP (right)

7.2.2 Fully-Composite Ultimate Moment

To calculate the fully-composite moment, one assumes that the entire panel acts as one beam, without strain discontinuity. Using strain compatibility, the following procedure can be used for mild-steel reinforced panels (with minor variation for prestressed panels):

$$a = \frac{A_{s1}f_{s1} + A_{s2}f_{s2}}{0.85f_c'b} \tag{7-4}$$

$$M_{FC} = A_{s1}f_{s1}\left(d_1 - \frac{a}{2}\right) + A_{s2}f_{s2}\left(d_2 + t_{wy_1} + t_{ins} - \frac{a}{2}\right) \tag{7-5}$$

7.2.3 Definition of Partial Percent Composite Action for Ultimate Moment

Utilizing the theoretical fully-composite moment, theoretical non-composite moment, and the actual measured moment from the test results or a prediction method, the degree of composite action, K_{Mn}, can be determined using Eq. (7-6).

$$K_{Mn} = \frac{M_{n,test} - M_{n,NC}}{M_{n,FC} - M_{n,NC}} \tag{7-6}$$

Where Mn_{test} = experimental maximum moment of the sandwich panel

Mn_{NC} = theoretical maximum moment of the non-composite sandwich panel

Mn_{FC} = theoretical maximum moment of the fully-composite sandwich panel

Figure 5-14 graphically demonstrates the relationship between moment and degree of composite action in Eq. (7-6).

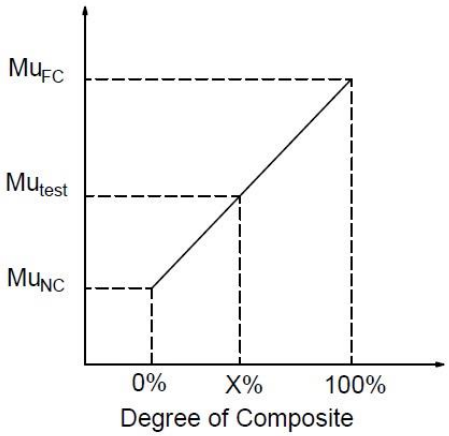

Figure 7-2 Visual demonstration of degree of composite action

7.3 Partially-Composite Strength Prediction Method

7.3.1 Overview and Discussion

The proposed Partially-Composite Strength Prediction Method procedure is based entirely upon first principles (i.e. equilibrium, strain compatibility), a "good enough" assumption about the slip profile along the length of the member, and shear deformation data of the connectors (which many connector companies already collect for ICC-ES certification, and which has been collected by several researchers). As such, this method is robust enough that it may be applied to situations outside of the simply supported panels presented in this report, although this would require validation. Furthermore, the reliance upon familiar first principles makes the procedure easily adopted by precast engineers and is a direct solution as long as recommendations are followed. For the purposes of validating the method, the approximate stress strain curve of the materials should be used (e.g., Hognestad's Concrete Material Model [Wight and MacGregor 2005], strain hardening of the steel) in lieu of common design assumptions; however, when used for design, standard assumptions (e.g., Whitney's stress block [Whitney, 1937], elastic-perfectly plastic rebar) can (and should) be used.

For the sake of illustrating the Partially-Composite Strength Prediction Method procedure, wythe 1 (or the "top wythe") is considered the fully-composite compression side of the member and wythe 2 (or the "bottom

wythe") is considered the fully-composite tension side of the member, as shown in Figure 7-1. The forces in a partially composite member are presented in Figure 7-3 which include the force of the connectors at the point of interest (F_{sum}) assumed to act at the center of each wythe. To maintain static equilibrium within a given wythe, the compression and tension forces in each wythe must transfer the difference between them to the other wythe; i.e.:

$$\sum F_{axial,1} = T_1 - C_1 - F_{sum} = 0 \qquad (7\text{-}7)$$

$$\sum F_{axial,2} = T_2 - C_2 + F_{sum} = 0 \qquad (7\text{-}8)$$

Where F_{sum} = is the sum of the connector forces from one end of the panel to the cross-section of interest

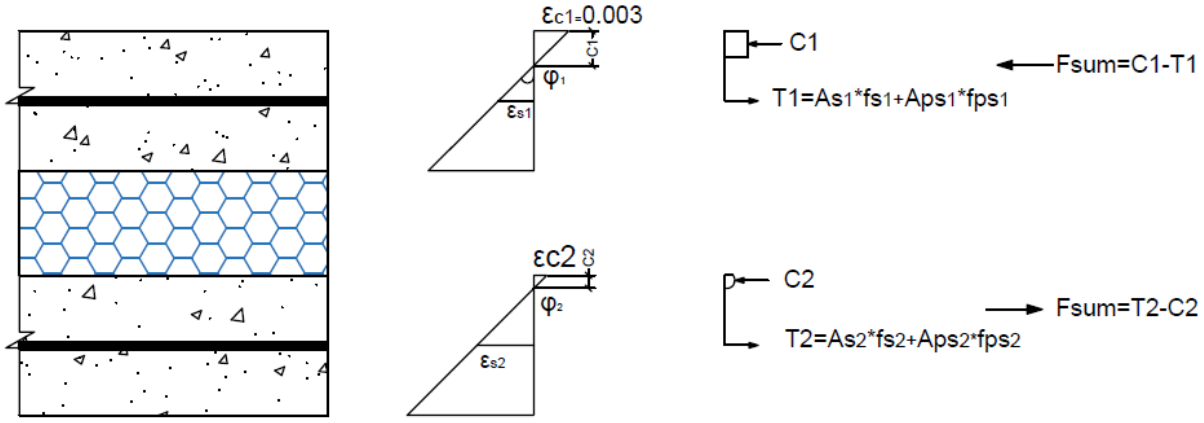

Figure 7-3 Strain and load profile of concrete sandwich wall panel

The shear force provided by the connectors can be estimated using the data from the push-off test depending on the number of connectors, the connector spacing, and a linear assumption about the slip distribution as shown in Figure 7-4.

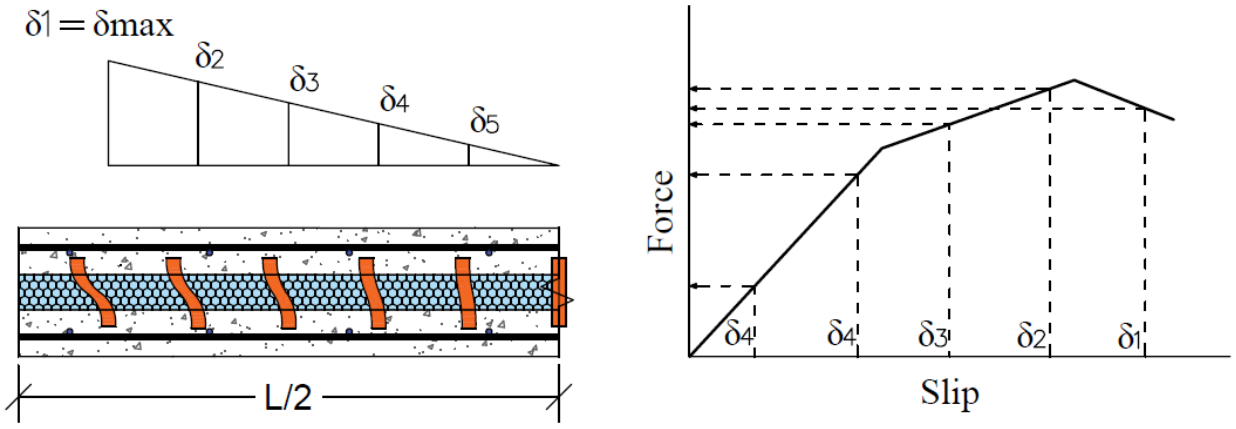

Figure 7-4 Slip distributed along the panel length

After the forces in each connector are determined, they can be summed for any given point along the length of the beam and applied to the beam cross-section as shown in Figure 7-3. With these simplifying assumptions, determining the moment capacity of a sandwich panel with an arbitrary distribution of shear connectors is no more difficult than determining the capacity of two separate beams with axial loads (F_{sum}, in this case). Similarly, it is known that the two wythes will have equal deflection and equal curvature:

$$\varphi_1 = \varphi_2 \qquad (7\text{-}9)$$

Where φ_1 = is the curvature of the wythe 1

φ_2 = is the curvature of the wythe 2

This method can be extended to all cross-sections along the panel and points on the load deflection curve, but the purpose of this chapter of the report is to determine the ultimate moment strength in a straightforward manner. The condition for failure is determined as either when the connectors fail or when the concrete on wythe 1 crushes (i.e., ε_{c1} = 0.003). It is assumed that designers would prefer to prevent the sudden failure of the connectors to ensure a ductile failure. Therefore, it is recommended to set a reasonable value for the force or slip in the connectors at the end of the panel connectors during design. Once the forces are resolved on the cross-section, one can use the following equation to calculate the nominal moment that can be carried by the cross-section:

$$M = M_1 + M_2 + F_{sum} * \left(\frac{t_{wy1} + t_{wy2}}{2} + t_{ins}\right) \qquad (7\text{-}10)$$

Where M_1 = is the moment in the top wythe created by C_1 and T_1:

M_2 = the moment in the bottom wythe created by C_2 and T_2:

The following sections outline the procedure for analysis of existing concrete sandwich panel walls, as well as a detailed design procedure.

7.3.2 Partially-Composite Strength Prediction Method Procedure

The following steps are proposed to predict the nominal moment capacity for a sandwich wall panel. The steps do not necessarily need to occur in this order, but the authors found this order convenient when analyzing a panel that was already created. A detailed design process is presented in the following section (Section 7.3.4).

1. Find the forces at each connector using the load-slip curve and assuming a linear distribution of slip (see Figure 7-4). The slip can be iterated until it maximizes the connector force, which will be the condition at ultimate, taking into account the post maximum strength of the connectors if desired. This can also be determined by using an influence line.

Design Note: As stated above, for design it may be important to prevent connector failure prior to panel failure by limiting slip or force carried by the most heavily loaded connectors. This can be conservatively done by assuming that the connectors at the end of the panel are at their maximum force (F_u). Connector behavior and mechanical property variation (e.g., ultimate strength, proportional limit, elastic limit, deformation at ultimate and shear deformation at rupture) are not always understood due to the private and proprietary nature of this part of the industry. Limiting connector forces at different limit states is an important consideration for PCI committees.

The slip at every connector location can be estimated heuristically (by assuming a linear slip profile based on the plot shown in Figure 7-4 or Figure 7-5 and Figure 7-6, which can then be used to create a robust spreadsheet), or by using the following equation (which is based on similar triangles):

$$\delta(i) = \delta_{Ult} * \frac{\frac{L}{2} - x_i}{\frac{L}{2} - x_1} \qquad (7\text{-}11)$$

Where $\delta(i)$ = the slip of the wythes at connector i

δ_{Ult} = Maximum slip of the end row of connectors at the ultimate moment

L = length of the panel

x_i = location of the connector from the end of the panel

i = connector line number from the end of the panel to the point of interest/analysis

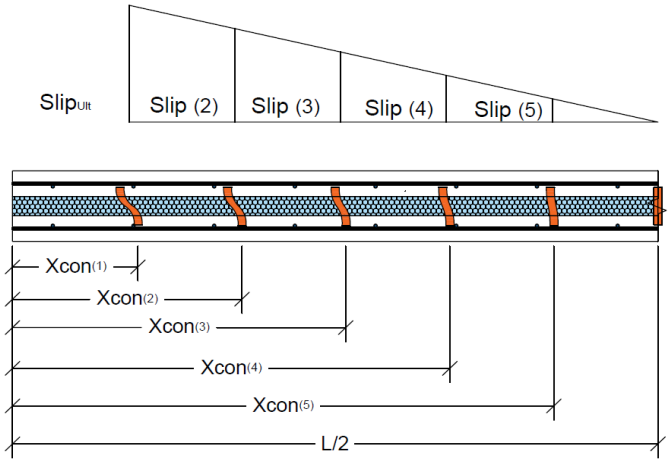

Figure 7-5 Slip diagram

Find the force, F_i, at each connector by using the appropriate load-slip curve.

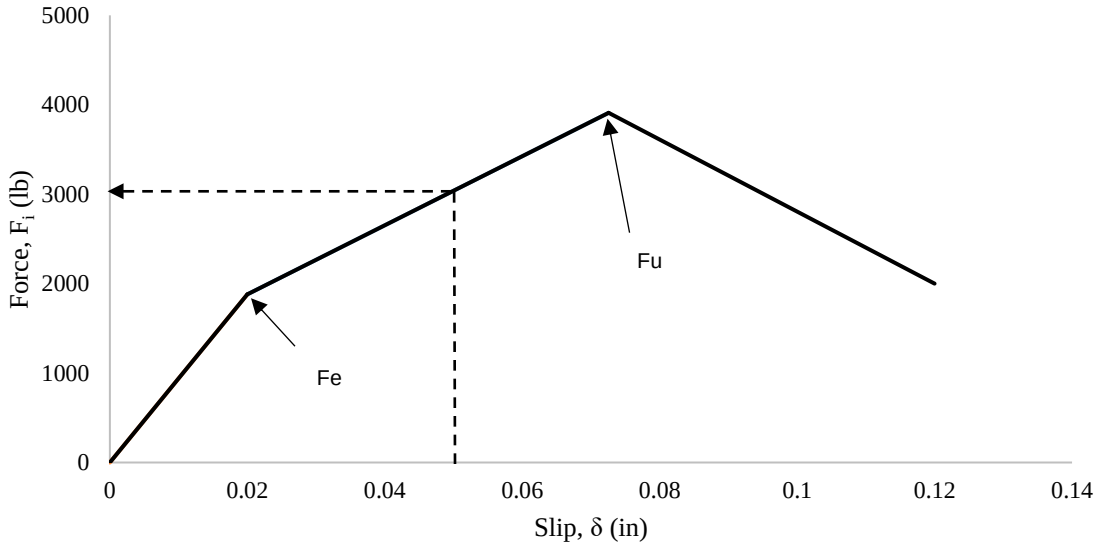

Figure 7-6 Typical load-slip curve

2. Find the total force provided by the connectors

$$F_{sum} = N * \sum F_i \leq A_s f_s + A_{ps} f_{ps} \qquad (7\text{-}12)$$

Where N = number of connectors per row

F_i = the force at connector i

The maximum connector force that can be transferred between wythes is limited to the smaller of the maximum force generated by connectors at the location of interest or maximum tensile force carried by the steel in the bottom wythe, hence the right-hand side of the inequality in Equation (7-12). In other words, adding additional connectors will not increase the strength of the panel over the fully-composite moment, although it is likely to influence deflections.

3. Find C_1 and T_1 for the top wythe as if it were an independent beam with an axial force F_{sum} (see Figure 7-8).

This process is exactly the same as any other reinforced/prestressed beam:

a. Assume the top fiber concrete strain is 0.003

b. Assume a value of the depth of the compression force in the concrete, c_1.

c. Calculate the curvature, φ_1. Assuming small angles, φ_1 may be calculated as

$$\varphi_1 = \frac{\varepsilon_c}{c_1} \qquad (7\text{-}13)$$

d. Calculate the compressive force in the top wythe. The compressive force in the concrete will utilize Hognestad's equation to estimate the concrete compressive strength. Hognestad's equation is not required for an accurate prediction of the top wythe, but it will become necessary for the bottom wythe if the panel is partially composite because Whitney's stress block is only valid when the maximum concrete strain is 0.003. The Hognestad formula is shown in Equation (7-14):

$$f_c = f_c' \left[\frac{2 * \varepsilon_c}{\varepsilon_o} - \left(\frac{\varepsilon_c}{\varepsilon_o} \right)^2 \right] \qquad (7\text{-}14)$$

Where f_c = stress in the concrete

f_c' = concrete compressive strength

ε_c = strain in the concrete

ε_o = 0.002.

Substituting Hognestad's equation, the concrete compressive force can be calculated as

$$C_1 = b * \int_0^{c_1} f_c \, dy = b * \int_0^{c_1} f_c' \left[\frac{2 * \varepsilon_c}{\varepsilon_o} - \left(\frac{\varepsilon_c}{\varepsilon_o} \right)^2 \right] dy$$

$$C_1 = b * \int_0^{c_1} f_c' \left[2 * \frac{\varphi_1 * c_1}{\varepsilon_o} - \left(\frac{\varphi_1 * c_1}{\varepsilon_o} \right)^2 \right] dy$$

$$C_1 = b * \left| f_c' \left[\frac{\varphi_1 * {c_1}^2}{\varepsilon_o} - \left(\frac{{\varphi_1}^2 * {c_1}^3}{3 * {\varepsilon_o}^2} \right) \right] \right|_0^{c1}$$

$$C_1 = b * f_c' \left[\frac{\varphi_1 * {c_1}^2}{\varepsilon_o} - \left(\frac{{\varphi_1}^2 * {c_1}^3}{3 * {\varepsilon_o}^2} \right) \right]$$

$$C_1 = b * f'c * \frac{\varphi_1 * c_1^2}{\varepsilon_o} * \left(1 - \frac{\varphi_1 * c_1}{3\varepsilon_o} \right) \qquad \textit{(7-15)}$$

Where C_1 = the compressive force in the concrete in wythe 1

b = width of the panel

$$x_{c1} = \frac{\int_0^{c_1} f_c' \left[\frac{2 * \varepsilon_c}{\varepsilon_o} - \left(\frac{\varepsilon_c}{\varepsilon_o} \right)^2 \right] * c_1 * \, dc_1}{\int_0^{c_1} f_c' \left[\frac{2 * \varepsilon_c}{\varepsilon_o} - \left(\frac{\varepsilon_c}{\varepsilon_o} \right)^2 \right] dc_1}$$

$$x_{c1} = \frac{\int_0^{c_1} f_c' \left[2 * \frac{\varphi_1 * {c_1}^2}{\varepsilon_o} - \frac{{\varphi_1}^2 * {c_1}^3}{{\varepsilon_o}^2} \right] dc_1}{\int_0^{c_1} f_c' \left[2 * \frac{\varphi_1 * c_1}{\varepsilon_o} - \frac{{\varphi_1}^2 * {c_1}^2}{{\varepsilon_o}^2} \right] dc_1}$$

$$x_{c1} = \frac{\left[\frac{2}{3} * \frac{\varphi_1 * {c_1}^3}{\varepsilon_o} - \frac{1}{4} * \frac{{\varphi_1}^2 * {c_1}^4}{{\varepsilon_o}^2} \right]}{\left[\frac{\varphi_1 * {c_1}^2}{\varepsilon_o} - \frac{1}{3} * \frac{{\varphi_1}^2 * {c_1}^3}{{\varepsilon_o}^2} \right]}$$

$$x_{c1} = c_1 - \frac{c_1 * (8 * \varepsilon_o - 3 * \varphi_1 * c_1)}{12 * \varepsilon_o - 4 * \varphi_1 * c_1} \qquad \textit{(7-16)}$$

Where x_{c1} = the centroid of compressive force in the concrete from extreme compressive fiber

Hognestad's concrete stress strain relationship is plotted along with the resultant force location in Figure 7-7.

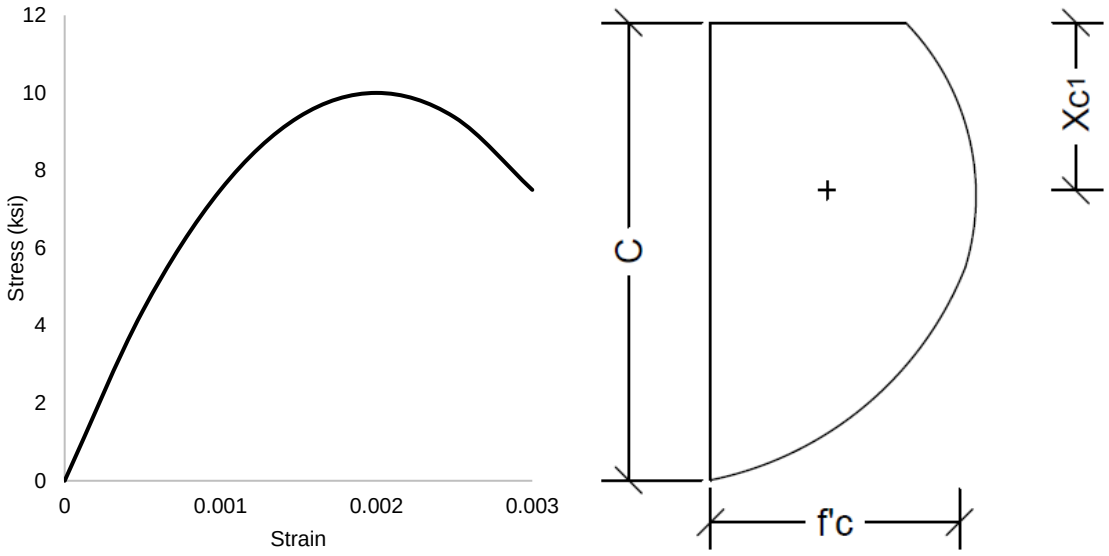

Figure 7-7 Stress vs strain of Hognestad (left) and stress profile (right)

Design Note: To facilitate design it is recommended to use Whitney's stress block. The Hognestad model is only used to analyze partially composite panels in this report and is still an approximation. It is recommended that when designing, the designer designs for a fully-composite panel, preventing compression in the bottom wythe and eliminating the need for and hassle of this more complex material model.

e. Calculate the strain and then stress in the steel. Strain can be determined using similar triangles (see Figure 7-8):

$$\varepsilon_s = \varepsilon_c \frac{d_1 - c_1}{c_1} \qquad (7\text{-}17)$$

Where d_1 = depth to the centroid of the steel measured from the top of wythe 1.

c_1 = depth to neutral axis of wythe 1 measured from the top of wythe 1.

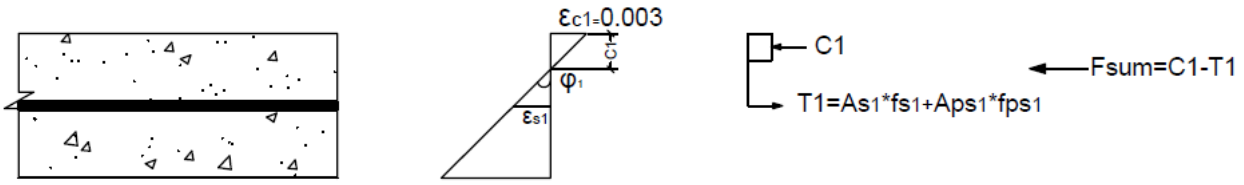

Figure 7-8 Strain and load profile for the top wythe

The stress is then calculated using an appropriate steel model:

Mild Steel for Design: Elastic Perfectly Plastic

$$f_s = \begin{cases} E_s * \varepsilon_s & if\ \varepsilon_s < \varepsilon_y \\ f_y & if\ \varepsilon_s \geq \varepsilon_y \end{cases} \qquad (7\text{-}18)$$

Where f_s = stress in the mild steel

E_s = modulus of elasticity of the steel

ε_s = strain in the mild steel

ε_y = strain of the mild steel at yielding

f_y = mild steel yield stress

For Prestressing Steel: The power formula (Devalapura and Tadros, 1992):

$$f_{ps} = \varepsilon_{ps} * \left\{ 887 + \frac{27600}{\left[1 + \left(112.4 * \varepsilon_{ps}\right)^{7.36}\right]^{7.36^{-1}}} \right\} < 270 \qquad (7\text{-}19)$$

Where f_{ps} = stress in the prestressing steel

Actual stress versus strain profile for the reinforcement, e.g. see Figure 5-1.

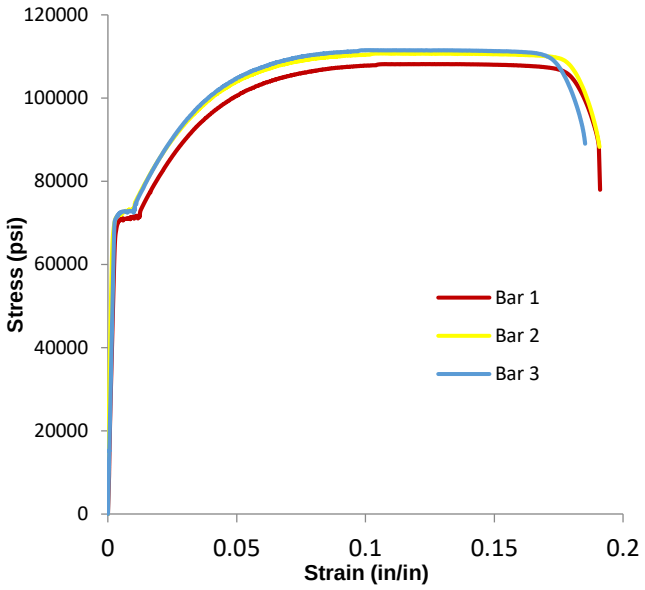

Figure 7-9 Stress vs. Strain for rebar

f. Calculate the tension force in the top wythe. This will just include the tension in the steel:

$$T_1 = f_{s1}A_{s1} + f_{ps1}A_{ps1} \qquad (7\text{-}20)$$

g. Determine if c_1 satisfies the force equilibrium for wythe 1. If not, repeat step 3 and iterate until force equilibrium is satisfied.

$$\sum F_x \rightarrow 0 = T_1 - C_1 - F_{sum} \qquad (7\text{-}21)$$

4. Find C_2 and T_2 for the second wythe as if it is a separate beam with F_{sum} acting as an axial force.
   a. Assume both wythes will deflect equally and maintain $\varphi_2 = \varphi_1$. This is a standard assumption for all composite or non-composite structures, steel, concrete or otherwise (Bai and Davidson 2015; Hassan and Rizkalla 2010; Newmark et al. 1951).
   b. Assume a value of c_2; however, in contrast to the previous example, the top fiber will *not* be 0.003 unless the panel is a non-composite design.

c. Calculate the compressive force in the bottom wythe, C_2. The compressive force in the concrete will again utilize Hognestad's equation to estimate the concrete compressive strength, but it is critical here because Whitney's stress block is only valid when the top fiber is at 0.003 strain and in the case of partial composite action, this will not be true. Substituting Hognestad's equation, the concrete compressive force can be calculated as before, with appropriate variables changed to reflect wythe 2, as:

$$C_2 = b * f'c * \frac{\varphi_2 * c_2^2}{\varepsilon_o} * \left(1 - \frac{\varphi_2 * c_2}{3\varepsilon_o}\right) \qquad (7\text{-}22)$$

Design note: To facilitate design it is recommended to use Whitney's stress block. The Hognestad model is only used to analyze partially composite panels in this report and is still an approximation. It is recommended that when designing, the designer designs for a fully-composite panel, preventing compression in the bottom wythe and eliminating the need to calculate C_2.

d. Calculate the strain and stress in the steel. Assuming small angles, the strain can be determined using the relationship in Equation (7-13) and (7-17) above and demonstrated in Figure 7-10 below as

$$\varepsilon_s = (d_2 - c_2) * \varphi_2 \qquad (7\text{-}23)$$

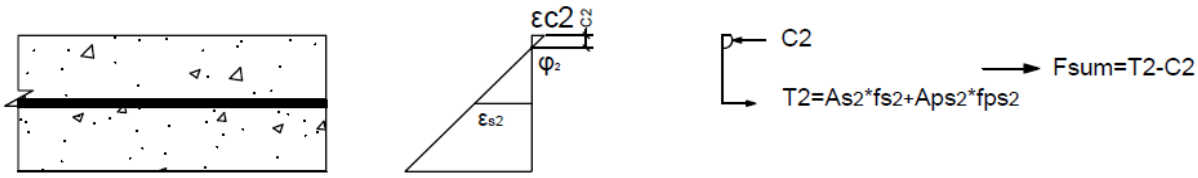

Figure 7-10 Strain and load profile for the bottom wythe

The stress can then be calculated using Equations (7-18) and (7-19) in Step 3e above.

e. Calculate the tension force in the bottom wythe:

$$T_2 = f_{s2}A_{s2} + f_{ps2}A_{ps2} \quad (7\text{-}24)$$

f. Determine if c_2 satisfies the force equilibrium for Wythe 2. If not, repeat step 4 and iterate until force equilibrium is satisfied.

$$\sum F_x \rightarrow 0 = T_1 - C_1 + F_{sum} \quad (7\text{-}25)$$

By enforcing equilibrium of each wythe using Equation (7-21) of step 3g and Equation (7-25) from step 4f, force equilibrium for the whole panel is now satisfied.

5. Find the ultimate moment of the concrete sandwich wall panel by taking the moments carried by the different parts of the panel presented in Figure 7-3:

$$M = M_1 + M_2 + F_{sum} * \left(\frac{t_{wy1} + t_{wy2}}{2} + t_{ins}\right) \quad (7\text{-}26)$$

Where M_1 = the moment in wythe 1 created by C1 and T1

M_2 = the moment in wythe 2 created by C_2 and T_2

M_1 and M_2 are most easily found by summing the moments about the steel locations:

$$M_1 = C_1 * (d_1 - x_{c1}) \quad (7\text{-}27)$$

$$M_2 = C_2 * (d_2 - x_{c2}) \quad (7\text{-}28)$$

Alternatively, the moment can be taken for all concrete and steel forces over the entire panel cross-section at a convenient location.

7.3.3 Validation of the Partially-Composite Strength Prediction Method

The Partially-Composite Strength Prediction Method presented in the previous section is compared below to the full-scale panel tests for its validation. Table 7-1 shows the experimental ultimate moment compared to predictions made by Partially-Composite Strength Prediction Method. The percent difference was, on average, about 8 percent less than the experimental ultimate moment results. This is a very common error metric, which is comparable to that of most other predictions for other members like normal reinforced concrete in bending or shear (Nowak and Collins 2000). Appendix C contains the detailed calculations for the panels from this study.

Table 7-1 Validation of Partially-Composite Strength Prediction Method

Panel	**Observed Ultimate Moment**		**Partially-Composite Strength Prediction Moment**	**Percent Difference**
	Specimen 1	**Specimen 2**		
	(k-ft)	*(k-ft)*	*(k-ft)*	*(%)*
Nu-Tie 343-2	43.36	-	39.5	8.9
Nu-Tie 343-4	60.86	-	55.37	9.0
HK	45.23	42.5	39.9	9.0
T A	45.1	41.3	41.1	4.9
T B	29.82	25.6	25.36	8.5
Average				**8.0**

7.3.4 Recommendations for Design

To make the Partially-Composite Strength Prediction Method easier to follow during the design stage, several recommendations are suggested to facilitate the strength calculation at failure:

a) Consider the panel as a fully-composite panel and find the required area of steel, which can be set equal to F_{sum} to select the total number of shear connectors. If satisfied, this assumption implies that the second wythe compression force (C_2) will be zero. Anything less than fully-composite requires the use of Hognestad's concrete material model (or another model of the engineer's choice) or another simplifying assumption. While Hognestad's material model is not complicated and the required equations derived and presented are above, it does add enough complication that a designer unfamiliar with it may not be comfortable.

b) Find the ultimate moment of the panel using the methods presented above. Several simplifications can be made to bring the method more in line with current reinforced concrete and prestressed concrete design:
    a. The Whitney stress block can be used as long as there is no compression force in the wythe 2.
    b. Elastic Plastic Mild Steel
    c. Power Formula or PCI formula for prestressing steel
    d. Limit end connector slip to the slip at maximum force (F_u) per the shear testing results
c) Find the number of connectors and spacing that provide the required F_{sum} for the cross-section. Although uniform spacing of connectors is recommended based on discussions with connector manufacturers and their in-house testing, alternate spacing layouts have been noted to be beneficial (Olsen and Maguire 2016).
d) Due to inherent variability associated with concrete bond, it is not recommended that designers use the fully bonded values from the push-off testing for strength and stiffness for long term strength without long term testing.

Some of these design assumptions are not appreciably different than those used by connector manufacturers, but are formalized here and fit within the design parameters discussed in this chapter. See Appendix D for Design Examples using the Partially-Composite Strength Prediction Method.

7.4 Conclusions

There is a significant need to develop an easy-to-use method based on first principles and good design assumptions that is easily fit into an engineer's design routine. This chapter presented a new method, the Partially-Composite Strength Prediction Method, to predict the nominal moment capacity of concrete sandwich wall panels that is easy to implement and shown to be accurate. The results of the method are compared to those in the full-scale testing chapter and use the results generated in the shear-testing chapter. The following conclusions can be made about the findings in this chapter:

- A design method based on familiar first principles and a series of assumptions was developed
- The developed Partially-Composite Strength Prediction Method was shown to be accurate to within 8% on average for the panels produced and tested in a preceding chapter. These panels represented very different configurations and were reinforced with different connectors and connector patterns, further demonstrating robustness.

- The developed method relies only on connector load-slip information extracted from the push-off tests.
- The developed, recommended, design procedure suggests designing for 100% composite action to facilitate design using standard assumptions, like Whitney's Stress block, and limiting connector end slip at ultimate to F_u.

8 CONCLUSIONS

8.1 Summary

In this report, a thorough literature review and history of composite action in PCSWP was presented and current design philosophies were described. In an attempt to develop general methods to predict PCSWP behavior an experimental program was undertaken in which push-off specimens and full-scale PCSWP were designed, fabricated and tested at the Utah State University SMASH lab. Using this valuable experimental data, two elastic models (one matrix-based and one based on first principles) were presented to predict important elastic deflections and cracking moments. Additionally, a first-principles based method was developed to predict ultimate load.

8.2 Push-off Testing

A total of 41 pure shear push-off specimens were created to evaluate the shear stiffness of the various commercially available sandwich panel wall shear connectors. The variables studied were connector type, foam thickness, foam type and foam bond. Due to project constraints, only a single specimen of each type could be constructed so there is no statistical information available regarding the connector strength and stiffness values. The following conclusions can be made from the push-off testing:

- For pin type connectors that fail mainly in dowel action (Connector B and D) or behave like a pin connector (Connector E), foam type and bond play a negligible role in strength and stiffness.
- For truss type connectors (Connectors A and C) that are loaded mainly in tension when shear is applied to the specimen, foam type and bond plays a more significant role in strength and stiffness.
- Connector types vary widely in stiffness, strength and ductility
- Bi-linear design curves were developed to be used in the prediction methodologies and limits on connector forces/deformation.
- Due to inherent variability associated with concrete bond, it is not recommended that designers use the fully bonded values for strength and stiffness for long term strength without long term testing.

- Future effort should investigate statistical information regarding the shear strength and stiffness in order to properly and safely set limits on elastic stresses and failure stresses in the connectors during different loading scenarios.

8.3 Full-Scale Testing

Eight full-scale concrete sandwich panels were tested to failure at the Utah State University Structures Lab. The purpose of the testing was to evaluate the percent composite action for the connector configurations and compare the results to those reported by composite connector manufacturers. The following conclusions can be made from the experimental program:

- The type and intensity of shear connectors significantly affect the degree of composite action achieved in a concrete sandwich panel wall. Doubling the number of shear connectors in the Connector A (Nu-Tie connector) panels resulted in a large gain in percent composite action. (Note that the A-2 panel was more lightly reinforced than would be detailed for an actual building)
- The manufacturer-reported degree of composite action can be considered conservative for the panel configurations and connectors and connector patterns tested in this paper.

8.4 Elastic Prediction Methods

In this section two methods to predict elastic deformations and cracking were developed. First, the Beam-Spring model is a simple, general, matrix analysis framework that allows for accurate prediction of sandwich panel behavior. The Elastic Hand Method was also developed which uses some simplifications and enforces equilibrium and slip kinematics. This method is general enough to predict cracking and deflections in most panels, but requires some iteration. Both models are limited to elastic behavior, although if inelasticity were introduced to the Beam-Spring model (non-linear springs and beam elements), ultimate deflections and ultimate strength could likely be determined, though this may not be necessary.

The Beam-Spring Model presented herein is a promising option for elastic analysis of precast concrete sandwich panel walls using composite shear connector systems, including those with unsymmetrical wythes, axial forces and irregular connector patterns, including P-δ and P-Δ effects.

The Elastic Hand Method presented herein relies on iteration, which is inconvenient, but easily programmed into excel or anther design aiding program. The iteration could be eliminated, but is difficult due to the summations of force required and this would limit the method's versatility and may require additional simplifying assumptions. The Elastic Hand Method is only evaluated on equal-wythe panels from this program, but could be extended to unsymmetrical wythes, axial forces, panels with openings and alternate connector patterns. The following conclusions can be made about the elastic prediction methods:

- A versatile, general matrix-based procedure, termed the Beam-Spring Model, can be used to predict elastic deflections and cracking very accurately, with a 0.97 and 0.96 test-to-prediction ratio for cracking load and deflections, respectively.
- Using first principles and a series of assumptions, a hand based method can be used to predict elastic deflections and cracking very accurately, with a 0.94 and 0.98 test-to-prediction ratio for cracking load and deflections, respectively.

8.5 Nominal Strength Method

There is a significant need to develop an easy-to-use method based on first principles and good design assumptions that is easily fit into an engineer's design routine. This chapter presented a new method to predict the nominal moment capacity of concrete sandwich wall panels that is easy to implement and shown to be accurate. The results of the method are compared to those in the full-scale testing chapter and use the results generated in the shear-testing chapter. The following conclusions can be made about the findings in this chapter:

- A design method based on familiar first principles and a series of assumptions was developed.
- The developed partially-composite nominal moment design procedure was shown to be accurate to within 8% on average for the panels produced and tested in this study. These panels represented very different configurations and were reinforced with different connectors and connector patterns, further demonstrating robustness.
- The developed method relies only on connector load-slip information extracted from the push-off tests.
- The design procedure developed herein and recommended for use in practice suggests designing for 100% composite action to facilitate design using standard assumptions, like Whitney's Stress block,

and limiting connector end slip at ultimate to F_u. However, the analysis method is not limited to these assumptions.

REFERENCES

Adams, R. C., Leabu, V., Barber, J. S., Cordon, W. A., Florian, J. O., Galezewski, S., . . . Burchett, K. R. (1971). "Design of Precast Concrete Wall Panels." *Journal of the American Concrete Institute*, 98(7), 504-513.

American Concrete Institute (ACI) Committee 318. (2014). *Building Code Requirements for Structural Concrete. ACI 318-14.* Farmington Hills, MI.

ASTM Standard A370-14 (2014) "Standard Test Methods and Definitions for Mechanical Testing of Steel Products." ASTM International. West Conshohocken, PA. 2014. DOI: 10.1520/A0370-14. www.astm.org.

ASTM Standard C31 (2015) "Standard Practice for Making and Curing Concrete Test Specimens in the Field." ASTM International. West Conshohocken, PA. 2015. DOI: 10.1520/C0031_C0031M-15AE01. www.astm.org.

ASTM Standard C39 (2015) "Standard Test Method for Compressive Strength of Cylindrical Concrete Specimens." ASTM International. West Conshohocken, PA. 2015. DOI: 10.1520/C0039_C0039M-15A. www.astm.org.

ASTM Standard C138 (2014) "Standard Test Method for Density (Unit Weight), Yield, and Air Content (Gravimetric) of Concrete." ASTM International. West Conshohocken, PA. 2014. DOI: 10.1520/C0138_C0138M-14. www.astm.org.

ASTM Standard C143 (2015) "Standard Test Method for Slump of Hydraulic-Cement Concrete." ASTM International. West Conshohocken, PA. 2015. DOI: 10.1520/C0143_C0143M-15A. www.astm.org.

ASTM Standard E488-96 (1996) "Standard Test Method for Strength of Anchors in Concrete and Masonry Elements." ASTM International. West Conshohocken, PA. 1996. DOI: 10.1520/E0488-96. www.astm.org.

Bai, F., and Davidson, J. S. (2015). "Analysis of Partially Composite Foam Insulated Concrete Sandwich Structures." *Journal of Engineering Structures*, 91, 197-209.

Bunn, W. G. (2011). "CFRP Grid/Rigid Foam Shear Transfer Mechanism for Precast, Prestressed Concrete Sandwich Wall Panels." Thesis, presented to North Carolina State University at Raleigh, NC in partial fulfillment of requirements for the degree of Master of Science.

Collins, F. T. (1954). “Precast Concrete Sandwich Panels for Tilt-up Construction.” *Journal of the American Concrete Institute*, 26, 149-164.

Devalapura, R. K and Tadros, M. K. (1992). “Stress-Strain Modeling of 270 ksi Low-Relaxation Prestressing Strands.” *PCI Journal*, 37(2), 100-106.

Drysdale, R. G., Hamid, A. A., and Baker, L. R. (1994). *Masonry Structures: Behavior and Design*. Prentice Hall, Englewood Cliffs, NJ.

Einea, A., Salmon, D. C., Fogarasi, G. J., Culp, T. D., and Tadros, M. K. (1991). “State-of-of-the-Art of Precast Concrete Sandwich Panels.” *PCI Journal*, 36(6), 78-98.

Einea, A., Salmon, D. C., Tadros, M. K., and Culp, T. D. (1994). “A New Structurally and Thermally Efficient Precast Sandwich Panel System.” *PCI Journal*, 39(4), 90-101.

Frankl, B. A., Lucier, G. W., Hassan, T. K., and Rizkalla, S. H. (2011). “Behavior of Precast, Prestressed Concrete Sandwich Wall panels Reinforced with CFRP Shear Grid.” *PCI Journal*, 56(2), 42-54.

Hassan, T. K., and Rizkalla, S. H. (2010). “Analysis and Design Guidelines of Precast, Prestressed Concrete, Composite Load-Bearing Sandwich Wall Panels Reinforced with CFRP Grid.” *PCI Journal*, 55(2), 147-162.

ICC-ES Acceptance Criteria AC320 (2015). “Acceptance Criteria for Fiber-Reinforced Polymer Composite or Unreinforced Polymer Connectors Anchored in Concrete.” International Code Council (ICC) Evaluation Service, LLC. Washington, DC. 2015. www.icc-es.org.

Lee, B. J., and Pessiki, S. (2007). “Design and Analysis of Precast, Prestressed Concrete, Three-Wythe Sandwich Wall Panels.” *PCI Journal*, 52(4), 70-83.

Lee, B. J., and Pessiki, S. (2008). “Experimental Evaluation of Precast, Prestressed Concrete, Three-Wythe Sandwich Wall Panels.” *PCI Journal*, 53(2), 95-115.

Losch, E. D., Hynes, P. W., Andrews Jr., R., Browning, R., Cardone, P., Devalapura, R., . . . Yan, L. (2011). “State of the Art of Precast/Prestressed Concrete Sandwich Wall Panels” (2nd Ed). *PCI Journal*, 56(2), 131-176.

Maguire, M., (2009) “Impact of 0.7-inch Diameter Prestressing Strands in Bridge Girders” Thesis, presented to University of Nebraska-Lincoln at Lincoln, NE in partial fulfillment of requirements for the degree of Master of Science.

Morcous, G., Hatami, A., Maguire, M., Hanna, K., and Tadros, M. (2012). "Mechanical and Bond Properties of 18-mm- (0.7-in.-) Diameter Prestressing Strands." *Journal of Materials in Civil Engineering*, 24(6), 735-744. DOI: 10.1061/(ASCE)MT.1943-5533.0000424, 735-744.

Naito, C. J., Hoemann, J., Beacraft, M., and Bewick, B. (2012). "Performance and Characterization of Shear Ties for Use in Insulated Precast Concrete Sandwich Wall Panels." *Journal of Structural Engineering*, 138(1), 52-61.

Naito, C. J., Hoemann, J. M., Shull, J. S., Saucier, A., Salim, H. A., Bewick, B. T., and Hammons, M. I. (2011). "Precast/Prestressed Concrete Experiments Performance on Non-Load Bearing Sandwich Wall Panels." *Air Force Research Laboratory Rep. AFRL-RX-TY-TR-2011-0021*. Tyndall Air Force Base, Panama City, FL.

Newmark, N. M., Siess, C. P., Viest, I. M. (1951). "Tests and Analysis of Composite Beams with Incomplete Interaction." *Proceedings of the Society of Experimental Stress Analysis*, 9 (1), 75–92.

Nowak, A. S. and Collins, K. R. (2000). *Reliability of Structures*. McGraw-Hill, Boston, MA. Print.

Olsen, J., Maguire, M., (2016). "Shear Testing of Precast Concrete Sandwich Wall Panel Composite Shear Connectors." PCI/NBC. Nashville, TN.

Pantelides, C. P., Surapaneni, R., Reaveley, L. D. (2008). "Structural Performance of Hybrid GFRP/Steel Concrete Sandwich Panels." *Journal of Composites for Construction*. 12(5), 570-576.

Pessiki, S., and Mlynarczyk, A. (2003). "Experimental Evaluation of the Composite Behavior of Precast Concrete Sandwich Wall Panels." *PCI Journal*, 48(2), 54-71.

Salmon, D. C., and Einea, A. (1995). "Partially Composite Sandwich Panel Deflections." *Journal of Structural Engineering*, 121, 778-783.

Salmon, D. C., Einea, A., Tadros, M. K., and Culp, T. D. (1997). "Full Scale Testing of Precast Concrete Sandwich Panels." *American Concrete Institute Structural Journal*, 94(4), 354-362.

Seeber, K. E., Andrews, R. J., Baty, J. R., Campbell, P. S., Dobbs, J. E., Force, G., . . . Wescott, H. E. (1997). "State-of-the-Art of Precast/Prestressed Sandwich Wall Panels." *PCI Journal*, 42(2), 92-134.

Seeber, K., Anderson, N. S., Barrett, C. T., Brecher, E. F., Cleland, N. M., D'Arcy, T. J., . . . Wynings, C. E. (2004). *PCI Design Handbook; Precast and Prestressed Concrete* (6th ed.). Chicago, IL. Precast/Prestressed Concrete Institute. Retrieved 2015.

Teixeira, N., Tomlinson, D. G., and Fam, A. (2016). “Precast Concrete Sandwich Wall Panels with Bolted Angle Connections Tested in Flexure Under Simulated Wind Pressure and Suction.” *PCI Journal*, 61(4), 65–83.

Tomlinson, D. G. (2015). “Behaviour of Partially Composite Precast Concrete Sandwich Panels under Flexural and Axial Loads.” Thesis, presented to Queen’s University at Kingston, Ontario, Canada in partial fulfillment of requirements for the degree of Doctor of Philosophy.

Whitney, C. S. (1937). “Design of Reinforced Concrete Members Under Flexure or Combined Flexure and Direct Compression.” *ACI Journal Proceedings*, 33(3), 483–498.

Wight, J. K., and MacGregor, J. G. (2005). *Reinforced Concrete Mechanics and Design*. Pearson Education, Inc., Upper Saddle River, NJ. Print.

Woltman, G., Tomlinson, D., and Fam, A. (2013). “Investigation of Various GFRP Shear Connectors for Insulated Precast Concrete Sandwich Wall Panels.” *Journal of Composites of Construction*, 3(17), 711-721. DOI:10.1061/(ASCE)CC.1943-5614.0000373.

APPENDICES

APPENDIX A. Elastic Hand Method Analysis Examples

This appendix contains examples and predictions for predicting cracking moment of the full-scale panels (which utilized HK Composite, Nu-Tie, and Thermomass connectors) using the Elastic Hand Method proposed in this report. Table A-1 Load, Deflection, and Slip predictions for panels using Table A-1 summarizes the results of this section. The calculations of the values in Table A-1 follow thereafter. These examples illustrate how the Elastic Hand Method predicts the deflection and cracking of a given panel. Note that the Elastic Hand Procedure is iterative.

Table A-1 Load, Deflection, and Slip predictions for panels using

Panel	**Load Considered**	**Load** *(psf)*	**Deflection** *(in)*	**Slip** *(in)*
A-2	Self-Weight	75	0.154	0.0184
	Four-Point	81.3	0.202	0.0239
	Total Applied	156.3	0.356	0.0423
A-4	Self-Weight	75.00	0.1130	0.0130
	Four-Point	119.52	0.2173	0.0247
	Total Applied	194.52	0.3303	0.0377
B-1 and B-2	Self-Weight	100	0.1074	0.0142
	Four-Point	49.4	0.0648	0.0085
	Total Applied	149.9	0.1722	0.0227
BC-1 and BC-2	Self-Weight	100	0.073	0.0103
	Four-Point	95.77	0.0845	0.0090
	Total Applied	195.77	0.1575	0.0193
D-1 and D-2	Self-Weight	100.00	0.0600	0.0071
	Four-Point	122.62	0.0888	0.0105
	Total Applied	222.62	0.1488	0.0176

A-2 Panel (Nu-Tie connectors) Analysis Example (Prestressed)

Panel Properties

$L = 16\ ft$ $\quad Span = 15\ ft$

$t_{wy1} = 3\ in$ $\quad t_{wy2} = 3\ in$

$t_{ins} = 4\ in$ $\quad b = 4\ ft$

$f_c' = 10.43\ ksi$ $\quad A_{ps} = 0.255\ in^2$ (three prestressing strands)

$x_i = \begin{bmatrix} 24 \\ 72 \end{bmatrix} in$ $\quad N = 2$

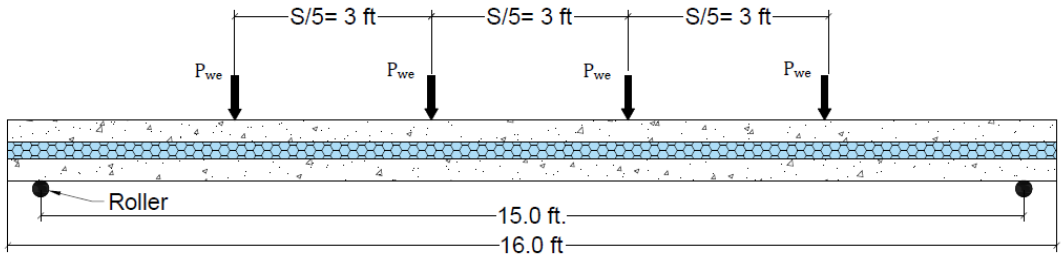

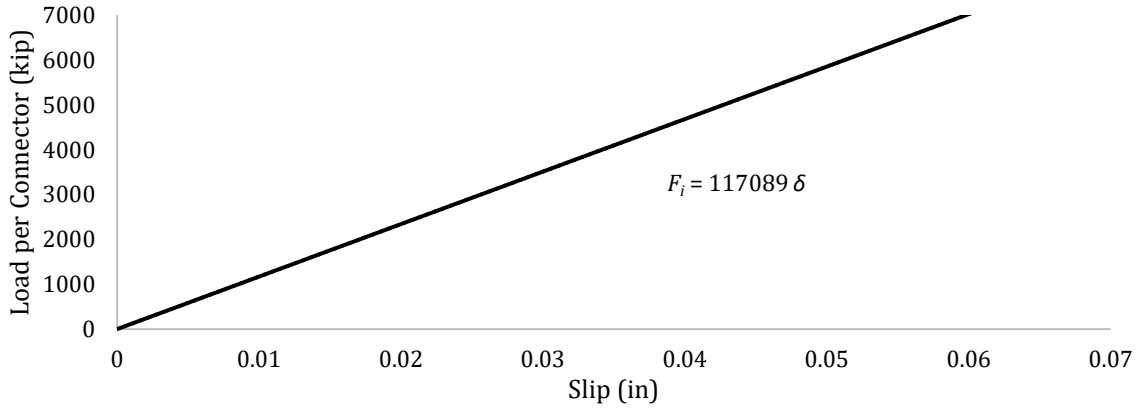

Figure A-1 Load vs Slip of Connector A (Nu-Tie connector)

Solution

1. Calculate the material and section properties of a non-composite sandwich panel.

$$x_{P1} = \frac{Span}{5} = 3\ ft \quad x_{P2} = 2 * x_{P1} = 6\ ft$$

$$E_c = 6191.46\ ksi$$

$$f_r = \frac{7.5\ ksi}{1000} * \sqrt{10430\ psi} + \frac{170\ ksi * 0.085\ in^2 * 3}{48\ in * 3\ in} = 1.067\ ksi$$

$$I_{NC1} = \frac{b}{12} * \left(t_{wy_1}^3\right) = \frac{4\ ft * 12\frac{in}{ft}}{12} * (3\ in)^3 = 108\ in^4$$

$$I_{NC2} = \frac{b}{12} * \left(t_{wy_2}^3\right) = \frac{4\ ft * 12\frac{in}{ft}}{12} * (3\ in)^3 = 108\ in^4$$

$$Z = \frac{t_{wy_1} + t_{wy_2}}{2} + t_{insul} = \frac{3\ in + 3\ in}{2} + 4\ in = 7\ in$$

2. Assume an end slip, which is the slip at the end connector line (see Figure 6-2). Calculate the slip in the other connectors using similar triangles or Eq. (6-5).

   Assuming δ_{max} = 0.0423 in

$$\delta(i) = \delta_{max} * \frac{\left(\frac{L}{2} - x_i\right)}{\left(\frac{L}{2} - x_1\right)} = \begin{bmatrix} 0.0423 \\ 0.0141 \end{bmatrix} in$$

3. Calculate the shear forces in each connector using Figure A-1.

$$F_i = 2 * \begin{bmatrix} 4955.7 \\ 1652 \end{bmatrix} lb$$

$$F_{sum} = \sum F_i = 13220\ lb$$

4. Calculate the cracking moment:

$$M_{wy_2} = 2 * I_{NC2} * \left(\frac{f_r}{t_{wy_2}} - \frac{F_{sum}}{b * t_{wy_2}^2}\right)$$

$$= 2 * 108\ in^4 * \left(\frac{1.067\ ksi}{3\ in} - \frac{13.22\ kip}{48\ in * (3\ in)^2}\right) = 5.851\ kip * ft$$

5. Calculate the equivalent load that wythe 2 can carry using equations (6-9).

$$w_{we2} = \frac{8 * M_{wy_2}}{Span^2} = \frac{8 * 5.851\ kip * ft}{(15\ ft)^2} = 0.208\frac{kip}{ft}$$

$$P_{we2} = \frac{M_{wy_2}}{(x_{P1} + x_{P2})} = \frac{5.851\ kip * ft}{(3\ ft + 6\ ft)} = 0.65\ kips$$

6. Using the equivalent load from the previous step, calculate axial and rotational displacement at the end connector using Eq. (6-10) and (6-11)

$$\theta_{w_{we2}} = \frac{w_{we2} * Span^3}{24 * E * I_{NC2}} = \frac{0.208\frac{kip}{ft} * (15\ ft)^3 * 144\ in^2/ft^2}{24 * 6191.46\ ksi * 108\ in^4} = 0.00630$$

$$\theta_{P_{we2}} = P_{we2}\left\{\frac{x_{P1}[(Span^2 - x_{P1}^2) + (Span - x_{P1})(2Span - x_{P1})]}{6 * Span * E_c * I_{NC2}} + \frac{x_{P2}[(Span^2 - x_{P2}^2) + (Span - x_{P2})(2Span - x_{P2})]}{6 * Span * E_c * I_{NC2}}\right\}$$

$$\theta_{P_{we2}} = 0.65\left\{\frac{3[(15^2 - 3^2) + (15 - 3)(30 - 3)]}{6 * 15 * 6191.46 * 108} + \frac{6[(15^2 - 6^2) + (15 - 6)(30 - 6)]}{6 * 15 * 6191.46 * 108}\right\}$$

$$= 0.00630$$

$$\Delta_{Rot} = \theta * Z = 0.00630 * 7\ in = 0.04410\ in$$

$$\Delta_{Axial} = 2 * \sum_{i=1}^{n} F(i) * \left(\frac{\frac{L}{2} - x_i}{b * E_c * t_{wy_1}}\right) = 0.00178 \text{ in}$$

7. Using Equation (6-11) and (6-12), calculate the slip at the end connector and compare to assumed value.

$$\delta_{max} = \Delta_{Rot} - \Delta_{Axial} = 0.0441\ in - 0.00178 \text{ in} = 0.04232\ in$$

$$\delta_{max} = Assumed\ \delta_{max} \quad \therefore \quad OK$$

8. Calculate the cracking moment using Equation (6-14).

$$M_{cr} = M_{wy_2} * 2 + F_{sum} * Z$$

$$= 2 * 5.851\ kip * ft + 13.22\ kip * 7\ in = \mathbf{19.4137\ kip * ft}$$

$$\Delta_{w_{we2}} = \frac{5 * w_{we2} * Span^4}{384 * E_c * I_{NC2}} = \frac{5 * 0.208\frac{kip}{ft} * (15\ ft)^4 * \left(12\frac{in}{ft}\right)^3}{384 * 6191.46\ ksi * 108\ in^4} = 0.3544\ in$$

$$\Delta_{P_{we2}} = \left(\frac{P_{we2}}{24 * E_c * I_{NC2}}\right)\{x_{P1} * (3 * Span^2 - 4 * x_{P1}^2) + x_{P2} * (3 * Span^2 - 4 * x_{P2}^2)\}$$

$$\Delta_{P_{we2}} = \left(\frac{0.559}{24 * 6191.46 * 108}\right)\{3 * (3 * 15^2 - 4 * 3^2) + 6 * (3 * 15^2 - 4 * 6^2)\} * 12^3$$

$$= 0.357\ in$$

Table A-2 Total Load, Equivalent Load Deflection, and Slip

Load Distribution	**Total Load, p_{Total}**	**Deflection from Equivalent Load, Δ_e** *(in)*	**Slip** *(in)*
Uniform Distributed Load	$\frac{M_{applied} * 8}{Span^2 * b} = \frac{19.4 * 8}{15^2 * 4} = 172.55\ psf$	0.3544	0.04232
Four-Point Loads	$\frac{4M_{applied}}{(x_{P1} + x_{P2}) * Span * b} = \frac{4 * 19.4}{9 * 15 * 4} = 143.79\ psf$	0.357	0.04232

The actual load on the sandwich wall panel included the four-point applied load as well as self-weight.

$$p_{self} = 150\ pcf * (6\ in) = 75\ psf$$

$$w_{self} = p_{self} * b = 75\ psf * 4\ ft = 300\ plf$$

$$M_{self} = \frac{\left(w_{self} * Span^2\right)}{8} = \frac{300\ plf * (15ft)^2}{8} = 8.4375\ kip * ft$$

$$M_{FourPt} = M_{cr} - M_{self} = 19.4137\ kip * ft - 8.4375\ kip * ft = 10.976\ kip * ft$$

$$P_{FourPt} = 4 * \left(\frac{10.976\ kip * ft}{36\ in + 72\ in}\right) = 4.878\ kip$$

$$p_{FourPt} = \frac{4878\ lbs}{15\ ft * 4\ ft} = 81.3\ psf$$

$$\boldsymbol{p_{TotalApplied} = p_{self} + p_{FourPt} = 75\ psf + 81.3\ psf = 156.3\ psf}$$

Similar effects can be calculated for deflection also, as well as slip. Since self-weight is a distributed load, the uniform distributed load values will be used from Table A-2.

$$\Delta_{self} = \frac{p_{self}}{p_{Total}} * \Delta_e = \frac{75\ psf}{172.55\ psf} * 0.3544\ in = 0.154\ in$$

$$\Delta_{FourPt} = \frac{p_{FourPt}}{p_{Total}} * \Delta_e = \frac{81.3\ psf}{143.79\ psf} * 0.357\ in = 0.202\ in$$

$$\boldsymbol{\Delta_{Total} = 0.154\ in + 0.202\ in = 0.356\ in}$$

$$\delta_{self} = \frac{p_{self}}{p_{Total}} * \delta_{max} = \frac{75\ psf}{172.55\ psf} * 0.04232\ in = 0.0184\ in$$

$$\delta_{FourPt} = \frac{p_{FourPt}}{p_{Total}} * \Delta_{max} = \frac{81.3\ psf}{143.79\ psf} * 0.04232\ in = 0.0239\ in$$

$$\boldsymbol{\delta_{Total} = \delta_{self} + \delta_{FourPt} = 0.0184\ in + 0.0239\ in = 0.0423\ in}$$

A-4 Panel (Nu-Tie connectors) Analysis Example (Prestressed)

Panel Properties

$L = 16\ ft$ $Span = 15\ ft$

$t_{wy1} = 3\ in$ $t_{wy2} = 3\ in$

$t_{ins} = 4\ in$ $b = 4\ ft$

$f_c' = 10.43\ ksi$ $A_{ps} = 0.255\ in^2$ (three prestressing strands)

$x_i = \begin{bmatrix} 24 \\ 72 \end{bmatrix} in$ $N = 4$

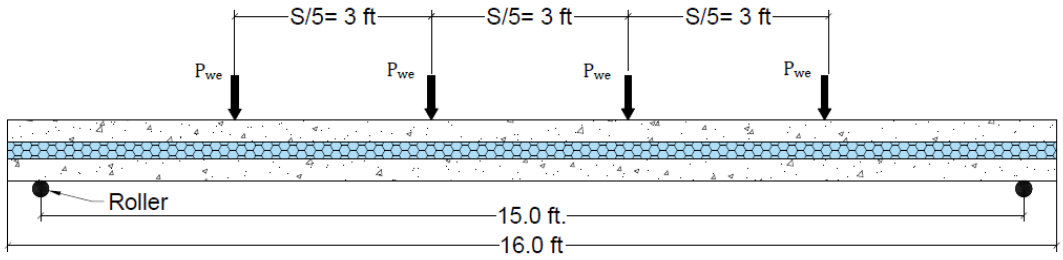

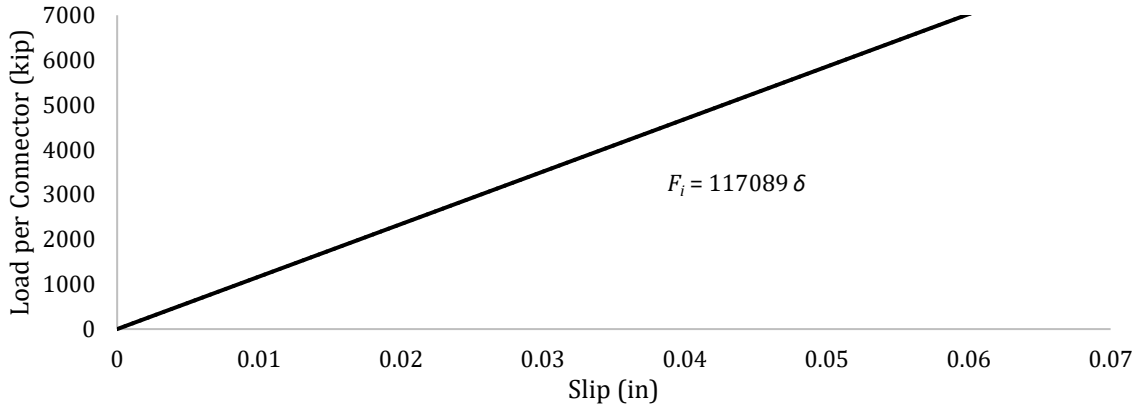

Figure A-2 Load vs Slip of Connector A (Nu-Tie connector)

Solution

1. Calculate the material and section properties of a non-composite sandwich panel.

$$x_{P1} = \frac{Span}{5} = 3\ ft \quad x_{P2} = 2 * x_{P1} = 6\ ft$$

$$E_c = 6191.46\ ksi$$

$$f_r = \frac{7.5\ ksi}{1000} * \sqrt{10430\ psi} + \frac{170\ ksi * 0.085\ in^2 * 3}{48\ in * 3\ in} = 1.067\ ksi$$

$$I_{NC1} = \frac{b}{12} * \left(t_{wy_1}^3\right) = \frac{4\ ft * 12\frac{in}{ft}}{12} * (3\ in)^3 = 108\ in^4$$

$$I_{NC2} = \frac{b}{12} * \left(t_{wy_2}^3\right) = \frac{4\ ft * 12\frac{in}{ft}}{12} * (3\ in)^3 = 108\ in^4$$

$$Z = \frac{t_{wy_1} + t_{wy_2}}{2} + t_{insul} = \frac{3\ in + 3\ in}{2} + 4\ in = 7\ in$$

2. Assume an end slip, which is the slip at the end connector line (see Figure 6-2). Calculate the slip in the other connectors using similar triangles or Eq. (6-5).

   Assuming δ_{max} = 0.0377 in

$$\delta(i) = \delta_{max} * \frac{\left(\frac{L}{2} - x_i\right)}{\left(\frac{L}{2} - x_1\right)} = \begin{bmatrix}0.0377\\0.0126\end{bmatrix} in$$

3. Calculate the shear forces in each connector using Figure A.

$$F_i = \begin{bmatrix}4413.4\\1471.1\end{bmatrix} lb$$

$$F_{sum} = 4 * \sum F_i = 23540\ lb$$

4. Calculate the cracking moment:

$$M_{wy_2} = 2 * I_{NC2} * \left(\frac{f_r}{t_{wy_2}} - \frac{F_{sum}}{b * t_{wy_2}^2}\right)$$

$$= 2 * 108\ in^4 * \left(\frac{1.067\ ksi}{3\ in} - \frac{23.54\ kip}{48\ in * (3\ in)^2}\right) = 5.421\ kip * ft$$

5. Calculate the equivalent load that wythe 2 can carry using equations (6-9).

$$w_{we2} = \frac{8 * M_{wy_2}}{Span^2} = \frac{8 * 5.421\ kip * ft}{(15\ ft)^2} = 0.1927\frac{kip}{ft}$$

$$P_{we2} = \frac{M_{wy_2}}{(x_{P1} + x_{P2})} = \frac{5.421\ kip * ft}{(3\ ft + 6\ ft)} = 0.602\ kips$$

6. Using the equivalent load from the previous step, calculate axial and rotational displacement at the end connector using Eq. (6-10) and (6-11).

$$\theta_{w_{we2}} = \frac{w_{we2} * Span^3}{24 * E * I_{NC2}} = \frac{0.1927\frac{kip}{ft} * (15\ ft)^3 * 144\ in^2/ft^2}{24 * 6191.46\ ksi * 108\ in^4} = 0.005837$$

$$\theta_{P_{we2}} = P_{we2}\left\{\frac{x_{P1}[(Span^2 - x_{P1}^2) + (Span - x_{P1})(2 * Span - x_{P1})]}{6 * Span * E_c * I_{NC2}} + \frac{x_{P2}[(Span^2 - x_{P2}^2) + (Span - x_{P2})(2 * Span - x_{P2})]}{6 * Span * E_c * I_{NC2}}\right\}$$

$$\theta_{P_{we2}} = 0.602\left\{\frac{3[(15^2 - 3^2) + (15 - 3)(30 - 3)]}{6 * 15 * 6191.46 * 108} + \frac{6[(15^2 - 6^2) + (15 - 6)(30 - 6)]}{6 * 15 * 6191.46 * 108}\right\}$$

$$= 0.005837$$

$$\Delta_{Rot} = \theta * Z = 0.005837 * 7\ in = 0.04086\ in$$

$$\Delta_{Axial} = 2 * \sum_{i=1}^{n} F(i) * \left(\frac{\frac{L}{2} - x_i}{b * E_c * t_{wy_1}}\right) = 0.003168 \text{ in}$$

7. Using Equation (6-11) and (6-12), calculate the slip at the end connector and compare to assumed value.

$$\delta_{max} = \Delta_{Rot} - \Delta_{Axial} = 0.04086\ in - 0.003168 \text{ in} = 0.0377\ in$$

$$\delta_{max} = Assumed\ \delta_{max} \quad \therefore \quad OK$$

8. Calculate the cracking moment using Equation (6-14).

$$M_{cr} = M_{wy_2} * 2 + F_{sum} * Z$$

$$= 2 * 5.421\ kip * ft + 23.54\ kip * 7\ in = \mathbf{24.573\ kip * ft}$$

$$\Delta_{w_{we2}} = \frac{5 * w_{we2} * Span^4}{384 * E_c * I_{NC2}} = \frac{5 * 0.1927\frac{kip}{ft} * (15\ ft)^4 * \left(12\frac{in}{ft}\right)^3}{384 * 6191.46\ ksi * 108\ in^4} = 0.3283\ in$$

$$\Delta_{P_{we2}} = \left(\frac{P_{we2}}{24 * E_c * I_{NC2}}\right)\{x_{P1} * (3 * Span^2 - 4 * x_{P1}^2) + x_{P2} * (3 * Span^2 - 4 * x_{P2}^2)\}$$

$$\Delta_{P_{we2}} = \left(\frac{0.602}{24 * 6191.46 * 108}\right)\{3 * (3 * 15^2 - 4 * 3^2) + 6 * (3 * 15^2 - 4 * 6^2)\} * 12^3$$

$$= 0.331\ in$$

Table A-3 Total Load, Equivalent Load Deflection, and Slip

Load Distribution	**Total Load, p_{Total}**	**Deflection from Equivalent Load, Δ_e** *(in)*	**Slip** *(in)*
Uniform Distributed Load	$\frac{M_{applied} * 8}{Span^2 * b} = \frac{24.57 * 8}{15^2 * 4} = 218.43\ psf$	0.3283	0.0377
Four-Point Loads	$\frac{4M_{applied}}{(x_{P1} + x_{P2}) * Span * b} = \frac{4 * 24.57}{9 * 15 * 4} = 182\ psf$	0.3310	0.0377

The actual load on the sandwich wall panel included the four-point applied load as well as self-weight.

$$p_{self} = 150\ pcf * (6\ in) = 75\ psf$$

$$w_{self} = p_{self} * b = 75\ psf * 4\ ft = 300\ plf$$

$$M_{self} = \frac{(w_{self} * Span^2)}{8} = \frac{300\ plf * (15ft)^2}{8} = 8.4375\ kip * ft$$

$$M_{FourPt} = M_{cr} - M_{self} = 24.573\ kip * ft - 8.4375\ kip * ft = 16.1355\ kip * ft$$

$$P_{FourPt} = 4 * \left(\frac{16.1355\ kip * ft}{36\ in + 72\ in}\right) = 7.171\ kip$$

$$p_{FourPt} = \frac{7171\ lbs}{15\ ft * 4\ ft} = 119.52\ psf$$

$$\boldsymbol{p_{TotalApplied} = p_{self} + p_{FourPt} = 75\ psf + 119.52\ psf = 194.52\ psf}$$

Similar effects can be calculated for deflection also, as well as slip. Since self-weight is a distributed load, the uniform distributed load values will be used from Table A-3.

$$\Delta_{self} = \frac{p_{self}}{p_{Total}} * \Delta_e = \frac{75\ psf}{218.43\ psf} * 0.3283\ in = 0.113\ in$$

$$\Delta_{FourPt} = \frac{p_{FourPt}}{p_{Total}} * \Delta_e = \frac{119.52\ psf}{182\ psf} * 0.3310\ in = 0.2173\ in$$

$$\boldsymbol{\Delta_{Total} = 0.113\ in + 0.2173\ in = 0.3303\ in}$$

$$\delta_{self} = \frac{p_{self}}{p_{Total}} * \delta_{max} = \frac{75\ psf}{218.43\ psf} * 0.0377\ in = 0.013\ in$$

$$\delta_{FourPt} = \frac{p_{FourPt}}{p_{Total}} * \Delta_{max} = \frac{119.52\ psf}{182\ psf} * 0.0377\ in = 0.02476\ in$$

$$\boldsymbol{\delta_{Total} = \delta_{self} + \delta_{FourPt} = 0.0130\ in + 0.02476\ in = 0.0377\ in}$$

B Panel (only Thermomass CC connectors) Analysis Example (Mild Reinforcement)

Panel Properties

$L = 16\ ft$ $Span = 14\ ft$

$t_{wy1} = 4\ in$ $t_{wy2} = 4\ in$

$t_{ins} = 3\ in$ $b = 3\ ft$

$f_c' = 9.23\ ksi$

$x_i = \begin{bmatrix} 30 \\ 82 \end{bmatrix} in$ $N = 3$

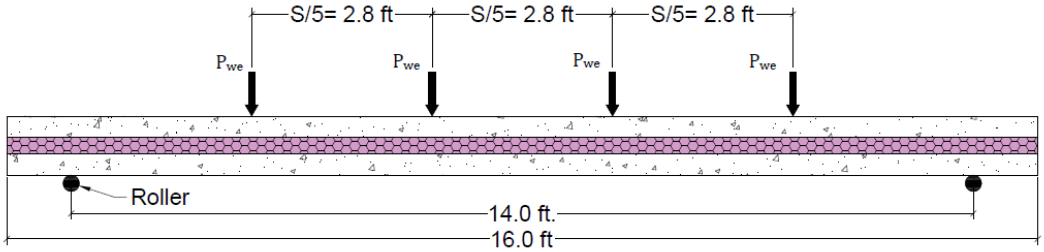

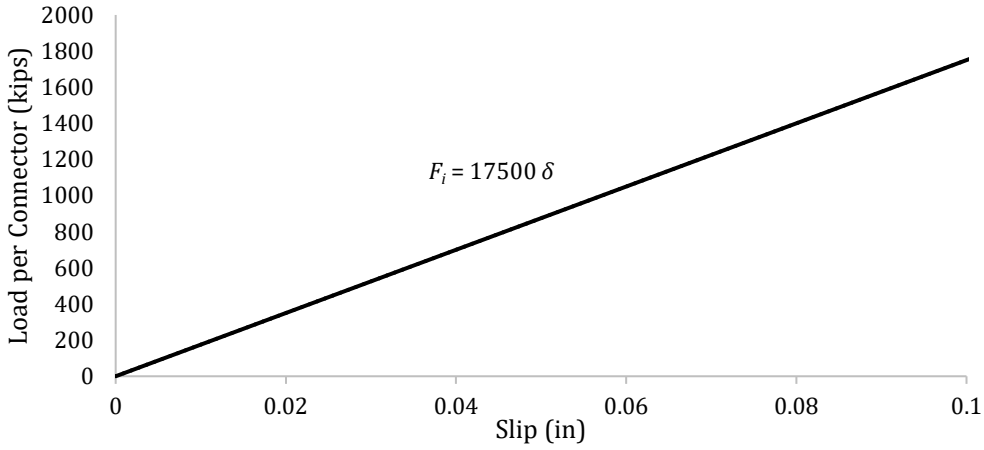

Figure A-3 Load vs slip of Connector B (Thermomass CC connector)

Solution

1. Calculate the material and section properties of a non-composite sandwich panel. The modulus of rupture of the concrete (f_r) was measured in this case, so the actual value is included here.

$$x_{P1} = \frac{Span}{5} = 2.8\ ft \quad x_{P2} = 2 * x_{P1} = 5.6\ ft$$

$$E_c = 5824.4\ ksi$$

$$f_r = 0.691\ ksi$$

$$I_{NC1} = \frac{b}{12} * \left(t_{wy_1}^3\right) = \frac{3\ ft * 12\frac{in}{ft}}{12} * (4\ in)^3 = 192\ in^4$$

$$I_{NC2} = \frac{b}{12} * \left(t_{wy_2}^3\right) = \frac{3\ ft * 12\frac{in}{ft}}{12} * (4\ in)^3 = 192\ in^4$$

$$Z = \frac{t_{wy_1} + t_{wy_2}}{2} + t_{insul} = \frac{4\ in + 4\ in}{2} + 3\ in = 7\ in$$

2. Assume an end slip, which is the slip at the end connector line (see Figure 6-2). Calculate the slip in the other connectors using similar triangles or Eq. (6-5).

   Assuming δ_{max} = 0.0227 in

$$\delta(i) = \delta_{max} * \frac{\left(\frac{L}{2} - x_i\right)}{\left(\frac{L}{2} - x_1\right)} = \begin{bmatrix}0.0227\\0.0048\end{bmatrix} in$$

3. Calculate the shear forces in each connector using Figure A-3.

$$F_i = 3 * \begin{bmatrix}405.5\\86\end{bmatrix} lb$$

$$F_{sum} = \sum F_i = 1475\ lb$$

4. Calculate the cracking moment:

$$M_{wy_2} = 2 * I_{NC2} * \left(\frac{f_r}{t_{wy_2}} - \frac{F_{sum}}{b * t_{wy_2}^2}\right)$$

$$= 2 * 192\ in^4 * \left(\frac{0.691\ ksi}{4\ in} - \frac{1.475\ kip}{36\ in * (4\ in)^2}\right) = 5.446\ kip * ft$$

5. Calculate the equivalent load that wythe 2 can carry using equation (6-9).

$$w_{we2} = \frac{8 * M_{wy_2}}{Span^2} = \frac{8 * 5.446\ kip * ft}{(14\ ft)^2} = 0.2223\frac{kip}{ft}$$

$$P_{we2} = \frac{M_{wy_2}}{(x_{P1} + x_{P2})} = \frac{5.446\ kip * ft}{(2.8\ ft + 5.6\ ft)} = \ 0.648\ kip$$

6. Using the equivalent load from the previous step, calculate axial and rotational displacement at the end connector using Eq. (6-10) and (6-11).

$$\theta_{w_{we2}} = \frac{w_{we2} * Span^3}{24 * E_c * I_{NC2}} = \frac{0.2223 \frac{kip}{ft} * (14\ ft)^3 * 144}{24 * 5824.4\ ksi * 192\ in^4} = \ 0.003273$$

$$\theta_{P_{we2}} = P_{we2}\left\{\frac{x_{P1}[(Span^2 - x_{P1}^2) + (Span - x_{P1})(2Span - x_{P1})]}{6 * Span * E_c * I_{NC2}}\right.$$

$$\left. + \frac{x_{P2}[(Span^2 - x_{P2}^2) + (Span - x_{P2})(2Span - x_{P2})]}{6 * Span * E_c * I_{NC2}}\right\}$$

$$\theta_{P_{we2}} = 0.648\left\{\frac{2.8[(14^2 - 2.8^2) + (14 - 2.8)(28 - 2.8)]}{6 * 14 * 5824.4 * 192}\right.$$

$$\left. + \frac{5.6[(14^2 - 5.6^2) + (14 - 5.6)(28 - 5.6)]}{6 * 14 * 5824.4 * 192}\right\} = 0.00327$$

$$\Delta_{Rot} = \theta * Z = 0.003273 * 7\ in = 0.02291\ in$$

$$\Delta_{Axial} = 2 * \sum_{i=1}^{n} F(i) * \left(\frac{\frac{L}{2} - x_i}{b * E_c * t_{wy_1}}\right) = 0.0002 \text{ in}$$

7. Using Eq. (6-11) and (6-12), calculate the slip at the end connector and compare to assumed value.

$$\delta_{max} = \Delta_{Rot} - \Delta_{Axial} = 0.02291\ in - 0.0002 \text{ in} = 0.02271\ in$$

$$\delta_{max} = Assumed\ \delta_{max} \quad \therefore \quad OK$$

8. Calculate the cracking moment using Equation (6-14).

$$M_{cr} = M_{wy_2} * 2 + F_{sum} * Z$$

$$= 2 * 5.446\ kip * ft + 1475\ lb * 7\ in = \mathbf{11.752\ kip * ft}$$

$$\Delta_{w_{we2}} = \frac{5 * w_{we2} * Span^4}{384 * E_c * I_{NC2}} = \frac{5 * 0.2223 \frac{kip}{ft} * (14\ ft)^4 * \left(12 \frac{in}{ft}\right)^3}{384 * 5824.4\ ksi * 192\ in^4} = 0.1718\ in$$

$$\Delta_{P_{we2}} = \left(\frac{P_{we2}}{24 * E_c * I_{NC2}}\right)\{x_{P1} * (3 * Span^2 - 4 * x_{P1}^2) + x_{P2} * (3 * Span^2 - 4 * x_{P2}^2)\}$$

$$\Delta_{P_{we2}} = \left(\frac{0.648}{24 * 5824.4 * 192}\right)\{2.8 * (3 * 14^2 - 4 * 2.8^2) + 5.6 * (3 * 14^2 - 4 * 5.6^2)\} * 12^3$$

$$= 0.1732\ in$$

Table A-4 Total Load, Equivalent Load Deflection, and Slip

Load Distribution	**Total Load, p_{Total}**	**Deflection from Equivalent Load, Δ_e** *(in)*	**Slip** *(in)*
Uniform Distributed Load	$\frac{M_{applied} * 8}{Span^2 * b} = \frac{11.75 * 8}{14^2 * 3} = 160\ psf$	0.1718	0.02271
Four-Point Loads	$\frac{4M_{applied}}{(x_{P1} + x_{P2})b * Span} = \frac{4 * 11.75}{8.4 * 3 * 14} = 133.2\ psf$	0.1732	0.02271

The actual load on the sandwich wall panel included the four-point applied load as well as self-weight.

$$p_{self} = 150\ pcf * (8\ in) = 100\ psf$$

$$w_{self} = p_{self} * b = 100\ psf * 3\ ft = 300\ plf$$

$$M_{self} = \frac{(w_{self} * Span^2)}{8} = \frac{300\ plf * (14ft)^2}{8} = 7.35\ kip * ft$$

$$M_{FourPt} = M_{cr} - M_{self} = 11.752\ kip * ft - 7.35\ kip * ft = 4.402\ kip * ft$$

$$P_{FourPt} = 4 * \left(\frac{4.402\ kip * ft}{33.6\ in + 67.2\ in}\right) = 2.096\ kip$$

$$p_{FourPt} = \frac{2096\ lbs}{14\ ft * 3\ ft} = 49.9\ psf$$

$$\boldsymbol{p_{TotalApplied} = p_{self} + p_{FourPt} = 100\ psf + 49.9\ psf = 149.9\ psf}$$

Similar effects can be calculated for deflection also, as well as slip. Since self-weight is a distributed load, the uniform distributed load values will be used from Table A-4.

$$\Delta_{self} = \frac{p_{self}}{p_{Total}} * \Delta_e = \frac{100\ psf}{160\ psf} * 0.1718\ in = 0.1074\ in$$

$$\Delta_{FourPt} = \frac{p_{FourPt}}{p_{Total}} * \Delta_e = \frac{49.9\ psf}{133.24\ psf} * 0.1732\ in = 0.0648\ in$$

$$\boldsymbol{\Delta_{Total} = 0.1074\ in + 0.0648\ in = 0.1722\ in}$$

$$\delta_{self} = \frac{p_{self}}{p_{Total}} * \delta_{max} = \frac{100\ psf}{160\ psf} * 0.0227\ in = 0.0142\ in$$

$$\delta_{FourPt} = \frac{p_{FourPt}}{p_{Total}} * \Delta_{max} = \frac{49.9\ psf}{133.24\ psf} * 0.0227\ in = 0.0085\ in$$

$$\boldsymbol{\delta_{Total} = \delta_{self} + \delta_{FourPt} = 0.0142\ in + 0.0085\ in = 0.0227\ in}$$

BC Panel (Thermomass CC and X connectors) Analysis Example (Mild Reinforcement)

Panel Properties

$L = 16\ ft$ $Span = 14\ ft$

$t_{wy1} = 4\ in$ $t_{wy2} = 4\ in$

$t_{ins} = 3\ in$ $b = 3\ ft$

$f_c' = 9.23\ ksi$ $A_s = 0.44\ in^2$

$x_{CCi} = \begin{bmatrix} 16 \\ 32 \\ 48 \\ 64 \\ 80 \end{bmatrix} in$ $N_{CC} = 3$

$x_{Xi} = [24] in$ $N_X = 3$

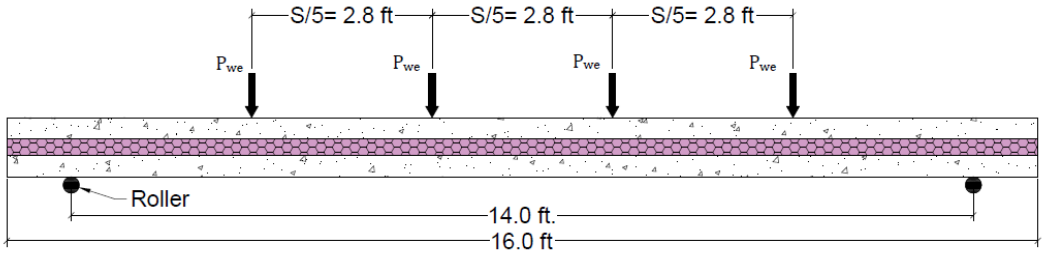

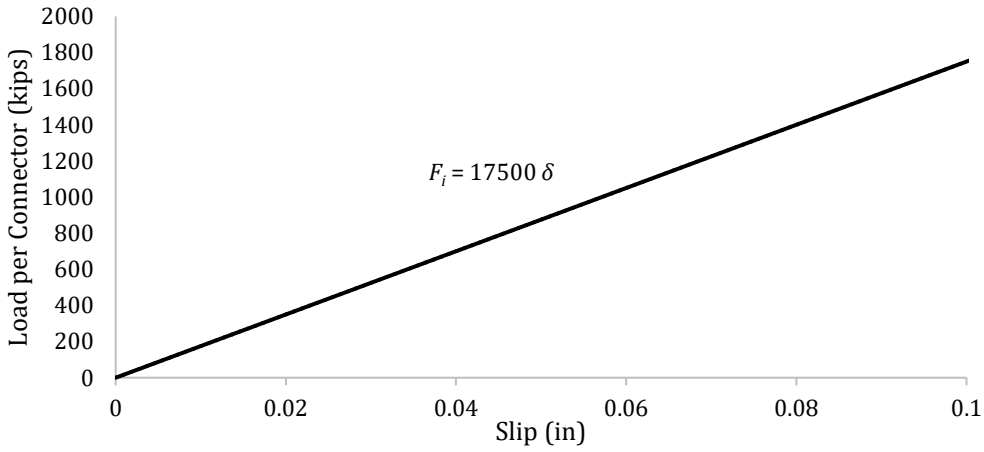

Figure A-4 Load vs slip of Connector B (Thermomass CC connector)

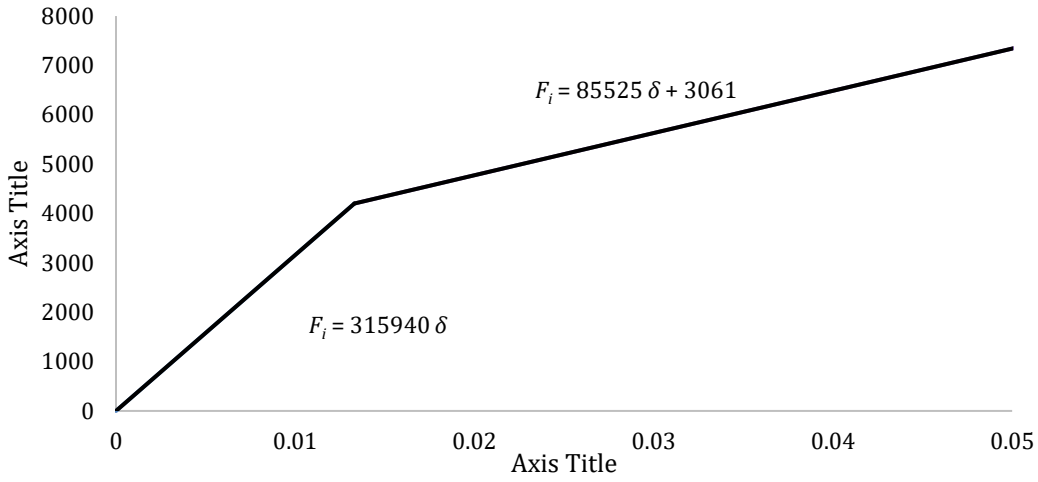

Figure A-5 Load vs slip of Connector C (Thermomass X connector)

Solution

1. Calculate the material and section properties of a non-composite sandwich panel. The modulus of rupture of the concrete (f_r) was measured in this case, so the actual value is included here.

$$x_{P1} = \frac{Span}{5} = 2.8\ ft \quad x_{P2} = 2 * x_{P1} = 5.6\ ft$$

$$E_c = 5824.4\ ksi$$

$$f_r = 0.691\ ksi$$

$$I_{NC1} = \frac{b}{12} * \left(t_{wy_1}^3\right) = \frac{3\ ft * 12\frac{in}{ft}}{12} * (4\ in)^3 = 192\ in^4$$

$$I_{NC2} = \frac{b}{12} * \left(t_{wy_2}^3\right) = \frac{3\ ft * 12\frac{in}{ft}}{12} * (4\ in)^3 = 192\ in^4$$

$$Z = \frac{t_{wy_1} + t_{wy_2}}{2} + t_{insul} = \frac{4\ in + 4\ in}{2} + 3\ in = 7\ in$$

2. Assume an end slip, which is the slip at the end connector line (see Figure 6-2). Calculate the slip in the other connectors using similar triangles or Eq. (6-5).

   Assuming δ_{max} = 0.01929 in

$$x_i = \begin{bmatrix} 16 \\ 24 \\ 32 \\ 48 \\ 64 \\ 80 \end{bmatrix} in \qquad \delta(i) = \delta_{max} * \frac{\left(\frac{L}{2} - x_i\right)}{\left(\frac{L}{2} - x_1\right)} = \begin{bmatrix} 0.01929 \\ 0.01736 \\ 0.01543 \\ 0.01157 \\ 0.00772 \\ 0.00386 \end{bmatrix} in$$

3. Calculate the shear forces in each connector using Figure A-4 and Figure A-5.

$$F_i = \begin{bmatrix} 3 * 344.4 \\ 2 * 3472 \\ 3 * 275.5 \\ 3 * 206.7 \\ 3 * 137.8 \\ 3 * 68.9 \end{bmatrix} lb$$

$$F_{sum} = \sum F_i = 10040\ lb$$

4. Calculate the cracking moment:

$$M_{wy_2} = 2 * I_{NC2} * \left(\frac{f_r}{t_{wy_2}} - \frac{F_{sum}}{b * t_{wy_2}^2}\right)$$

$$= 2 * 192\ in^4 * \left(\frac{0.691\ ksi}{4\ in} - \frac{10.04\ kip}{36\ in * (4\ in)^2}\right) = 4.97\ kip * ft$$

5. Calculate the equivalent load that wythe 2 can carry using equations (6-9).

$$w_{we2} = \frac{8 * M_{wy_2}}{Span^2} = \frac{8 * 4.97\ kip * ft}{(14\ ft)^2} = 0.203 \frac{kip}{ft}$$

$$P_{we2} = \frac{M_{wy_2}}{(x_{P1} + x_{P2})} = \frac{4.97\ kip * ft}{(2.8\ ft + 5.6\ ft)} = 0.5917\ kip$$

6. Using the equivalent load from the previous step, calculate axial and rotational displacement at the end connector using Eq. (6-10) and (6-11).

$$\theta_{w_{we2}} = \frac{w_{we2} * Span^3}{24 * E * I_{NC2}} = \frac{0.203 \frac{kip}{ft} * (14\ ft)^3 * 144}{24 * 5824.4\ ksi * 192\ in^4} = 0.00299$$

$$\theta_{P_{we2}} = P_{we2} \left\{ \frac{x_{P1}[(Span^2 - x_{P1}^2) + (Span - x_{P1})(2Span - x_{P1})]}{6 * Span * E_c * I_{NC2}} \right.$$

$$\left. + \frac{x_{P2}[(Span^2 - x_{P2}^2) + (Span - x_{P2})(2Span - x_{P2})]}{6 * Span * E_c * I_{NC2}} \right\}$$

$$\theta_{P_{we2}} = 0.5917 \left\{ \frac{2.8[(14^2 - 2.8^2) + (14 - 2.8)(28 - 2.8)]}{6 * 14 * 5824.4 * 192} \right.$$

$$\left. + \frac{5.6[(14^2 - 5.6^2) + (14 - 5.6)(28 - 5.6)]}{6 * 14 * 5824.4 * 192} \right\} = 0.00299$$

$$\Delta_{Rot} = \theta * Z = 0.00299 * 7\ in = 0.0209\ in$$

$$\Delta_{Axial} = 2 * \sum_{i=1}^{n} F(i) * \left(\frac{\frac{L}{2} - x_i}{b * E_c * t_{wy_1}} \right) = 0.001618 \text{ in}$$

7. Using Equation (6-11) and (6-12), calculate the slip at the end connector and compare to assumed value.

$$\delta_{max} = \Delta_{Rot} - \Delta_{Axial} = 0.0209\ in - 0.001618 \text{ in} = 0.01928\ in$$

$$\delta_{max} = Assumed\ \delta_{max} \quad \therefore \quad OK$$

8. Calculate the cracking moment using Equation (6-14).

$$M_{cr} = M_{wy_2} * 2 + F_{sum} * Z$$

$$= 2 * 4.97\ kip * ft + 10040\ lb * 7\ in = \mathbf{15.797\ kip * ft}$$

$$\Delta_{w_{we2}} = \frac{5 * w_{we2} * Span^4}{384 * E_c * I_{NC2}} = \frac{5 * 0.203 \frac{kip}{ft} * (14\ ft)^4 * \left(12 \frac{in}{ft}\right)^3}{384 * 5824.4\ ksi * 192\ in^4} = 0.157\ in$$

$$\Delta_{P_{we2}} = \left(\frac{P_{we2}}{24 * E_c * I_{NC2}} \right) \{ x_{P1} * (3 * Span^2 - 4 * x_{P1}^2) + x_{P2} * (3 * Span^2 - 4 * x_{P2}^2) \}$$

$$\Delta_{P_{we2}} = \left(\frac{0.559}{24 * 5824.4 * 192} \right) \{ 2.8 * (3 * 14^2 - 4 * 2.8^2) + 5.6 * (3 * 14^2 - 4 * 5.6^2) \} * 12^3$$

$$= 0.158\ in$$

Table A-5 Total Load, Equivalent Load Deflection, and Slip

Load Distribution	**Total Load, p_{Total}**	**Deflection from Equivalent Load, Δ_e** *(in)*	**Slip** *(in)*
Uniform Distributed Load	$\frac{M_{applied} * 8}{Span^2 * b} = \frac{15.8 * 8}{14^2 * 3} = 214.95\ psf$	0.1570	0.01929
Four-Point Loads	$\frac{4M_{applied}}{(x_{P1} + x_{P2})b * Span} = \frac{4 * 15.8}{8.4 * 3 * 14} = 179.1\ psf$	0.1581	0.01929

The actual load on the sandwich wall panel included the four-point applied load as well as self-weight.

$$p_{self} = 150\ pcf * (8\ in) = 100\ psf$$

$$w_{self} = p_{self} * b = 100\ psf * 3\ ft = 300\ plf$$

$$M_{self} = \frac{\left(w_{self} * Span^2\right)}{8} = \frac{300\ plf * (14ft)^2}{8} = 7.35\ kip * ft$$

$$M_{FourPt} = M_{cr} - M_{self} = 15.797\ kip * ft - 7.35\ kip * ft = 8.447\ kip * ft$$

$$P_{FourPt} = 4 * \left(\frac{8.447\ kip * ft}{33.6\ in + 67.2\ in}\right) = 4.02\ kip$$

$$p_{FourPt} = \frac{4020\ lbs}{14\ ft * 3\ ft} = 95.77\ psf$$

$$\boldsymbol{p_{TotalApplied} = p_{self} + p_{FourPt} = 100\ psf + 95.77\ psf = 195.77\ psf}$$

Similar effects can be calculated for deflection also, as well as slip. Since self-weight is a distributed load, the uniform distributed load values will be used from Table A-5.

$$\Delta_{self} = \frac{p_{self}}{p_{Total}} * \Delta_e = \frac{100\ psf}{214.95\ psf} * 0.157\ in = 0.0730\ in$$

$$\Delta_{FourPt} = \frac{p_{FourPt}}{p_{Total}} * \Delta_e = \frac{95.77\ psf}{179.13\ psf} * 0.158\ in = 0.0845\ in$$

$$\boldsymbol{\Delta_{Total} = 0.0730\ in + 0.0845\ in = 0.1575\ in}$$

$$\delta_{self} = \frac{p_{self}}{p_{Total}} * \delta_{max} = \frac{100\ psf}{214.95\ psf} * 0.01929\ in = 0.00897\ in$$

$$\delta_{FourPt} = \frac{p_{FourPt}}{p_{Total}} * \Delta_{max} = \frac{95.77\ psf}{179.13\ psf} * 0.01929\ in = 0.0103\ in$$

$$\boldsymbol{\delta_{Total} = \delta_{self} + \delta_{FourPt} = 0.00897\ in + 0.0103\ in = 0.01928\ in}$$

D Panel (HK Composite connectors) Panel Analysis Example (Mild Reinforcement)

Panel Properties

$L = 16\ ft$ $Span = 14\ ft$

$t_{wy1} = 4\ in$ $t_{wy2} = 4\ in$

$t_{ins} = 3\ in$ $b = 3\ ft$

$f_c' = 9.23\ ksi$

$x_i = \begin{bmatrix} 16 \\ 32 \\ 48 \\ 64 \\ 80 \end{bmatrix} in$ $N = 3$

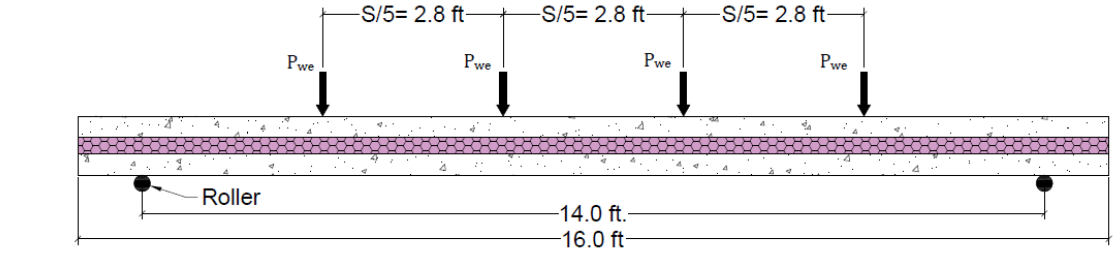

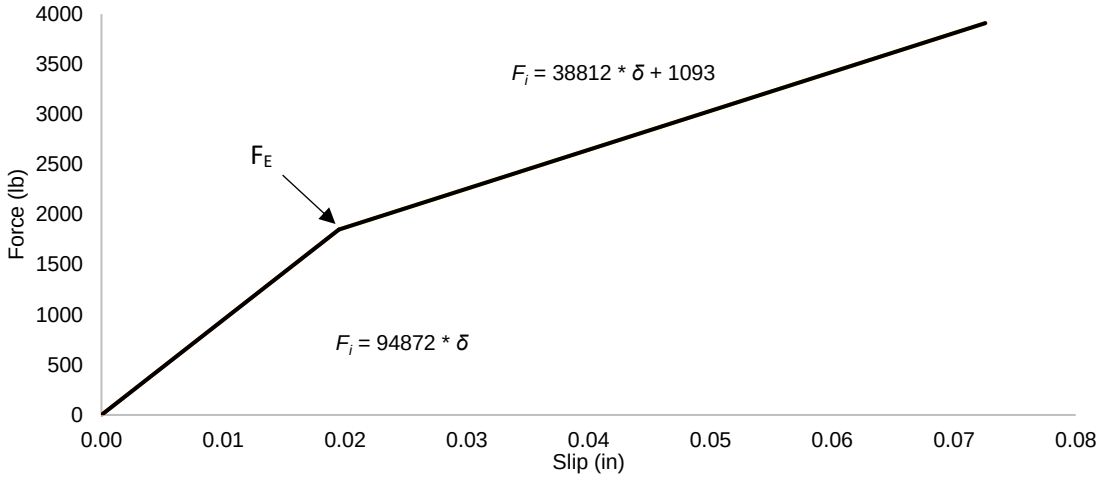

Figure A-6 Load vs slip of HK connector

Solution

1. Calculate the material and section properties of a non-composite sandwich panel. The modulus of rupture of the concrete (f_r) was measured in this case, so the actual value is included here.

$$x_{P1} = \frac{Span}{5} = 2.8\ ft \quad x_{P2} = 2 * x_{P1} = 5.6\ ft$$

$$E_c = 5824.4\ ksi$$

$$f_r = 0.691\ ksi$$

$$I_{NC1} = \frac{b}{12} * \left(t_{wy_1}^3\right) = \frac{3\ ft * 12\frac{in}{ft}}{12} * (4\ in)^3 = 192\ in^4$$

$$I_{NC2} = \frac{b}{12} * \left(t_{wy_2}^3\right) = \frac{3\ ft * 12\frac{in}{ft}}{12} * (4\ in)^3 = 192\ in^4$$

$$Z = \frac{t_{wy_1} + t_{wy_2}}{2} + t_{insul} = \frac{4\ in + 4\ in}{2} + 3\ in = 7\ in$$

2. Assume an end slip, which is the slip at the end connector line (see Figure 6-2). Calculate the slip in the other connectors using similar triangles or Eq. (6-5).

   Assuming δ_{max} = 0.01763 in

$$\delta(i) = \delta_{max} * \frac{\left(\frac{L}{2} - x_i\right)}{\left(\frac{L}{2} - x_1\right)} = \begin{bmatrix} 0.01763 \\ 0.01410 \\ 0.01058 \\ 0.00705 \\ 0.00353 \end{bmatrix} in$$

3. Calculate the shear forces in each connector using Figure A-6.

$$F_i = \begin{bmatrix} 1673 \\ 1338 \\ 1004 \\ 669 \\ 335 \end{bmatrix} lb$$

$$F_{sum} = 3\sum F_i = 15053\ lb$$

4. Calculate the cracking moment:

$$M_{wy_2} = 2 * I_{NC2} * \left(\frac{f_r}{t_{conc_2}} - \frac{F_{sum}}{b * t_{wy_2}^2}\right)$$

$$= 384\ in^4 * \left(\frac{0.691\ ksi}{4\ in} - \frac{15.053\ kip}{36\ in * (4\ in)^2}\right) = 4.692\ kip * ft$$

5. Calculate the equivalent load that wythe 2 can carry using equation (6-9).

$$w_{we2} = \frac{8 * M_{wy_2}}{Span^2} = \frac{8 * 4.692\ kip * ft}{(14\ ft)^2} = 0.1917\frac{kip}{ft}$$

$$P_{we2} = \frac{M_{wy_2}}{(x_{P1} + x_{P2})} = \frac{4.692\ kip * ft}{(2.8\ ft + 5.6\ ft)} = 0.559\ kip$$

6. Using the equivalent load from the previous step, calculate axial and rotational displacement at the end connector using Eq. (6-10) and (6-11).

$$\theta_{w_{we2}} = \frac{w_{we2} * Span^3}{24 * E * I_{NC2}} = \frac{0.1915 \frac{kip}{ft} * (14\ ft)^3 * 144}{24 * 5824.4\ ksi * 192\ in^4} = 0.00282$$

$$\theta_{P_{we2}} = P_{we2} \left\{ \frac{x_{P1}[(Span^2 - x_{P1}^2) + (Span - x_{P1})(2Span - x_{P1})]}{6 * Span * E_c * I_{NC2}} + \frac{x_{P2}[(Span^2 - x_{P2}^2) + (Span - x_{P2})(2Span - x_{P2})]}{6 * Span * E_c * I_{NC2}} \right\}$$

$$\theta_{P_{we2}} = 0.559 \left\{ \frac{2.8[(14^2 - 2.8^2) + (14 - 2.8)(28 - 2.8)]}{6 * 14 * 5824.4 * 192} + \frac{5.6[(14^2 - 5.6^2) + (14 - 5.6)(28 - 5.6)]}{6 * 14 * 5824.4 * 192} \right\} = 0.00282$$

$$\Delta_{Rot} = \theta * Z = 0.00282 * 7\ in = 0.01974\ in$$

$$\Delta_{Axial} = 2 * \sum_{i=1}^{n} F(i) * \left(\frac{\frac{L}{2} - x_i}{b * E_c * t_{wy_1}} \right) = 0.002106 \text{ in}$$

7. Using Equation (6-11) and (6-12), calculate the slip at the end connector and compare to assumed value.

$$\delta_{max} = \Delta_{Rot} - \Delta_{Axial} = 0.01974\ in - 0.00211 \text{ in} = 0.01763\ in$$

$$\delta_{max} = Assumed\ \delta_{max} \quad \therefore \quad OK$$

8. Calculate the cracking moment using Equation (6-14).

$$M_{cr} = M_{wy_2} * 2 + F_{sum} * Z$$

$$= 2 * 4.692\ kip * ft + 15053\ lb * 7\ in = \mathbf{18.165\ kip * ft}$$

$$\Delta_{w_{we2}} = \frac{5 * w_{we2} * Span^4}{384 * E_c * I_{NC2}} = \frac{5 * 0.1917 \frac{kip}{ft} * (14\ ft)^4 * \left(12 \frac{in}{ft}\right)^3}{384 * 5824.4\ ksi * 192\ in^4} = 0.148\ in$$

$$\Delta_{P_{we2}} = \left(\frac{P_{we2}}{24 * E_c * I_{NC2}} \right) \{x_{P1} * (3 * Span^2 - 4 * x_{P1}^2) + x_{P2} * (3 * Span^2 - 4 * x_{P2}^2)\}$$

$$\Delta_{P_{we2}} = \left(\frac{0.559}{24 * 5824.4 * 192} \right) \{2.8 * (3 * 14^2 - 4 * 2.8^2) + 5.6 * (3 * 14^2 - 4 * 5.6^2)\} * 12^3$$

$$= 0.1493\ in$$

Table A-6 Total Load, Equivalent Load Deflection, and Slip

Load Distribution	**Total Load, p_{Total}**	**Deflection from Equivalent Load, Δ_e** *(in)*	**Slip** *(in)*
Uniform Distributed Load	$\frac{M_{applied} * 8}{Span^2 * b} = \frac{18.16 * 8}{14^2 * 3} = 247.1\ psf$	0.1480	0.01763
Four-Point Loads	$\frac{4M_{applied}}{(x_{P1} + x_{P2})b * Span} = \frac{4 * 18.16}{8.4 * 3 * 14} = 205.95\ psf$	0.1492	0.01763

The actual load on the sandwich wall panel included the four-point applied load as well as self-weight.

$$p_{self} = 150\ pcf * (8\ in) = 100\ psf$$

$$w_{self} = p_{self} * b = 100\ psf * 3\ ft = 300\ plf$$

$$M_{self} = \frac{(w_{self} * Span^2)}{8} = \frac{300\ plf * (14ft)^2}{8} = 7.35\ kip * ft$$

$$M_{FourPt} = M_{cr} - M_{self} = 18.165\ kip * ft - 7.35\ kip * ft = 10.815\ kip * ft$$

$$P_{FourPt} = 4 * \left(\frac{10.815\ kip * ft}{33.6\ in + 67.2\ in}\right) = 5.15\ kip$$

$$p_{FourPt} = \frac{5150\ lbs}{14\ ft * 3\ ft} = 122.62\ psf$$

$$\boldsymbol{p_{TotalApplied} = p_{self} + p_{FourPt} = 100\ psf + 122.62\ psf = 222.62\ psf}$$

Similar effects can be calculated for deflection also, as well as slip. Since self-weight is a distributed load, the uniform distributed load values will be used from Table A-6.

$$\Delta_{self} = \frac{p_{self}}{p_{Total}} * \Delta_e = \frac{100\ psf}{247.13\ psf} * 0.148\ in = 0.06\ in$$

$$\Delta_{FourPt} = \frac{p_{FourPt}}{p_{Total}} * \Delta_e = \frac{122.62\ psf}{205.95\ psf} * 0.1492\ in = 0.0888\ in$$

$$\boldsymbol{\Delta_{Total} = 0.06\ in + 0.0888\ in = 0.1488\ in}$$

$$\delta_{self} = \frac{p_{self}}{p_{Total}} * \delta_{max} = \frac{100\ psf}{247.13\ psf} * 0.01763\ in = 0.00713\ in$$

$$\delta_{FourPt} = \frac{p_{FourPt}}{p_{Total}} * \Delta_{max} = \frac{122.62\ psf}{205.95\ psf} * 0.01763\ in = 0.0105\ in$$

$$\boldsymbol{\delta_{Total} = \delta_{self} + \delta_{FourPt} = 0.00713\ in + 0.0105\ in = 0.01763\ in}$$

APPENDIX B. Elastic Hand Method Design Examples

This appendix serves to clarify the Beam-Spring and Elastic Hand Method prediction methodology described in Chapter 6. The example included herein illustrates the design method to predict the deflection and cracking of a given panel. Note that the Elastic Hand Procedure is iterative.

Panel Properties

$L = 37\ ft$ $Span = 35\ ft$

$t_{wy1} = 3\ in$ $t_{wy2} = 3\ in$

$t_{ins} = 3\ in$ $b = 8\ ft$

$f_c' = 6.0\ ksi$ $f_y = 60\ ksi$

$Wind\ Load = W_L = 30\ psf$ Insulation Type: XPS

$K_E = 94.8\ kips/in$

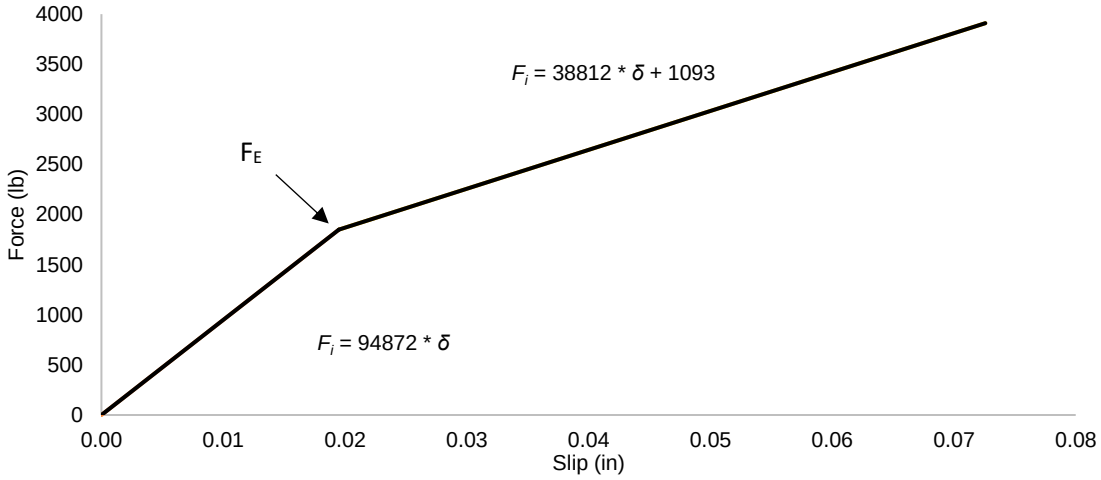

Figure B-1 Load vs slip of HK connector

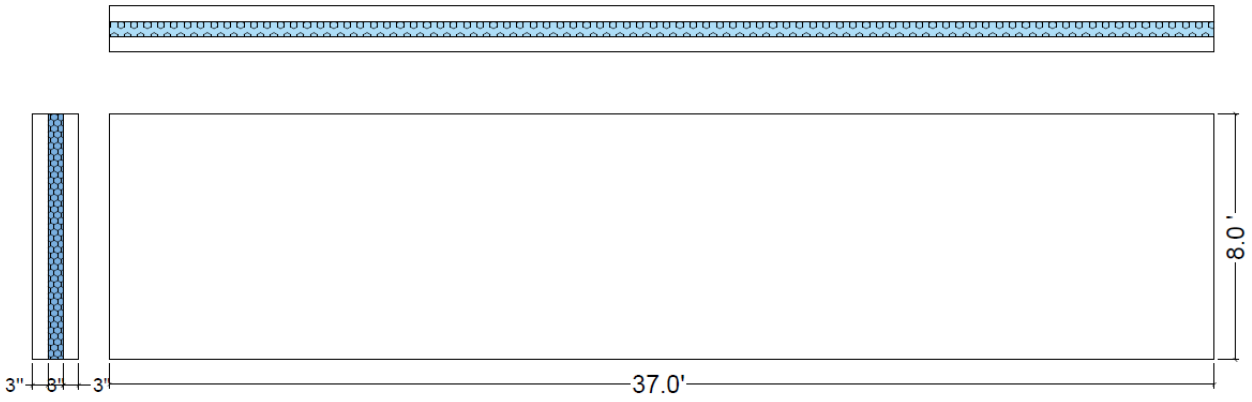

Figure B-2 Design example sandwich panel dimensions

Elastic Hand Method

Solution

1. Calculate the material and section properties of a non-composite sandwich panel.

$$E_c = 4696\ ksi$$

$$f_r = 7.5 * \sqrt{f'c} = 7.5 * \sqrt{6000} = 0.581\ ksi$$

$$I_{NC2} = \frac{b}{12} * \left(t_{wy_2}^3\right) = \frac{8 * 12}{12} * (3^3) = 216\ in^4$$

$$Z = \frac{t_{wy_1} + t_{wy_2}}{2} + t_{insul} = 3\ in + 3\ in = 6\ in$$

$$M_{service} = 1.0 * \frac{W_L * L * Span^2}{8} = \frac{30\ psf * 8\ ft * (35\ ft)^2}{8} = 36.75\ kip.ft$$

2. Assume four connectors in a row (***N* = 4**) with 24 in. longitudinal spacing. This spacing means there will be 9 connector rows in half of the span (***n* = 9**).

   Now assume the slip at the end connector line and then calculate the shear forces in the connectors. A good initial assumption is to assume the ultimate elastic slip of the connectors.

   Assume $\delta_{end} = 0.02\ in$

$$x_i = \begin{bmatrix} 12 \\ 36 \\ 60 \\ 84 \\ 108 \\ 132 \\ 156 \\ 180 \\ 204 \end{bmatrix} in \quad \therefore \quad \delta(i) = \delta_{end} * \frac{\left(\frac{L}{2} - x_i\right)}{\left(\frac{L}{2} - x_1\right)} = \begin{bmatrix} 0.02 \\ 0.0177 \\ 0.0154 \\ 0.0131 \\ 0.0109 \\ 0.0086 \\ 0.0063 \\ 0.0040 \\ 0.0017 \end{bmatrix} in$$

Calculate the forces in each connector and connector line using Equations (6-6) and (6-7) or use Figure 6-2 and Figure B-1 to find the forces that correspond to connector slip

$$F_i = \delta(i) N_i * K_E = \begin{bmatrix} 0.02 \\ 0.0177 \\ 0.0154 \\ 0.0131 \\ 0.0109 \\ 0.0086 \\ 0.0063 \\ 0.0040 \\ 0.0017 \end{bmatrix} in * 4 * 94.8 \frac{kips}{in} = \begin{bmatrix} 7584 \\ 6717 \\ 5851 \\ 4984 \\ 4117 \\ 3250 \\ 2384 \\ 1517 \\ 650 \end{bmatrix} lb$$

$$F_{sum} = \sum F_i = 37{,}053.3\ lb$$

3. Calculate the cracking moment for a mild reinforced non-composite wythe using Equation (6-8).

$$M_{wy_2} = \frac{M_{service} - F_{sum} * Z}{2} = \frac{36.75\ kip * ft - 37.05\ kip * 6\ in * \frac{1\ ft}{12\ in}}{2} = 9.112\ kip * ft$$

4. Calculate the equivalent load using Equations (6-9).

$$w_{we2} = \frac{8 * M_{wy_2}}{Span^2} = \frac{8 * 9.112\ kip * ft}{(35\ ft)^2} = 0.0595 \frac{kip}{ft}$$

5. Using the equivalent load, calculate the axial and rotational displacement assuming the equivalent load distribution by using Equations (6-10) through (6-12).

$$\theta = \frac{w_{we2} * Span^3}{24 * E * I_{NC2}} = \frac{0.0595\ \frac{kip}{ft} * (35\ ft)^3}{24 * 4696\ ksi * 216\ in^2} = 0.0151$$

$$\Delta_{Rot} = \theta * Z = 0.0151 * 6\ in = 0.0905 in$$

$$\Delta_{Axial} = 2 * \sum_{i=1}^{n} F(i) * \left(\frac{\frac{L}{2} - x_i}{b * E * t_{wy_2}} \right)$$

$$= \frac{2}{b * E * t_{wy_2}} * \sum_{i=1}^{n} F(i) * \left(\frac{L}{2} - x_i\right)$$

$$= \frac{2}{8\ ft * 4696\ ksi * 3\ in} * \sum_{i=1}^{n} \begin{bmatrix} 7584 \\ 6717 \\ 5851 \\ 4984 \\ 4117 \\ 3250 \\ 2384 \\ 1517 \\ 650 \end{bmatrix} lb * \left(\frac{444\ in}{2} - \begin{bmatrix} 12 \\ 36 \\ 60 \\ 84 \\ 108 \\ 132 \\ 156 \\ 180 \\ 204 \end{bmatrix} in \right)$$

$$= 0.00809\ in$$

6. Calculate a new δ_{end} using equation (6-13).

$$\delta_{end} = \Delta_{Rot} - \Delta_{Axial} = 0.0906\ in - 0.00809\ in = 0.0825\ in$$

Check to see if $\delta_{end} < \delta_E$

$$\delta_{end} = 0.0825\ in > \delta_E = 0.02\ in$$

This **violates the linear elastic assumption**, therefore more connectors are required. Repeat steps 2 through 6 and iterate until this limit is satisfied.

2. This time assume six connectors in a row (***N* = 6**) with 16 in. longitudinal spacing. This spacing means there will result in 13 connector rows in half of the span (***n* = 13**).

Again assume a slip at the end connector line and then calculate the shear forces in the connectors.

Assume $\delta_{end} = 0.01568\ in$

$$x_i = \begin{bmatrix} 16 \\ 32 \\ 48 \\ 64 \\ 80 \\ 96 \\ 112 \\ 128 \\ 144 \\ 160 \\ 176 \\ 192 \\ 208 \end{bmatrix} in \quad \therefore \quad \delta(i) = \delta_{end} * \frac{\left(\frac{L}{2} - x_i\right)}{\left(\frac{L}{2} - x_1\right)} = \begin{bmatrix} 0.0157 \\ 0.0145 \\ 0.0132 \\ 0.012 \\ 0.0108 \\ 0.0096 \\ 0.0084 \\ 0.0072 \\ 0.0059 \\ 0.0047 \\ 0.0035 \\ 0.0023 \\ 0.0011 \end{bmatrix} in$$

Calculate the forces in each connector and connector line using Equations (6-6) and (6-7) or use Figure 6-2 and Figure B-1 to find the forces that correspond to connector slip

$$F_i = (i)N_i * K_E = \begin{bmatrix} 0.0157 \\ 0.0145 \\ 0.0132 \\ 0.012 \\ 0.0108 \\ 0.0096 \\ 0.0084 \\ 0.0072 \\ 0.0059 \\ 0.0047 \\ 0.0035 \\ 0.0023 \\ 0.0011 \end{bmatrix} in * 6 * 94.8\ kips/in = \begin{bmatrix} 8922 \\ 8229 \\ 7536 \\ 6843 \\ 6150 \\ 5457 \\ 4764 \\ 4071 \\ 3378 \\ 2685 \\ 1992 \\ 1299 \\ 606 \end{bmatrix} lb$$

$$F_{sum} = \sum F_i = 61{,}932\ lb$$

3. Calculate the cracking moment for a mild reinforced non-composite wythe using Equation (6-8).

$$M_{wy_2} = \frac{M_{service} - F_{sum} * Z}{2} = \frac{36.75\ kip.ft - 61.932\ kip * 6\ in * \frac{1\ ft}{12\ in}}{2} = 2.892\ kip * ft$$

4. Calculate the equivalent load using Equations (6-9).

$$w_{we2} = \frac{8 * M_{wy_2}}{Span^2} = \frac{8 * 2.892\ kip * ft}{(35\ ft)^2} = 0.01889 \frac{kip}{ft}$$

5. Using the equivalent load, calculate axial and rotational displacement assuming equivalent load distribution using equations by using Equations (6-10) through (6-12).

$$\theta = \frac{w_{we2} * Span^3}{24 * E * I_{NC2}} = \frac{0.01889 \frac{kip}{ft} * (35\ ft)^3}{24 * 4696\ ksi * 216\ in^2} = 0.00479$$

$$\Delta_{Rot} = \theta * Z = 0.00479 * 6\ in = 0.02874\ in$$

$$\Delta_{Axial} = 2 * \sum_{i=1}^{n} F(i) * \left(\frac{\frac{L}{2} - x_i}{b * E * t_{wy_2}} \right)$$

$$= \frac{2}{b * E * t_{wy_2}} * \sum_{i=1}^{n} F(i) * \left(\frac{L}{2} - x_i \right)$$

$$= \frac{2}{8\ ft * 4696\ ksi * 3\ in} * \sum_{i=1}^{13} \begin{bmatrix} 8922 \\ 8229 \\ 7536 \\ 6843 \\ 6150 \\ 5457 \\ 4764 \\ 4071 \\ 3378 \\ 2685 \\ 1992 \\ 1299 \\ 606 \end{bmatrix} lb * \left(\frac{444\ in}{2} - \begin{bmatrix} 16 \\ 32 \\ 48 \\ 64 \\ 80 \\ 96 \\ 112 \\ 128 \\ 144 \\ 160 \\ 176 \\ 192 \\ 208 \end{bmatrix} in \right)$$

$$= 0.0130 \text{ in}$$

6. Calculate a new δ_{end} using equation (6-13).

$$\delta_{end} = \Delta_{Rot} - \Delta_{Axial} = 0.0287 - 0.013 = 0.0157\ in$$

$$\delta_{end} = 0.01568 = Assumed\ \delta_{end}$$

Check to see if $\delta_{end} < \delta_E$

$$\delta_{end} = 0.0157\ in < \delta_E = 0.02\ in \quad \therefore \quad OK$$

7. Check tension stress to verify it is less than modulus of rupture of the concrete with Equation (6-19).

$$f = \frac{M_{wy_2} * t_{wy_2}}{2 * I_{NC2}} + \frac{F_{sum}}{b * t_{wy_2}} = \frac{2.892\ kip * ft * 3\ in}{2 * 216\ in^4} + \frac{61.932\ kip}{8ft * 3\ in} = 0.456\ ksi$$

$$f < fr \quad \therefore \quad OK$$

Therefore, use six connectors per row with 16 in. longitudinal spacing.

8. Calculate deflection at midspan using Equation (6-15) for a uniform distributed load.

$$\Delta = \frac{5 * w_{we2} * Span^4}{384 * E_c * I_{NC2}} = \frac{5 * 0.01889 \frac{kip}{ft} * (35ft)^4 * (12\ in/ft)^3}{384 * 4696\ ksi * 216\ in^4} = 0.628\ in$$

Beam-Spring Model

Creating the Beam-Spring model requires a two-dimensional finite element software and only requires assignment of gross individual wythe properties and connector shear stiffness. Assuming the connector spacing is equal to 16 inches in both directions, each spring will have a shear stiffness of $N * K_E$. Figure B-3 shows the Beam-Spring model for this example.

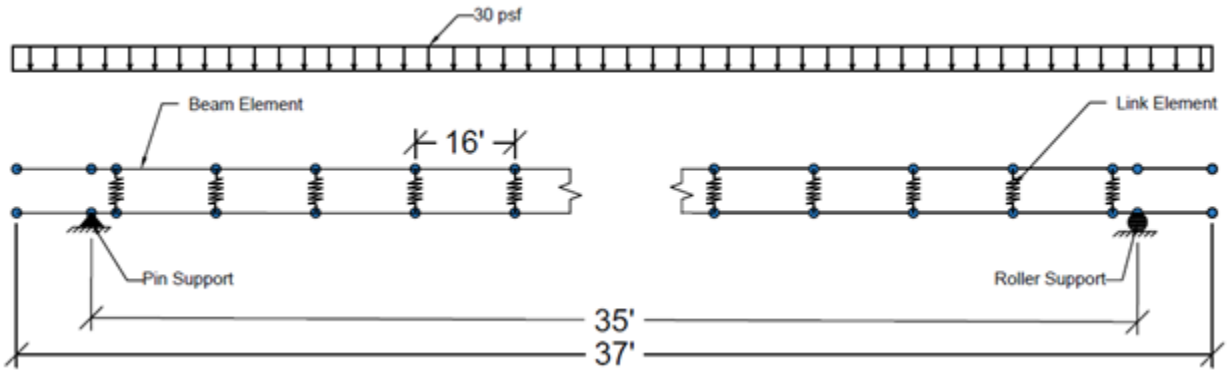

Figure B-3 Beam-Spring Model of design example

Table B-1 shows the results from the Beam-Spring Model.

Table B-1 Results from the Beam-Spring Model for wythe 2

Moment (kip-ft)	2.72 kip-ft
Tension force (kip)	61.7 kips
Slip (in)	0.014 in
Deflection at mid span (in)	0.58 in

$$f = \frac{P}{A} + \frac{M * c}{I}$$

$$f = \frac{61.7\ kip}{288\ in^2} + \frac{2.67\ kip * ft * \frac{12\ in}{ft} * 1.5\ in}{216} = 441\ psi\ < f_r\ \therefore OK$$

APPENDIX C. Partially-Composite Strength Prediction Method Analysis Examples

This appendix presents the analysis for predicting the ultimate moment using the partially composite moment prediction method presented above for the HK, Nu-Tie, and Thermomass panels tested in this report.

A-2 Panel Analysis Example (Nu-Tie connectors, Prestressed Reinforcement)

Strain Compatibility

Section and Material Properties

$f_{ps} = 270\ ksi$ $\quad A_{ps} = 0.255\ in^2$

$f_c' = 10.43\ ksi$ $\quad b = 48\ in$

$t_{wy1} = 3\ in$ $\quad t_{wy2} = 3\ in$

$t_{ins} = 4\ in$ $\quad L = 192\ in$

$x_{conX} = \begin{bmatrix}24\\72\end{bmatrix} in$ $\quad N = 2$

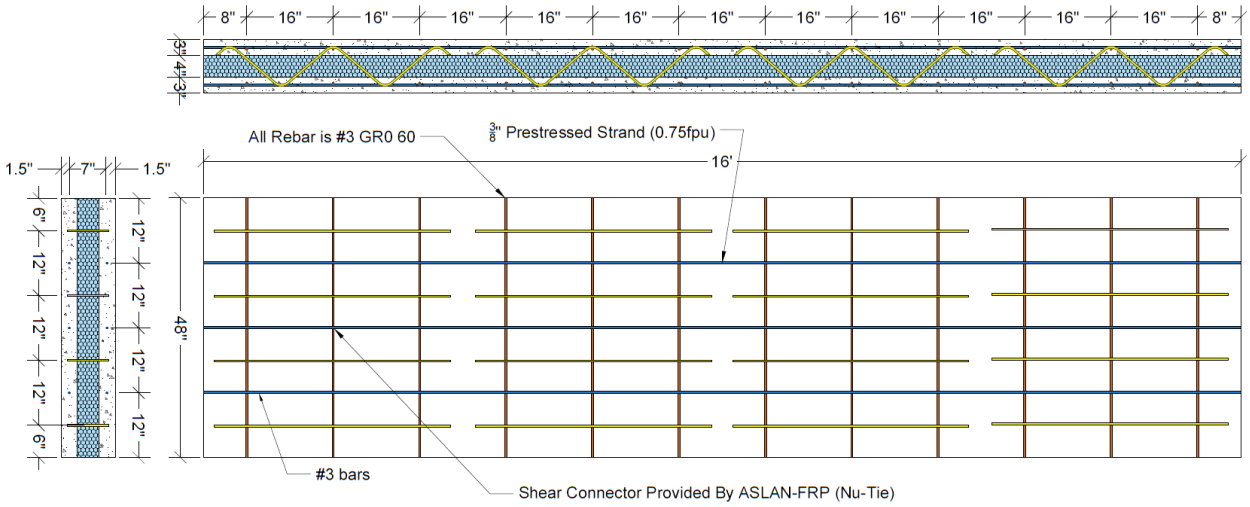

Solution

1. Find the forces in each connector using the load-slip relation. Using an influence line, the ultimate slip (δ_{Ult}) that occurs at the maximum force is determined to be 0.267 in.

$$\delta(i) = \frac{\delta_{Ult}}{\frac{L}{2} - x_1} * \left(\frac{L}{2} - x_i\right)$$

$$\delta(i) = \frac{0.267\ in}{\frac{192}{2} in - 24\ in} * \begin{bmatrix} \frac{192}{2} - 24 \\ \frac{192}{2} - 72 \end{bmatrix} \text{in} = \begin{bmatrix} 0.267 \\ 0.089 \end{bmatrix} in$$

Find F_i at each connector by using Figure C-1.

$$F(i) = \begin{bmatrix} 11.25 \\ 9.26 \end{bmatrix} \text{kips}$$

The full load-slip diagram for the connector is used to obtain the most accurate prediction

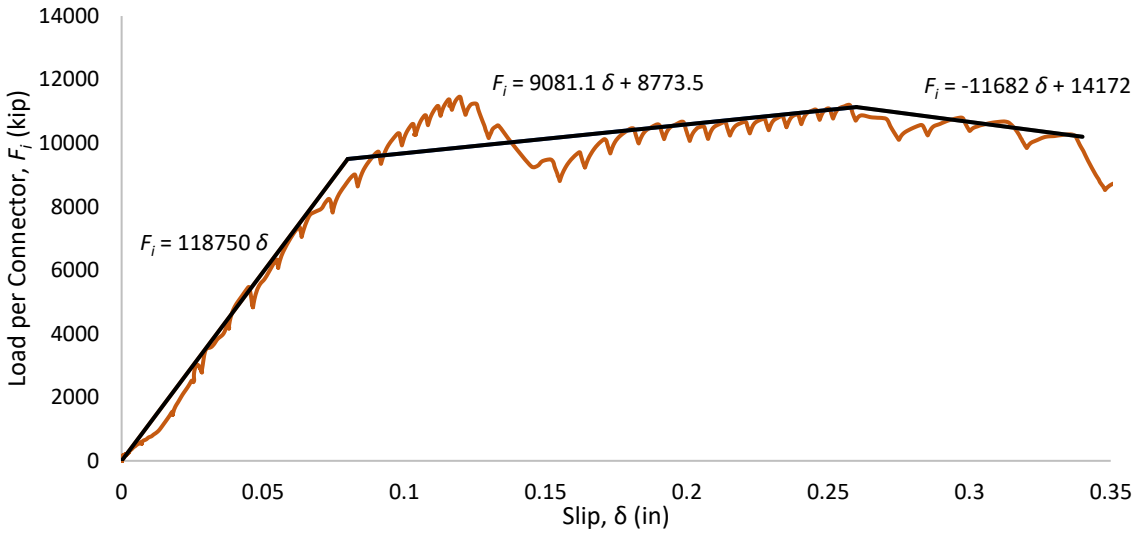

Figure C-1 Load-slip curve for Nu-Tie Panels

2. Find the total sum of the connector forces using Equation (7-12):

$$F_{sum} = N * \sum F_i = 41.0\ kips$$

$$F_{sum} \leq A_{ps} * f_{pu} = 0.255\ in^2 * 270\ ksi = 68.9\ kips \quad \therefore \quad OK$$

3. Find C_1 and T_1 for the first wythe

   a. Assume ε_c = 0.003.

b. Assume a value of c_1. We will assume c_1 = 0.287 in

c. Calculate curvature using Equation (7-13):

$$\varphi = \frac{0.003}{0.287} = 0.01045$$

d. Calculate the compressive force in the top wythe using Equation (7-15). This will incorporate Hognestad's Equation (7-14).

$$C_1 = b * f_c' * \frac{\varphi_1 * c_1^2}{\varepsilon_0} * \left(1 - \frac{\varphi_1 * c_1}{3\varepsilon_0}\right)$$

$$C_1 = 48\ in * 10.43\ ksi * \frac{0.01045 * 0.287^2}{0.002} * \left(1 - \frac{0.01045 * 0.287}{0.006}\right) = 107.83\ kips$$

e. Calculate the strain and stress in the steel using Equations (7-17) and (7-19).

$$\varepsilon_1 = \frac{f_{pe}}{E_{ps}} = \frac{170}{28500} = 0.00596 \qquad \varepsilon_2 \approx 0$$

$$\varepsilon_{ps} = 0.003 * \frac{1.5 - 0.287}{0.287} + 0.00596 + 0 = 0.01864$$

$$f_{ps} = \varepsilon_{ps} * \left\{ 887 + \frac{27600}{\left[1 + \left(112.4 * \varepsilon_{ps}\right)^{7.36}\right]^{7.36^{-1}}} \right\} = 261.98\ ksi$$

f. Calculate the tension force in wythe 1 with Equation (7-20)

$$T_1 = 261.98\ ksi * 0.255\ in^2 = 66.8\ kips$$

g. Enforce force equilibrium for wythe 1 with Equation (7-21):

$$C_1 - T_1 = 107.83\ kips - 66.8\ kips = 41.0\ kips = F_{sum} \ \therefore \ OK$$

4. Find C_2 and T_2 for the second wythe

a. Assume both wythes will deflect equally, therefore assume $\varphi_2 = \varphi_1 = 0.01045$

b. Assume a value of c_2. We will assume c_2 = 0.11154 in (neutral axis in the bottom wythe)

c. Calculate the compressive force in the bottom wythe, C_2, using Equation (7-22). The compressive force in the concrete will again utilize Hognestad's equation to estimate the concrete compressive strength, but it is critical here because Whitney's stress block is only valid when the top fiber is at 0.003 strain and in the case of partial composite action, this will not be true.

$$C_2 = b * f_c' * \frac{\varphi_2 * c_2^2}{\varepsilon_0} * \left(1 - \frac{\varphi_2 * c_2}{3\varepsilon_0}\right)$$

$$C_2 = 48\ in * 10.43\ ksi * \frac{0.01045 * 0.11154^2}{0.002} * \left(1 - \frac{0.01045 * 0.11154}{0.006}\right) = 26.2\ kips$$

d. Calculate the strain and stress in the steel.

$$\varepsilon_{ps} = (d - c_2) * \varphi_2 + \varepsilon_1$$

$$\varepsilon_{ps} = \left(1.5 - (0.11154)\right) * 0.01045 + 0.00596 = 0.02052$$

$$f_{ps} = \varepsilon_{ps} * \left\{887 + \frac{27600}{\left[1 + \left(112.4 * \varepsilon_{ps}\right)^{7.36}\right]^{7.36^{-1}}}\right\} = 263.68\ ksi$$

e. Calculate the tension force in wythe 2 using Equation (7-24):

$$T_2 = 263.68\ ksi * 0.255\ in^2 = 67.2\ kips$$

f. Enforce force equilibrium for wythe 2 with Equation (7-25):

$$T_2 - C_2 = 67.2\ kips - 26.2\ kips = 41.0\ kips = F_{sum}\ \therefore\ OK$$

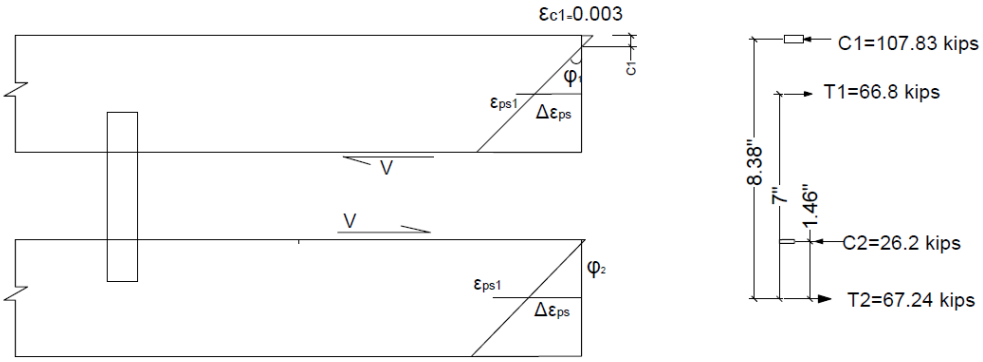

Figure C-2 Nu-Tie 343-2 Panel Design Example

5. Calculate the ultimate moment of the concrete sandwich wall panel using Equation (7-26). In addition, Using Equation (7-16) to calculate the centroid of C_1 and C_2.

$$x_{c1} = c_1 - \frac{c_1 * (8 * \varepsilon_o - 3 * \varphi_1 * c_1)}{12 * \varepsilon_o - 4 * \varphi_1 * c_1} = 0.287 - \frac{0.287\ * (8 * 0.002 - 3 * 0.01045 * 0.287)}{12 * 0.002 - 4 * 0.01045 * 0.287} = 0.12\ in$$

$$M_1 = C_1 * (d_1 - X_{c1}) = 107.83 * (1.5 - 0.12) = 148.8\ kip.in$$

$$x_{c2} = c_2 - \frac{c_2 * (8 * \varepsilon_o - 3 * \varphi_2 * c_2)}{12 * \varepsilon_o - 4 * \varphi_2 * c_2} = 0.1115 \ - \frac{0.1115 \ * (8 * 0.002 - 3 * 0.01045 * 0.1115 \ )}{12 * 0.002 - 4 * 0.1115 \ * 0.01045} = 0.0348 \ in$$

$$M_2 = C_2 * (d_2 - x_{c2}) = 26.2 * (1.5 - 0.0348) = 38.4 \ kip.in$$

$$M = M_1 + M_2 + F_{sum} * \left(\frac{t_{wy1} + t_{wy2}}{2} + t_{ins}\right)$$

$$= 148.8 + 38.4 + 41 * \left(\frac{3+3}{2} + 4\right) = 474.2 \ kip * in$$

$$= \mathbf{39.5} \ \boldsymbol{kip} * \ \boldsymbol{ft}$$

A-4 Panel Analysis Example (Nu-Tie connectors, Prestressed Reinforcement)

Strain Compatibility

Section and Material Properties

$f_{ps} = 270\ ksi$ $\quad A_{ps} = 0.255\ in^2$

$f_c' = 10.43\ ksi$ $\quad b = 48\ in$

$t_{wy1} = 3\ in$ $\quad t_{wy2} = 3\ in$

$t_{ins} = 4\ in$ $\quad L = 192\ in$

$x_i = \begin{bmatrix} 24 \\ 72 \end{bmatrix} in$ $\quad N = 4$

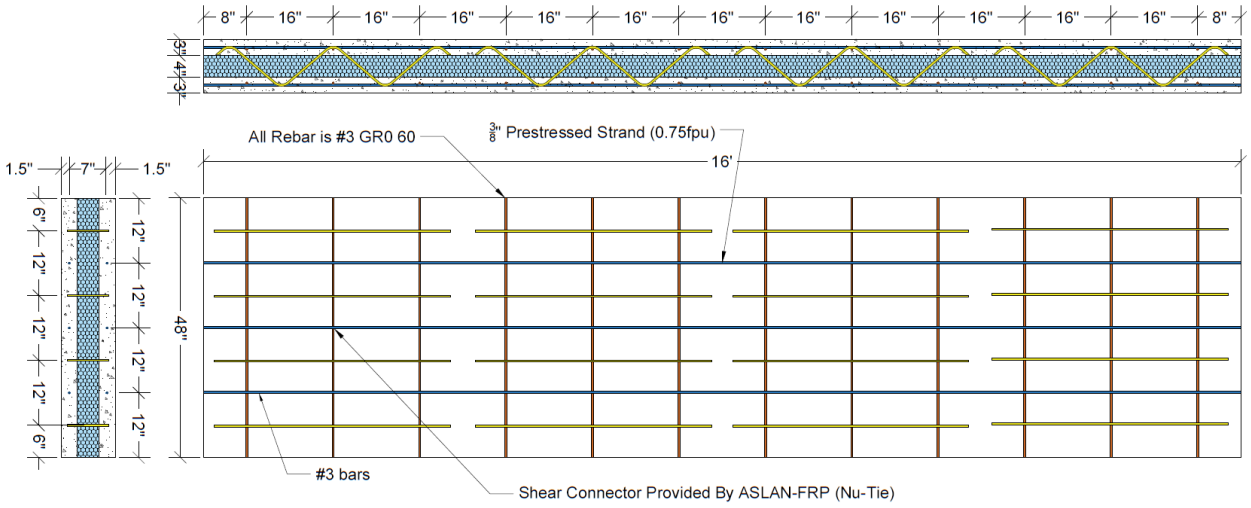

Solution

1. Find the forces in each connector using the load-slip relation. Using an influence line, the ultimate slip (δ_{Ult}) that occurs at the maximum force is 0.267 in., but because of the limit $F_{sum} \leq A_{ps} * f_{pu}$, the ultimate slip will actually occur at a force of F_{sum}, which is δ_{Ult} = 0.187 in. Calculate slip using Equation (7-11):

$$\delta(i) = \frac{\delta_{Ult}}{\frac{L}{2} - x_1} * \left(\frac{L}{2} - x_i\right)$$

$$\delta(i) = \frac{0.187\ in}{\frac{192}{2} in - 24\ in} * \begin{bmatrix} \frac{192}{2} - 24 \\ \frac{192}{2} - 72 \end{bmatrix} \text{in} = \begin{bmatrix} 0.187 \\ 0.0623 \end{bmatrix} in$$

Find F_i at each connector by using Figure C-3.

$$F(i) = \begin{bmatrix} 9.928 \\ 7.3 \end{bmatrix} \text{kips}$$

The full load-slip curve for the connector is used to obtain the most accurate prediction. In a design, the bilinear curve recommended above should be used.

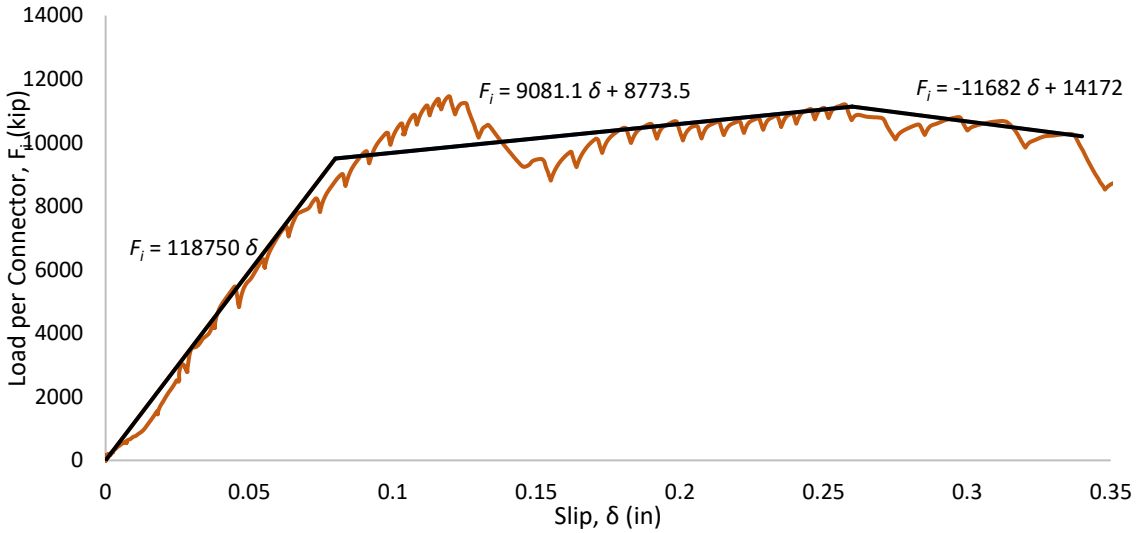

Figure C-3 Load-slip curve for Nu-Tie Panels

2. Find the total sum of the connector forces using Equation (7-12):

$$F_{sum} = N * \sum F_i = 68.9\ kips$$

$$F_{sum} \leq A_{ps} * f_{pu} = 0.255\ in^2 * 270\ ksi = 68.9\ kips \quad \therefore \quad OK$$

3. Find C_1 and T_1 for the first wythe

   a. Assume ε_c = 0.003.

   b. Assume a value of c_1. We will assume c_1 = 0.359 in.

   c. Calculate curvature using Equation (7-13):

$$\varphi = \frac{0.003}{0.359} = 0.00835$$

d. Calculate the compressive force in the top wythe using Equation (7-15). This will incorporate Hognestad's Equation (7-14).

$$C_1 = b * f_c' * \frac{\varphi_1 * c_1^2}{\varepsilon_0} * \left(1 - \frac{\varphi_1 * c_1}{3\varepsilon_0}\right)$$

$$C_1 = 48\ in * 10.43\ ksi * \frac{0.00835 * 0.359^2}{0.002} * \left(1 - \frac{0.00835 * 0.359}{0.006}\right) = 134.9\ kips$$

e. Calculate the strain and stress in the steel using Equations (7-17) and (7-19).

$$\varepsilon_1 = \frac{f_{pe}}{E_{ps}} = \frac{170}{28500} = 0.00596 \qquad \varepsilon_2 \approx 0$$

$$\varepsilon_{ps} = 0.003 * \frac{1.5 - 0.359}{0.359} + 0.00596 + 0 = 0.01554$$

$$f_{ps} = \varepsilon_{ps} * (887 + \frac{27600}{\left(1 + \left(112.4 * \varepsilon_{ps}\right)^{7.36}\right)^{7.36^{-1}}}) = 258.8\ ksi$$

f. Calculate the tension force in wythe 1 with Equation (7-20)

$$T_1 = 258.8\ ksi * 0.255\ in^2 = 66.0\ kips$$

g. Enforce force equilibrium for wythe 1 with Equation (7-21):

$$C_1 - T_1 = 134.9\ kips - 66.0\ kips = 68.9\ kips = F_{sum} \ \therefore \ OK$$

4. Find C_2 and T_2 for the second wythe

a. Assume both wythes will deflect equally, therefore assume $\varphi_2 = \varphi_1 = 0.00835$

b. Assume a value of c_2. We will assume c_2 = -1.11 in (neutral axis in the foam)

c. Calculate the compressive force in the bottom wythe, C_2, using Equation (7-22). The compressive force in the concrete will again utilize Hognestad's equation to estimate the concrete compressive strength, but it is critical here because Whitney's stress block is only valid when the top fiber is at 0.003 strain and in the case of partial composite action, this will not be true.

$$C_2 = b * f_c' * \frac{\varphi_2 * c_2^2}{\varepsilon_0} * \left(1 - \frac{\varphi_2 * c_2}{3\varepsilon_0}\right)$$

$$C_2 = 0\ kips$$

d. Calculate the strain and stress in the steel.

$$\varepsilon_{ps} = (d - c_2) * \varphi_2 + \varepsilon_1$$

$$\varepsilon_{ps} = \big(1.5 - (-1.112)\big) * 0.00835 + 0.00596 = 0.02783$$

$$f_{ps} = \varepsilon_{ps} * (887 + \frac{27600}{\Big(1 + \big(112.4 * \varepsilon_{ps}\big)^{7.36}\Big)^{7.36^{-1}}}) = 270\ ksi$$

e. Calculate the tension force in wythe 2 using Equation (7-24):

$$T_2 = 270\ ksi * 0.255\ in^2 = 68.9\ kips$$

f. Enforce force equilibrium for wythe 2 with Equation (7-25):

$$T_2 - C_2 = 68.9\ kips - 0\ kips = 68.9\ kips = F_{sum}\ \ \therefore\ \ OK$$

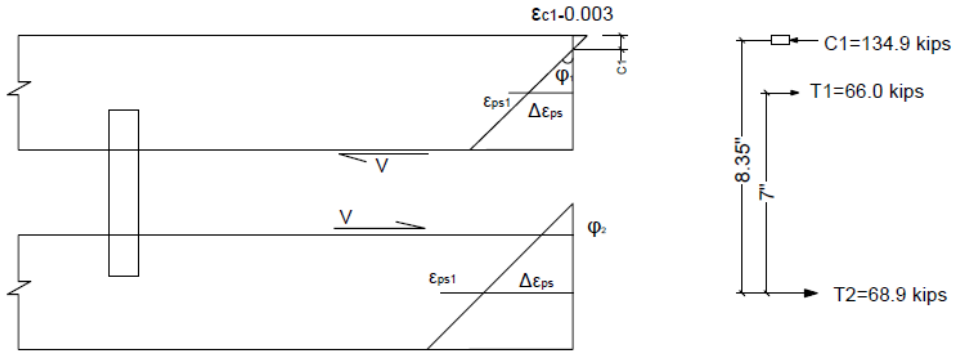

Figure C-4 Nu-Tie 343-2 Panel Design Example

5. Calculate the ultimate moment of the concrete sandwich wall panel using Equation (7-26). In addition, Using Equation (7-16) to calculate the centroid of C_1 and C_2.

$$x_{c1} = c_1 - \frac{c_1 * (8 * \varepsilon_o - 3 * \varphi_1 * c_1)}{12 * \varepsilon_o - 4 * \varphi_1 * c_1} = 0.359 - \frac{0.359\ * (8 * 0.002 - 3 * 0.00835 * 0.359)}{12 * 0.002 - 4 * 0.00835 * 0.359} = 0.15\ in$$

$$M_1 = C_1 * (d_1 - x_{c1}) = 134.9 * (1.5 - 0.15) = 182.1\ kip * in$$

$$M_2 = C_2 * (d_2 - x_{c2}) = 0$$

$$M = M_1 + M_2 + F_{sum} * \left(\frac{t_{wy1} + t_{wy2}}{2} + t_{ins}\right)$$

$$= 182.1 + 0 + 68.9 * \left(\frac{3+3}{2} + 4\right) = 664.4\ kip * in$$

$$= \mathbf{55.4\ kip * ft}$$

B Panel Analysis Example (Thermomass CC connectors only, Mild Reinforcement)

Section and Material Properties

$f_c' = 9.23\ ksi$ $A_s = 0.44\ in^2$

$b = 36\ in$ $t_{wy1} = 4\ in$

$t_{wy2} = 4\ in$ $t_{ins} = 3\ in$

$L = 192\ in$

$x_i = \begin{bmatrix} 30 \\ 82 \end{bmatrix} in$ $N = 3$

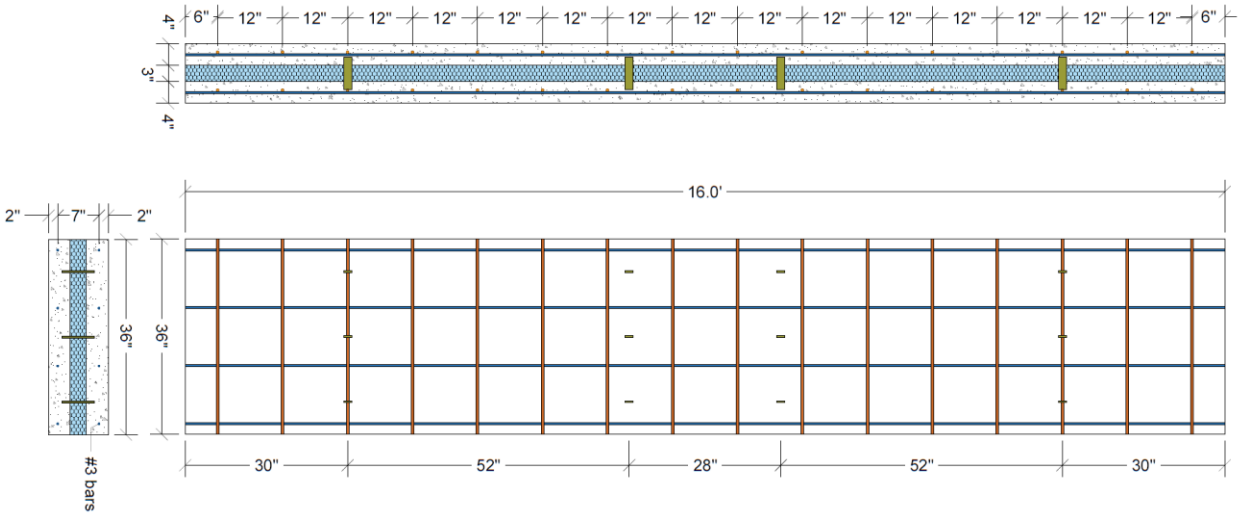

Solution

1. Find the forces in each connector using the load-slip relationship. Using an influence line, the ultimate slip (δ_{Ult}) that occurs at the maximum force is determined to be 0.18 in. In addition, the sum of the forces should be less than or equal to A_s * f_s in the bottom wythe. Calculate slip using Equation (7-11):

$$\delta(i) = \frac{\delta_{Ult}}{\frac{L}{2} - x_1} * \left(\frac{L}{2} - x_i\right)$$

$$\delta(i) = \frac{0.833\ in}{\frac{192}{2} in - 30\ in} * \begin{bmatrix} \frac{192}{2} - 30 \\ \frac{192}{2} - 82 \end{bmatrix} \text{in} = \begin{bmatrix} 0.833 \\ 0.1767 \end{bmatrix} in$$

Find F_i at each connector by using Figure C-5.

$$F(i) = \begin{bmatrix} 4.99 \\ 2.56 \end{bmatrix} \text{kips}$$

Note that the full connector load-slip diagram is used to obtain the most accurate answer.

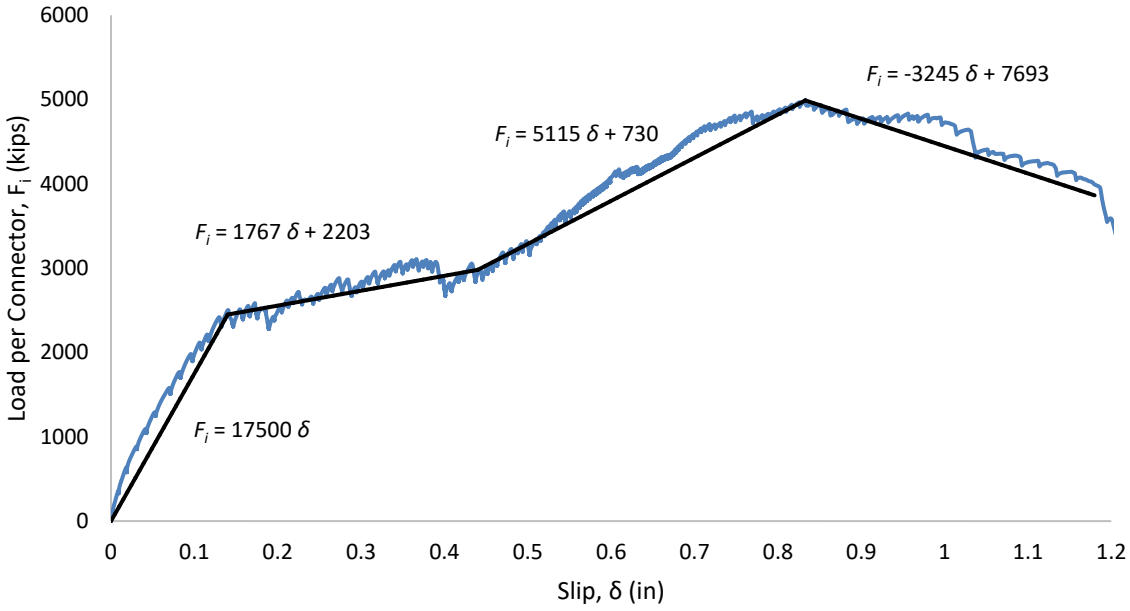

Figure C-5 Load-slip curve for Thermomass B

2. Find the total sum of the connector forces using Equation (7-12):

$$F_{sum} = N * \sum F_i = 22.65\ kips$$

$$F_{sum} \leq A_s * f_u = 0.44\ in^2 * 110\ ksi = 48.4\ kips \quad \therefore \quad OK$$

3. Find C_1 and T_1 for the first wythe

   a. Assume $\varepsilon_c = 0.003$.

   b. Assume a value of c_1. We will assume $c_1 = 0.242$ in

   c. Calculate curvature using Equation (7-13):

$$\varphi = \frac{0.003}{0.242} = 0.01238$$

   d. Calculate the compressive force in the top wythe using Equation (7-15). This will incorporate Hognestad's Equation (7-14).

$$C_1 = b * f_c' * \frac{\varphi_1 * c_1^2}{\varepsilon_0} * \left(1 - \frac{\varphi_1 * c_1}{3\varepsilon_0}\right)$$

$$C_1 = 36\ in * 9.23\ ksi * \frac{0.01238 * 0.242^2}{0.002} * \left(1 - \frac{0.01238 * 0.242}{0.006}\right) = 60.38\ kips$$

e. Calculate the strain and stress in the steel using Equations (7-17) and the experimental stress-strain curve for the actual steel in the panel (see Chapter 5).

$$\varepsilon_s = 0.003 * \frac{2.0 - 0.242}{0.242} = 0.02176$$

$$f_s = 85.75\ ksi$$

f. Calculate the tension force in wythe 1 with Equation (7-20)

$$T_1 = 85.75\ ksi * 0.44\ in^2 = 37.73\ kips$$

g. Enforce force equilibrium for wythe 1 with Equation (7-21):

$$C_1 - T_1 = 60.38\ kips - 37.73\ kips = 22.65\ kips = F_{sum}\ \therefore\ OK$$

4. Find C_2 and T_2 for the second wythe

a. Assume both wythes will deflect equally, therefore assume $\varphi_2 = \varphi_1 = 0.01238$

b. Assume a value of c_2. We will assume c_2 = 0.0982 in (neutral axis in the bottom wythe)

c. Calculate the compressive force in the bottom wythe, C_2, using Equation (7-22). The compressive force in the concrete will again utilize Hognestad's equation to estimate the concrete compressive strength, but it is critical here because Whitney's stress block is only valid when the top fiber is at 0.003 strain and in the case of partial composite action, this will not be true.

$$C_2 = b * f_c' * \frac{\varphi_2 * c_2^2}{\varepsilon_0} * \left(1 - \frac{\varphi_2 * c_2}{3\varepsilon_0}\right)$$

$$C_2 = 36\ in * 9.23\ ksi * \frac{0.01238 * 0.0982^2}{0.002} * \left(1 - \frac{0.01238 * 0.0982}{0.006}\right) = 15.8\ kips$$

d. Calculate the strain and stress in the steel using experimental curve (Chapter 5).

$$\varepsilon_s = (d - c_2) * \varphi_2$$

$$\varepsilon_s = (2.0 - 0.0982) * 0.01238 = 0.02358$$

$$f_s = 87.42\ ksi$$

e. Calculate the tension force in wythe 2 using Equation (7-24):

$$T_2 = 87.42\ ksi * 0.44\ in^2 = 38.46\ kips$$

f. Enforce force equilibrium for wythe 2 with Equation (7-25):

$$T_2 - C_2 = 38.46\ kips - 15.8\ kips = 22.66\ kips = F_{sum}\ \therefore\ OK$$

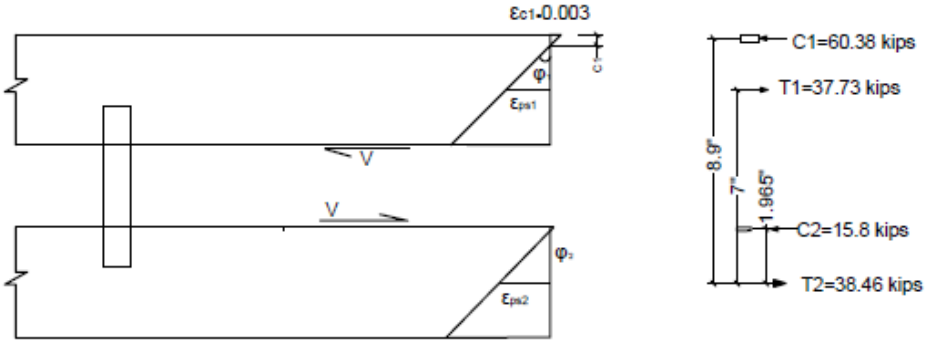

Figure C-6 Thermomass B Panel Design Example

5. Calculate the ultimate moment of the concrete sandwich wall panel using Equation (7-26). In addition, Using Equation (7-16) to calculate the centroid of C_1 and C_2.

$$x_{c1} = c_1 - \frac{c_1 * (8 * \varepsilon_o - 3 * \varphi_1 * c_1)}{12 * \varepsilon_o - 4 * \varphi_1 * c_1} = 0.242 - \frac{0.242\ * (8 * 0.002 - 3 * 0.01238 * 0.242)}{12 * 0.002 - 4 * 0.01238 * 0.242} = 0.10\ in$$

$$M_1 = C_1 * (d_1 - x_{c1}) = 60.38\ kips * (2.0\ in - 0.1\ in) = 114.7\ kip * in$$

$$x_{c2} = c_2 - \frac{c_2 * (8 * \varepsilon_o - 3 * \varphi_2 * c_2)}{12 * \varepsilon_o - 4 * \varphi_2 * c_2} = 0.0982 \text{ in} - \frac{0.0982\ * (8 * 0.002 - 3 * 0.01238 * 0.0982)}{12 * 0.002 - 4 * 0.0982 * 0.01238} = 0.0348\ in$$

$$M_2 = C_2 * (d_2 - x_{c2}) = 15.8\ kips * (2.0\ in - 0.0348\ in) = 31.05\ kip *\ in$$

$$M = M_1 + M_2 + F_{sum} * \left(\frac{t_{wy1} + t_{wy2}}{2} + t_{ins}\right)$$

$$= 114.7 + 31.05 + 22.66 * \left(\frac{4+4}{2} + 3\right) = 304.4\ kip * in$$

$$= \mathbf{25.36\ kip * ft}$$

BC Panel Analysis Example (both Thermomass CC and X connectors, Mild Reinforcement)

Section and Material Properties

$f_c' = 9.23\ ksi$ $A_s = 0.44\ in^2$

$b = 36\ in$ $t_{wy1} = 4\ in$

$t_{wy2} = 4\ in$ $t_{ins} = 3\ in$

$L = 192\ in$

$x_{CCi} = \begin{bmatrix} 16 \\ 32 \\ 48 \\ 64 \\ 80 \end{bmatrix} in$ $N_{CC} = 3$

$x_{Xi} = [24] in$ $N_X = 2$

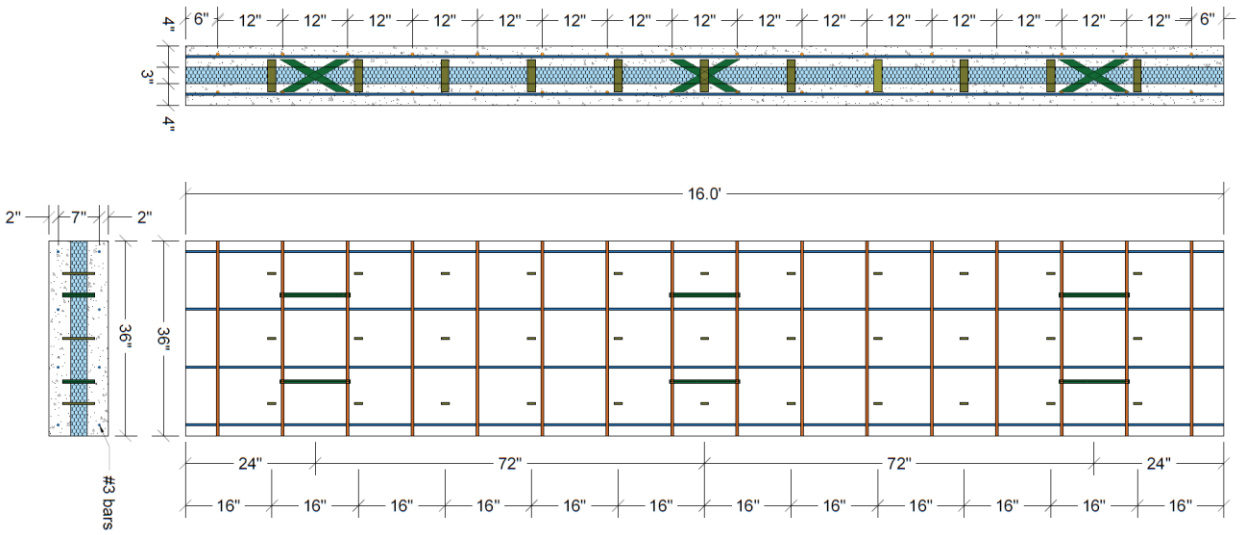

Solution

1. Find the forces in each connector using the load-slip relationship. Using an influence line, the ultimate slip (δ_{Ult}) that occurs at the maximum force is determined to be 0.18 in. Calculate slip using Equation (7-11):

$$\delta(i) = \frac{\delta_{Ult}}{\frac{L}{2} - x_1} * \left(\frac{L}{2} - x_i\right)$$

$$\delta(i) = \frac{0.18\ in}{\frac{192}{2} in - 16\ in} * \begin{bmatrix} \frac{192}{2} - 16 \\ \frac{192}{2} - 24 \\ \frac{192}{2} - 32 \\ \frac{192}{2} - 48 \\ \frac{192}{2} - 64 \\ \frac{192}{2} - 80 \end{bmatrix} \text{in} = \begin{bmatrix} 0.18 \\ 0.162 \\ 0.144 \\ 0.108 \\ 0.072 \\ 0.036 \end{bmatrix} in$$

Find F_i at each connector by using Figure C-7. The entire curve is used to obtain the most accurate prediction. Because there are different N values for each connector (N_{CC} = 3 and N_X = 2), we incorporate that into this step.

$$F(i) = \begin{bmatrix} 3 * 2.567 \\ 2 * 12.17 \\ 3 * 2.5 \\ 3 * 1.93 \\ 3 * 1.28 \\ 3 * 0.643 \end{bmatrix} \text{kips}$$

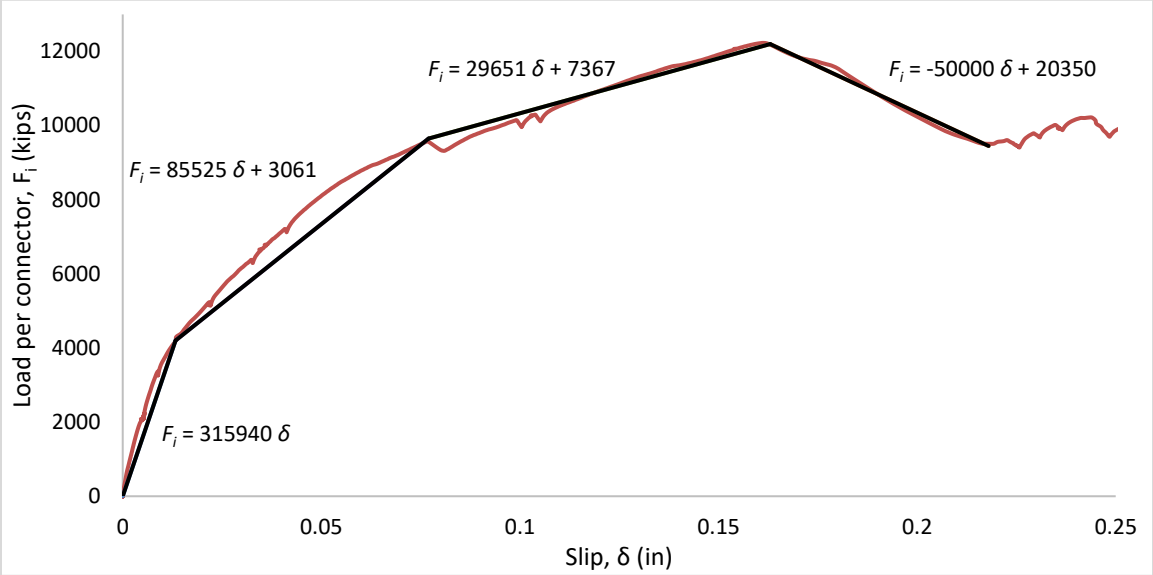

Figure C-7 Load-slip curve for Thermomass A

2. Find the total sum of the connector forces using Equation (7-12). Note that we already accounted for N values in the previous step in this example only because there were two different values for N_{CC} and N_X.

$$F_{sum} = \sum F_i = 51.13\ kips$$

$$F_{sum} \geq A_s * f_u = 0.44\ in^2 * 110\ ksi = 48.4\ kips \quad \therefore \quad \text{Use } F_{sum} = 48.4\ kips$$

Ultimate Slip corresponding to $F_{sum} = 48.4\ kips$ is $\delta_{Ult} = 0.162\ in$

3. Find C_1 and T_1 for the first wythe

    a. Assume ε_c = 0.003.

    b. Assume a value of c_2. We will assume c_1 = 0.33307 in.

    c. Calculate curvature using Equation (7-13):

$$\varphi = \frac{\varepsilon_c}{c_1} = \frac{0.003}{0.33307} = 0.009007$$

    d. Calculate the compressive force in the top wythe using Equation (7-15). This will incorporate Hognestad's Equation (7-14).

$$C_1 = b * f_c' * \frac{\varphi_1 * c_1^2}{\varepsilon_0} * \left(1 - \frac{\varphi_1 * c_1}{3\varepsilon_0}\right)$$

$$C_1 = 36\ in * 9.23\ ksi * \frac{0.009007 * 0.33307^2}{0.002} * \left(1 - \frac{0.009007 * 0.33307}{0.006}\right) = 83\ kips$$

    e. Calculate the strain and stress in the steel using Equations (7-17). The stress will come from a stress-strain curve for the actual steel in this panel as shown in Figure 7-9.

$$\varepsilon_s = 0.003 * \frac{2.0 - 0.33307}{0.33307} = 0.01501$$

$$f_s = 78.65\ ksi$$

    f. Calculate the tension force in wythe 1 with Equation (7-20)

$$T_1 = 78.65\ ksi * 0.44\ in^2 = 34.6\ kips$$

    g. Enforce force equilibrium for wythe 1 with Equation (7-21):

$$C_1 - T_1 = 83\ kips - 34.6\ kips = 48.4\ kips = F_{sum} \quad \therefore \quad OK$$

4. Find C_2 and T_2 for the second wythe

    a. Assume both wythes will deflect equally, therefore assume $\varphi_2 = \varphi_1 = 0.009007$

    b. Assume a value of c_2. Assume c_2 = -6.5 (the neutral axis is not in the bottom wythe; no compression force)

c. Calculate the compressive force in the bottom wythe, C_2, using Equation (7-22). The compressive force in the concrete will again utilize Hognestad's equation to estimate the concrete compressive strength, but it is critical here because Whitney's stress block is only valid when the top fiber is at 0.003 strain and in the case of partial composite action, this will not be true.

$$C_2 = b * f_c' * \frac{\varphi_2 * c_2^2}{\varepsilon_0} * \left(1 - \frac{\varphi_2 * c_2}{3\varepsilon_0}\right)$$

$$C_2 = 0\ kips$$

d. Calculate the strain and stress in the steel. This step is only necessary to calculate the tension force in wythe 2, and since we discovered in step 2 that the steel yields, this step is unnecessary and we move to step 4e.

e. Calculate the tension force in wythe 2. Because the Steel has yielded:

$$T_2 = 48.4\ kips$$

f. Enforce force equilibrium for Wythe 2 with Equation (7-25):

$$T_2 - C_2 = 48.4\ kips - 0\ kips = 48.4\ kips = F_{sum} \ \therefore \ OK$$

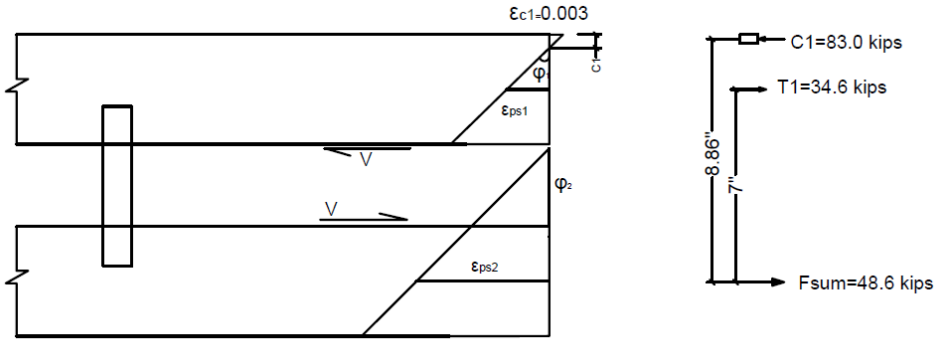

Figure C-8 Thermomass A Panel Design Example

5. Calculate the ultimate moment of the concrete sandwich wall panel using Equation (7-26). In addition, Using Equation (7-16) to calculate the centroid of C_1

$$x_{c1} = c_1 - \frac{c_1 * (8 * \varepsilon_o - 3 * \varphi_1 * c_1)}{12 * \varepsilon_o - 4 * \varphi_1 * c_1} = 0.333 - \frac{0.333 \ * (8 * 0.002 - 3 * 0.009 * 0.333)}{12 * 0.002 - 4 * 0.009 * 0.333} = 0.139 \ in$$

$$M_1 = C_1 * (d_1 - x_{c1}) = 83 * (2.0 - 0.139) = 154.5 \ kip * in$$

$$M_2 = C_2 * (d_2 - x_{c2}) = 0$$

$$M = M_1 + M_2 + F_{sum} * \left(\frac{t_{wy1} + t_{wy2}}{2} + t_{ins}\right)$$

$$= 154.5 + 0 + 48.4 * \left(\frac{4 + 4}{2} + 3\right) = 493.3 \ kip * in$$

$$= \mathbf{41.1 \ kip * ft}$$

D Panel Analysis Example (HK Composite connectors, Mild Reinforcement)

Section and Material Properties

$f_c' = 9.23\ ksi$ $\quad A_s = 0.44\ in^2$

$b = 36\ in$ $\quad t_{wy1} = 4\ in$

$t_{wy2} = 4\ in$ $\quad t_{ins} = 3\ in$

$L = 192\ in$

$x_i = \begin{bmatrix} 16 \\ 32 \\ 48 \\ 64 \\ 80 \end{bmatrix} in$ $\quad N = 3$

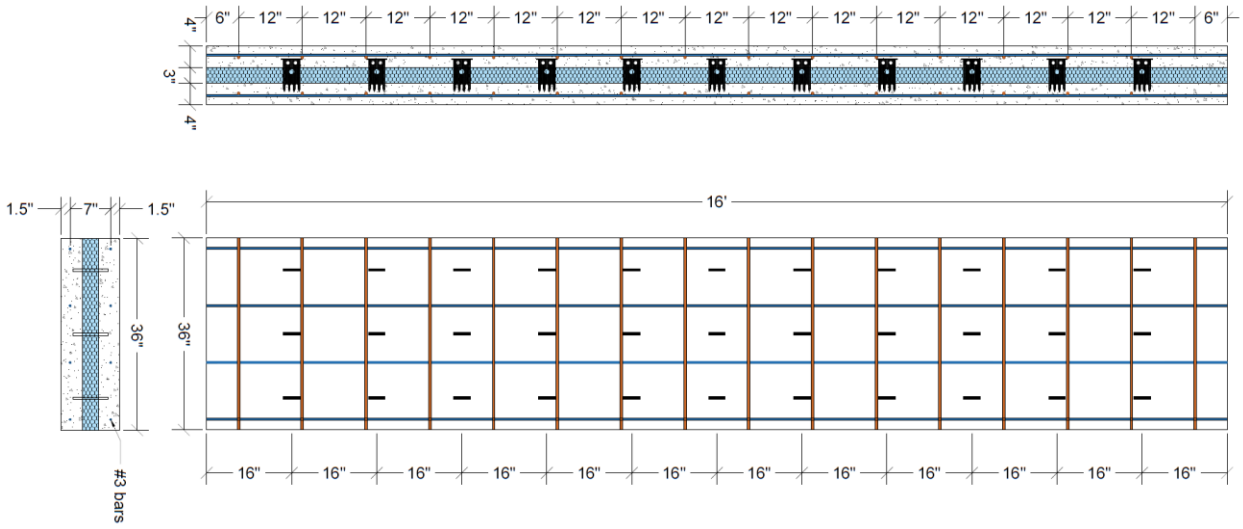

Solution

1. Find the forces in each connector using the load-slip relationship. Using an influence line, the ultimate slip (δ_{Ult}) that occurs at the maximum force is determined to be 0.12 in. In addition, the sum of the forces should be less than or equal to A_s * f_s in the bottom wythe. Calculate slip using Equation (7-11):

$$\delta(i) = \frac{\delta_{Ult}}{\frac{L}{2} - x_1} * \left(\frac{L}{2} - x_i\right)$$

$$\delta(i) = \frac{0.12\ in}{\frac{192}{2} in - 16\ in} * \begin{bmatrix} \frac{192}{2} - 16 \\ \frac{192}{2} - 32 \\ \frac{192}{2} - 48 \\ \frac{192}{2} - 64 \\ \frac{192}{2} - 80 \end{bmatrix} \text{in} = \begin{bmatrix} 0.12 \\ 0.0968 \\ 0.0726 \\ 0.0484 \\ 0.0242 \end{bmatrix} in$$

Find F_i at each connector by using Figure C-9.

$$F(i) = \begin{bmatrix} 3.13 \\ 3.52 \\ 3.91 \\ 2.97 \\ 2.03 \end{bmatrix} kips$$

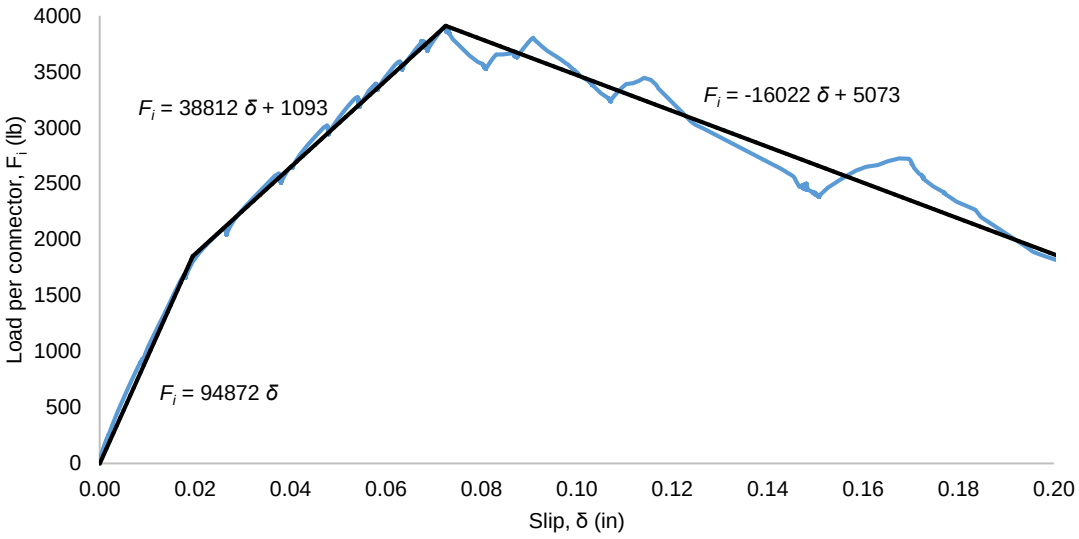

Figure C-9 Load-slip curve for HK

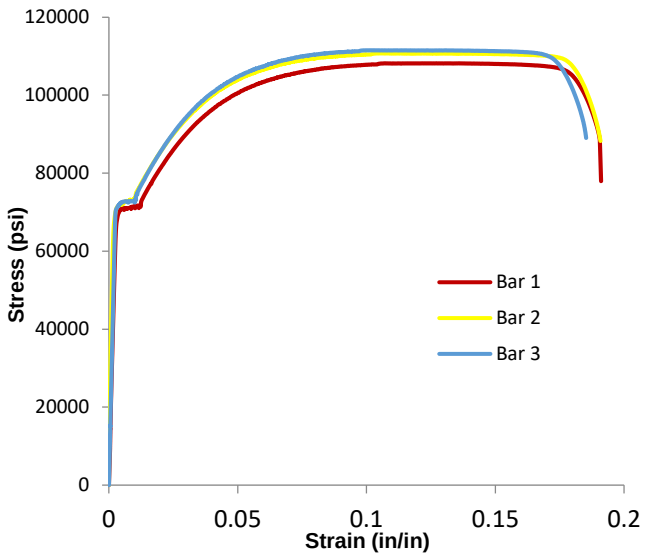

Figure C-10 Actual stress vs strain of HK and Thermomass panel

2. Find the total sum of the connector forces using Equation (7-12):

$$F_{sum} = N * \sum F_i = 46.7\ kips$$

$$F_{sum} \leq A_s * f_u = 0.44\ in^2 * 110\ ksi = 48\ kip \quad \therefore \quad OK$$

3. Find C_1 and T_1 for the first wythe

   a. Assume ε_c = 0.003.

   b. Assume a value of c_1. We will assume c_1 = 0.327 in.

   c. Calculate curvature using Equation (7-13):

$$\varphi_1 = \frac{\varepsilon_c}{c_1} = \frac{0.003}{0.327} = 0.00917$$

   d. Calculate the compressive force in the top wythe using Equation (7-15). This will incorporate Hognestad's Equation (7-14).

$$C_1 = b * f_c' * \frac{\varphi_1 * c_1^2}{\varepsilon_0} * \left(1 - \frac{\varphi_1 * c_1}{3\varepsilon_0}\right)$$

$$C_1 = 36\ in * 9.23\ ksi * \frac{0.00917 * 0.327^2}{0.002} * \left(1 - \frac{0.00917 * 0.327}{0.006}\right) = 81.5\ kips$$

   e. Calculate the strain and stress in the steel using Equations (7-17) and (7-18). The stress will come from a stress-strain curve for the actual steel used in the panel as shown in Figure 7-9.

$$\varepsilon_s = 0.003 * \frac{2.0 - 0.327}{0.327} = 0.01535$$

$$f_s = 79.0\ ksi$$

f. Calculate the tension force in wythe 1 with Equation (7-20)

$$T_1 = 79.0\ ksi * 0.44\ in^2 = 34.8\ kips$$

g. Enforce force equilibrium for wythe 1 with Equation (7-21):

$$C_1 - T_1 = 81.5\ kips - 34.8\ kips = 46.7\ kips = F_{sum}\ \therefore\ OK$$

4. Find C_2 and T_2 for the second wythe

a. Assume both wythes will deflect equally, therefore assume $\varphi_2 = \varphi_1 = 0.00917$.

b. Assume a value of c_2. Assume c_2 = -4.7 (neutral axis in the foam, no compression force)

c. Calculate the compressive force in the bottom wythe, C_2, using Equation (7-22). The compressive force in the concrete will again utilize Hognestad's equation to estimate the concrete compressive strength, but it is critical here because Whitney's stress block is only valid when the top fiber is at 0.003 strain and in the case of partial composite action, this will not be true.

$$C_2 = b * f_c' * \frac{\varphi_2 * c_2^2}{\varepsilon_0} * \left(1 - \frac{\varphi_2 * c_2}{3\varepsilon_0}\right)$$

$$C_2 = 0\ kips$$

d. Calculate the strain and stress in the steel using the actual stress strain relationship for the steel in the panel as shown in Figure 7-9.

$$\varepsilon_s = \varphi_2\ (d_2 - c) = 0.00917 * \big(2 - (-4.7)\big) = 0.0614$$

$$f_s = 106.1\ ksi$$

e. Calculate the tension force in wythe 2 using Equation (7-24):

$$T_2 = f_s * A_s = 106.1\ ksi * 0.44\ in^2 = 46.7\ kips$$

f. Enforce force equilibrium for wythe 2 with Equation (7-25):

$$T_2 - C_2 = 46.7\ kips - 0\ kips = 46.7\ kips = F_{sum}\ \therefore\ OK$$

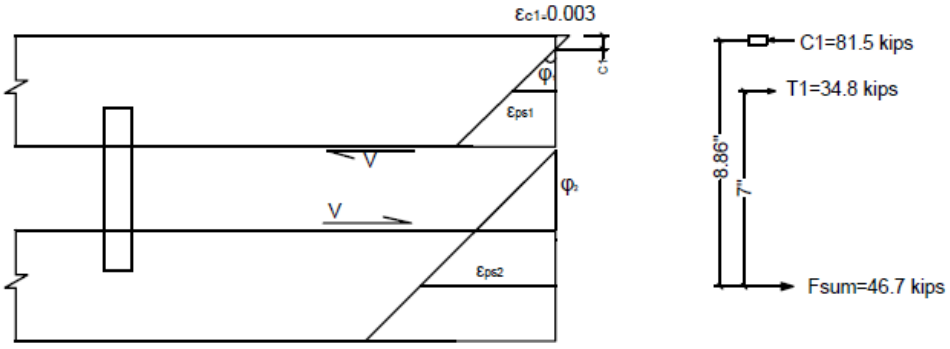

Figure C-11 HK Panel Design Example

5. Calculate the ultimate moment of the concrete sandwich wall panel using Equation (7-26). In addition, Using Equation (7-16) to calculate the centroid of C_1

$$x_{c1} = c_1 - \frac{c_1 * (8 * \varepsilon_o - 3 * \varphi_1 * c_1)}{12 * \varepsilon_o - 4 * \varphi_1 * c_1} = 0.327\ in - \frac{0.327\ \text{in} * (8 * 0.002 - 3 * 0.00917 * 0.327)}{12 * 0.002 - 4 * 0.00917 * 0.327} = 0.1362\ in$$

$$M_1 = C_1 * (d_1 - x_{c1}) = 81.5\ kips * (2.0 - 0.1362) = 151.9\ kip * in$$

$$M_2 = C_2 * (d_2 - x_{c2}) = 0$$

$$M = M_1 + M_2 + F_{sum} * \left(\frac{t_{wy1} + t_{wy2}}{2} + t_{ins}\right)$$

$$= 151.9\ kip * ft + 0 + 46.7\ kips * \left(\frac{4\ in + 4\ in}{2} + 3\ in\right) = 478.8\ kip * in$$

$$= \mathbf{39.9\ kip * ft}$$

APPENDIX D. Partially-Composite Strength Prediction Method Design Example

As with many design problems, an example may clarify the ultimate moment method described in Chapter 7. This example only takes into account a single load case, but illustrates the design method to achieve full-composite action at failure. There are two major stages to consider in this design of concrete sandwich panel walls. The first stage is to find the required area of steel, and the second stage is to determine the number and spacing of connectors needed. Figure D-1 depicts the sandwich panel used in this example.

Panel Properties

$L = 37\ ft$ $Span = 35\ ft$

$t_{wy1} = 3\ in$ $t_{wy2} = 3\ in$

$t_{ins} = 3\ in$ $b = 8\ ft$

$f_c' = 6.0\ ksi$ $f_y = 60\ ksi$

$Wind\ Load = W_L = 30\ psf$ Insulation Type: XPS

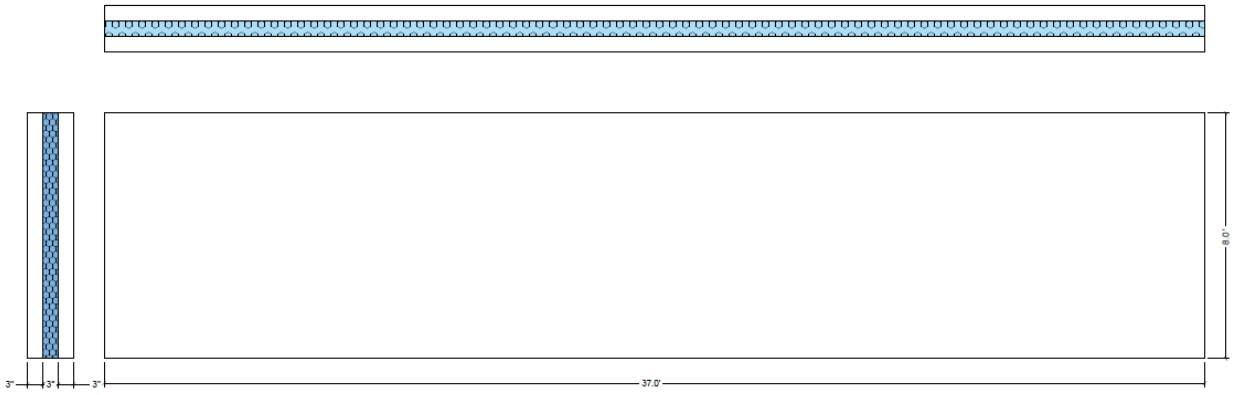

Figure D-1 Design example sandwich panel dimensions

Solution

a. First, assume the panel acts with full-composite action and find the required area of steel.

$$\phi = 0.9 \qquad d_1 = 1.5\ in \qquad d_2 = 1.5\ in$$

Nominal moment may be calculated using Equation (7-5) as

$$M_n = \frac{M_u}{\phi} = A_{s1} * f_{s1} * \left(d_1 - \frac{a}{2}\right) + A_{s2} * f_{s2} * \left(d_2 + t_{wy_1} + t_{ins} - \frac{a}{2}\right)$$

Ultimate factored moment is calculated as

$$M_u = \frac{1.6 * W_L * b * L^2}{8} = \frac{1.6 * 30\ psf * (8\ ft) * (35\ ft)^2}{8} = 58.8\ k.ft$$

Assume $As_1 = As_2 = 1.514\ in^2\ and\ (f_{s1}\ \&\ f_{s1})\ are\ yield$

$$a = \frac{(As_1 + As_2) * f_y}{0.85 * f_c' * b} = \frac{(1.514 + 1.514) in^2 * 60\ kis}{0.85 * 6\ ksi * 8\ ft * \frac{12in}{ft}} = 0.371\ in$$

Using strain compatibility, the stress in the steel is calculated as

$$f_s = E_s * \left(\varepsilon_c * \frac{\left(d - \frac{a}{\beta_1}\right)}{\frac{a}{\beta_1}} \right) \leq f_y$$

Where

$$\beta_1 = 0.85 - 0.05 * (f_c' - 4\ ksi) = 0.85 - 0.05 * (6\ ksi - 4ksi) = 0.75$$

Stress is then calculated as

$$f_{s1} = 29000 * \left(0.003 * \frac{\left(1.5 - \frac{0.317}{0.75}\right)}{\frac{0.317}{0.75}} \right) = 222\ ksi > f_y\ \therefore f_{s1} = 60$$

$$f_{s2} = 29000 * \left(0.003 * \frac{\left(7.5 - \frac{0.317}{0.75}\right)}{\frac{0.317}{0.75}} \right) = 1457\ ksi > f_y\ \therefore f_{s2} = 60$$

Substituting, we can solve for A_s:

$$\frac{58.8\ k.ft}{0.9} = A_s * 60\ ksi * \left(1.5\ in - \frac{a}{2}\right) + A_s * 60\ ksi * \left(7.5\ in - \frac{a}{2}\right)$$

$$A_s = 1.52\ in^2 = Assumed\ A_s\ \therefore OK$$

Therefore, **use eight #4 bars in each wythe**.

Assume the shear force provided by the connectors at midspan is equal to the area of steel times the steel yield stress.

$$F_{sum} = A_s * f_y = (8 * 0.2\ in^2) * 60\ ksi = 96\ kips.$$

b. Find the ultimate moment of the panel:

i. Find C_1 and T_1 for wythe 1

a. Assume $c_1 = 0.523\ in$

b. Calculate curvature as

$$\phi_1 = \frac{\varepsilon_c}{c_1} = \frac{0.003}{0.523} = 0.005736$$

c. Using Whitney Stress block, we calculate compressive force of

$$C_1 = 0.85 * f_c' * b * \beta_1 * c_1$$

$$C_1 = 0.85 * 6\ ksi * 96\ in * 0.75 * 0.523\ in = 192\ kips$$

d. Strain and stress of steel are calculated as

$$\varepsilon_s = \varepsilon_c \frac{d_1 - c_1}{c_1} = 0.003 * \frac{1.5 - 0.523}{0.523} = 0.056$$

$$f_s = \varepsilon_s * E_s = 0.056 * 29000\ ksi = 1624\ ksi > 60ksi\ \ \therefore\ f_s = f_y = 60\ ksi$$

e. Tension force in the wythe is calculated by

$$T_1 = f_s * A_s = 60\ ksi * (8 * 0.20\ in^2) = 96\ kips$$

f. Check for $C_1 - T_1 = F_{sum}$

$$C_1 - T_1 = 192\ kips - 96\ kips = 96\ kips = F_{sum}\ \ \therefore\ OK$$

ii. Find C_2 and T_2 for wythe 2

a. Assume $\varphi_2 = \varphi_1 = 0.005736$

b. Guess $c_2 = 0$ (neutral axis at top fiber of wythe 2)

c. It is recommended to facilitate design that there is zero compressive force in wythe 2, therefore

$$C_2 = 0\ kips$$

d. We also assume the steel has yielded, therefore

$$f_s = f_y = 60\ ksi$$

e. Tensile force in the bottom wythe will be calculated as

$$T_2 = f_s * A_s = 60\ ksi * (8 * 0.20\ in^2) = 96\ kips$$

f. Check for $C_2 - T_2 = F_{sum}$

$$C_2 - T_2 = 96\ kips - 0\ kips = 96\ kips = F_{sum}\ \ \therefore\ OK$$

iii. The moment is determined to be

$$M_1 = C_1 * \left(d_1 - \frac{a_1}{2}\right) = 192\ kips * \left(1.5 - 0.523 * \frac{0.75}{2}\right) = 250.3\ kip * in$$

$$M_2 = C_2 * \left(d_2 - \frac{a_2}{2}\right) = 0\ kip * in$$

$$M_n = M_1 + M_2 + F_{sum} * \left(\frac{t_{wy1}+t_{wy2}}{2} + t_{ins}\right) = 250.3\ kip * in + 96\ kips * 6\ in =$$

826.3 k-in = **68.8 k-ft**

$$M_u = 58.8\ kip.ft < (\phi M_n = 0.9 * 68.8 = 61.92\ kip.ft) \quad \therefore OK$$

c. Find the number of connectors and the spacing that provide the required shear force.

Assume 4 HK Composite connectors at 24 spacing. First calculate the slip using Equation (7-11).

$$\delta(i) = \frac{\delta_{Ult}}{\frac{L}{2} - x_1} * \frac{L}{2} - x_i$$

$$\delta(i) = \frac{0.0726\ in}{222\ in - 24\ in} * \begin{bmatrix} 222-24 \\ 222-48 \\ 222-72 \\ 222-96 \\ 222-120 \\ 222-144 \\ 222-168 \\ 222-192 \end{bmatrix} \text{in} = \begin{bmatrix} 0.0726 \\ 0.0638 \\ 0.055 \\ 0.0462 \\ 0.0374 \\ 0.0286 \\ 0.0198 \\ 0.011 \end{bmatrix} in$$

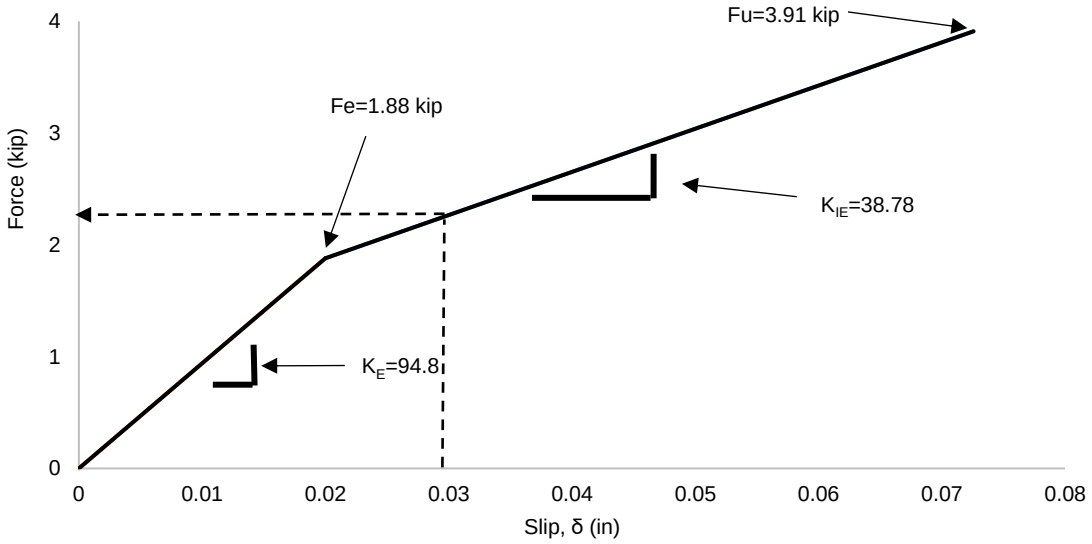

Figure D-2 Load-slip curve for D connector

Using Table 4-12, a design curve may be created for the recommended design. The force at each connector location can then be determined using the load-slip curve for the HK connector (see Figure D-2). Alternatively, the following equations may be used to calculate the force at each value of slip.

$$F(i) = \begin{cases} K_E * \delta(i) & if\ \delta \le \delta_E \\ (F_e - K_{IE} * \delta_E) + K_{IE} * Slip & if\ \delta > \delta_E \end{cases}$$

$$F(i) = \begin{cases} 94.8 * \delta & if\ \delta \le \delta_E \\ 1.11 + 38.78 * \delta & if\ \delta > \delta_E \end{cases}$$

$$F(i) = \begin{bmatrix} 3.91 \\ 3.57 \\ 3.23 \\ 2.89 \\ 2.55 \\ 2.21 \\ 1.861 \\ 1.0 \end{bmatrix} kip$$

These values can then be used with Equation (7-12) to calculate F_{sum}:

$$F_{sum} = 4 * 21.26\ kip = 85\ kip < A_s * f_y \quad \therefore \quad Not\ OK$$

Therefore, Assume 4 HK Composite connectors at 20 spacing.

Again, calculate the slip using Equation (7-11) as

$$\delta(i) = \frac{\delta_{Ult}}{\frac{L}{2} - x_1} * \left(\frac{L}{2} - x_i\right)$$

$$\delta(i) = \frac{0.0726\ in}{222\ in - 20\ in} * \begin{bmatrix} 222 - 20 \\ 222 - 40 \\ 222 - 60 \\ 222 - 80 \\ 222 - 100 \\ 222 - 120 \\ 222 - 140 \\ 222 - 160 \\ 222 - 180 \\ 222 - 200 \end{bmatrix} \text{in} = \begin{bmatrix} 0.0726 \\ 0.0654 \\ 0.0582 \\ 0.051 \\ 0.0438 \\ 0.0366 \\ 0.0295 \\ 0.0223 \\ 0.0151 \\ 0.008 \end{bmatrix} in$$

The force at each connector location can then be determined using the load-slip curve for the HK connector (see Figure D-2).

$$F(i) = \begin{bmatrix} 3.91 \\ 3.63 \\ 3.35 \\ 3.07 \\ 2.79 \\ 2.51 \\ 2.24 \\ 1.96 \\ 1.43 \\ 0.75 \end{bmatrix} kip$$

These values can then be used with Equation (7-12) to calculate F_{sum}:

$$F_{sum} = 4 * 25.65\ kip = 102.6\ kip > A_s * f_y \quad \therefore OK$$

Therefore, using 4 HK Composite connectors at 20 in. center-to-center spacing.

as shown in Figure D-3 is acceptable.

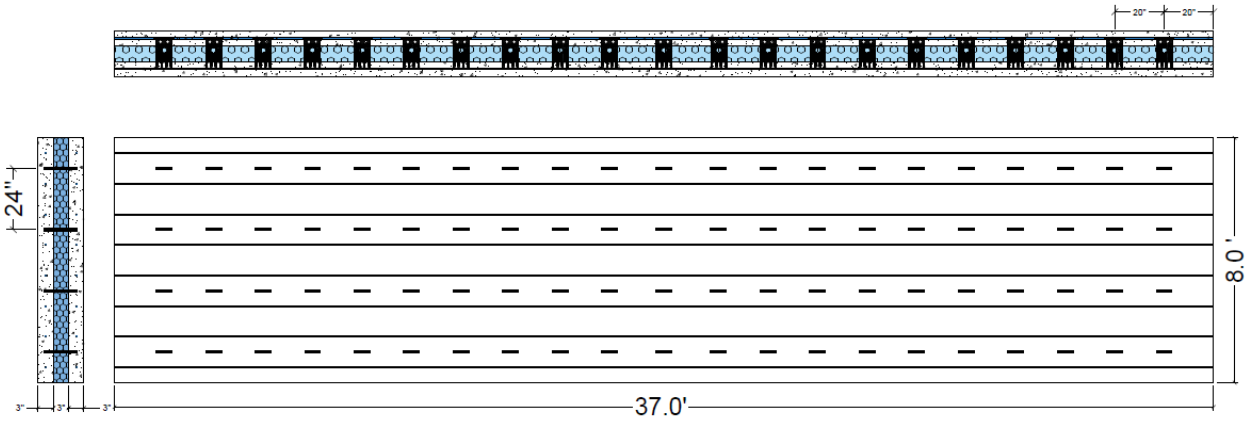

Figure D-3 Sandwich panel detail for Design Example